Responsive Hydrogels using Self-Assembling Polymer-Peptide Conjugates

A thesis submitted to the University of Manchester
for the degree of Doctor of Philosophy
in the Faculty of Engineering and Physical Sciences

2010

Antons Maslovskis

School of Chemical Engineering and Analytical Science

TABLE OF CONTENTS

List of Tables 6
List of Figures 7
List of Abbreviations and Symbols 12
Abstract 13
Declaration 14
Copyright Statement 14
Acknowledgements 15
The Author 16
Dedication 18

Chapter 1. General Introduction 22
Chapter 2. Literature Review 28
2.1. Temperature-responsive polymer: poly(*N*-isopropylacrylamide) 30
2.1.1. Introduction 30
2.1.2. Single chain PNIPAAm synthesis 31
2.1.2.1. Free radical polymerisation (FRP) of NIPAAm 32
2.1.3. PNIPAAm behaviour in aqueous solution 35
2.1.3.1. LCST phenomenon 35
2.1.3.2. LCST characterisation methods 37
2.1.3.3. Polymer chain conformation studies with light scattering and fluorescence 38
2.1.4. Factors that influence the LCST 39
2.1.4.1. Polymer molecular weight 39
2.1.4.2. Copolymerisation of *N*-isopropylacrylamide 40
2.1.4.3. Solvent effect on the LCST 41
2.1.4.4. Salt effect on the LCST 42
2.1.4.5. Surfactant effect on the LCST 42
2.1.5. Applications of PNIPAAm 43
2.1.5.1. Biological application 43
2.1.5.2. PNIPAAm in cell growth 45
2.1.5.3. Separation technologies 46
2.1.6. Summary 47
2.2. Amino acids and peptide formation 48
2.2.1. Introduction 48
2.2.2. Amino acids 48
2.2.3. The amide bond and peptides primary structure 50
2.2.4. Secondary structures 51
2.2.4.1. α-Helix 51
2.2.4.2. Pleated-sheet structures 52
2.2.5. Tertiary and quaternary structure 53
2.2.6. Solid phase peptide synthesis 54
2.2.7. Summary 57
2.3. Peptide self-assembly 58
2.3.1. Introduction 58

2.3.2. Self-assembling peptide systems 60
2.3.2.1. Systems based on β-sheet structures – ionic complementary peptides 61
2.3.2.2. Systems based on β-hairpins 61
2.3.2.3. Systems based on surfactant-like peptides 63
2.3.2.4. Systems based on α-helical structure 65
2.3.2.5. Systems based on aromatic interactions 66
2.3.3. Ionic-complementary peptides and their self-assembly 67
2.3.4. Different factors that affect self-assembly of ionic-complementary peptides 69
2.3.4.1. Peptide sequence effect 69
2.3.4.2. Concentration effect 70
2.3.4.3. pH effect 71
2.3.4.4. Salt effect 72
2.3.5. Applications of self-assembling peptides 73
2.3.5.1. Tissue engineering 73
2.3.5.2. Drug delivery 74
2.3.6. Summary 75
2.4. Conjugates of polymers and peptides 76
2.4.1. Introduction 76
2.4.2. Polymer-peptide conjugation strategies 76
2.4.2.1. Convergent conjugation methods 77
2.4.2.1.1. Amine-reactive polymers 78
2.4.2.1.2. Thiol-reactive polymers 81
2.4.2.1.3. Oxime formation 83
2.4.2.1.4. Conjugate formation via cycloaddition 83
2.4.2.1.5. Ligand-modified polymers 84
2.4.2.2. Divergent conjugation 85
2.4.2.2.1. Polymerisation from a peptide 85
2.4.3. Self-assembly of polymer-peptide conjugates 86
2.4.4. Applications of smart polymer-peptide/protein conjugates 90
2.4.4.1. Drug delivery and tissue engineering 90
2.4.4.2. Separation and purification technology 93
2.4.5. Summary 93
2.5. Aims of the study 94
References 95

Chapter 3. Materials and Methods 104
3.1. Introduction 106
3.2. Material 106
3.3. Synthetic procedures 106
3.3.1. Solid phase peptide synthesis (SPPS) 106
3.3.2. Modification of FEFEFKFK with 3-mercaptopropionic acid (MPA) 108
3.3.3. Polymerisation of *N*-isopropylacrylamide (NIPAAm) 109
3.3.4. PNIPAAm functionalisation with peptide 109
3.3.5. Determination of the polymer/conjugate ratio 110
3.3.6. Gelation and phase behaviour of polymer/conjugate mixtures 110
3.4. Instrumental techniques 111

3.4.1. Nuclear magnetic resonance (NMR) spectroscopy....111
3.4.1.1. Theory behind NMR spectroscopy....111
3.4.1.2. General procedure for NMR spectroscopy....112
3.4.2. Static Light Scattering (SLS)....112
3.4.2.1. Principle of SLS....112
3.4.2.2. General procedure for SLS....114
3.4.3. Viscometry....115
3.4.3.1. Introduction to viscometry....115
3.4.3.2. General procedure for viscometry measurements....116
3.4.4. Reversed phase high performance liquid chromatography(RP-HPLC)....116
3.4.4.1. Principle of RP-HPLC....116
3.4.4.2. General procedure for RP-HPLC analysis....117
3.4.5. Size exclusion chromatography (SEC)....117
3.4.5.1. Introduction to SEC....117
3.4.5.2. General procedure for GPC....119
3.4.6. Oscillatory rheology....119
3.4.6.1. Principle of rheology....119
3.4.6.2. General procedure for oscillatory rheology....120
3.4.7. Micro differential scanning calorimetry (micro DSC)....121
3.4.7.1. Principle of micro DSC....121
3.4.7.2. General procedure for micro DSC....123
3.4.8. Transmission electron microscopy (TEM)....123
3.4.8.1. Principle of TEM....123
3.4.8.2. General procedure for TEM....124
3.4.9. Atomic force microscopy (AFM)....124
3.4.9.1. Principle of AFM....124
3.4.9.2. General procedure for AFM....126
3.4.10. Small-angle neutron scattering (SANS)....127
3.4.10.1. Principles of SANS....127
3.4.10.2. SANS spectrometer D22 and general procedure for SANS experiment....134
References....137

Chapter 4. Peptide-PNIPAAm Conjugate Based Hydrogels: Synthesis and Characterisation....140
4.1. Introduction....142
4.2. Synthesis and characterisation of polymer/conjugate mixtures....142
4.3. Characterisation of the mixtures of polymer and polymer-peptide conjugate....152
4.3.1. Gelation and thermal behaviour in water....152
4.3.2. Thermal behaviour....160
4.3.3. Gel morphology and microstructure....165
4.4. Summary....167
References....170

Chapter 5. Thermo-Responsive Peptide-Rich Hydrogels from Physical Mixtures of Peptide and Polymer/Conjugate Mixture....172
5.1. Introduction....174

5.2. Thermal behaviour of the peptide-rich gels 175
5.3. Rheological studies 179
5.4. Summary 184
References 186

Chapter 6. Thermo-Responsive Peptide-Based Composite Gels 188
6.1. Introduction 190
6.2. Gels macroscopic phase separation 190
6.3. Micro DSC studies of the composite gels 194
6.4. Mechanical properties of the gels 196
6.5. Gel network morphology 202
6.6. Self-assembly scheme 212
6.7. Summary 214
References 215

Chapter 7. General Conclusions and Future Work 216
7.1. General Conclusions 218
7.2. Future Work 222

Appendices 224
Appendix 1. 226
Appendix 2. 229

Final word count: 58,496

LIST OF TABLES

Table 2.1: PNIPAAm molecular weight effect on the LCST.....40
Table 2.2: Natural amino acids.....49
Table 2.3: LCST of PNIPAAM, its copolymer with AAc and conjugates with alanine.....81
Table 3.1: PNIPAAm functionalisation with FEFEFKFK and FEFKFEFK.....109
Table 3.2: Gradient of solvents used for the RP-HPLC method.....117
Table 3.3: Types of radiation used in scattering.....128
Table 3.4: Scattering length densities for the peptide, polymer and solvents.....129
Table 3.5: Molar volumes of the amino acids.....129
Table 4.1: Summay of the polymer/conjugate mixtures prepared in this study.....145
Table 4.2 : Summary of the characterisation data for the polymer/conjugate mixtures prepared in this study.....148
Table 4.3: Peptide content in the polymer/conjugate mixtures at their *C**.....154
Table 4.4: Different β-sheet fibre forming peptides and G' values of their gels.....157
Table 5.1: Peptide weight fractions ($W_{pept.}$) in the conjugates PS3 and PA3 used for the preparation of the peptide-rich gels and conjugate weight fractions ($W_{conj.}$) in the peptide-rich gels studied.....175
Table 5.2: G' values of the gels FEFEFKFK/PS3 and FEFKFEFK/PA3 before heating and after 4 consecutive heating/cooling cycles.....183
Table 6.1: Peptide weight fraction ($W_{pept.}$) in the conjugate used for the preparation of the composite gels and conjugate weight fractions ($W_{conj.}$) in the peptide-rich gels studied.....192

LIST OF FIGURES

Figure 2.1: Chemical structure of PNIPAAm 31
Figure 2.2: Homolytical decomposition of AIBN 32
Figure 2.3: α-Cyanoalkyl radical attack of monomer double bond 32
Figure 2.4: PNIPAAm macromolecular chain growth 33
Figure 2.5: Termination of macromolecular chains via combination 33
Figure 2.6: Termination of macromolecular chains via disproportionation 33
Figure 2.7: Inactivation of active radicals with oxygen 34
Figure 2.8: Chain-transfer reaction using 3-mercaptopropionic acid 34
Figure 2.9: Phase diagram of an aqueous solution of PNIPAAm 35
Figure 2.10: Schematic representation of the reversible phase separation of PNIPAAm: A) linear chains, B) terminally-grafted PNIPAAm surfaces, and C) multi-point grafted PNIPAAm surfaces 36
Figure 2.11: Cloud point (A) and differential scanning calorimetry (DSC) (B) measurements of the LCST of aqueous solution of PNIPAAm 37
Figure 2.12: The effect of AAm and NtBAAm on the LCST of the copolymers with NIPAAm 41
Figure 2.13: General chemical structure of an amino acid 48
Figure 2.14: Scheme of peptide bond formation 50
Figure 2.15: Resonance structures of a peptide bond 50
Figure 2.16: Cis/trans isomers of peptide bond 51
Figure 2.17: Scheme of hydrogen bond formation 51
Figure 2.18: Representation of α-helix: a) schematic, b) molecular, c) view from the top 52
Figure 2.19: Schematic representation of anti-parallel β-sheets. Arrows represent the direction of β-sheet strands 53
Figure 2.20: Stabilising interchain interactions between amino acid residues: a) disulfide bridge, b) hydrogen bond, c) ionic bond (salt bridge), d) hydrophobic interaction 53
Figure 2.21: Scheme of solid-phase peptide synthesis 55
Figure 2.22: Schematic representation of Wang resin 55
Figure 2.23: Protecting group strategies in SPPS 56
Figure 2.24: Scheme showing various building blocks and different structures in which they can self-assemble through various intermolecular interactions 58
Figure 2.25: Scheme showing peptide folding into β-hairpin structure, driven by different stimuli, and assembly of β-hairpins 62
Figure 2.26: Chemical structure of TSS1 peptide 63
Figure 2.27: Molecular models of nanotube (A) and nanovesicle (B) formed by surfactant-like peptides with negatively charged heads (in red) and glycine tails (in green) 64
Figure 2.28: Schematic representation of self-assembly of peptide-amphiphile upon acidification and intermolecular crosslinking upon oxidation. 64
Figure 2.29: Schematic representation of peptide heptades that adopt α-helical conformation. **a** and **d** positions are usually occupied by apolar residues, whereas other residues are polar65
Figure 2.30: A) SEM pictures of vertically aligned nanotubes of diphenylalanine and B) high-resolution SEM revealed their open-ended structure 66
Figure 2.31: Scheme of EAK16-II self-assembly through hydrophobic interactions and ionic complementarity 67
Figure 2.32: Self-assembly of peptide tapes 68
Figure 2.33: Scheme of self-assembly of EAK16-II 70
Figure 2.34: Scheme of peptide self-assembling into fibrillar network 70
Figure 2.35: Scheme of various conjugation strategies 77
Figure 2.36: Different ways to obtains amine-reactive polymers via: A) dichlorotriazine formation, B) thioimidoester formation, C) aldehyde formation 79

Figure 2.37: Amide bond formation reaction via active sulfo-NHS ester formation.....80
Figure 2.38: Conjugation of poly(NIPAAm-co-NASI) with protein A 80
Figure 2.39: Synthesis of vinyl sulfone end-functionalised PNIPAAm 82
Figure 2.40: Synthesis of maleimide end-functionalised polystyrene 82
Figure 2.41: Synthesis of α,ω-pyridyl disulfide activated Pluronic.....82
Figure 2.42: Oxime formation.....83
Figure 2.43: Synthesis of the PEG modified CCL-5 via oxime formation 83
Figure 2.44: Bioconjugate formation via [3+2] cycloaddition 84
Figure 2.45: Formation of PNIPAAm-streptavidin thermo-responsive nanoparticles 84
Figure 2.46: PNIPAAm polymerisation from streptavidin macroinitiator.....85
Figure 2.47: ATRP polymerisation of NIPAAm from the protein macroinitiator 85
Figure 2.48: Schematic representation of different structures of copolymer PNIPAAm(PLG-co-PLLys) at different pH 87
Figure 2.49: Schematic representation of the self-assembly of polymer-peptide conjugates into β-sheet fibres.....89
Figure 2.50: Design of multi-functionalised polymeric micelles 90
Figure 2.51: Schematic representation of the formation of micelles of Dox-conjugated PEG-b-PD block copolymer.....91
Figure 2.52: Schematic representation of cell encapsulation above the LCST of the PPGMA-co-PEGMA particles 93
Figure 3.1: A Zimm plot using the double extrapolation method 114
Figure 3.2: Schematic representation of the separation process in SEC: A) sample injection, B) size separation, C) elution of large molecules, D) elution of small molecules.....118
Figure 3.3: Schematic representation of a typical oscillatory rheometer with the sample placed between two parallel plates.....120
Figure 3.4: Schematic representation of: (A) the calorimetric block and (B) an experimental vessel of the micro DSC instrument.....121
Figure 3.5: Schematic representation of a transmission electron microscope.....124
Figure 3.6: Principle of AFM.....125
Figure 3.7: Curve of interatomic force versus tip-to-sample distance.....125
Figure 3.8: Schematic representation of the scattering principle.....127
Figure 3.9: Schematic illustration of the contrast matching concept in SANS 132
Figure 3.10: The plots of $(a_{Pep} - Y_{Pep}a_S)^2$, $(a_{Pol} - Y_{Pol}a_S)^2$ and $2(a_{Pep} - Y_{Pep}a_S)(a_{Pol} - Y_{Pol}a_S)$ versus volume fraction of H_2O 134
Figure 3.11: D22 instrument layout.....135
Figure 4.1: Chemical structures of the polymer-peptide conjugates: A) PNIPAAm-FEFEFKFK and B) PNIPAAm-FEFKFEFK.....143
Figure 4.2: ^{1}H NMR spectra of: A) PNIPAAm, B) PS3 and C) FEFEFKFK (DMSO-d_6, 400 MHz) 144
Figure 4.3: Calibration curve for the determination of the monomer/peptide molar ration in the polymer/conjugate mixtures 145
Figure 4.4: ^{1}H NMR spectra of: A) non-purified polymer/conjugate mixture P400FEFEFKFK, B) PNIPAAm and C) conjugate after the purification via centrifugation (DMSO-d_6, 400 MHz) 146
Figure 4.5: A) Second virial coefficient as a function of the weight fraction of PNIPAAm/peptide conjugate in the polymer mixtures. B) Second virial coefficient as a function of the number average molecular weight of the polymers.....149
Figure 4.6: Variation of dynamic viscosity with the concentration of the polymeric products in 1 mM PB at 10ºC.....150
Figure 4.7: Reduced and inherent for the different polymer/conjugate mixtures and for PNIPAAm (P0) as a function of their concentration in 1mM PB at 10°C.....151

Figure 4.8: A) Huggins coefficient as a function of the weight fraction of PNIPAAm-peptide conjugate in the polymer mixtures. B) Huggins coefficient as a function of the number average molecular weight of the polymers. 152
Figure 4.9: Critical gelation concentration (measured with the tilt test on formulations in test tubes) as a function of the weight fraction of PNIPAAm-peptide conjugate in the polymer mixtures 153
Figure 4.10: Strain amplitude sweeps at angular frequency of 1 rad s^{-1} of: A) PS3 and B) PA3 at different concentrations at 20°C. C) Variation of yield strain with polymer/conjugate mixture concentration 155
Figure 4.11: Variation of G' and G" as a function of frequency of: A) PS3 and B) PA3 at different concentrations. Variation of tan δ as a function of angular frequency of: C) PS3 and D) PA3 at different concentrations 156
Figure 4.12: Plateau values of G' as a function of concentration of: A) PS1, PS2, PS3 and FEFEFKFK; B) PA1, PA2, PA, and FEFKFEFK at pH 5.5 159
Figure 4.13: Photographs showing phase behaviour of the polymer/conjugate mixtures at their critical gelation concentrations: A) 1-PS1: 150 mg ml^{-1}, 2-PS2: 50 mg ml^{-1}, 3-PS3: 35 mg ml^{-1} and B) 4-PA1: 190 mg ml^{-1}, 5-PA2: 150 mg ml^{-1}, 6-PA3: 75 mg ml^{-1} at 25ºC, 40ºC and 80ºC 161
Figure 4.14: Micro DSC thermographs of PS3 over a range of concentrations in comparison to pure PNIPAAm during: A) heating from 20 to 80°C and B) cooling from 80 to 20°C ... 162
Figure 4.15: Plots of the LCST transitions (upper) and enthalpies of phase separation (lower) as a function of PNIPAAm (P0) concentration and of polymer concentration in: A) PS1, PS2, PS3 and B) PA1, PA2, PA3 163
Figure 4.16: A) Variation of G' and G" of PS3 at 60 mg ml^{-1}during heating from 20 to 45°C and cooling from 45 to 20°C; B) Variation of G' of PS3 at different concentrations during heating from 20 to 45°C. C) Variation of tan δ of PS3 at 60 mg ml^{-1} with temperature. 164
Figure 4.17: Typical TEM images of: A) PS3 and B) PA3 at concentration of 10 mg ml^{-1}, C) FEFEFKFK at concentration of 1 mg ml^{-1} 166
Figure 4.18: Typical AFM images of: A) PS3 at concentration of 5 mg ml^{-1}, B) PA3 at concentration of 10 mg ml^{-1}, C) PNIPAAm at concentration of 5 mg ml^{-1} and D) FEFEFKFK at concentration of 2 mg ml^{-1} 167
Figure 4.19: Schematic representation of the polymer/conjugate gel. A) Polymer and polymer-peptide conjugate are dissolved in water. B, C) Self-assembly of the conjugates and fibre formation. Free polymers float around the fibrillar network. D) Phase separation due to the collapse of PNIPAAm above the LCST ..... .169
Figure 5.1: Photographs of: A) FEFEFKFK/PS3 gels and B) FEFKFEFK/PA3 gels at the following peptide/(polymer/conjugate mixture) weight ratios: 1) 20-10, 2) 15-10, 3) 10-10, 4) 10-15, 5) 10-20 at 25°C , 40°C and 80°C 176
Figure 5.2: Micro DSC plots of the gels of: A, B) FEFEFKFK/ PS3 and C, D) FEFKFEFK/PA3 at different weight ratios. B) and D) images correspond to the magnifications of the heating region from 55 to 80°C to show the 2nd endothermic transitions. Micro DSC plots for the peptides FEFEFKFK and FEFKFEFK at 20 mg ml^{-1} each are given for comparison 177
Figure 5.3: Plots of the LCST (A, C) and enthalpy (B, D) values versus the weight fraction of polymer and weight fraction of peptide in the gels of FEFEFKFK/PS3 and FEFKFEFK/PA3 178
Figure 5.4: Strain amplitude sweeps of the gels of: A) FEFEFKFK/PS3 and B) FEFKFEFK/PA3 at different peptide/(polymer/conjugate mixture) weight ratios at 20°C. Frequency sweeps of the gels of: C) FEFEFKFK/PS3 and D) FEFKFEFK/PA3 at different peptide/(polymer/conjugate mixture) weight ratios at 20°C. E) Variation of yield strain with peptide concentration. 180
Figure 5.5: Plateau values of G' as a function of peptide concentration of the gels FEFEFKFK/PS3 and FEFKFEFK/PA3 at peptide/(polymer/conjugate mixture) ratios of

20-10, 15-10 and 10-10; and of pure FEFEFKFK and FEFKFEFK gels.....181
Figure 5.6: Variation of G' and G" of the gels: A, B) FEFEFKFK/PS3 (20/10) and C, D) FEFKFEFK/PA3 (20/10) during 1st heating/cooling cycle (A, C) and 2nd heating/cooling cycle (B, D) in the temperature range from 20 to 80°C.....182
Figure 5.7: Photographs of the stable gel of the physical mixture FEFEFKFK/PS3 after 4 consecutive heating/cooling cycles: A) below and B) above the LCST of PNIPAAm.....184
Figure 5.8: Schematic representation of peptide-rich gel obtained by incorporating polymer/conjugate mixture into peptide matrix. A) Peptide and polymer/conjugate mixture are dissolved in water. B, C) Self-assembly and peptide fibre formation. Free polymers float around the fibrillar network. D) Phase separation due to the collapse of PNIPAAm above the LCST 185
Figure 6.1: ^{1}H NMR spectra of : A) PNIPAAm, B) PNIPAAm-FEFEFKFK and C) FEFEFKFK (DMSO-d_6, 400 MHz).....191
Figure 6.2: Gelation and macroscopic phase behaviour of the composite gels: (1) series of 10 mg ml^{-1} of peptide and 2) series of 20 mg ml^{-1} of peptide and various conjugate content at: A) ambient temperature and B) 45ºC.....192
Figure 6.3: A) Absorbance profile of an aqueous solution of the conjugate of 10 mg ml^{-1} and composite gel 20-10 at 500 nm and B) magnification of the composite gel profile 193
Figure 6.4: Micro DSC plots of the composite gel 20-10 during 4 consecutive: A) heating and B) cooling cycles.....194
Figure 6.5: LCST and phase separation enthalpy (ΔH) values for polymer and conjugate aqueous solutions and for the composite gels at peptide concentration of 10 mg ml^{-1} and 20 mg ml^{-1} with various conjugate concentration as a function of polymer concentration...195
Figure 6.6: Strain amplitude sweeps of: A) composite gel series 10-3, 10-5, 10-10 and FEFEFKFK at 10 mg ml^{-1}, B) composite gel series 20-3, 20-5, 20-10 and FEFEFKFK at 20 mg ml^{-1} at 20°C 197
Figure 6.7: Variation of: A) yield strain and B) modulus at the cross-over point of G' and G" profiles with conjugate concentration incorporated into the peptide gels of 10 mg ml^{-1} and 20 mg ml^{-1} 197
Figure 6.8: Frequency sweeps for: A) composite gel series 10-3, 10-5, 10-10 and FEFEFKFK at 10 mg ml^{-1}, B) composite gel series 20-3, 20-5, 20-10 and FEFEFKFK at 20 mg ml^{-1} at 20°C 198
Figure 6.9: A) Variation of G' for the composite gels of peptide at 10 mg ml^{-1}, 20 mg ml^{-1} as a function of conjugate concentration and for the physical mixture of 20 mg ml^{-1} of peptide as a function of polymer concentration. B) Plateau values of G' as a function of peptide concentration in: pure FEFEFKFK, composite gels 10-3, 10-5, 10-10 and composite gels 20-3, 20-5, 20-10.....199
Figure 6.10: Dynamic temperature sweeps for the composite gels: A) 10-3, 10-5, 10-10 and C) 20-3, 20-5, 20-10 during heating from 20 to 80°C. Dynamic temperature sweeps for the composite gels: B) 10-3, 10-5, 10-10 and D) 20-3, 20-5, 20-10 during cooling from 80 to 20°C. Heating rate 1 °C min^{-1}.....201
Figure 6.11: Variation of G' and G" of FEFEFKFK at 20 mg ml^{-1} as a function of temperature 201
Figure 6.12: $I_N(q)$ versus plot of the deuterated PNIPAAm (3 mg ml^{-1}) and the composite gel of protonated peptide (10 mg ml^{-1}) and deuterated PNIPAAm (3 mg ml^{-1}) in D_2O.....203
Figure 6.13: $I_N(q)$ versus q plot for the peptide (10 mg ml^{-1}) in H_2O, D_2O and their mixtures.....203
Figure 6.14: SANS profiles of the two series of the composites gels in D_2O at 25°C. Pure peptide FEFEFKFK at 10 and 20 mg ml^{-1} is given for comparison.....205
Figure 6.15: SANS profiles of the two series of the composites gels in D_2O at 45°C.....206
Figure 6.16: SANS profiles of the two series of the composites gels in the solvent mixture of 58 vol.% H_2O / 42 vol.% D_2O at 25°C.....208

Figure 6.17: SANS profiles of the two series of the composites gels in the solvent mixture of 58 vol.% H_2O / 42 vol.% D_2O at 45°C 209
Figure 6.18: SANS profiles of the composites gel 20-10 in: A) D_2O and B) in the solvent mixture of 58 vol.% H_2O / 42 vol.% D_2O at 25, 45 and 25°C 210
Figure 6.19: Typical TEM images of: A) composite gel 10-3, B) composite gel 20-3 and B) FEFEFKFK at 10 mg ml^{-1}. Gels were diluted to the concentration of 1 mg ml^{-1} of peptide. 210
Figure 6.20: AFM images of the composite gels 10-10 (A - scan size 2 μm^2, D - scan size 0.25 μm^2), 20-10 (B - scan size 2 μm^2, E - scan size 0.25 μm^2), and peptide solution at concentration of 2 mg ml^{-1} (C - scan size 2 μm^2, F - scan size 0.25 μm^2C) on mica at ambient temperature 211
Figure 6.21: Self-assembly scheme 213
Figure 7.1: Variation of: A) G' and B) yield strain with conjugate weight fraction ($W_{conjugate}$) in the gels studied..... 221

LIST OF ABBREVIATIONS AND SYMBOLS

AAm	acrylamide
AAc	acrylic acid
NASI	*N*-acryloyloxysuccinimide
ATRP	atom transfer radical polymerisation
AFM	atomic force microscopy
AIBN	azobisisobutyronitrile
BMA	butylmethacrylate
CIPAAm	carboxyisopropylacrylamide
C^*	critical gelation concentration
DCM	dichloromethane
DSC	differential scanning calorimetry
DIPEA	*N*,*N*-diisopropylethylamine
DMAc	dimethylacetamide
DMAPAAm	*N*,*N*-dimethylaminopropylacrylamide
DMF	*N*,*N*-dimethylformamide
DMSO	dimethylsulfoxide
G'	elastic modulus
Fmoc	fluorenylmethyloxycarbonyl
FRP	free radical polymerisation
GPC	gel permeation chromatography
k_H	Huggins constant
HEMA	2-hydroxyethyl methacrylate
HPMAAm	*N*-(2-hydroxypropyl)methacrylamide
NHS	*N*-hydroxysuccinimide
IgG	immunoglobulin G
NIPAAm	*N*-isopropylacrylamide
k_K	Kraemer constant
LCST	lower critical solution temperature
MPA	3-mercaptopropionic acid
NMP	*N*-methyl-2-pyrrolidone
MVA	*N*-methyl-*N*-vinylacetamide
$\overline{M}_n$	number-average molecular weight
PEG	poly(ethylene glycol)
PLG	poly(L-glutamic acid)
PLLA	poly(L-lactic acid)
PLL	poly(L-lysine)
PPO	polypropylene oxide
^{1}H NMR	proton nuclear magnetic resonance
A_2	second virial coefficient
SANS	small angle neutron scattering
SPPS	solid phase peptide synthesis
SLS	static light scattering
TEM	transmission electron microscopy
R_g	radius of gyration
RP HPLC	reverse phase high performance liquid chromatography
RAFT	reversible addition-fragmentation chain-transfer polymerisation
NtBAAm	*N*-*tert*-butyl acrylamide
TFA	trifluoroacetic acid
VPL	*N*-vinyl-2-pyrrolidinone
G''	viscous modulus
$\overline{M}_w$	weight-average molecular weight

ABSTRACT

Stimuli-responsive polymers and self-assembling peptides represent two classes of materials with interesting properties and great potential to be used as biomaterials. The conjugation of polymer with peptide offers a way to combine the controlled chemical, mechanical, and thermal properties of polymer with the functionality of designed bioactive group. Pure hybrid materials with the characteristics of individual components or systems containing hybrid materials became attractive for applications in drug delivery and tissue engineering.

This work focused on systems where the thermo-responsive properties of a polymer were combined with the gelling properties of two different ionic-complementary peptides via conjugation. The prototypical thermo-responsive polymer poly(*N*-isopropylacrylamide) (PNIPAAm) was chosen due to its lower critical solution temperature (LCST) ~32°C being close to body temperature. Ionic-complementary oligo-peptides, containing the alternating hydrophobic/hydrophilic and charged/uncharged amino acids, phenylalanine (F), glutamic acid (E) and lysine (K), were selected as they are known to form β-sheet rich fibrillar networks at low concentrations. Two peptide sequences with different charge distribution were chosen: FEFEFKFK and FEFKFEFK which form self-supporting gels at ~ 17 and 10 mg ml^{-1} respectively. Polymer-peptide conjugates were used to confer self-assembling and thermo-responsive behaviour to the system.

Thermo-responsive PNIPAAm-rich hydrogels were obtained by targeting different degrees of functionalisation of PNIPAAm with the self-assembling peptides. Two series of such systems were prepared by using either a thiol-modified FEFEFKFK or a thiol-modified FEFKFEFK peptide as the chain-transfer agent in the free radical polymerisation of NIPAAm. The resulting polymer/conjugate mixtures were studied by proton nuclear magnetic resonance (^{1}H NMR). The polymer/conjugate ratios were calculated and showed that the conjugate fraction in the mixtures increased with increasing concentration of peptide used for the polymerisation. Static light scattering (SLS) and viscometry showed the aggregation of the polymer/conjugate mixtures presumably due to the presence of peptide. The $\overline{M}_n$ values from gel permeation chromatography (GPC), which were mostly attributed to the unconjugated polymers, were higher than those obtained from ^{1}H NMR and centrifugation for the conjugates. The polymer/conjugate mixtures formed self-supporting gels where the critical gelation concentration decreased with increasing conjugate content. Oscillatory rheology experiments confirmed gels had formed and revealed that their elastic modulus, G' varied from ~ 10 to 400 Pa depending on the sample. TEM and AFM studies proved the formation of β-sheet fibres of ~ 4.5 ± 1.5 nm in diameter. The PNIPAAm-rich hydrogels were also characterised by micro DSC to reveal their thermo-responsiveness and phase separation and showed the LCST at ~ 30°C. The results of the study showed that varying the peptide sequence did not have an effect on thermal, mechanical or morphological properties of the hydrogels. By exploiting the self-assembly of the ionic-complementary peptides, it was possible to create PNIPAAm-rich, thermo-responsive hydrogels with controllable properties.

Further in the study pure PNIPAAm-FEFEFKFK conjugate was incorporated into the FEFEFKFK peptide matrix to create peptide-rich thermo-responsive composite gels. Two series of the composite gels were prepared by varying separately the peptide matrix and polymer-peptide conjugate concentration. Micro DSC measurements revealed an endothermic peak at ~ 30ºC characteristic of the LCST of PNIPAAm. Oscillatory rheology studies showed that the composite gels became stronger with increasing conjugate concentration (G' ~ 20 – 200 Pa). Network morphology was studied by SANS. Using contrast variation and contrast matching techniques it was possible to distinguish between the peptide fibres and the PNIPAAm chains. Below and above the LCST the scattering curves showed a q^{-1} behaviour which is typical of rod-like objects. TEM and AFM also proved the formation of fibres of ~4.0 ± 0.8 nm and ~4.5 ± 1 nm respectively. AFM studies showed that the fibres of the composite gels were decorated with polymer chains. The thermo-responsiveness and the gelation properties of these conjugate-based scaffolds have potential for use as drug delivery vehicles or tissue engineering scaffolds.

Keywords: poly(*N*-isopropylacrylamide), stimuli-responsive polymer, LCST, peptide, β-sheet fibre, self-assembly, hydrogel, polymer-peptide conjugate.

DECLARATION

No portion of the work referred to in the thesis has been submitted in support of an application for another degree or qualification of this or any other university or other institute of learning.

COPYRIGHT STATEMENT

i. The author of this thesis (including any appendices and/or schedules to this thesis) owns certain copyright or related rights in it (the "Copyright") and s/he has given The University of Manchester certain rights to use such Copyright, including for administrative purposes.

ii. Copies of this thesis, either in full or in extracts and whether in hard or electronic copy, may be made **only** in accordance with the Copyright, Designs and Patents Act 1988 (as amended) and regulations issued under it or, where appropriate, in accordance with licensing agreements which the University has from time to time. This page must form part of any such copies made.

iii. The ownership of certain Copyright, patents, designs, trade marks and other intellectual property (the "Intellectual Property") and any reproductions of copyright works in the thesis, for example graphs and tables ("Reproductions"), which may be described in this thesis, may not be owned by the author and may be owned by third parties. Such Intellectual Property and Reproductions cannot and must not be made available for use without the prior written permission of the owner(s) of the relevant Intellectual Property and/or Reproductions.

iv. Further information on the conditions under which disclosure, publication and commercialisation of this thesis, the Copyright and any Intellectual Property and/or Reproductions described in it may take place is available in the University IP Policy (see http://www.campus.manchester.ac.uk/medialibrary/policies/intellectual-property.pdf), in any relevant Thesis restriction declarations deposited in the University Library, The University Library's regulations (see http://www.manchester.ac.uk/library/aboutus/regulations) and in The University's policy on presentation of Theses.

ACKNOWLEDGEMENTS

I would like to express my gratitude to my supervisors Dr Aline F. Miller and Dr Alberto Saiani for the opportunity to pursue science in the Polymers and Peptides Research Group in Manchester Interdisciplinary Biocentre at The University of Manchester. I would also like to thank my supervisors for their support, guidance, fruitful discussions, patience, and encouragement throughout my PhD.

I would like to thank Marie Curie Early Stage Research Training that enabled to fund this research project and the attendance of various seminars and conferences.

My separate gratitude goes to Prof. Nicola Tirelli for the possibility to use the facilities in his laboratory in the School of Pharmacy at The University of Manchester. I also thank Prof. Nicola Tirelli for his time, help, ideas and l'accueil chaleureux.

I would like to thank other members of the Polymer and Peptide Research Group for being always helpful, supportive and nice. I thank also my friends in Latvia and here in Manchester for their advice and patience, especially Cat "Le Bouffon" and Jelena Chobotova.

I would also like to acknowledge Dr Nigel Hodson for his help with AFM imaging, Ms Polly Crook for the help with the experiments in the School of Materials, Dr Isabelle Grillo for the help with SANS experiments in ILL (Grenoble, France), Mr Keith Nixon for his help with GPC analysis.

Finally, I would like to thank my parents and my family for their constant support and encouragement.

THE AUTHOR

Antons Maslovskis graduated from The University of Latvia (Riga) with the BSc in Chemistry in 2005 and the MSc in Chemistry in 2007. He was awarded a scholarship from the French association "Le Pont Neuf" to undertake a one-year research project in Paris (France) leading to the award of a Master's degree in Fundamental and Applied Chemistry, Polymer Materials at the 6th University of Paris (Université Pierre et Marie Curie) in 2007.

He started his PhD research at The University of Manchester, School of Chemical Engineering and Analytical Science in September 2007 under the supervision of Dr Aline F. Miller. The project focused on the design and characterisation of new family of thermo-responsive hydrogels that would possess both characteristics of the gelling peptide and the thermo-responsive poly(*N*-isopropylacrylamide) (PNIPAAm). The research work is described in this thesis and also parts of this work have been accepted for publication in *Macromolecular Symposia* and are being prepared for submission to *Soft Matter* and *Langmuir*.

The results of this research have been also presented on a number of national and international conferences. The oral contribution were given at the European Polymer Congress in Graz, Austria (12-17 July 2009), at the 22nd European Conference on Biomaterials in Lausanne, Switzerland (7-11 September 2009), as well as at the Hydrogels '09 Meeting in Manchester, UK (22-23 September 2009). Posters were presented at various conferences such as MRS Spring 2010 Meeting in San Francisco, USA (5-9 April 2010), Macro Group Young Researchers Meeting in Nottingham, UK (29-30 April 2010) and the 43rd IUPAC World Polymer Congress Macro2010 in Glasgow, UK (11-16 July 2010).

To my family

The gem cannot be polished without friction,
nor man perfected without trials.

Chinese proverb

Chapter 1

General Introduction

Hydrogels are widely used in the biomedical and pharmaceutical fields due to their similarity to hydrated body tissues. They can be obtained either via polymerisation or copolymerisation using chemical cross-linking agents to create covalent bonds, or via the self-assembly of small molecules where three-dimensional structure is obtained via physical interactions or entanglement. The structure and mechanical properties of such materials can be tuned simply by varying the chemistry of the initial monomer, cross-linking agent and/or the self-assembling building block.

Self-assembling materials possess amphiphilic nature as they contain both hydrophobic and hydrophilic segments. Amphiphilic molecules are lipids, block copolymers, proteins and peptides. Self-assembly of various peptide sequences gives various nanostructures such as β-sheets, β-hairpins, α-helices that form higher level hierarchical structures which can mimic the native extracellular matrix. Ionic-complementary peptides are one class of peptides that form gels composed of interwoven β-sheet fibres. Self-assembling peptide hydrogels have already been successfully employed in different areas of biomedical applications such as scaffolds for tissue regeneration and controlled drug delivery. Peptide scaffolds are successful because they are highly biocompatible, biodegradable, possess good mechanical properties, and various biological functionality can be introduced that are important for successful cell adhesion, proliferation and differentiation.

Stimuli-responsive materials are studied widely due to their potential applications in controlled drug delivery, tissue engineering, separation technologies and biosensors. External stimuli fall into three categories: physical (temperature, ionic strength, solvent), chemical (pH, salt effect), and biochemical (reaction to enzyme). They can be used solely or can be combined to expand the versatility and application of the system. Under the influence of these cues stimuli-responsive materials change their characteristic properties, such as solubility or conformation, they undergo self-assembly or phase separation. Normally these transformations are reversible when the stimulus is removed.

Typically a polymer confers the responsiveness to the system. Depending on the monomer nature, different types of stimuli-responsive materials can be obtained. Thermo-responsive polymers are the most widely studied and the typical representative is poly(*N*-isopropylacrylamide) (PNIPAAm) whose aqueous solution possesses the lower critical solution temperature (LCST) close to the temperature of body fluid (~ 32°C). At the LCST the polymer undergoes a sharp coil-to-globule transition resulting in the dispersion of the collapsed and aggregated polymer chains in water. The LCST of PNIPAAm can be controlled by a variety of external stimuli such as solvent, ionic strength, surfactant, but most importantly

the LCST can be increased or decreased by using hydrophilic or hydrophobic co-monomers respectively.

Self-assembling peptide systems can also be considered as stimuli-responsive materials, as the gelation (sol-to-gel transition), conformational changes can be triggered by various environmental stimuli, such as pH, ionic strength and enzyme. For some peptide systems temperature is another stimulus to trigger the gelation but for others, only gel melting is observed upon heating. Also the peptides with the LCST behaviour were reported. For example, short elastin-like peptides based on GVGVP (G – glycine, V – valine, P - proline) sequence exhibited the LCST behaviour in water, however the LCST values were very high, i.e. ~100-200°C.

Little attention has been paid to self-assembling peptide systems with thermo-responsive behaviour similar to that of thermo-responsive polymers. One strategy to obtain thermo-responsive gels is to use thermo-responsive polymers, such as PNIPAAm. The polymer can be conjugated to the peptide and the peptide will confer hierarchical self-assembly to the system. Peptide hybrid materials or conjugates of peptides and polymers represent a class of materials with interesting properties. Such systems are attractive for biomaterials applications as they combine the controlled chemical, mechanical, and thermal properties of a polymer with the structural properties and functionality of a peptide. One other strategy consists of introducing thermo-responsive micelles, nanoparticles into a non-thermo-responsive gel matrix or into already thermo-responsive gel to accentuate its thermo-responsiveness and to improve gel network swelling/shrinking and gel mechanical properties. The possibility to combine the properties of polymer with those of peptide influenced the choice of the strategy of conjugation.

This research work focuses on the combination of two synthetic components: ionic-complementary peptide and thermo-responsive polymer via conjugation. Two ionic complementary octapeptides containing alternating hydrophobic/hydrophilic and charged/uncharged amino acids of phenylalanine (F), glutamic acid (E) and lysine (K), i.e. FEFEFKFK and FEFKFEFK were selected for the study. The peptides FEFEFKFK and FEFKFEFK are known to form a β-sheet rich fibrillar network at considerably low concentrations: ~17 mg ml^{-1} and 10 mg ml^{-1} respectively. PNIPAAm has been chosen as the thermo-responsive polymer due to its sharp and reversible phase separation upon heating.

The general purpose of the current research work is to combine the thermo-responsive behaviour of PNIPAAm with the gelling properties of FEFEFKFK and FEFKFEFK peptides by synthesising bioconjugates of PNIPAAm-peptide and to use these conjugates to confer self-assembling and thermo-responsive behaviour to the system. Polymer and peptide

conjugation is possible by using a sulfhydryl end-functionalised peptide as the chain-transfer agent in the free radical polymerisation of NIPAAm. Two main aims are defined for the research. The first aim is to create PNIPAAm-rich gels by doping in different quantities of PNIPAAm-peptide conjugates. It is postulated that the peptide segments will retain their self-assembling behaviour after conjugation and will form the β-sheet fibres decorated with PNIPAAm chains once dissolved in water. The effect of the peptide sequence on the self-assembly and gel properties is also explored. The gelling, mechanical and thermo-responsive properties and results correlated to gel morphology will be probed using various techniques. The second aim is to create thermo-responsive peptide-rich composite gels by incorporating pure polymer-peptide conjugate into a peptide matrix which does not exhibit a phase separation similar to that of PNIPAAm. It is postulated that the conjugate will incorporate into the peptide fibres and confer its thermo-responsiveness to the gel. This research aims to reveal thermo-responsive behaviour of the composite gels, to understand how the conjugate behaves in the gel network upon heating and cooling, to reveal fibre morphology and how the incorporation of the conjugate into gel matrix influences the overall mechanical properties of the composite gel.

The overall structure of the study takes the form of seven chapters, including this introductory Chapter 1. Chapter 2 reviews the literature concerning the four key themes: the thermo-responsive polymer PNIPAAm; theory on different types of amino acids, peptide structures and peptide synthesis; peptide self-assembly, and the application of self-assembling peptide materials and finally, various methods to obtain polymer-peptide conjugates and their application. Chapter 3 focuses on the experimental procedures and methodologies employed in this study. Some theoretical principles of each experimental technique employed are also discussed here. Chapters 4, 5 and 6 present the research findings and include a discussion of the results. Three chapters study polymer/conjugate based systems. Chapter 4 outlines the synthesis route for thermo-responsive polymers with different degrees of peptide functionalisation leading to control over the gelation properties of PNIPAAm. The products prepared contain pure polymer and controllable quantities of PNIPAAm-FEFEFKFK or PNIPAAm-FEFKFEFK conjugate. In all samples in this chapter the free polymer concentration is much higher than conjugate concentration. These polymer/conjugate mixtures are characterised by various methods to reveal their structural properties and thermal phase behaviour. Chapter 5 focuses on a range of samples made up of pure FEFEFKFK and FEFKFEFK peptide mixed with the pure polymer and polymer-conjugate mixtures obtained in Chapter 4. In this study peptide concentration is greater than polymer (free and conjugated) concentration. In Chapter 6 small quantities of purified polymer-peptide conjugate are added

to pure peptide. In this case the peptide content is higher than conjugated polymer content. General conclusions from the work are presented in Chapter 7 along with some recommendations for future work.

Chapter 2

Literature Review

The overall structure of the literature review takes the form of four sections. Section 1 introduces responsive polymers and looks closer at the properties of the prototypical thermo-responsive polymer poly(*N*-isopropylacrylamide) (PNIPAAm). Section 2 focuses on the peptides. General information about amino acid types, peptide bond formation, and peptide structure will be given initially. Then the solid phase peptide synthesis possibilities using Fmoc protocol will be discussed. Section 3 describes the self-assembly behaviour of the peptides and the applications of self-assembling materials in tissue engineering and controlled drug delivery. Finally, section 4 presents recent achievements on the synthetic routes to conjugate a polymer with a peptide and some examples of conjugates applications will be given there. There is a significant body of research focused on the thermo-responsive polymers, self-assembling peptides and polymer-peptide conjugates. Only the most salient points will be covered here.

2.1. TEMPERATURE-RESPONSIVE POLYMER: POLY(*N*-ISOPROPYLACRYLAMIDE)

2.1.1. Introduction

Stimuli-responsive polymers have become very popular recently due to their various properties and potential applications. These polymers are classified as polymers that change their characteristic properties due to changes in their environment. They are also known as "smart" or "intelligent" polymers. The stimuli that influence their properties fall into three categories: physical (temperature, ionic strength, solvent), chemical (pH, salt effect), and biochemical (reaction to enzyme). Doubly sensitive polymers also exist, where polymers change their properties during the application of two stimuli, for example, temperature and pH. Under the influence of various stimuli, responsive and doubly responsive polymers change their conformation, solubility, surface characteristics and undergo self-assembly. Normally these transformations are reversible when the stimulus is removed [1, 2].

Thermo-responsive polymers are the most widely studied. They undergo a phase separation in aqueous solution upon heating. The conformation of a macromolecule in solution is determined by polymer-solvent and polymer-polymer interactions. The polymer-solvent interactions are predominant in a good solvent, where solvent molecules open the chain to a random coil conformation. In this conformation the interactions between polymer segments are minimised. The polymer segments start to aggregate when the quality of the solvent decreases and polymer-polymer interactions become predominant. Subsequently in a poor solvent the formation of a globule containing collapsed chains is observed. This

transition is called coil-to-globule transition and the temperature at which this transition occurs is called the lower critical solution temperature (LCST) or cloud point (CP) [3].

Materials based on thermo-responsive polymers have become very popular during the last 30 years owing to their application in cell encapsulation [4], drug delivery [4, 5], and tissue engineering scaffolding [6, 7]. The reviews of Taylor and Cerankowski [8], Galaev *et al.* [9] and Saunders *et al.* [10] introduce a great variety of polymers that exhibit LCST behaviour upon heating. The majority of thermo-responsive polymers belong to three main groups of polymers:

- poly(*N*-substituted (meth)acrylamides), for example, the LCST of poly(*N*-ethylacrylamide) is 74°C and of poly(*N*-ethylmethacrylamide) is 58°C [8]
- poly(*N*-vinyl-*N*,*N*-disubstituted amides), such as poly(*N*-vinyl caprolactam) with LCST of 31°C and atactic poly(vinyl methyl ether) with LCST of 34°C [11]
- ethylene oxide-containing polymers

Polymers with amide functional groups form the largest class of thermo-responsive polymers. Poly(*N*-isopropylacrylamide) (PNIPAAm) is the typical representative which has been employed in many studies due to its sharp phase separation in aqueous solution at temperatures close to body temperature. Its chemical structure is given in Fig. 2.1.

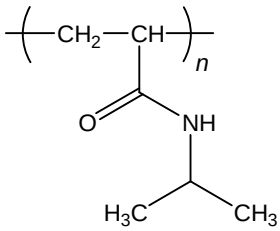

Figure 2.1: *Chemical structure of PNIPAAm (n – polymerisation index)*

There are several literature reviews [3, 12, 13] that describe the properties and application of this polymer in great detail. One of the most comprehensive is the review of H.G. Schild published in 1992 [12].

2.1.2. Single chain PNIPAAm synthesis

PNIPAAm can be obtained by different polymerisation methods including free radical polymerisation (FRP) [12, 14-16], atom transfer radical polymerisation (ATRP) [17-21], and reversible addition-fragmentation chain-transfer polymerisation (RAFT) [22-25]. There are also examples of PNIPAAm obtained by redox polymerisation [26-28]. Living polymerisation techniques offer an array of advantages in comparison with traditional chain polymerisation; they allow the reactions to be carried out in a controlled way, giving polymers with a low

polydispersity, predetermined molecular weight and the controlled introduction of functional groups [25, 29].

The reviews of Schild [12] and Dimitrov *et al.* [13] give further insight into the different polymerisation routes to prepare PNIPAAm. The following section will describe the synthesis of PNIPAAm via free radical polymerisation as this method has been employed in this research work.

2.1.2.1. Free radical polymerisation (FRP) of NIPAAm

Different organic solvents and initiators can be used in FRP and this can affect the molecular weight and molecular weight distribution of the polymer chains [30].

For the synthesis of PNIPAAm and its copolymers, FRP usually gives high polydispersity indices (PDI = 1.5, if chains are terminated by combination of two radicals and PDI = 2, if chains are terminated via disproportionation or chain-transfer) and poorly defined end-group chemistries [31]. Every FRP reaction consists of three stages: initiation, propagation and termination and each of these is outlined below [32].

Initiation. Two radicals are formed under the thermal decomposition of organic peroxides or azo compounds. Fig. 2.2 shows the homolytic scission of azo (-N=N-) linkage of 2,2'-azobisisobutyronitrile (AIBN) upon heating.

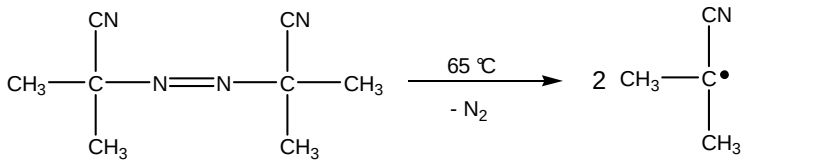

Figure 2.2: *Homolytical decomposition of AIBN*

Each radical attacks the π-bond of a NIPAAm monomer, thus creating an active centre and initiating the reaction (Fig. 2.3).

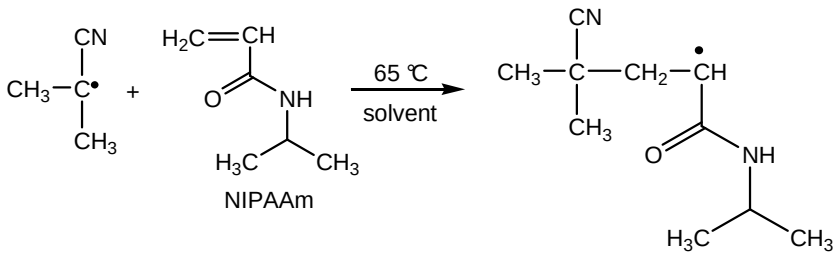

Figure 2.3: *a-Cyanoalkyl radical attack of monomer double bond*

Propagation. The propagation step involves growth of the polymer chain by rapid sequential addition of monomer to the active centre (Fig. 2.4).

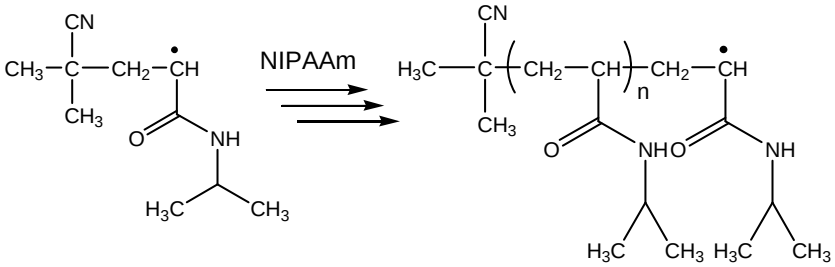

Figure 2.4: *PNIPAAm macromolecular chain growth*

Termination. Finally, growth of the polymer chain is terminated. There are two common mechanisms of termination that involve bimolecular reaction of growing polymer chains: combination and disproportionation. During combination, two growing chains couple together to form a single polymer molecule with initiator fragments at both ends (Fig 2.5).

Figure 2.5: *Termination of macromolecular chains via combination*

During disproportionation, a hydrogen atom can be abstracted from one growing chain by another, hence two polymer molecules with initiator fragments at one end are formed (Fig. 2.6). Polymer chains with unsaturated end groups can undergo further reactions.

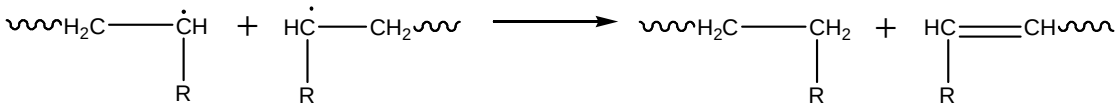

Figure 2.6: *Termination of macromolecular chains via disproportionation*

Radical reaction with oxygen. Carbon-centered radicals can react with oxygen, thus deactivating the radicals and forming unwanted products. After the reaction of oxygen with an α-cyanoalkyl radical (Fig 2.7A), an alkylperoxy radical (Fig 2.7B) can form, which may initiate polymerisation and thus form a relatively unstable peroxidic end group (Fig. 2.7C).

The hydroperoxy radical (Fig. 2.7B) has a tendency to abstract hydrogen from the polymer, monomer, or other components in the reaction media forming a potentially reactive hydroperixide (Fig. 2.7D) and a new radical (R·) which may initiate further polymerisation.

The process can become more complicated when the species (C) and (D) undergo homolysis under polymerisation conditions. In addition, the peroxides derived from (C) and (D) may act as chain-transfer agents (CTA) [32]. To minimise these reactions, all dissolved gases should be removed from solvents prior to polymerisation.

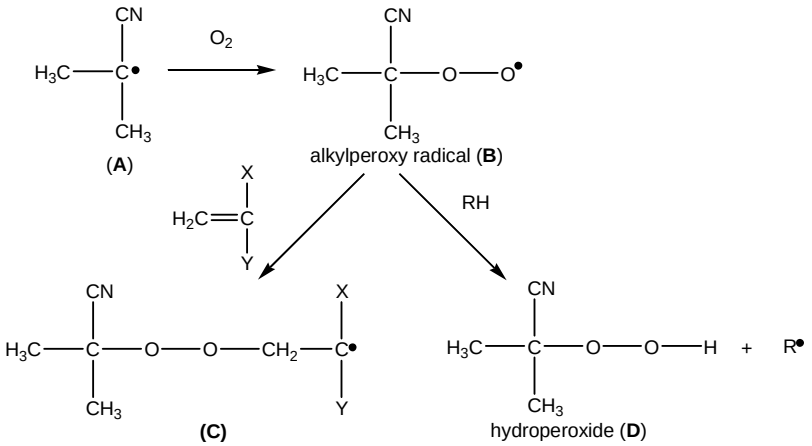

Figure 2.7: *Inactivation of active radicals with oxygen*

Chain-transfer. It is well known that the use of a CTA allows the synthesis of polymers with well-defined functional end-groups. One of the CTAs used widely in FRP of NIPAAm is 3-mercaptopropionic acid (MPA) [16, 33, 34]. This enables the synthesis of PNIPAAm with functional carboxylic groups which are then used to link PNIPAAm to different biomolecules. Normally, high CTA concentrations allow short chain oligomers to be synthesised.

The general scheme of chain-transfer reaction of MPA is given in Fig. 2.8 [16]. One initiator molecule creates two active radicals that initiate the polymerisation reaction of monomer. Some of these growing chains become terminated and this way free polymer chains are created, but some of them abstract a hydrogen atom from the chain-transfer agent molecule thus transferring the active centre to it. Then the polymer chains functionalised with the CTA propagate. The reaction is terminated by adding the hydrogen atom from CTA.

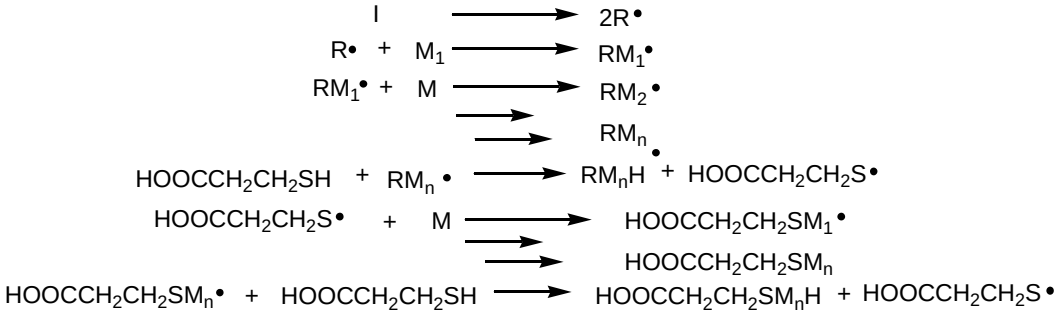

Figure 2.8: *Chain-transfer reaction using 3-mercaptopropionic acid*

Typically the polydispersity indices (PDI) of end-functionalised PNIPAAm obtained through this type of chain-transfer varies from 1.20 to 1.50 indicating a fairly narrow polydispersity.

2.1.3. PNIPAAm behaviour in aqueous solution

2.1.3.1. LCST phenomenon

Many polymers exhibit a lower critical solution phenomenon where their solubility increases with decreasing temperature, and vice versa. The temperature at which this phase transition occurs is called the LCST [35].

In 1967 Scarpa *et al.* [36] reported such a phase separation of a 2% aqueous solution of PNIPAAm at 31°C. This phase separation was reversible upon cooling. Heskins and Guillet [37] reported the same phenomenon in 1968 and this paper is cited more often. In both studies the macroscopic phase separation of an aqueous solution of PNIPAAm was observed visually. Below the LCST the solution was transparent and above the LCST it became cloudy. This is an easy way of determining the LCST of the polymer solution [12].

Below the LCST in dilute aqueous solution, PNIPAAm chains form extended coils that are isolated and flexible because the polymer chains are hydrated and the intermolecular hydrogen bonds between the polymer carbonyl, polar amide groups and water molecules are formed (Fig. 2.9) [12].

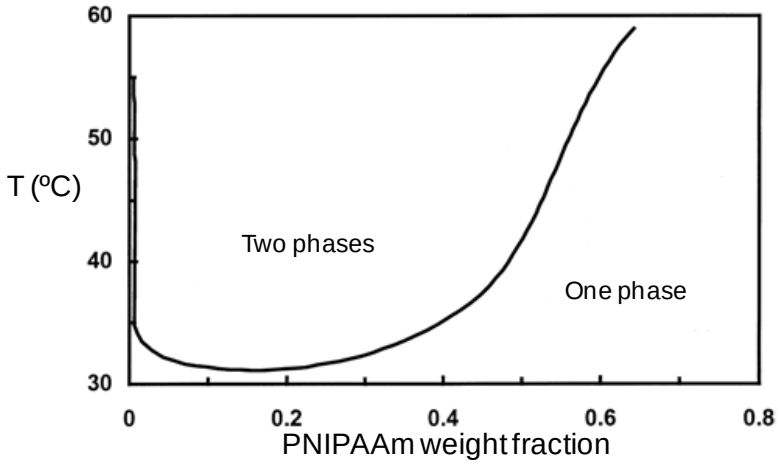

Figure 2.9: *Phase diagram of an aqueous solution of PNIPAAm [37]. Below the LCST one phase exists when polymer is hydrophilic and adopts coil conformation. Above the LCST, coil-to-globule transition occurs and 2 phases are formed.*

Thermo micro-attenuated total reflection Fourier transform infrared (ATR FT-IR) spectroscopy proved the formation of intermolecular hydrogen bonding between PNIPAAm and water [38]. At and above the LCST, these hydrogen bonds broke, bound water was expelled and hydrophobic interactions between hydrophobic polymer segments were strengthened. ATR FT-IR revealed that above the LCST intramolecular hydrogen bonding were predominant. In fact, the hydrophobic interaction of the methyl groups of PNIPAAm increased 1.5 times when the temperature was above the LCST [38]. When this happened, water switched from being a good solvent to a poor solvent. As a result, polymer chains

collapsed and then aggregated. This resulted in the formation of a second phase that was suspended in a water-rich phase.

The reason for the phase separation is purely thermodynamic and can be explained with the Gibbs free energy equation: $\Delta G_{mix} = \Delta H_{mix} - T \times \Delta S_{mix}$ where ΔG_{mix}, ΔH_{mix} and ΔS_{mix} are the Gibbs free energy, enthalpy and entropy of mixing respectively and T is temperature. A polymer is soluble in a solvent when $\Delta G_{mix} < 0$ (favourable free energy) which can be achieved when $\Delta S_{mix} > 0$ and $\Delta H_{mix} < 0$. Negative ΔH_{mix} is facilitated by hydrogen bond interactions and ordered ("ice-like") structure of water around polymer chains. When the temperature increases above the LCST, hydrogen bonds start to break, polymer-polymer interactions become predominant and phase separation occurs resulting in unfavourable ΔG_{mix} ($\Delta G_{mix} > 0$). Above the LCST the entropic term becomes predominant and a positive ΔG_{mix} can be obtained when the magnitude of ΔH_{mix} ($|\Delta H_{mix}|$) becomes smaller than $|T \times \Delta S_{mix}|$ [12].

Linear and grafted PNIPAAm chains behave differently in the same conditions. PNIPAAm grafting is possible after the introduction of functional groups, such as carboxyl groups, into its structure. These groups can be introduced terminally or into the polymer chains during the copolymerisation with acrylic acid (AAc). Carboxyl groups allow polymer attachment to different biomolecules and surfaces to create different bioconjugates and terminally grafted or multi-point grafted surfaces [39]. Fig. 2.10 illustrates the phase behaviour of linear and grafted PNIPAAm chains.

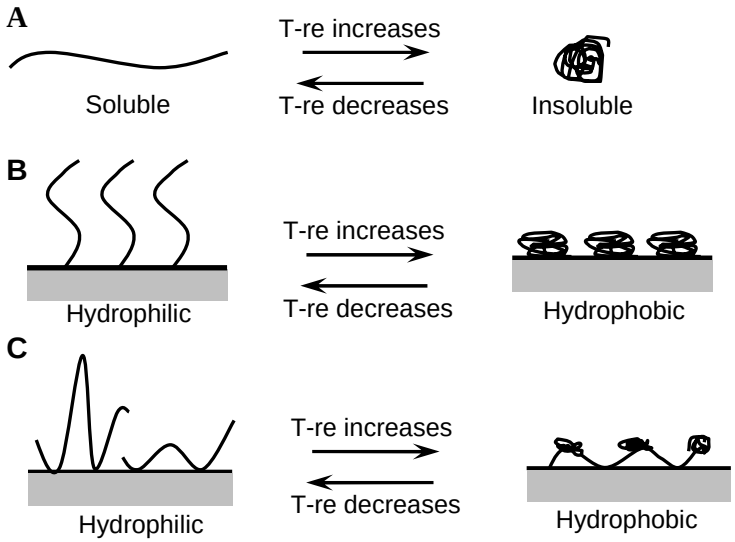

Figure 2.10: *Schematic representation of the reversible phase separation of PNIPAAm: A) linear chains, B) terminally-grafted PNIPAAm surfaces, and C) multi-point grafted PNIPAAm surfaces (adapted from [39])*

In Fig. 2.10A linear chains collapse and aggregate freely above the LCST. Therefore linear chains have a sharp phase transition. Fig. 2.10B shows terminally grafted polymers. Above the LCST the chains collapse and remain on the surface. In the multi-point grafted surfaces the short polymer chain loops between the grafted points will collapse upon heating (Fig. 2.10C). These surfaces are less hydrophobic above the LCST than terminally grafted surfaces due to terminal carboxyl groups that can form hydrogen bonding with water [39].

2.1.3.2. LCST characterisation methods

There are a number of methods that can be used to study the LCST phenomenon. Optical and UV turbidimetric techniques are typically used to determine the LCST value [40-42]. Differential scanning calorimetry (DSC) measures both the LCST and the enthalpy of the phase transition [43-46]. Light scattering, viscometry, and fluorescence provide information on polymer chain conformation, chain interaction and environment around chains below and above the LCST [42, 47-50]. Infrared spectroscopy (IR) provides information on inter- and intramolecular interactions between functional groups below and above the LCST accordingly [38]. ^{1}H NMR has also been used to study the conformational changes of PNIPAAm in aqueous solution upon heating and cooling [51, 52]. Nevertheless, the most common methods for determination and observation of the phase separation in aqueous solutions of PNIPAAm are optical or UV turbidimetric methods and micro-DSC.

In UV and optical turbidimetric measurements the term "cloud point" is commonly used and is the temperature at which the opaqueness of the solution appears [53]. Fig. 2.11A gives an example of a cloud point curve measured by turbidimetric method at 500 nm. Cloud point techniques are sensitive to the macroscopic phase separation phenomenon which is a slow process at very low PNIPAAm concentrations [53].

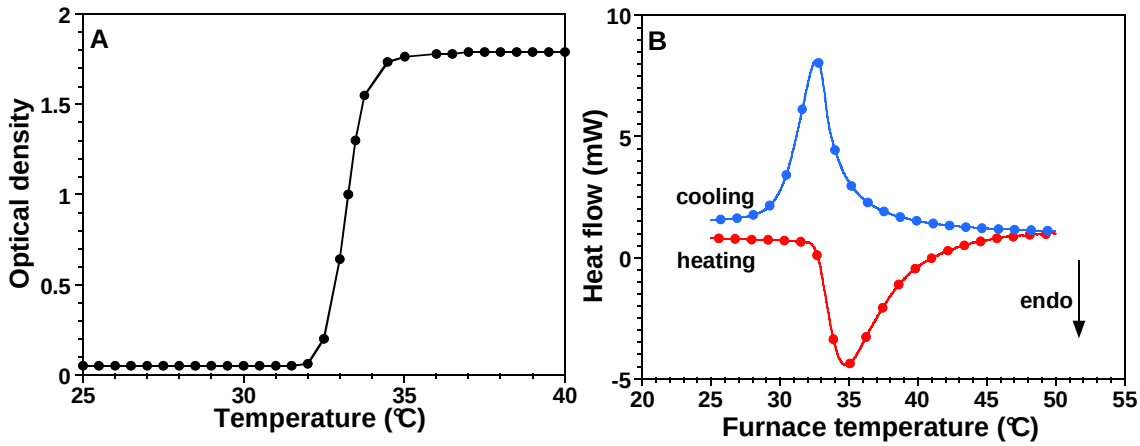

Figure 2.11: *Cloud point (A) and differential scanning calorimetry (DSC) (B) measurements of the LCST of aqueous solution of PNIPAAm*

DSC determines the LCST and measures the heat associated with the hydrogen bonding breakage, which is the first stage of the phase separation process upon heating [53]. It is known that when phase separation occurs the macromolecular chains aggregate into larger aggregates that are sustained by intramolecular hydrogen bonding and non-polar interactions [38]. Heskins and Guillet [37] were the first to report the LCST of PNIPAAm. They reported that the heats associated with the transition had an endothermic effect and that the heats varied with concentration. Such heats were ascribed to the energy necessary to break the hydrogen bonds that formed between the polymer and water. Typical DSC plots for the aqueous solution of PNIPAAm are given in Fig. 2.11B. The transition is reversible upon cooling. Schild and Tirrell [46] showed that the values of the phase transition in DSC correlate with those observed in the cloud point experiments.

2.1.3.3. Polymer chain conformation studies with light scattering and fluorescence

Light scattering. It is possible to determine the shape, size and orientation of macromolecules using light scattering [54, 55]. Heskins and Guillet [37] observed that the apparent molecular weight increased 4.5 times when heating a PNIPAAm solution from 25 to 33°C. They proposed that collapsed polymer chains start to aggregate. Dynamic and static light scattering techniques were used to detect a coil-to-globule transition. Intramolecular polymer-polymer bonds, that form at the LCST, govern the collapse of the polymer chains consequently forms a hard sphere, i.e., globule [55].

Hirotsu *et al.* [47] studied a dilute solution of PNIPAAm ($\overline{M}_w$ ~ 1.3×10^6 g mol^{-1}) and observed a coil-globule transition of a single polymer chain at 34.1°C. The hydrodynamic radius was observed to decrease sharply from 1000 to 600 Å upon an increase in temperature.

Hirotsu *et al.* [47] and Fujishige *et al.* [56] suggested a mechanism for the LCST behaviour based on the results from quasi-elastic light scattering (QELS). Initially, a single polymer chain will collapse, because water-polymer hydrogen bondings become less favourable than polymer-polymer and water-water interactions. Secondly, the collapsed polymer chains will aggregate, because PNIPAAm macromolecular chain units interact with the nearest units of the same macromolecule. These findings correlate well with the previous concepts about the LCST transition.

Fujishige [57] studied PNIPAAm solutions below the LCST using light scattering in conjunction with viscosimetry. Results showed that water is a good solvent for PNIPAAm and its statistical segment takes a more extended form in water than in THF, as water is a better solvent than THF. Similar results were obtained by Chiantore *et al.* [30]. They observed

that PNIPAAm chains behave as normal flexible chains in methanol, while the structure is more extended in aqueous solution and becomes subsequently unstable upon heating.

Fluorescence. Fluorescence enables the changes in PNIPAAm chain mobility and the degree of coil compaction to be monitored as a function of temperature [58]. Winnik [59-61] widely studied fluorescently-labelled PNIPAAm to determine different properties of the polymer such as polarity and mobility and confirmed that solvated coils of PNIPAAm shrink upon heating into a collapsed state and these subsequently aggregate to form larger particles. Swanson *et al.* [58] also studied fluorescently-labelled samples and observed similar conformational changes from open coil below the LCST to the compact globular structure above the LCST.

2.1.4. Factors that influence the LCST

The LCST of the aqueous solution of PNIPAAm is influenced by salts [46, 62], surfactants [62, 63] and comonomers [64, 65]. As mentioned previously, polymer behaviour in solution depends on the interactions between its segments and water molecules. The additives such as surfactants and salts bind to the polymer or change the water structure around it. Also the hydrophilic comonomers increase the LCST, whereas the hydrohpobic comonomers decrease it. Here the effect of polymer molecular weight, copolymerisation, and various additives on the LCST will be described.

2.1.4.1. Polymer molecular weight

Fujishige and coworkers [56] stated that the LCST of PNIPAAm was not affected by either the molecular weight of the polymer within the range of 5×10^4 to 840×10^4 g mol^{-1} or by its concentration (0.01 to 1 wt.%). However, there is some evidence that is in conflict with this belief [44, 46, 66-68].

It has been reported that the molecular weight of PNIPAAm affects the phase transition both inversely [46, 66] and directly [67, 68]. Table 2.1 demonstrates the inverse dependence of the LCST on molecular weight of PNIPAAm. This conflicting behaviour may be due to the polydispersity of the polymer, different initiators or chain-transfer agents used in the synthesis of PNIPAAm.

Table 2.1: *PNIPAAm molecular weight effect on the LCST [46]*

$\overline{M}_n$, g mol^{-1}	$\overline{M}_w / \overline{M}_n$	LCST, °C
5,400	2.3	34.3
11,000	6.9	34.2
13,000	1.2	32.6
160,000	2.8	32.2
300,000		31.8

The majority of the research to date has been done on linear PNIPAAm. Winnik *et al.* [69] studied the behaviour of cyclic PNIPAAm as a function of temperature. This polymer was obtained through ring closure of a α,ω-heterodifunctional telechelic PNIPAAm precursor. The phase transitions of linear precursors have been compared with the phase transitions of cyclic polymers with the same molecular weight of 6,000, 12,000 and 19,000 g mol^{-1}. Cyclic polymers had higher LCST temperatures and the values decreased with increasing ring size. The LCST values varied from ~ 36 to 40°C depending on the molecular weight of the sample, for example, the samples of 6,000 g mol^{-1} had the LCST of 37.0 and 40.4°C for linear and cyclic PNIPAAm respectively. The higher temperatures for cyclic polymers have been attributed to the repulsion between the rings, the absence of end groups and steric hindrance.

2.1.4.2. Copolymerisation of *N*-isopropylacrylamide

NIPAAm can be easily copolymerised with other comonomers. This property enables the synthesis of a great variety of new polymers with different properties that can be employed in many areas. Numerous studies investigated the changes of the LCST after the copolymerisation of NIPAAm with different comonomers. Schild and Dimitrov generalised them in their excellent reviews [12, 13].

In 1975, Taylor and Cerankowski [8] stated that the LCST of a polymer soluble in water is strongly dependent on its hydrophilic/hydrophobic balance. The more hydrophilic the comonomer, the higher the LCST [8, 12, 70, 71]. They studied different poly(*N*-alkyl acrylamides) that had different LCSTs and solubilities depending on the alkyl group. They concluded that the longer was the alkyl chain, the higher was the LCST and the more insoluble were the final copolymers. In 1989, Schild and Tirrell [12] were the first to study the copolymerisation of NIPAAm with *N*-hexadecylacrylamide (HDAAm) and they noticed that the LCST of the copolymer slightly decreased.

As there is a great variety of potential comonomers either hydrophilic or hydrophobic, the number of possible combinations is vast. Fig. 2.12 perfectly illustrates the LCST behaviour

of copolymers of NIPAAm. When NIPAAm monomer is copolymerised with more hydrophilic monomers, for example acrylamide (AAm), the LCST increases. When AAm content is high, the copolymers do not show the LCST behaviour. On the other hand, when the comonomers are hydrophobic, for example *N-tert*-butyl acrylamide (NtBAAm), the LCST decreases.

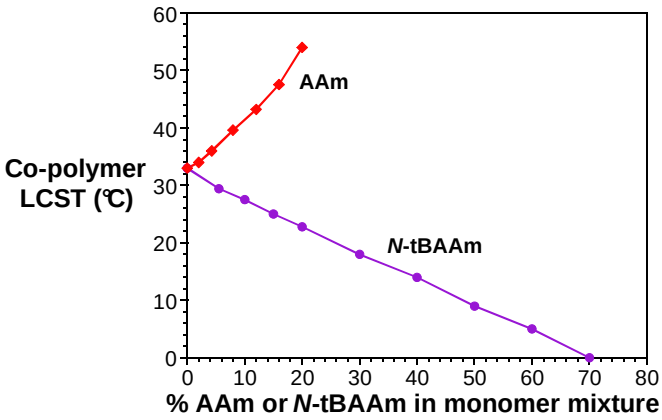

Figure 2.12: *The effect of AAm and NtBAAm on the LCST of the copolymers with NIPAAm [72]*

Copolymerisation of NIPAAm with other comonomers also allows the combination of polymer thermo-responsiveness with other types of stimuli, for example pH, light, magnetic field and solvent quality [73, 74]. Moreover comonomers can be used not only to change the responsiveness of the polymer [60, 75] but also to label the polymers to enable the observation of behaviour of polymer chains [60] and to introduce biological activity [76, 77]. In aqueous solutions amphiphilic block and random copolymers can self-assemble into micelles, lamellar aggregates, vesicles and hydrogels offering various interesting application possibilities [13]. The self-assembly of the amphiphilic molecules will be discussed later.

2.1.4.3. Solvent effect on the LCST

PNIPAAm is soluble in organic solvents that can form hydrogen bonds with polymer molecules, for example ethanol, methanol, acetone, dioxane, chloroform, THF and methyl ethyl ketone. According to Mark-Houwink-Sakurada theory these solvents are good solvents and no LCST is observed because PNIPAAm is soluble up to the solvent's boiling point [57].

As discussed elsewhere, the addition of organic solvents that form hydrogen bonds with PNIPAAm could theoretically improve the solubility of PNIPAAm and increase the LCST [3]. In practice, these organic solvents suppress the LCST initially and then increase it. When a mixture of two non-solvents for a polymer forms a good solvent, this phenomenon is called cononsolvency. Winnik *et al.* [78] observed this cononsolvency phenomenon for PNIPAAm

in water/methanol mixtures where methanol was a non-aqueous solvent and hence reduced the polymer-water contacts.

2.1.4.4. Salt effect on the LCST

Salts change the water structure and reduce the quantity of water molecules bound by hydrogen bonds. Consequently, the free energy of interaction between the polymer and water is reduced, polymer chains become more hydrophobic and the LCST of the phase separation decreases. This occurs due to the salting out effect of the macromolecular chains from aqueous solution [79, 80].

Behaviour of PNIPAAm in the presence of salts follows the classical Hoffmeister series. Salts efficiency to decrease the LCST of the aqueous solution of PNIPAAm follows this ranking: NaI < KI < LiCl < NaBr ~ KBr < $MgCl_2$ < NaCl ~ KCl ~ CsCl < RbCl < $CaCl_2$ < $SrCl_2$ < $BaCl_2$ < NaOH ~ KOH < NaF ~ KF < $LiSO_4$ < $MgSO_4$ < K_2SO_4 < K_2CO_3 ~ Na_2CO_3 < $Na_2P_2O_7$ ~ Na_3PO_4 ~ Na_2SO_4. The LCST also decreases with the increase in salt concentration [3, 79].

2.1.4.5. Surfactant effect on the LCST

Usually, surfactants increase the LCST of PNIPAAm in the following order: non-ionic < cationic < anionic. This is also a general order of surfactant adsorption onto the polymers. In the case of linear alkyl sulfonates, the transition temperature increases as the alkyl chain length increases. Amighi *et al.* [79] used sodium salts of fatty acids as surfactants varying the length of the hydrocarbon aliphatic tail. At high surfactant concentrations, surfactants with short chains (hydrocarbon aliphatic tails containing less than eight carbon atoms) suppressed the LCST. On the other hand, surfactants with alkyl tails containing more than eight carbon atoms, increased the LCST. At low concentrations, a certain decrease of the LCST was observed, due to the surfactant concentration being under the critical aggregation concentration (CAC). When surfactant concentration reached the critical micelle concentration (CMC), the increase of the LCST was observed. Typically, CAC is lower than the CMC. At CAC the surfactant self-associated into the aggregates and at CMC the surfactant spontaneously formed micelles.

Eliassaf [81] reported that the addition of 1% of sodium dodecyl sulfate (SDS) to an aqueous solution of PNIPAAm prevented it from precipitating and increased the viscosity of the solution. As the SDS concentration increased, the surfactant molecules adsorbed on the PNIPAAm chain. This enhanced its solubility without affecting the phase transition.

Other surfactants have also been studied and the results obtained were summarised in the review of Schild [12].

2.1.5. Applications of PNIPAAm

According to the literature, researchers appear to mostly use the copolymers of PNIPAAm for drug delivery and tissue engineering. These copolymers tune behaviour to appropriate application and allow the formation of conjugates with different bioactive molecules, drugs and proteins. Applications of PNIPAAm cover the fields of separation [82-84], controlled drug release [85], gene delivery [86], and tissue engineering [87-90]. The following section includes a brief description of the ways these polymers can be applied.

2.1.5.1. Biological application

It has been reported that enzyme immobilisation on stimuli-responsive polymers has various advantages, such as affinity-based enzyme precipitation or recovery from the solution, control of the enzyme activity, prolonged enzyme activity in aqueous solutions, and use of the enzyme in organic solvents [77, 91-94]. It has been demonstrated that PNIPAAm can also be conjugated with enzymes, such as trypsin or cyclodextrin glycosyltransferase [95]. The results showed that the enzymes retained their activity during the cycles of conjugate precipitation and solubilisation. It was concluded that PNIPAAm can serve as an enzyme support in homogeneous biocatalysis. Moreover, Nguyen and Luong [76] prepared a conjugate of the copolymer of NIPAAm and glycidyl acrylate and a strong trypsin inhibitor. The conjugate selectively bound to trypsin and its separation was possible upon heating when the complex of the copolymer and the enzyme precipitated due to the collapse of PNIPAAm.

The delivery of drugs and chemical agents by thermo-responsive polymer vehicles is a growing field of research where the LCST phenomenon of PNIPAAm plays a key role. When considering the application of such thermo-responsive polymers in drug delivery, it is necessary that the phase transition occurs at a temperature higher than the human body temperature. The system should be soluble at 37°C and exhibit a phase separation that is sharper than that of the homopolymer. Eeckman *et al.* [62] used thermo-responsive polymers to create new drug delivery agents. They copolymerised NIPAAm with hydrophilic comonomers: acrylamide (AAm), *N*-methyl-*N*-vinylacetamide (MVA), *N*-vinylacetamide (NVA) and *N*-vinyl-2-pyrrolidinone (VPL). The result was that all copolymers had the LCST higher than 37°C. Subsequently, the authors studied the drug release from Na_2SO_4-loaded copolymer-coated tablets. It was noted that the salt from the tablets decreased the solubility rates of the copolymer coating, thereby retarding drug release. When salt concentration in the

coating decreased, the polymer became more soluble and drug release occurred. As a result of the salting out effect, the time before drug release for PNIPAAm-co-NVA and PNIPAAm-co-MVA coated tablets was increased up to 80-90% [62].

Some studies showed the potential application of the copolymers of PNIPAAm in cancer therapy. It was found that the polymer should be soluble when injected *in vivo* after which it will become insoluble and accumulate selectively on locally heated tumour cells. In this case, the phase transition of the polymer in aqueous solution has to be between a physiological temperature (~ 37°C) and the temperature of the heated tumour tissue (local hyperthermia) (~ 40°C) [96]. For example, when a selective part of tissue was heated, it was found that selective accumulation of rhodamine-poly(*N*-isopropylacrylamide-co-acrylamide) P(NIPAAm-*co*-AAm) in the tumour tissues occurred [97, 98]. Using a polymer matrix as a drug carrier improves poor drug solubility in aqueous media and poor pharmacokinetics of drug, and decreases the toxic side effects of drug [99].

PNIPAAm also showed promising results in *in vivo* studies. Kim *et al.* [100] prepared a thermo-responsive PNIPAAm coating for heparin release to prevent surface-induced thrombosis. This coating was obtained by the blending and co-precipitation of two linear polymers: Biomer (multiple block co-polyether-urethane-urea) and PNIPAAm. At room temperature the resulting network-like structure had many entanglements and swelled in heparin solution and consequently absorbed it. At body temperature, heparin was released as the network shrank. The researchers used this heparin-loaded thermo-responsive coating to cover intravenous polyurethane catheters in a canine animal model. Results showed significant reduction of thrombus formation.

Okano *et al.* [101] obtained block copolymer poly(*N*-isopropylacrylamide-*b*-butylmethacrylate) (PNIPAAm-*b*-PBMA) that formed micelles. The hydrophobic inner core of the micelles was composed of self-aggregated PBMA segments and was loaded with the anti-cancer drug, adriamycin. The outer shell contained PNIPAAm segments that stabilised the micelles and were responsible for the thermo-responsiveness. At locally-heated sites, the outer core turned hydrophobic releasing the drug. Adriamycin-loaded micelles showed *in vitro* cytotoxicity only when heated above the LCST of 32.5°C.

Hsieu *et al.* [102] studied the application of PNIPAAm in ophthalmic drops to release the ophthalmic agent, epinephrine, for glaucoma therapy. Two systems were studied. One type of drops was based on linear PNIPAAm and the other type was based on the mixture of linear PNIPAAm and cross-linked PNIPAAm nanoparticles. The drugs were administered into the eyes of rabbits. Both systems showed good results and prolonged release times (~ 6 h), especially ophthalmic drops with the mixture of linear PNIPAAm and crosslinked

PNIPAAm nanoparticles. Also both systems were found to show no cytotoxic activity on the epithelial cells of cornea.

2.1.5.2. PNIPAAm in cell growth

Thermo-responsive polymers have been widely used in cell growth. The actual role of the polymer here is to facilitate cell detachment upon cooling without using enzymes that can alter the morphology and function of cells [87, 103]. Cells adhere selectively onto hydrophobic surfaces. Hence cell detachment occurs upon cooling when the polymer switches from a hydrophobic to a hydrophilic state [104, 105].

PNIPAAm is considered to be a poor substrate for cell growth and proliferation. However, this property can be improved by copolymerisation with appropriate comonomers [106]. Normally PNIPAAm and its copolymers are grafted onto surfaces suitable for cell growth, such as polystyrene culture dishes. A substantial amount of research work has been done in this field [107-111].

Okano's group was one of the first to start applying PNIPAAm as an active agent to release cells from culture plates. Their contribution to the development of thermo-responsive systems was considerable and the majority of today's scientists do their research, relying on the early work of Okano's group.

In 1990, Okano *et al.* studied bovine hepatocytes and discovered that the cells easily detached from the surfaces modified with PNIPAAm-grafted chains when the culture temperature was reduced below 32°C [87]. In 1995, the same research group [112] grafted PNIPAAm with the LCST of 25°C in physiological phosphate-buffered saline solution (pH 7.4) and 32°C in water onto polystyrene cell culture dishes. Endothelial cells and hepatocytes attached and proliferated on these surfaces at 37°C. Hepatocytes detached at 10°C and endothelial cells detached at 20°C. Since hepatocytes and endothelial cells have different temperatures for cellular metabolism and detachment, it is important to find the optimum temperature for these two processes [112]. Sodium azide was used as detachment inhibitor, suggesting that cell metabolism directly affects cell detachment. The cells detached due to reduced cell-surface interaction and due to morphological changes of active cells. Okano *et al.* [112] proposed a mechanism of cell detachment that involved two stages. According to them, cell rounding occurs when the surface of Petri dish grafted with PNIPAAm changes its nature from hydrophobic to hydrophilic (passive detachment). Subsequently, active detachment occurs involving cellular metabolism.

Other copolymers of PNIPAAm, such as poly(NIPAAm-*co*-AAc) or poly(NIPAAm-co-CIPAAm), were also studied. As AAc made PNIPAAm-grafted surfaces excessively

hydrophilic, cell proliferation was suppressed at 37°C. Since 2-carboxyisopropylacrylamide (CIPAAm) was more hydrophobic than AAc, cell adhesion and proliferation was found to be better on these surfaces at 37°C. When temperature decreased, cell detachment was faster on CIPAAm copolymer grafted surfaces than on the surfaces with pure PNIPAAm as a result of the carboxyl groups of CIPAAm that made it more hydrophilic [113].

Okano *et al.* [114] extended further the study of P(NIPAAm-co-CIPAAm) grafted tissue culture dishes by attaching the cell adhesion promoter RGDS (arginine – glycine – asparagine - serine) sequences via the carboxyl groups of CIPAAm and studying human umbilical vein endothelial cells. At 37°C the copolymer collapsed exposing the functional RGDS sequence on the surface which promoted cell proliferation via integrin receptors. Below the LCST, swollen polymer chains restricted integrin receptors access to the RGDS sequence and mechanically disrupted cell-surface interaction resulting in cells detachment.

Moran *et al.* [108] prepared copolymers of NIPAAm and *N-tert*-butyl acrylamide (NtBAAm) and coated them with cell adhesion promoters, such as collagen, poly-L-lysine, and laminin that bind physically to the copolymer surface to improve cell adhesion and growth. The researchers reported that cell detachment was slower when the copolymers were highly hydrophobic, i.e. the NtBAAm content was high.

Vihola *et al.* [115] studied the cytotoxicity of PNIPAAm and found that the monomer was more toxic than the polymer. The tests showed that PNIPAAm was not toxic to cells in the concentration range from 0.01 to 10 mg ml^{-1}.

2.1.5.3. Separation technologies

PNIPAAm has also been used to modify the stationary phase of an aqueous chromatography column. The fact that water can be used as an eluent instead of organic solvents makes this chromatography very interesting in terms of maintaining the structure and activity of bioactive compounds.

Kanazawa *et al.* [35] prepared thermo- and pH-responsive poly(NIPAAm-*co*-BMA5%-*co*-DMAPAAm5%) copolymers where butyl methacrylate (BMA) is a hydrophobic comonomer and *N,N*-dimethylaminopropylacrylamide (DMAPAAm) is a cationic monomer. The LCST of this copolymer in water was at 31.1°C. The LCST decreased when the pH increased from 6.0 to 9.0 (38.7 to 29.7°C accordingly) because deprotonation of amino groups in DMAPAAm increased the hydrophilicity of the polymer. At pH 4.5 – 6.0 the LCST was roughly constant (~ 38.8°C). At pH = 3.0, protonation took place and the LCST decreased to 35.6°C [15]. Subsequently, poly(NIPAAm-co-BMA-co-DMAPAAm) copolymer was grafted onto aminopropyl silica beads and used as the packing material for a high performance liquid

chromatography (HPLC) column. This column was used to separate steroids [35], non-steroidal anti-inflammatory drugs such as ibuprofen, ketoprofen and naxoprofen [15] and anionic biologically active substances, such as proteins and peptides. The retention in these systems was maintained by the hydrophobic interactions between the solute molecules and the hydrophobic polymer chains immobilised on the stationary phase surface. Steroids, peptides, and proteins can be separated using columns packed with PNIPAAm-modified silica simply by changing the temperature of an aqueous mobile phase and consequently the phase separation temperature of the polymer.

2.1.6. Summary

In summary, this section introduced thermo-responsive polymers and described the prototypical example, poly(*N*-isopropylacrylamide) (PNIPAAm) in some detail. This polymer has been widely studied and used in different applications due to its LCST being close to body temperature. Different LCST and polymer conformation detection techniques were described, as well as the various parameters that can alter the LCST behaviour: polymer molecular weight, copolymerisation, and different additives. This polymer can easily be used in different model studies where temperature stimulus is important. The range of PNIPAAm applications is very diverse and the most prominent are the fields of controlled drug delivery and tissue engineering.

2.2. AMINO ACIDS AND PEPTIDE FORMATION

2.2.1. Introduction

This section will focus on the amino acids and peptide formation. Different types of amino acids and peptide structures will be discussed here. The principle of solid phase peptide synthesis will also be introduced.

2.2.2. Amino acids

Peptides and proteins are composed of **amino acids** (2-aminocarboxylic acids). There are only 20 naturally occurring amino acids. Synthetic amino acids can be obtained via enzymatic conversions. All amino acids, with an exception of glycine, have four different substituents around the central α-carbon atom (C-2): a carboxyl group, an amino group, a hydrogen, and a side chain (R), which is different to all amino acids (Fig. 2.13). All naturally occurring amino acids, except glycine, are chiral and found in L-enantiomeric form [116].

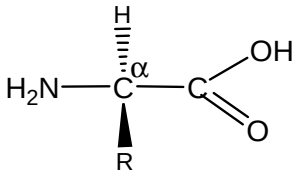

Figure 2.13: *General chemical structure of an amino acid*

Amino acids are classified according to the nature of the side chain. This classification is described below and the chemical structures of the 20 natural amino acids are given in the Table 2.2.

The **aliphatic** amino acids are *glycine*, *alanine*, *valine*, *leucine* and *isoleucine*. They are strongly apolar as they do not contain any heteroatoms like N, O or S [116]. Peptides that contain glycine are more flexible than those with other amino acids because there are two hydrogen atoms in its structure that help to overcome any steric hindrance usually imposed by the amino acids side chains [117]. The **aromatic** amino acids possess resonance-stabilised rings in their side chains. This class includes *phenylalanine* (strongly apolar), *tyrosine* (intermediate polarity), *tryprophan* (intermediate polarity), and *histidine* (strongly polar). Since the imidazole ring of histidine can be easily protonated at neutral and weak pH, it can also be classified as a basic amino acid.

The **sulfur-containing** amino acids, such as *cysteine* and *methionine*, are also apolar (in the case of cysteine it refers to the undissociated state only). A disulfide bond can be formed between two cysteine molecules which commonly stabilises protein secondary structure.

The side chains of **neutral** amino acids contain hydroxyl groups (*serine*, *threonine*) or amide groups (*asparagine*, *glutamine*). The amide groups of asparagine and glutamine are very

polar. Aliphatic and aromatic amino acids are hydrophobic amino acids, whereas neutral and acidic amino acids are hydrophilic amino acids.

Table 2.2: *Natural amino acids*

Aliphatic				
Glycine (Gly)	Alanine (Ala)	Valine (Val)	Leucine (Leu)	Isoleucine (Ile)
G	A	V	L	I
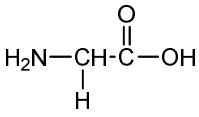	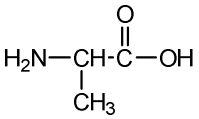	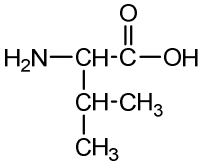	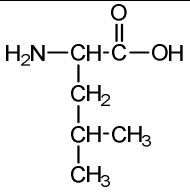	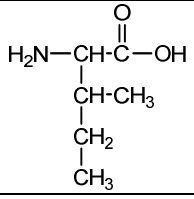
Sulfur-containing		**Aromatic**		
Cysteine (Cys)	Methionine (Met)	Phenylalanine (Phe)	Tyrosine (Tyr)	Tryptophan (Trp)
C	M	F	Y	W
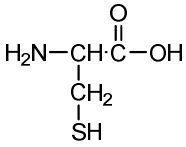	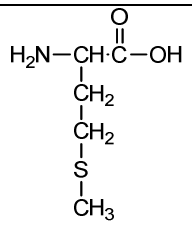	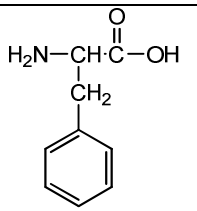	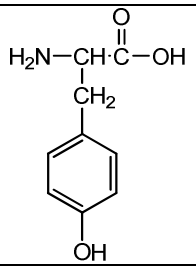	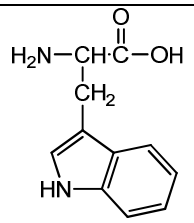
Imino acid	**Neutral**			
Proline (Pro)	Serine (Ser)	Threonine (Thr)	Asparagine (Asn)	Glutamine (Gln)
P	S	T	N	Q
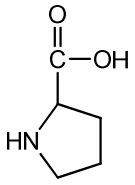	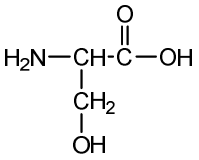	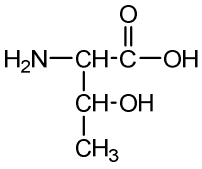	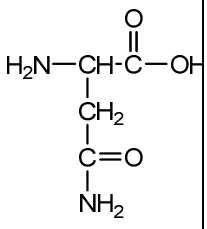	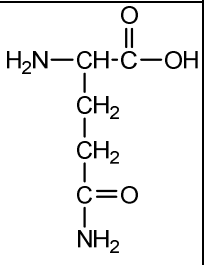
Acidic		**Basic /aromatic**	**Basic**	
Aspartic acid (Asp)	Glutamic acid (Glu)	Histidine (His)	Lysine (Lys)	Arginine (Arg)
D	E	H	K	R
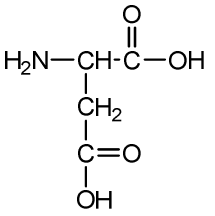	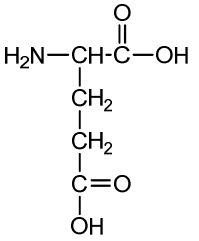	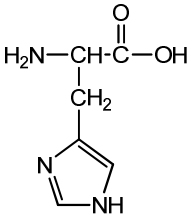	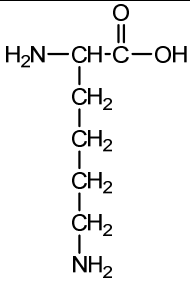	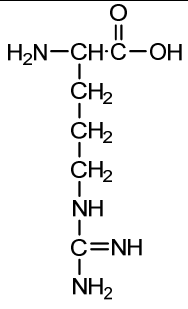

The **acidic** amino acids, such as *aspartic acid* and *glutamic acid*, contain carboxyl groups that are almost completely ionised at physiological pH values. Also the side chains of the **basic** amino acids, *lysine* and *arginine*, are fully protonated at neutral pH. Arginine has the guanido group and is therefore very basic and very polar.

Proline is a different amino acid. It has a five-membered ring and includes a chiral carbon and an α-amino group in the side chain. This is why proline is an imino acid. The nitrogen atom of proline is weakly basic and therefore not protonated at physiological pH. Within peptide chains, proline residues cause bends that interrupt secondary structure [116]. Proline also makes the peptide more rigid because of the locked conformation as the side chain is covalently linked to the amino terminus [117].

2.2.3. The amide bond and peptides primary structure

In the **primary structure** of peptides and proteins amino acids are linked through an **amide bond** (peptide bond); the bond between the carboxyl group of one amino acid and the amine group of another amino acid (Fig. 2.14). Many properties of peptides and proteins can be explained by properties of the peptide bond [118].

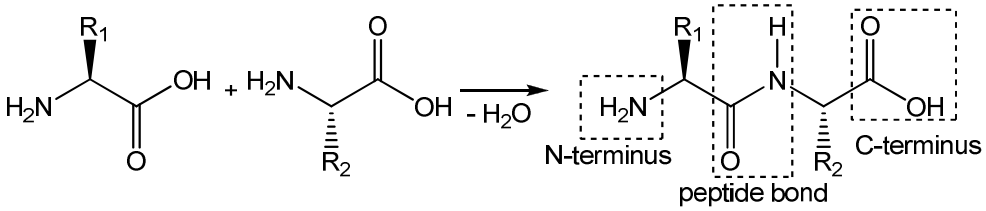

Figure 2.14: *Scheme of peptide bond formation*

The linking of two amino acids results in a dipeptide. In dipeptides, one of the two residues contains a free amino group (the *N-terminal* amino acid), while the other a free carboxyl group (the *C-terminal* amino acid). The naming and representation of peptides always begins at the left with the N-terminal amino acid.

The peptide bond is planar due to stabilisation by resonance (Fig. 2.15), i.e., the delocalisation of electrons between the carbonyl oxygen and the amide nitrogen.

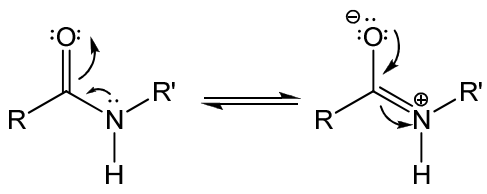

Figure 2.15: *Resonance structures of a peptide bond*

The planar conformation can form *trans* and *cis* isomers (Fig. 2.16). *Trans* form is more stable than *cis* form because the *cis* form has greater steric repulsion between the C_α atoms and their attached groups. The *trans* peptide bonds dominate protein structure.

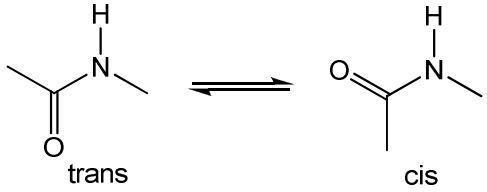

Figure 2.16: *Cis/trans isomers of peptide bond*

Each amino acid in a peptide is involved in the formation of two peptide bonds, the only exception being the terminal residues.

2.2.4. Secondary structures

Secondary structure refers to interactions within localised domains that result in three-dimensional structure. As the residues can rotate around N-C_α and C_α-C bonds, the type of secondary structure formed depends on the stabilisation of the peptides intramolecular or intermolecular hydrogen bonds between the NH group (hydrogen bond donor) and the carbonyl oxygen atom (hydrogen bond acceptor) (Fig. 2.17).

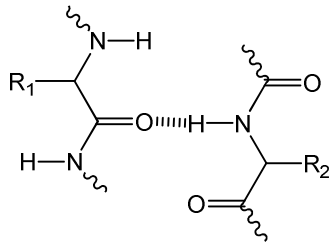

Figure 2.17: *Scheme of hydrogen bond formation*

There are various types of secondary structure including α-helices and coiled coils, β-sheets, β-hairpins and β-turns. Only α-helical and β-sheet structures will be described in the following sub-sections, as they are most relevant to this work.

2.2.4.1. α-Helix

The right-handed α-helix is the most common secondary structure (Fig. 2.18). Each turn of the helix contains 3.6 amino acid residues. The intramolecular hydrogen bonds between the NH and CO groups stabilise the α-helices. The right-handed α-helices (from L-amino acids) is the preferred conformation energetically and stereochemically [116, 119].

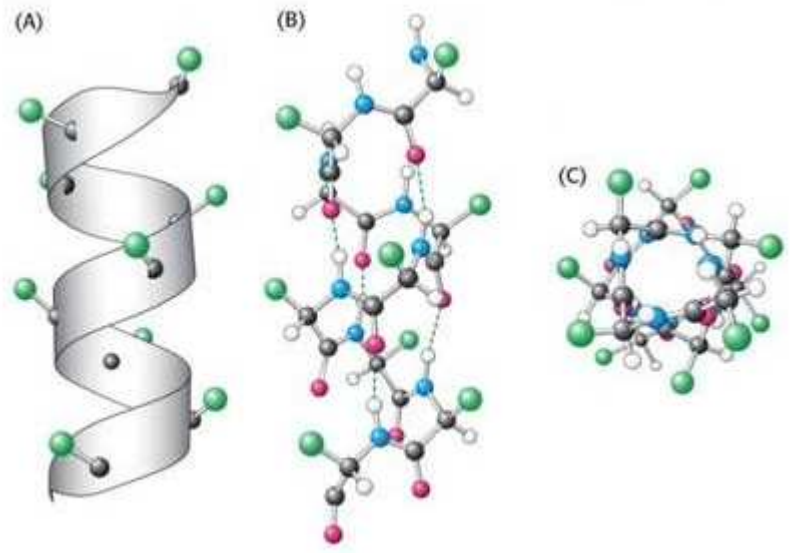

Figure 2.18: *Representation of a-helix: a) schematic, b) molecular, c) view from the top (adapted from [119])*

The nature of the amino acids in the primary structure is essential for helix formation and stability. According to the amino acids propensity scale to form α-helix, developed by Pace and Scholtz [120], alanine has the highest helix propensity. Also methionine, leucine, uncharged glutamate and lysine are compatible with helical structures. However, glycine, proline and negatively charged aspartate showed low propensities for helical structures. These amino acids do not act as hydrogen bond donors and consequently decrease helix stability [118].

In nature the left-handed helix structure is scarcely represented, except in the collagens, which are important constituents of the connective-tissue matrix. In the α-helices of collagen hydrogen bonds are not possible, but the conformation is stabilised by the association of three left-handed helices to form a right-handed collagen triple helix structure [116]. When α-helices wrap around each other, they form a stable structure, known as coiled coils [121].

2.2.4.2. Pleated-sheet structures

In pleated-sheet structures the peptide planes repeat the arrangement of a regularly folded sheet of paper. The hydrogen bonds form only between neighbouring chains. If the N- and C-termini alternate, the peptides form an **antiparallel pleated β-sheet** (β_a) (Fig. 2.19). When all C-termini of the peptide chains are in one direction, a **parallel pleated β-sheet** (β_p) is formed. β_a structure is energetically more favourable due to almost linear hydrogen bonds [116].

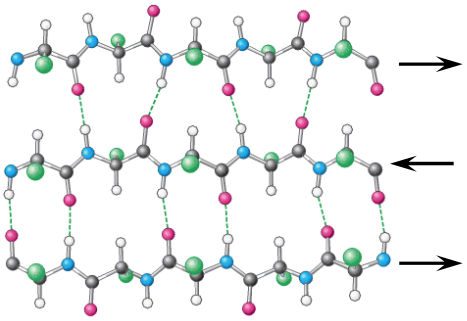

Figure 2.19: *Schematic representation of anti-parallel β-sheets. Arrows represent the direction of β-sheet strands (adapted from [119])*

It was reported that β-branched (valine, isoleucine and threonine) and aromatic amino acids usually form β-sheets. Glycine and proline do not have a pronounced tendency to form β-sheets [118].

Both helices and β-sheets can be amphiphilic, meaning that they contain both hydrophilic and hydrophobic characteristics.

2.2.5. Tertiary and quaternary structure

The three-dimensional arrangement of secondary structural elements is called the **tertiary structure**. Quaternary structure refers to interactions between subunits, or individual polypeptide chains, in multichain protein. Not only hydrogen bonds but also other interactions, such as disulfide, ionic bonds and/or hydrophobic interactions, stabilise these structures (Fig. 2.20).

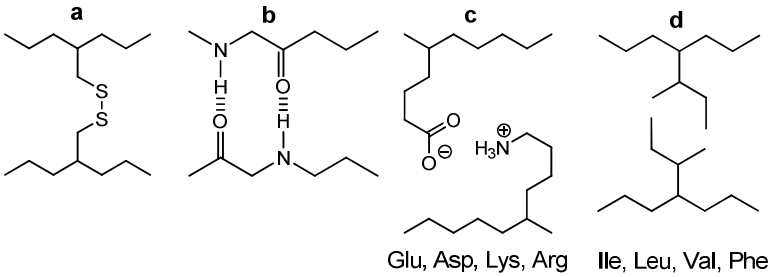

Figure 2.20: *Stabilising interchain interactions between amino acid residues: a) disulfide bridge, b) hydrogen bond, c) ionic bond (salt bridge), d) hydrophobic interaction [118]*

A typical example of a protein that adopts quaternary structure is insulin [116]. Insulin is composed of two peptide chains, referred to as A and B with 21 and 30 amino acids respectively. The A chain contains two sections of α-helices that lie alongside and the B chain wraps around it. The tertiary structure is stabilised by two disulfide bonds between A and B chains and an additional disulfide bond formed within the A chain. The quaternary structure

of insulin consists of hexamers (six insulin molecules as described above, grouped around two zinc ions) due to interactions between hydrophobic surfaces [116].

2.2.6. Solid phase peptide synthesis

In 1963, R.B. Merrifield introduced the concept of solid phase peptide synthesis (SPPS), where the growing peptide is attached to a solid support (resin) allowing the removal of excess reagents and by-products by filtration [122]. SPPS is conducted on functionalised solid support and consists of assembling amino acids from the C- to the N-terminus.

The solid support is typically composed of spherical beads of polystyrene, crosslinked with divinylbenzene. They contain active sites where the first amino acid of the peptide to be synthesised is usually attached to the beads. Beads can be purchased with different mesh size and different amino acid loadings. The porosity of the filter in the reaction vessel should also be taken into account when choosing the resin. Normally, 100 – 200 mesh (particle size distribution) is the recommended bead size. The beads swell in organic, or similarly polar solvents (except methanol, ether and water) and form a well-solvated gel with mobile polymeric chains, thus facilitating the access of the reagents to the active sites [118].

The general principle of SPPS is shown in Fig. 2.21 [118]. First, the anchoring group, or linker, is introduced onto the polymeric support (Fig. 2.21, step 1). There are many linkers for polystyrene core resins depending on the nature of the C-terminus of the desired peptide and cleavage conditions. Wang resin with a polystyrene core functionalised with a Wang linker (4-hydroxymethylphenoxy) was used in this work (Fig. 2.22).

Peptides are synthesised from the C- to the N-terminus beginning at the benzylic alcohol of the Wang linker (Fig. 2.21, step 2). In most cases, Wang resin can be purchased with the first amino acid preloaded. In this work, Wang resin preloaded with lysine (K) was employed, hence the SPPS synthesis starts from step 3 in Fig. 2.21. When the protecting group is removed, the next amino acid can be coupled (step 4). Then steps 3 and 4 are repeated (step 5) until the desired peptide sequence has been completed. Finally, the covalent bond between the linker and the peptide chain is cleaved. Usually the side chain-protecting groups may also be removed during the cleavage step (step 6). Subsequently, this peptide is present in solution and can be separated from the insoluble polymeric support by filtration.

Every deprotection and coupling step is followed by the Kaiser test to ensure that reaction has taken place. Hinhydrin, present in the solution for the Kaiser test, reacts solely with primary and secondary amines, forming a deep blue coloured compound. If the coupling step is successful, no colouring occurs.

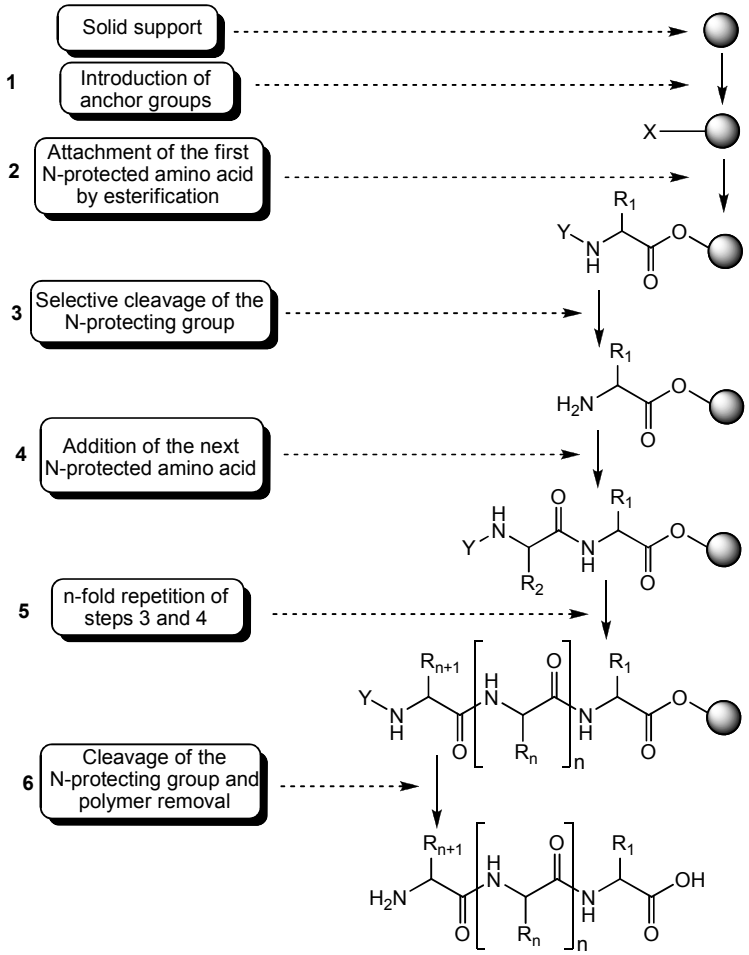

Figure 2.21: *Scheme of solid-phase peptide synthesis (adapted from [118])*

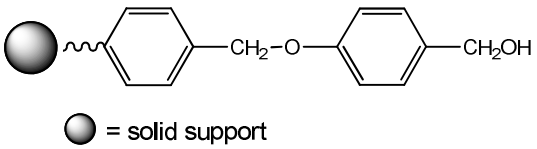

Figure 2.22: *Schematic representation of Wang resin*

Ten of the proteinogenic amino acids (S, T, Y, D, E, K, R, H, U and C) have functional groups in the side chain that have to be protected before coupling. There are intermediary (temporary or transient) and semipermament protecting groups. The temporary groups are used for temporary protection of the amino or carboxy functional group, involved in subsequent bond formation. The semipermanent groups are cleaved at the end of the synthesis.

Each deprotection-coupling cycle is initiated by selective cleavage of the N^{α}-protecting group. The linker and the semipermanent amino acid side chain-protecting groups must be chosen correctly with the respect to the protecting group chemistry of the temporary N^{α}-protecting group.

In SPPS, either the acid labile *tert*-butyloxycarbonyl (Boc) group or the base-labile fluorenyl-9-methyloxycarbonyl (Fmoc) group are applied as temporary N-α-protecting groups. Boc is usually cleaved with TFA. Repetitive TFA acidolysis in Boc-group deprotection could lead to alternation of sensitive peptide bonds as well as acid catalysed reactions. That is why in SPPS using Fmoc protocol the growing peptide is subjected to mild base treatment using piperidine during Fmoc-deprotection. TFA is only required for the final cleavage when side-chain protecting groups are cleaved simultaneously with detachment from the peptide resin. Fig. 2.23 shows the protecting group and cleavage strategy for Fmoc chemistry [123].

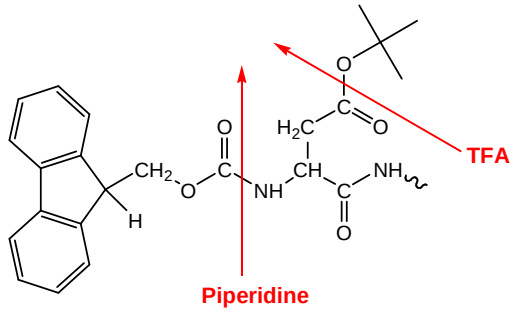

Figure 2.23: *Protecting group strategies in SPPS*

SPPS possesses many advantages over solution peptide synthesis [123]:

- good yields of 80 - 90% of the peptide are possible due to its attachment to a solid support
- excess reagents and by-products can be removed by washing and filtering the solid support
- the process can be automated
- the use of excess reagents leads to the completion of the reaction
- poor chemoselectivity of some reagents can be improved by attachment of the appropriate component to the solid support to give only the desired product
- selective derivatisation of peptide end is possible.

However, there are some limitations [118]:

- heterogeneity of the final product if all deprotection and coupling steps are not quantitative
- use of a lot of starting materials as they are added in excess
- undesirable side reactions during activation, coupling and deprotection may occur
- it is sometimes difficult to swell the resin efficiently to ensure diffusion of the reagents and amino acid coupling at all active sites
- aggregation of the growing peptide chain may complicate the synthesis
- peptide can be damaged during cleavage

2.2.7. Summary

This section presented some general aspects about amino acids chemical nature, peptide bond formation, and peptides structure. The notion of SPPS using Fmoc protocol has also been introduced, describing important parameters for the correct choice of resin, amino acids protecting groups and reaction conditions.

2.3. PEPTIDE SELF-ASSEMBLY

2.3.1. Introduction

Molecular self-assembly can be defined as spontaneous organisation of molecules under certain conditions into structurally well defined and stable arrangements through non-covalent interactions such as hydrogen bonding, electrostatic, hydrophobic and van der Waals interactions. Although these forces are weak on their own, they form very stable structures when combined [124].

Self-assembling materials have an amphiphilic nature as they contain both hydrophobic and hydrophilic segments. Amphiphilic molecules are widely present in nature and include lipids, peptides and proteins. They serve as building blocks for the construction of functional assemblies, such as cellular membranes, the cytoskeleton, and the extracellular matrix. Three most widely used classes of self-assembling molecules are lipids, block copolymers, and peptides/proteins and they are depicted in Fig. 2.24 along with the forces that drive their self-assembly into various structures [125]. When dissolved in an appropriate solvent (solvent choice depends on the building blocks), the self-assembly of these molecules is driven by weak, non-covalent interactions and depending on the monomer structure different morphologies of assembled structures can be obtained ranging from vesicles, micelles, tubes to fibrillar rich networks.

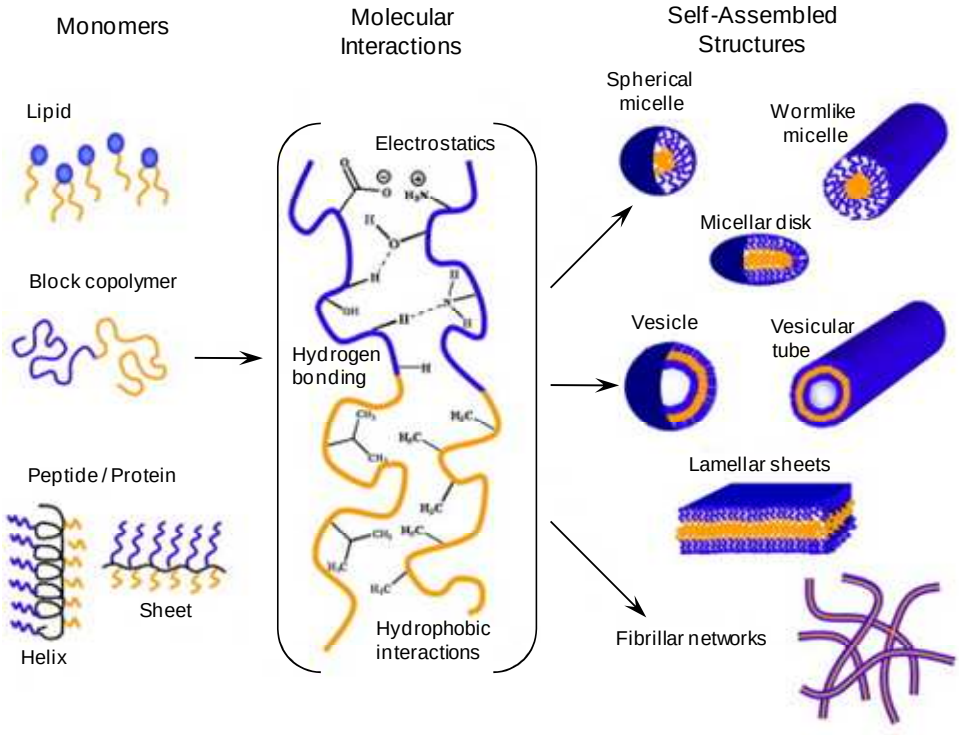

Figure 2.24: *Scheme showing various building blocks and different structures in which they can self-assemble through various intermolecular interactions (hydrophilic part is depicted in blue, hydrophobic part – in orange) (adapted from [125])*

Lipids represent the simplest naturally occurring amphiphilic material. Synthetic block copolymers [126-132], and peptides/proteins [133-135] have been shown to form various morphologies due to the balance between their hydrophilic and hydrophobic parts. Hybrid materials, derived from combining peptides, polymers and lipids, have also been reported [136-138].

Peptide and protein self-assembly is a widespread phenomenon in nature [124]. The widely cited examples include the process of protein folding [135], the self-assembly of tobacco mosaic virus [139] or formation of pyruvate dehydrogenase complex [121]. Regulated self-assembly of proteins plays a major role in many biological processes, for example, the association of four hemoglobin molecules into a tetramer or six insulin molecules into hexamer [124, 140]. Amyloid fibrils are the key example of protein self-assembly. Unregulated self-assembly resulting from the misfolding and aggregation of proteins is characteristic of degenerative amyloid disorders such as Alzheimer's disease, Parkinson's disease, and type II diabetes [133]. In these diseases the misfolded proteins assemble into insoluble amyloid fibrils that aggregate into plaques in different organs and tissues and are considered neurotoxic [141].

Peptides afford design of self-assembled materials with controllable structural features and simultaneous tuning of physicochemical and biological properties. Self-assembly of various peptide sequences give various nanostructures that form higher level hierarchical associations which mimic the structure of native extracellular matrix. A great variety of natural and synthetic amino acids are available for peptide synthesis using relatively simple preparation techniques, such as SPPS (see sub-section 2.2.6.) [142]. Self-assembled peptide networks are widely used as substrates for cell culture and scaffolds in regenerative medicine, where the role of the scaffold is crucial in successful cell adhesion, proliferation and differentiation [143-146].

Self-assembling systems can be also considered as stimuli-responsive materials because their structure, assembly and disassembly can be triggered by environmental changes such as temperature, ionic strength, pH or enzymes [132, 147-153]. Some researchers think that since the self-assembly is driven by weak interactions, the aggregates stability and strength can be affected during the response to environmental stimuli. This can be a limiting factor for the application of such materials [154]. However, there are many examples of successful application of self-assembling materials, mostly as scaffolds in tissue engineering and as drug carriers in controlled drug delivery. The study of self-assembling systems will also provide more understanding about molecular mechanisms in protein-folding disorders and will facilitate the development of therapeutic strategies.

2.3.2. Self-assembling peptide systems

Zhang *et al.* [155] was one of the first research groups that reported self-assembly of short peptides, whose structure was based on the principle of ionic complementarity. They also showed various examples of their application possibilities [142, 156-162]. There are four different types of self-assembling peptide according to Zhang and coworkers [155, 163]. These are introduced below.

Type I peptides can assemble spontaneously into well defined nanostructures and form β-sheet structures in water due to the alternating negatively, positively charged and neutral hydrophobic and hydrophilic residues [158, 164-166]. Type I peptides are also called ionic complementary peptides. **Type II** peptides can change their properties abruptly in a response to environmental changes. An example of this is a dipolar 16 amino acids-long peptide ADADADADARARARAR (DAR16-IV, where A is alanine, D is aspartic acid, and R is arginine; IV means that the peptide has four consecutive positively and/or negatively charged residues). This peptide formed a β-sheet structure at ambient temperature and changed to α-helix at high temperatures [167, 168]. Upon cooling an α-helical structure was retained, however the peptide returned partially to the initial β-sheet conformation over several weeks at ambient temperature. Similar conformational changes can be induced by changing pH [167]. **Type III** peptides undergo self-assembly on surfaces to form monolayers that can be used for cell patterning or for interaction with other molecules. They have three distinct features: the ligand segment that ensures recognition by other molecules or cells due to some functional groups in its structure, the central linker that is responsible for the flexibility and rigidity of the system, and the surface anchor to form a covalent bond with the surface. This system is thought to be useful in biomedical engineering and biology [124, 159, 169]. **Type IV** peptides are biphasic hydrophobic-hydrophilic peptides, called surfactant-like peptides. They have a hydrophobic tail with various degrees of hydrophobicity, and a hydrophilic head.

During the last few decades there has been an increased interest in self-assembling peptides owing to their interesting properties and promising application. This generated a great number of research papers on peptides that can self-assemble into different architectures and this is why another classification system appeared. The classification is based on the structure of monomeric units that participate in the self-assembly [117, 170-172]. These motifs usually are amphiphilic peptides that form different secondary structures, for example, α-helices, β-sheets, and β-turns, also surfactant-like and hydrophobic peptides, such as short aromatic peptides. Examples of these peptides will be given below.

2.3.2.1. Systems based on β-sheet structures – ionic complementary peptides

This type is consistent with Zhang's Type I peptides. The structure of these materials is based on the principle of ionic complementarity because the peptide sequences contain alternating positively, negatively charged and neutral amino acids. Self-assembly of such peptides is governed not only by hydrogen bonding and hydrophobic interactions but also by ionic interactions. These peptides form β-sheet secondary structure and then form fibrils, membranes and hydrogels when peptide concentration is increased. The self-assembly can be affected by the peptide sequence, concentration, pH, and presence of salts. These materials can be used in tissue engineering, drug/gene delivery and biological surface patterning [143, 160, 173-175]. Since this type of peptides was used in the research project, further description of these systems will be given in section 2.3.3.

2.3.2.2. Systems based on β-hairpins

Another class are β-hairpins which consist of two amino acid sequences connected centrally with a short turn sequence. Groups of Pochan and Schneider made a significant contribution in the development and understanding of these systems and reported a number of peptides that exhibit this behaviour [176-179]. They connected two valine and lysine containing sequences with tetrapetide $V^{D}PPT$ (V - valine, P – proline, and T - threonine). Non-natural proline in its D-form in this tetrapeptide adopted a β-turn conformation under certain conditions (basic pH, temperature, ionic strength), thus imposing a hairpin-like structure to a whole peptide sequence. These hairpins subsequently self-assembled into larger fibrillar aggregates, i.e. gels, due to hydrophobic interactions and intramolecular hydrogen bonding. For example, Pochan and Schneider reported that 20 amino acid long peptides VKVKVKVK-V^{D}PPT-KV***K***VKVKV-NH_2 (MAX1) and VKVKVKVK-V^{D}PPT-KV***E***VKVKV-NH_2 (MAX8) with alternating valine and lysine residues were β-hairpin peptides that underwent self-assembly triggered by increased ionic strength. At pH 7.4, 37°C and low ionic strength MAX1 was soluble and unfolded due to electrostatic repulsions between positively charged lysine residues. When the salt concentration increased, the charges were screened and the peptide adopted a β-hairpin structure stabilised by intramolecular hydrogen bonds. Since one face of the hairpin contained hydrophilic lysine residues and the other hydrophobic valine residues, hairpins started to collapse into fibrillar structures stabilised by intermolecular hydrogen bonds [177]. MAX8 was an analogue of MAX1 and contained glutamic acid instead of lysine in position 15. It was observed that MAX8 underwent faster folding and self-assembly in comparison to MAX1 under the same conditions due to reduced positive charge and reduced electrostatic repulsion [178].

Later Pochan and Schneider [179] claimed that increasing the temperature of MAX1 peptide solution at pH 7.4 resulted in peptide folding and subsequent self-assembly. They stated that at low ionic strength, at pH 9 and at temperatures below 20°C, the peptide remained unfolded. At 37°C hydrophobic valine residues were more solvated, leading to the peptide folding and self-assembly. Aggregation and shielding of hydrophobic valine sides from water was energetically more favorable than electrostatic repulsion of lysines. Schneider *et al.* [180] extended the gelation kinetic studies of 20-residues long amino acids. They designed two more MAX1 analogues in which they replaced the lysine (K) in position 15 with glutamine (Q) and threonine (T) and obtained the peptides K15Q and K15T accordingly. Glutamine and threonine are neutral amino acids. The replacement of K in position 15 in the peptide MAX8 with E gave the peptide K15E. By replacing lysine with glutamine, threonine and glutamic acid, the total charge of the peptide decreased from +9 (MAX1) to +8 (K15Q and K15T) and +7 (K15E). Peptides with the decreased charge formed gels quicker.

The researchers stated that folding and self-assembly of this type of peptides can be triggered by different stimuli: by pH to obtain reduced point charge of the lysine residues, by ionic strength to screen the charges, or by temperature to facilitate the attraction of hydrophobic residues (Fig. 2.25).

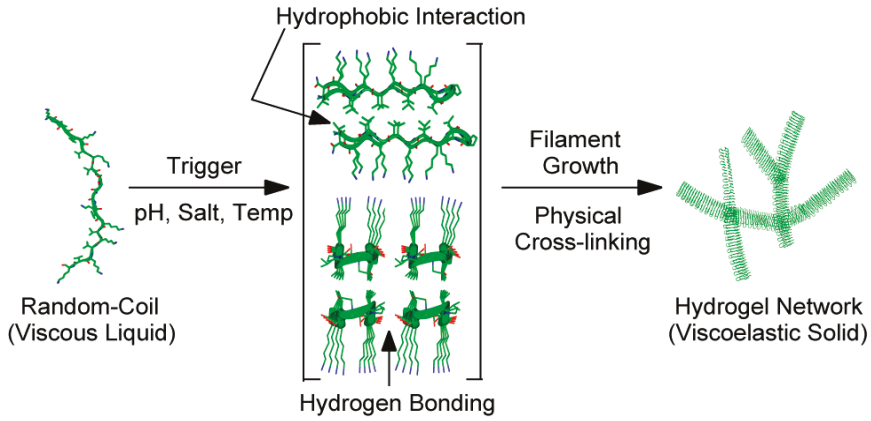

Figure 2.25: *Scheme showing peptide folding into β-hairpin structure, driven by different stimuli, and assembly of β-hairpins (adapted from [180])*

The same research groups of Pochan and Schneider designed and studied 32 amino acid long peptide TSS1 with alternating valine and lysine residues and two tetrapeptides VKVKVKVKV^{D}PPTKVKVKVKV^{D}PPTKVKVKVKV-NH_2 (V^{D}PPT) in its structure (Fig. 2.26) [181].

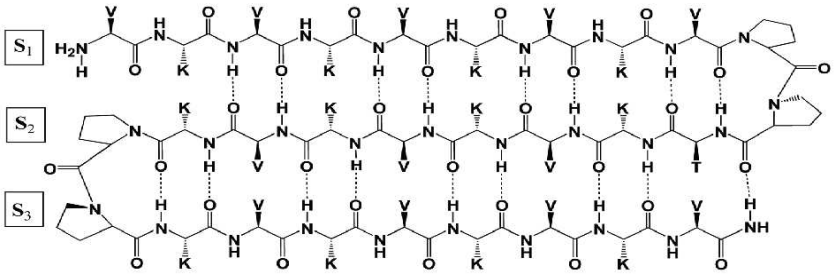

Figure 2.26: *Chemical structure of TSS1 peptide* [181].

This peptide adopted three-stranded β-sheet structure upon heating leading to the self-assembly into gels of well-defined β-sheet fibrils. These gels possessed good mechanical properties (at pH 9 elastic modulus, *G′* varied from 1750 to 9000 Pa and at pH 7 *G′* was ~ 9000 Pa) which made them attractive for the cell culture applications.

2.3.2.3. Systems based on surfactant-like peptides

This classification is consistent with Type IV peptides from Zhang's classification. Surfactant-like peptides have a hydrophobic tail and a hydrophilic head. Zhang reported that seven to eight amino acid long peptide monomers with the head composed of negatively charged aspartic acid (D) and glutamic acid (E) or positively charged lysine (K) or histidine (H), and the tail with alanine (A), valine (V), or leucine (L), behaved as typical surfactant. The length of each peptide was ~ 2 nm, similar to that of biological phospholipids. Surfactant-like peptides, such as A_6D, V_6D, V_6D_2 and L_6D_2, interacted not only through packing of the hydrophobic tail, but also through intermolecular hydrogen bond formed along the backbone. These peptides formed nanotubes and nanovesicles with diameters ranging from 30 to 50 nm [182, 183].

Zhang *et al.* [182] also studied surfactant-like peptides which contained glycine (G) residues in the hydrophobic tail and aspartic acid (D) residues in hydrophilic head. Authors assumed that the peptides would form a bilayer similar to phospholipids to hide hydrophobic glycine tails from water molecules. They prepared four peptides: G_4D_2, G_6D_2, G_8D_2 and $G_{10}D_2$, and noticed that at neutral pH in water these peptides formed nanotubes and nanovesicles with the expected bilayer structure (Fig. 2.27). Results showed that G_4D_2 formed mostly nanotubes, G_6D_2 formed more vesicles and nanotubes similar to those of G_4D_2. G_8D_2 and $G_{10}D_2$ formed more entangled nanotubes with some globular aggregates. The length of glycine tail determined the structural morphology of the assemblies [182].

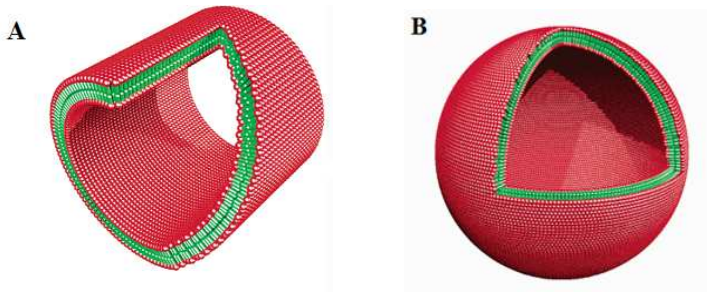

Figure 2.27: *Molecular models of nanotube (A) and nanovesicle (B) formed by surfactant-like peptides with negatively charged heads (in red) and glycine tails (in green) (adapted from [182])*

Stupp and Hartgerink [161] observed pH triggered assembly of a peptide amphiphile resulting in the fibrillar network. The peptides contained a long alkyl tail that made them hydrophobic, four consecutive cysteine residues that could be oxidised and form disulfide bridges to enhance structural stability of the assembly, a linker of three glycine residues, a single phosphorylated serine residue, and an RGD sequence to improve cell adhesion. The peptides self-assembled into a cylindrical structure, in which alkyl tails were hidden inside and the peptide segments were exposed on the surface. The cylindrical micelles were similar to fibrillar structures. They studied the mineralisation of the peptide fibres which formed a composite material that mimicked the lowest level of structural orientation between collagen and hydroxyapatite observed in bone. Furthermore, Stupp and Hartgerink [184] used the same peptide-amphiphile model and studied the effect of alkyl chain length and peptide sequence composition on the self-assembly and nanofiber morphology. The study included a family of peptide amphiphiles that self-assembled reversibly into nanofibers in response to change of pH. This occurred due to the presence of cysteine residue in the peptide sequence (Fig. 2.28).

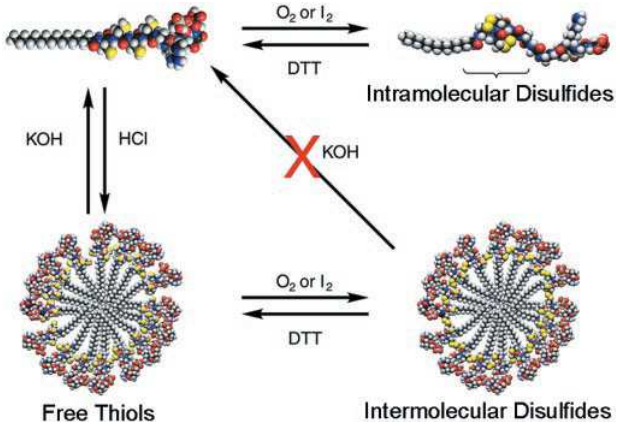

Figure 2.28: *Schematic representation of self-assembly of peptide-amphiphile upon acidification and intermolecular cross-linking upon oxidation. The processes are reversible upon pH increase and reduction of disulfide bridges (adapted from [184])*

Peptides self-assembled upon acidification and disassembled at neutral and basic pH. Oxidation of self-assembled nanofibers resulted in their increased structural stability due to intermolecular disulfide bonds. This crosslinked system was stable over a broad pH range.

2.3.2.4. Systems based on α-helical structure

As described before, the α-helix is one of the key secondary structures and is characterised by a single spiral chain of amino acids stabilised by hydrogen bonds. Woolfson *et al.* [185] have studied extensively the self-assembly of α-helical peptides. The majority of coiled-coil structures are based on the 7-residue (heptad) sequence repeat, **abcdefg**, where **a** and **d** are usually hydrophobic and the remaining residues tend to be polar. When folded, the **a** and **d** positions of such sequences align along one face of the helix making it amphipathic (Fig. 2.29). Two or more such amphipathic helices assemble through their hydrophobic faces to make the coiled-coil oligomer. Charged residues at **e** and **g**, which flank the **a/d** core, couple with an electrostatically-appropriate residue to form the hetero-oligomeric assemblies.

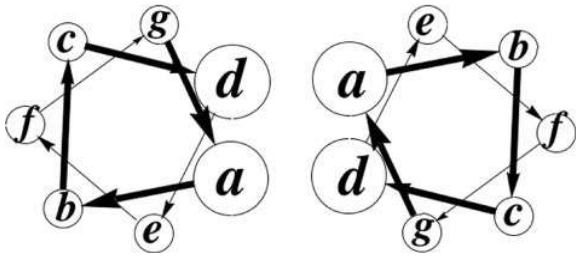

Figure 2.29: *Schematic representation of peptide heptades that adopt α-helical conformation.* ***a*** *and* ***d*** *positions are usually occupied by apolar residues, whereas other residues are polar (adapted from [185])*

In 1997, Kojima *et al.* [186] were the first to study the peptide that adopted α-helical conformation. They studied α_3-peptide that contained three repeats of the seven-residue sequence LETLAKA. They observed that at low salt concentration and at pH 6.0 many fibrils of 5 - 10 nm in width were formed. An increase in salt concentration resulted in the assembly of many filaments into larger fibres.

Woolfson *et al.* [187] studied two 28-residue self-assembling fiber (SFA) peptides SFA-p1 and SFA-p2 which had a staggered hydrophobic interface or "sticky end" in their structure. A peptide formed a coiled-coil interface with another peptide through this "sticky end" principle. Authors reported that the peptides SFA-p1 and SFA-p2 formed extended coiled-coil fibres.

Kajava *et al.* [188] also studied α-helical coiled-coil structures. They studied pH influence on the behaviour of α-helical fibril-forming peptide of 34 residues. They reported that, at slightly acidic pH values, it assembled into long fibrils of 2.5 nm in diameter. The fibrils were composed of five-stranded coiled coils as expected. At pH 7 spherical aggregate were formed. The authors reported that these gels could be used to encapsulate and to release bioactive molecules in a controlled fashion.

2.3.2.5. Systems based on aromatic interactions

Gazit *et al.* [189] studied aromatic dipeptide, dipehylalanine, that is known to be present in Alzheimer's β-amyloid peptide sequence. The dipeptide was dissolved in organic solvent and this solution was depositied onto siliconised glass. After solvent evaporation a highly ordered arrangement of vertically aligned nanotubes was observed (Fig. 2.30). Other diphenylalanine analogues showed similar behaviour and assembled in tubular structures [190]. Authors suggested that not only intermolecular hydrogen bonds were responsible for the self-assembly, but also π-π interactions of aromatic side chains, resulting in increased meachanical stability and strength of the nanotubular structure [189].

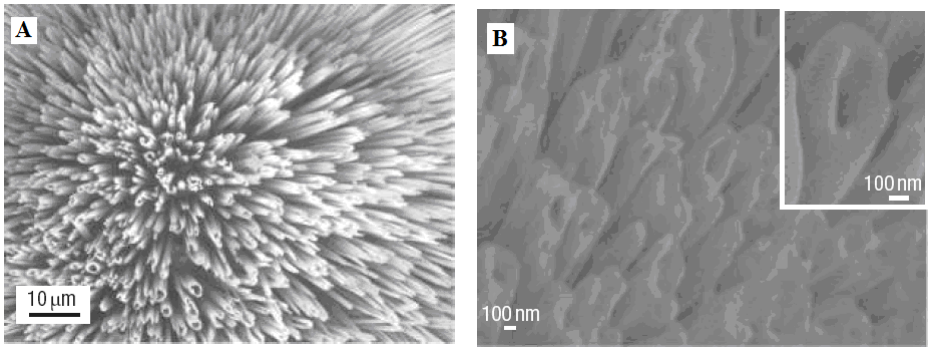

Figure 2.30: *SEM pictures of vertically aligned nanotubes of diphenylalanine (A) and high-resolution SEM revealed their open-ended structure (B) [190]*

One other aromatic dipeptide, diphenylglycine, was reported to form nanospherical assemblies [191]. When cysteine was introduced into diphenylalanine structure, the peptide formed spherical particles similar to those of diphenylglycine. Authors claimed that in this case the formation of the spherical structure was driven by disulfide bridges that drove the closure of the two-dimensional layer into more tightly packed spherical structure. These aromatic nanostructures showed excellent stability in acidic and alkaline conditions [191].

Ulijn *et al.* [150, 192, 193] extended the study on short aromatic self-assembling peptides. They introduced fluorenylmethoxycarbonyl (Fmoc), naphatlene or benzyloxycarbonyl groups at the N-terminus of di- and tripeptides. The results showed that the self-assembly was driven not only by antiparallel β-sheet forming peptides, but also by π-π stacking interactions of aromatic rings. Recently, the study of Fmoc-FF revealed that the peptides formed anti-parallel β-sheets with the Fmoc groups acting as a zipper to bring neighbouring sheets together. The neighbouring sheets were rotated in relation to one another because of the twist introduced by the β-sheet structure, thus creating a cylindrical structure [192]. They also showed that pH had an effect on the self-assembly of Fmoc-FF [194]. At high pH, an entangled network of flexible

fibrils was formed resulting in a weak gel, whereas at intermediate pH values flat, rigid ribbons were observed that did not entangle and hence did not form a gel.

2.3.3. Ionic-complementary peptides and their self-assembly

As described previously (see section 2.3.2) ionic-complementary peptides are characterised by an alternating arrangement of negatively and positively charged or uncharged amino acid residues. There are three types of charge distribution: Type I: -+; Type II: - - ++; Type III: - - - +++, and Type IV: - - - - ++++ [163].

In general, ionic-complementary peptides form β-sheets in water solutions, but random coil and β-α transitional structures are also found [155, 163, 167]. Peptides with short amino acids sequences usually form random coil structures but the peptides of type IV have propensity to undergo a β-α conformational change in response to temperature increase.

The first ionic-complementary peptide studied by Zhang *et al.* [164] was EAK16 that contained 16 alternating hydrophobic and hydrophilic amino acid residues. EAK16 had different molecular structure depending on charge alternation: EAK16-I, EAK16-II and EAK16-IV. This peptide formed β-sheets and further stable membrane-like structures when a salt was added. EAK16-II peptide is present in nature as a repeated segment in a yeast protein. Its structure is given in Fig. 2.31. It is seen from the structure of the peptide that β-sheets are stabilised by hydrogen bonding, hydrophobic and electrostatic interactions (Fig. 2.31A). Fig. 2.31B shows the self-assembly of the β-sheets in an anti-parallel manner.

The amino acid residues can be easily replaced by different residues, offering a wide range of primary sequences and leading to different self-assembled aggregates with various properties. For example, DAR16 peptide sequence can be easily obtained by replacing charged residues in EAK16 sequence.

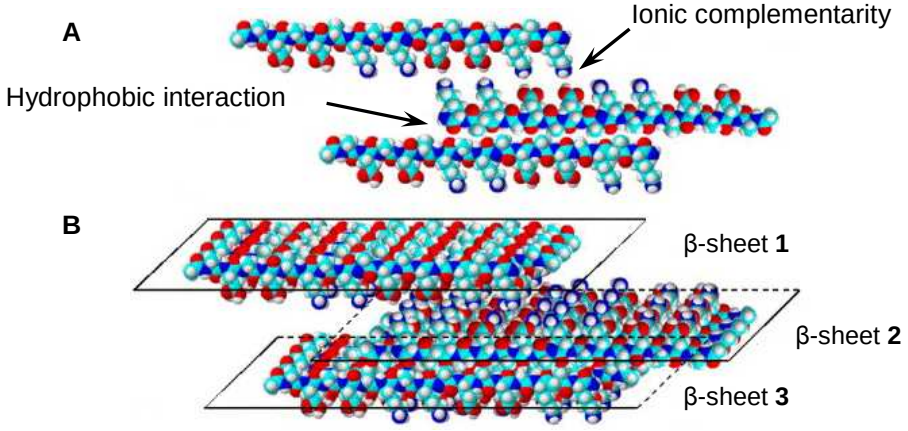

Figure 2.31: *Scheme of EAK16-II self-assembly through hydrophobic interactions and ionic complementarity (adapted from [164, 195])*

β-sheets formed by many ionic-complementary peptides are extremely stable under different physiological conditions and are impermeable to denaturing agents. Their stability can be explained by hydrogen bonds formed by peptide groups on the backbone itself, by interactions of charges residues via hydrogen and ionic bonds, and by hydrophobic interactions of nonpolar residues [195].

Saiani *et al.* [196, 197] and Nilsson *et al.* [198] developed self-assembling systems based on ionic-complementary octa-peptides. Saiani *et al.* studied four octa-peptides AEAEAKAK, AEAKAEAK, FEFEFKFK and FEFKFEFK. The self-assembly and gelation properties of theses peptides in water have been studied by Fourrier transform infrared spectroscopy (FTIR), transmission electron microscopy (TEM), atomic force microscopy (AFM) and small angle neutron scattering (SANS). No self-assembly was observed for AEAKAEAK. Only fibres of ~ 6 nm in radius were observed for AEAEAKAK which did not associate into a three dimensional (3D) network. This peptide formed α-helix rich fibres that did not form gel due to their rigidity. Thus no gelation was observed for AEAEAKAK. FEFKFEFK and FEFEFKFK peptides adopted β-sheet conformation as expected and formed gels at concentrations higher than 8 mg ml^{-1}. Below this concentration these peptides formed fibrillar structures with average radii of ~ 4 nm. Above 8 mg ml^{-1} the mesh size of the gel network varied between 15 and 30 nm depending on the gel concentration as determined by SANS [196].

β-sheet peptides can form different higher level hierarchical structures depending on their concentration. Aggeli *et al.* [199] reported two 11-residues long peptides P_{11}-I (CH_3CO-QQRQQQQQEQQ-NH_2) and P_{11}-II (CH_3CO-QQRFQWQFEQQ-NH_2) that adopted β-sheet secondary structure and assembled in one dimension into antiparallel β-sheet tapes, ribbons, fibrils and fibres (Fig. 2.32). The final structure was controlled by peptide and salt concentration. Peptide monomers self-assembled into tapes, two of which formed a ribbon. As the peptide concentration increased, higher level assemblies were possible, such as fibrils and fibres.

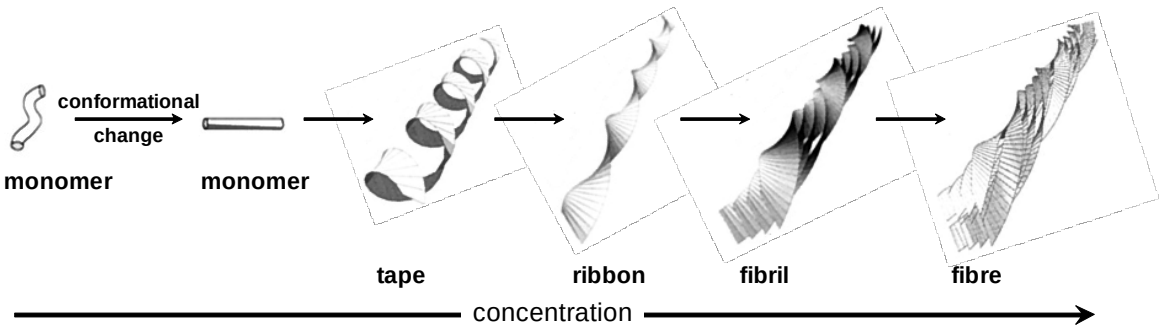

Figure 2.32: *Self-assembly of peptide tapes. Different structures can be formed depending on peptide concentration (adapted from [199])*

2.3.4. Different factors that affect self-assembly of ionic-complementary peptides

2.3.4.1. Peptide sequence effect

The amino acid sequence determines the structure and properties of the peptide and protein. Each amino acid has its own impact on the secondary structure which is influenced mainly by its hydrophilic and hydrophobic nature (see section 2.2.2) [200].

Hong *et al.* [201] reported that EAK16-II formed fibrillar assemblies at pH values between 4 and 11, whereas EAK16-IV formed globular nanostructures at near neutral pH (pH 6.5 – 7.5). At 7.5 < pH < 6.5 the peptide EAK16-IV formed fibrillar assemblies similar to those of EAK16-II. Regarding the mechanism for the self-assembly of these two peptides, Hong *et al.* stated that EAK16-II peptide first formed fibres that subsequently aggregated into fibrillar assemblies. At neutral pH hydrophobic sides of EAK16-IV were exposed to the solvent and then hydrophobic attraction took place, resulting in globular structures.

Dobson *et al.* [202] reported that at pH 2.6 KTVIIE formed β-sheet structures, whereas KTVLIE and KTVIYE formed random coil secondary structures (I - isoleucine, Y - tyrosine). The formation of the antiparallel β-sheets was determined by the ionic-complementarity between K and E residues and the hydrophobic interaction of the middle four residues. Leucine is less hydrophobic than isoleucine, therefore the interactions of antiparallel β-sheets of KTVLIE were weaker than of KTVIIE. Authors also assumed that tyrosine residue in KTVIYE might interact with the tyrosine residues of other peptides, forming β-sheet structure.

The team of Lauffenburger [203] studied the salt effect on the self-assembly of three 12-amino acid-long peptides ($(IKIE)_3$, $(FKFE)_3$ and $(VKVE)_3$)). They found that since the peptide self-assembly was driven by hydrophobic attraction of peptide side chains, the critical coagulation concentration decreased as the hydrophobicity of the peptide increased. The hydrophobicity of the residues increased in the following ranking: F < V < I.

Nilsson *et al.* [198] took $(FKFE)_2$ peptide as a model system to study the effect of aromatic and hydrophobic residues. They prepared $(FKFE)_2$ analogues in which they replaced F by other amino acid residues such as A, V, L, and cyclohexylalanine (Cha). Cha residue was more hydrophobic than F. Their results showed that the self-assembly of short amphiphilic peptides was not driven only by the interactions of aromatic residues but also by the hydrophobic interactions. Four of the peptides studied ($(FKFE)_2$, $(LKLE)_2$, $(VKVE)_2$ and $(ChaKChaEChaKChaE)_2$) self-assembled and formed fibres. $(AKAE)_2$ did not show self-assembly. These results were consistent with those observed by Saiani *et al.* [196].

Cha-containing peptide formed thinner fibres than F-containing peptide due to its hydrophobic nature and consequently rapid nucleation and elongation.

2.3.4.2. Concentration effect

The concentration dependence of peptide self-assembly is similar to that of surfactants. Below the critical aggregation concentration (CAC) the peptides would be in a form of dispersion, and at, or above, the CAC they would aggregate. As mentioned in section 2.3.3, concentration of β-sheet peptides influenced directly the formation of higher level structures.

Fung *et al.* [204] studied the effect of concentration on self-assembly of EAK16-II by different techniques, such as surface tension measurements, light scattering and atomic force microscopy (AFM). They stated that the nanostructure formation was concentration-dependent and proposed a model for self-assembly, which included two stages for fibre formation (Fig. 2.33). During the first stage, the peptide monomers self-assembled into protofibrils and this process depended on the peptide concentration. The protofibrils could be globular or filamentous, but in both structures β-sheets were present. Above the CAC of 0.1 mg ml^{-1}, the protofibrils associated into fibrils or larger globules. It was anticipated that small globules could align along the filaments, resulting in larger fibrils. Studies of EAK16-II peptide showed that an increase in concentration did not influence the width of fibrils, only their length. Hence, the fibrillar network became more dense.

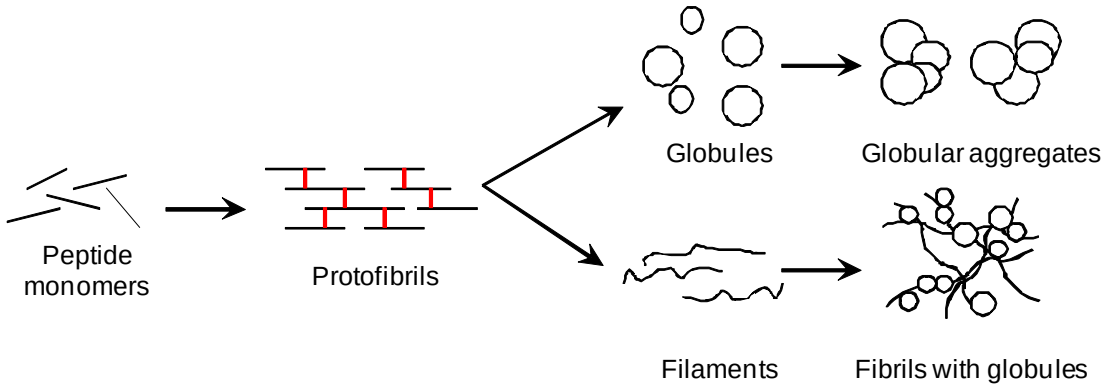

Figure 2.33: *Scheme of self-assembly of EAK16-II [204]. Red segments in the structure of protofibrils represent hydrogen bonds.*

The scheme in Fig. 2.33 is slightly different from that proposed by Saiani *et al.* (Fig. 2.34) [197].

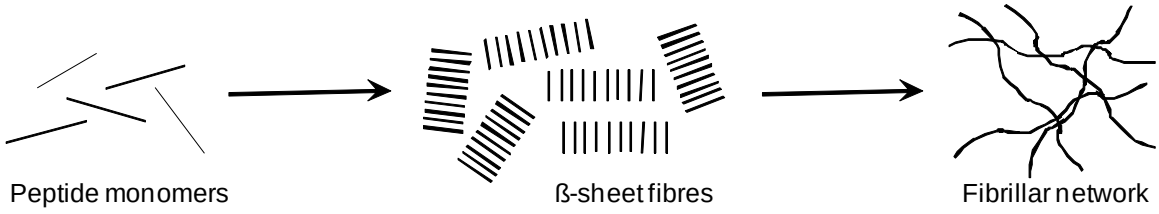

Figure 2.34: *Scheme of peptide self-assembling into fibrillar network [197]*

According to this scheme peptides started to self-assemble into β-sheet fibres once dissolved in water. Then these fibres started to grow in length when the concentration increased, forming a dense network of interwoven fibres. The fibre width was ~ 4 nm which was equal to the width of peptide in a stretched conformation. The self-assembly of ionic-complementary peptides is likely to occur according to scheme depicted in Fig. 2.34.

2.3.4.3. pH effect

pH is an important parameter when considering the use of peptides and proteins, since it can directly affect their ionisation state. When amino acids are charged, they can play a major role in the stabilisation of peptide and protein conformation through electrostatic interactions and hydrogen bonds.

Hong *et al.* [201] studied two peptides EAK16-II and EAK16-IV. They observed the changes in nanostructure with pH variation. It was found that EAK16-IV showed the propensity to form globular structures at pH 6.5 – 7.5 due to strong intramolecular electrostatic interaction. At pH values below 6.5 when most of the glutamic acid residues were neutralised and intramolecular electrostatic attractions were weakened, fibrillar structures were observed. Similar structures were detected at pH higher than 7.5 when most of the lysine residues were neutralised. In contrast, EAK16-II peptide formed fibrillar nanostructures in the pH range from 4 to 11.

In addition, Aggeli *et al.* [205] investigated the effect of pH on the assembly of the peptide QQRFQWQFEQQ (P_{11}-II). At pH < 5, when only arginine was positively charged, a gel was formed due to stabilisation of the fibrillar dispersion. At pH > 5, when both glutamic and arginine residues were charged, flocculation occurred due to electrostatic interactions of neighbouring charged residues.

WEAALAEALAEALAEHLAEALAEALEALAA peptide (GALA) [206] and its analogue, WEAKLAKALAKALAKHLAKALAKALKACEA peptide (KALA) [207] are other examples of pH-mediated systems. When the pH was lowered from 7 to 5 for solution of the GALA and when pH was increased from 5 to 7.5 for solution of the KALA, both peptides underwent conformational changes from a random coil to an amphipathic α-helix. In the case of the GALA peptide, electrostatic repulsions of glutamic acid residues destabilised the helical conformation at pH 7 (α-helices - 19%, β-sheets - 20%), whereas at pH 5 neutralisation of glutamic acid residues promoted α-helix formation (α-helices - 69%, β-sheets - 20%). In the case of the KALA peptide, when the pH was lowered from 8, seven lysine residues were positively charged and two glutamic acid residues were negatively charged. This promoted α-helical structure formation. When the pH decreased below 7, the histidine

residue became protonated and neutralised the negative charge of glutamic acid, thus increasing total positive charge of the peptide. This facilitated the disruption of α-helices. Thus, at pH 8.6 the content of α-helices was 51% and at pH 4.5 their content decreased to 41%.

As ionic-complementary peptides contain both negatively and positively charged residues, pH changes will have an effect on their self-assembly. This ability to change their secondary structure can be applied in drug delivery systems [208]. For example, it is known that the pH in tumour tissue is lower than in normal tissue [209] and this property can be used during the design of cancer targeted drug carriers. Namely, the drug vehicles can be loaded with bioactive molecules at neutral pHs and their release will occur selectively in acidic conditions.

2.3.4.4. Salt effect

Salt concentration and valency of the salt is known to influence the conformation, stability, solubility, activity, and self-assembly of biological molecules [210, 211]. Once present in a peptide solution, salt ions will screen the charge of the peptide, thus reducing the effect of the interactions between two molecules.

Lauffenburger *et al.* [203] studied the salt effect on the gelation properties of oligopeptides $(FKFE)_3$, $(IKIE)_3$ and $(VKVE)_3$. As discussed above the hydrophobic attraction of the hydrophobic peptide side chains was favourable for gel formation in comparison to the electrostatic repulsion between side chains. The effect of the electrostatic repulsion was diminished by adding salt. Thus, the critical coagulation concentration (CCC) was 0.1 – 0.5 mM of NaCl for $(IKIE)_3$; 0.1 – 1.0 mM of NaCl for $(FKFE)_3$, and 0.5 – 5.0 mM of NaCl for $(VKVE)_3$. Below CCC no gel was formed, whereas above it the oligopeptides self-assembled into β-sheet fibres.

de la Paz *et al.* [202] reported that the rate of formation of β-sheet rich fibrils from hexapeptide sequences increased with increasing ionic strength of NaCl up to 0.1 M. When the concentration of NaCl was higher than 0.1 M, they observed only the formation of short filaments and amorphous aggregates due to the screening of charge interactions.

Chen *et al.* [212] also studied the salt effect on the self-assembly of peptides. In the case of surfactants, salt decreased the CMC due to charge screening between head groups. In contrast, the critical self-assembly concentration of EAK16-I increased from 0.3 mg ml^{-1} in water to 0.8 mg ml^{-1} in the presence of 20 mM NaCl. The results showed that NaCl facilitated fibrillar structure formation.

Zhang *et al.* [164] reported that in the case of EAK16-II only monovalent cations caused the formation of larger-sized peptide self-assemblies. The formation of these assemblies

decreased with the decrease of hydrated radii in the following order $Li^+ > Na^+ > K^+ > Cs^+$. Authors stated that the divalent ions facilitated only the formation of disordered aggregates. Salts screened the charge, thus reducing electrostatic interaction and facilitating the formation of large size assemblies.

Schneider and Pochan [176, 177] reported in several papers that increased ionic strength triggered the folding of MAX1 and MAX8 peptides into β-hairpins and subsequent self-assembly of the β-hairpins into fibrillar structures. In this case salt screened the positive charges of the lysine residues and the peptides consequently changed their conformation.

2.3.5. Applications of self-assembling peptides

2.3.5.1. Tissue engineering

Many studies showed that self-assembling peptide gels could be used for cell culture and various cell lines could be used such as neuronal cells [160, 175], osteoblasts [213], human microvascular endothelial cells [214] and chrondrocytes [174]. Even neurite outgrowth and synapse formation was possible in these gels [160]. Peptide scaffolds are successful because they are highly biocompatible, biodegradable, possess good mechanical properties, and various biological functionalities can be introduced for successful cell adhesion, proliferation, and differentiation [215-226]. Some examples are discussed below in more detail.

The large self-assembled aggregates, formed by EAK16-II and RAD16-II, can be employed as scaffolds for growing mammalian cells such as mouse fibroblast, bovine aortic endothelial cells, human foreskin fibroblast and many others. These hydrogels showed excellent cell attachment and proliferation compared to conventional tissue culture dishes [158]. RAD16-I and RAD16-II hydrogels composed of interwoven fibrils proved to be applicable as substrates for neutrite outgrowth and synapse formation [160].

3D hydrogels of Ac-KLDLKLDLKLDL-$CONH_2$ (KLD12-I) were reported to be suitable for cartilage tissue repair [174]. Chrondrocytes readily proliferated in this gel forming a cartilage-like extracellular matrix (ECM), rich in proteoglycans and type II collagen.

RADA16 peptide was used as a 3D scaffold to prepare synthetic dermis by incubating human fibroblasts and synthetic skin was prepared by incubating human epidermal keratinocytes in layers. Results showed successful proliferation of human fibroblasts inside this peptide scaffold and secretion of type I collagen typical to natural dermal fibroblasts was detected [227].

Xie *et al.* [228] reported a new peptide scaffold by mixing two peptides RADA16 and RGDA16. Peptide RADA16 and the mixture of two peptides were used to study the attachment, spreading and proliferation of pre-osteoblasts. RGDA16 did not form a gel at

required concentration but did so when mixed with RADA16. The results showed that this new scaffold significantly promoted the initial attachment and proliferation of the cells compared to pure RADA16 scaffold. RGD sequence was recognised by the cells integrin receptors thus improving the proliferation [229].

2.3.5.2. Drug delivery

Drug delivery devices are designed to entrap the drug molecule in their structure either physically or chemically and to release the drug in a controlled fashion where and when appropriate. These drug carriers also protect the drug molecule from undesirable enzyme effects, thus maintaining drug activity over a prolonged period of time [159, 230]. The ability of peptide hydrogels to load and to release the drug can easily be tailored by changing the sequence of hydrophilic and hydrophobic residues.

Zhang *et al.* [231] used self-assembling peptide Ac-$(RADA)_4$-$CONH_2$ $(RADA)_4$ to create a hydrogel scaffold for controlled drug delivery applications. They encapsulated four different proteins including lysozyme, trypsin inhibitor, bovine serum albumine (BSA) and immunoglobulin G (IgG) within these gels and studied their release. The results showed an initial burst release of the protein through a 1% (wt./vol.) peptide hydrogel occurred within the first hour and then the release slowed until it reached a plateau. Authors demonstrated successfully that protein release through this gel depended on the protein size and the density of peptide fibrils. Densely packed network physically entrapped the molecules thus slowing their diffusion. IgG with the highest molecular weight showed the slowest release rate of all four proteins. Protein conformation and functionality was not affected by encapsulation and subsequent release.

Schneider *et al.* [232] showed that their MAX1 and MAX8 hydrogels could also encapsulate and subsequently release biomolecules. They used dextran molecules and the protein lactoferin as model drugs and found that their release depended on the hydrogel mesh size and electrostatic interaction between the hydrogel network and the molecules. In more concentrated gels with smaller mesh size the mobility of probes became hindered. The mesh size could be controlled by peptide concentration and peptide sequence. Since MAX1 (+9) was more electropositive than MAX8 (+7), negatively charged dextrans interacted more with MAX1 fibrillar network than with MAX8, consequently their diffusion was restricted. In contrast, positively charged protein lactoferin was released more quickly than dextrans due to electrostatic repulsions from the peptide network.

Davis *et al.* [233] reported another example of successful application of self-assembling peptide in drug delivery. They created biotinylated RAD16-II hydrogels for specific and

controlled delivery of insulin-like growth factor 1 (IGF-1) to the myocardial microenvironment. The possibility of IGF-1 delivery could improve cells therapy after myocardial infarction.

2.3.6. Summary

This section introduced self-assembling systems with an emphasis on peptide self-assembly. Different classes of peptides that undergo self-assembly were discussed. Specifically, ionic complementary peptides were discussed in more detail as they were more relevant to this research. Results of numerous investigations suggested that peptide self-assembly depended on various factors, either structural or chemical. These factors need to be taken into consideration when designing and studying these peptides. It was shown that the peptide self-assembling systems possess a lot of potential to be employed in tissue regeneration and controlled drug delivery.

2.4. CONJUGATES OF POLYMERS AND PEPTIDES

2.4.1. Introduction

Over the past decades polymeric materials have gained a lot of interest in the fields of drug delivery, regenerative medicine and tissue engineering due to their biocompatibility and suitable mechanical properties. Conjugates of polymers with peptides or proteins represent a large group of these materials. Börner *et al.* [234, 235], Kiick *et al.* [236], Maynard *et al.* [237] as well as Klok *et al.* [238, 239] have published excellent reviews on the latest achievements in the synthesis and applications of the conjugates. Section 2.4 does not pretend to be exhaustive, but aims to familiarise the reader with the subject.

Conjugation involves the covalent linking of two or more molecules to form a new complex that will combine the characteristic properties and functions of its individual components. Usually peptides or proteins (peptidic drugs, enzymes) are linked to synthetic polymers and these materials are also called hybrid materials. Peptidic drug conjugation to a polymer offers many advantages, such as improvement of drug solubility via its conjugation to a hydrophilic polymer; drug protection from degradation and interactions with enzymes and antibodies, hence increased stability. Also drug circulation times can be increased after the drug conjugation to the polymer, hence ensuring the prolonged drug activity [236, 239]. Conjugation or cross-linking is also used to introduce various detectable groups to study protein interactions and structure. This opens a large area for therapeutic design. Moreover, the polymer backbone also brings responsive and tunable properties allowing targeted and controlled drug release by changing temperature, pH, or enzyme concentration [236, 237]. This will be discussed later in further detail.

2.4.2. Polymer-peptide conjugation strategies

The synthesis of the first conjugate goes back to 1954 when Jatzkewitz combined the pre-synthesised glycyl-L-leucyl-mescaline (mescaline - naturally occurring alkaloid) with the copolymer of *N*-vinyl-α-pyrrolidinone and methyl acrylate. The conjugate was created to improve drug efficiency and the drug was cleaved from the polymer by an enzyme [240]. In 1977, Abuchowski *et al.* reported another example of a polymer-protein conjugate which was obtained by PEGylation (PEG – poly(ethylene glycol)) of bovine serum albumin (BSA). PEG groups and protein molecules were chemically linked via 2,4,6-trichloro-*s*-triazine. The conjugates were administered into rabbits intravenously and intramuscularly. The results showed that PEG proved to hide the protein from recognition by the immune system, thus prolonging its effect [241].

The synthesis of peptide or protein can be achieved using one of the following routes. Peptides or proteins can be obtained via α-amino acid *N*-carboxyanhydride ring-opening polymerisation, solid phase peptide synthesis (SPPS) or protein biosynthesis. Several polymer and peptide/protein conjugation strategies are presented in Fig. 2.35.

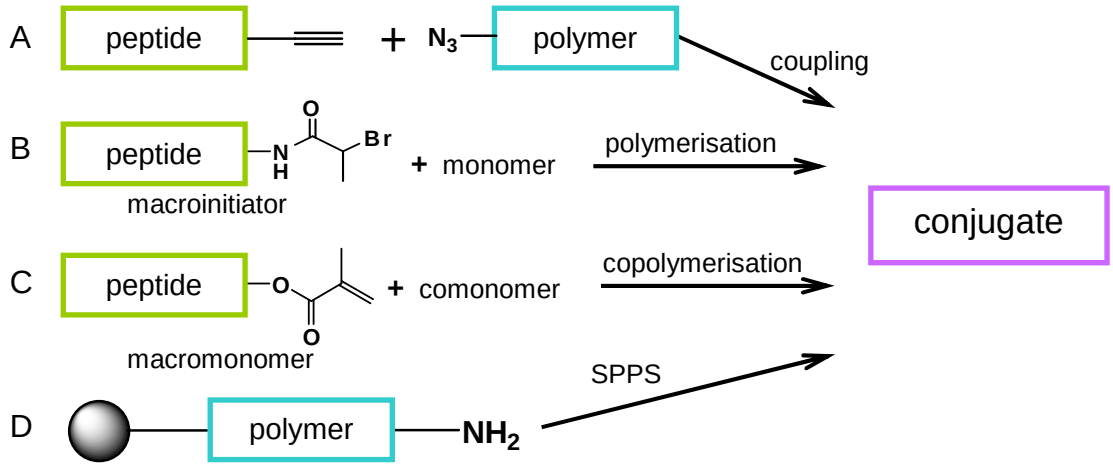

Figure 2.35: *Scheme of various conjugation strategies*

Conjugates can be synthesised in either a convergent or divergent way. In the convergent way (Fig. 2.35A) both the polymer and peptide components are pre-synthesised and then coupled together. This method is also called cross-linking where coupling reagents with different reactive groups are used to link two molecules together. In the divergent method (Fig. 2.35 B to D) the conjugates are obtained either via polymerisation of monomers using a peptide macroinitiator, by peptide synthesis on a solid support that contains a polymer, or from polymers in solution [238, 239]. Modern synthetic techniques such as atom transfer radical polymerisation (ATRP), reverse addition-fragmentation chain-transfer (RAFT) polymerisation or "click" chemistries have been extremely useful for conjugate preparation as they offer many advantages in terms of controlled molecular weight, different architectures and functionalities in comparison to the conventional FRP.

2.4.2.1. Convergent conjugation methods

In this section, some of the classical convergent conjugation methods are described. A comprehensive guide for convergent conjugation methods can be found in the review of Klok *et al.* [238].

Peptides may be conjugated to the polymer chain end or pendant groups via the chemical reaction between their functional groups. The functional groups can be introduced to the polymer via ATRP, RAFT or copolymerisation [242]. Peptides contain the following functional groups appropriate for bioconjugation:

- **primary amine (-NH_2)** – the group is present in each peptide/protein as the N-terminus, as well as in the side chain, for example in lysine (K)
- **carboxyl group (-COOH)** - the group is present in each peptide/protein as C-terminus, as well as in the side chain of aspartic acid (N) and glutamic acid (E)
- **sulfhydryl group (-SH)** – the group is present in the side chain of cysteine (C)
- **carbonyl group (-CHO)** – the group can be formed as a result of polysaccharide oxidation in glycoproteids.

These functional groups of amino acid residues and polymers can also be modified following classical organic chemistry methods [243]. The choice of an appropriate modification will depend on the type of amino acid residues or functional group subjected to coupling.

Typically, the peptide is conjugated to the polymer using the cross-linker, reagent that links the functional group of the peptide with the functional group of the polymer [244]. If there are two or more reactive sites on the polymer, it can be conjugated more than once to the same protein molecule or to several protein molecules. The cross-linkers vary in length and they can be hydrolitycally or enzymatically degradable, or can contain reducible disulfide groups that ensure controlled release of the conjugated protein.

One limitation of the convergent approach, however, is that sometimes the functional groups of large macromolecules may not be accessible for coupling, thus reducing conversion rates and product isolation.

2.4.2.1.1. Amine-reactive polymers

Here, various ways to obtain amine-reactive polymers will be presented. Different post-polymerisation modification strategies exist that offer a great variety of conjugation possibilities. Amine reactive groups can be obtained easily using the reactions outlined in Fig. 2.36. Initially hydroxyl group modification reactions were used for the modification of the hydroxyl groups of PEG to enable them to react with amines. Peptide modification with PEG or PEGylation is widely used for conjugates preparation owing to its biocompatibility, high solubility, and chain flexibility [245, 246]. The terminal hydroxyl group of PEG can be transformed in different ways and these reactions are also applicable for other polymers with hydroxyl end-groups. Some examples of the hydroxyl group modification reactions are given in Fig. 2.36. In Fig. 2.36A the hydroxyl group of PEG reacted with one chlorine of 2,4,6-trichloro-*s*-triazine and then, the amine group of the protein reacted with second chlorine. Following this procedure PEG was linked to bovine serum albumin (BSA) [241] and bovine liver catalase [247].

Fig. 2.36B shows the example of the formation of thioimidoester end-group that can react with amine groups such as in the side chains of lysine, forming amidinated linkages. Using this reaction, ribosome inactivating protein gelonin was coupled to PEG. Protein retained the positive charge after the conjugation, thus maintaining its biological activity [248].

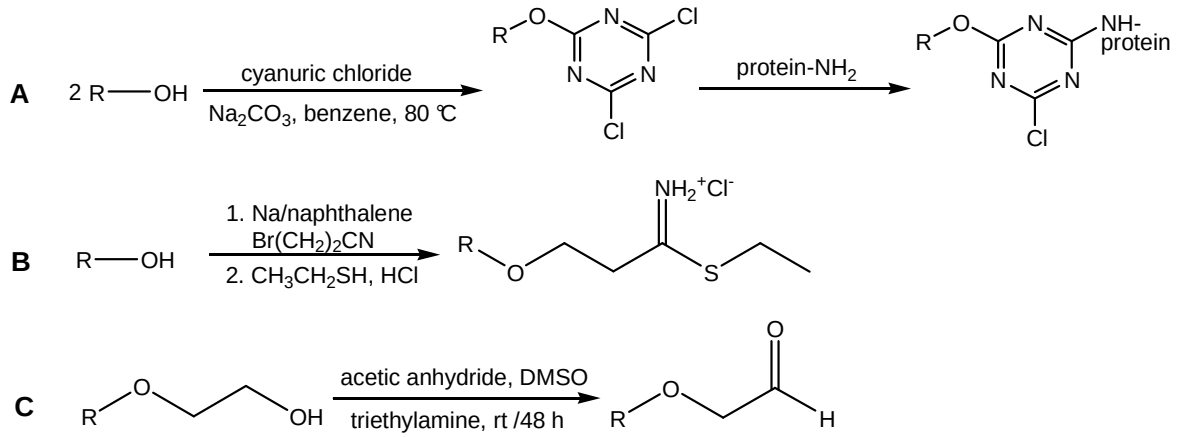

Figure 2.36: *Different ways to obtain amine-reactive polymers via: A) dichlorotriazine formation, B) thioimidoester formation, C) aldehyde formation*

Fig. 2.36C shows the formation of aldehyde group via Moffatt oxidation [249, 250]. Aldehyde-functionalised PEG was coupled to the glycoprotein CD4-IgG (CD4 is the primary receptor for human deficiency virus type I and IgG is immunogammaglobulin) via amine groups of lysine residues. The coupling ensured its prolonged circulation time [249]. Heterogeneous bioconjugates could also form due to the non-specific coupling with multiple and random lysine residues. However, the conjugates retained their biological activity [250].

Stable amide bond formation between two molecules is also possible via the formation of intermediate active esters, for example *N*-hydroxysuccinimidyl (NHS) esters. Figure 2.37 presents the typical reaction scheme for the formation of an amide bond through the formation of an active ester. Active *N*-hydroxysuccinimidyl (NHS) ester can be obtained via the reaction of the carboxyl group of the polymer with NHS and carbodiimide [251]. This strategy was used to prepare PNIPAAm-trypsin conjugates [252].

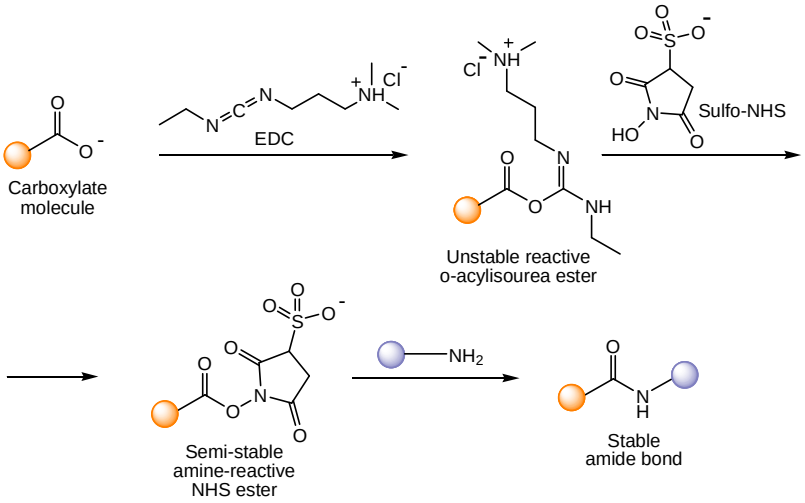

Figure 2.37: *Amide bond formation reaction via active sulfo-NHS ester formation*

One other example shows the incorporation of the *N*-hydroxysucinimide group into a copolymer structure and then its linking with the amine group of the desired peptide/protein. Nguyen and Luong [253] prepared copolymers of PNIPAAm with *N*-acryloyloxysuccinimide (NASI) and glycidyl methacrylate (GMA) and made them react with amino groups of proteins. A trypsin inhibitor, *p*-aminobenzamidine, was attached to the polymer and trypsin was separated selectively from the trypsin-chymotrypsin mixture. Also PNIPAAm-GDA reacted with IgG and alkaline phosphotase (AP). IgG selectively bound to protein A and precipitated upon heating. AP retained its activity after conjugation. Chen and coworkers [254] studied a similar system. They prepared a copolymer of PNIPAAm and *N*-acryloxysuccinimide (NASI) that was later conjugated with protein A (major component of the cell wall of certain strains of *Staphylococcus aureus*) (Fig. 2.38) via the primary amine groups of the lysine residue in protein A. Human immunogammaglobulin formed the complex with this conjugate and precipitated upon heating (> 32°C) thus enabling its separation from the protein mixture.

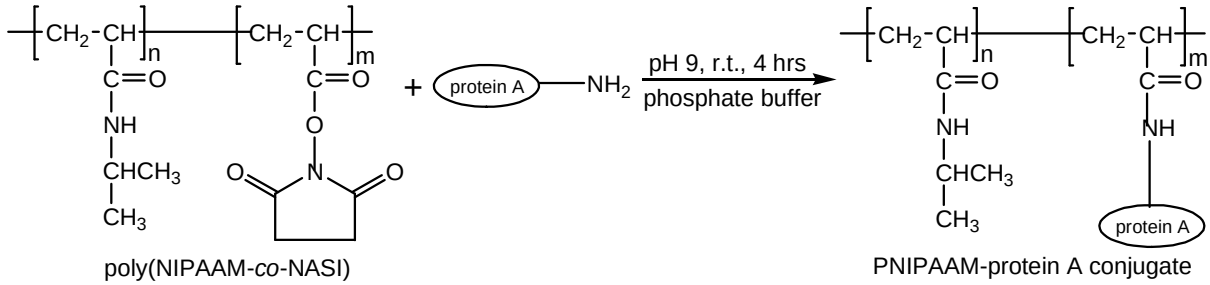

Figure 2.38: *Conjugation of poly(NIPAAm-co-NASI) with protein A*

Hatti-Kaul *et al.* [255] conjugated trypsin to PNIPAAm through *N*-acryloxysuccinimide (NASI) reactive groups. The conjugated enzyme exhibited higher heat stability in comparison to the free enzyme. The authors claimed that the enzyme stability was enhanced due to the enzyme multipoint attachment to the copolymer and not due to the presence of polymer.

Takei *et al.* [16] prepared COOH-end-functionalised PNIPAAm using 3-mercaptopropionic acid (MPA) as a chain-transfer agent. PNIPAAm then was grafted onto collagen using active ester formation with NHS and dicyclohexylcarbodiimide (DCC). The phase separation and precipitation occurred at 34°C enabling easy separation of the conjugates. Pişkin *et al.* [256] copolymerised NIPAAm with acrylic acid (AAc) and subsequently conjugated the polymer via the carboxyl group of AAc with the amine group of monoalanine, dialanine and trialanine using water-soluble carbodiimide. Alanine (A) residue was COOH-protected with methylester group which was hydrolysed with KOH solution to form the carboxylic group prior to conjugation. The LCST of poly(NIPAAm-co-AAc) increased in comparison with pure PNIPAAm (Table 2.3). When the pH increased, carboxylic acid groups of AAc became ionised. This made the copolymer more hydrophilic and hence the LCST increased. At pH 4.0 the LCST was 37.7 ± 0.5°C, at pH 7.4 the LCST was > 60°C. The LCST increased with the increase of the number of conjugated amino acids as more peptide bonds were formed [256].

Table 2.3: *LCST of PNIPAAm, its copolymer with AAc and conjugates with alanine (A) [256]*

Polymer, conjugates	LCST at pH 4.0 (°C)	LCST at 7.4 (°C)
PNIPAAm	29.9	28.7
Poly(NIPAAmco-AAc)	37.7 ± 0.5	> 60
A-OCH_3 conjugate	35.1 ± 0.4	41.6 ± 0.3
AA-OCH_3 conjugate	43.3 ± 0.1	46.2 ± 0.3
AAA-OCH_3 conjugate	45.8 ± 0.3	> 60

2.4.2.1.2. Thiol-reactive polymers

Many peptides contain cysteine residues, therefore it is important to synthesise thiol-reactive polymers. Thiol-reactive end-groups include vinyl sulfone, maleimide, and functionalised disulfide end-groups.

Hoffman, Stayton *et al.* reported the first results on responsive polymer bioconjugates [242, 257-259]. They reported α-hydroxyl-functionalised PNIPAAm prepared by FRP with AIBN as the initiator and β-mercaptoethanol as the chain-transfer agent. The α-hydroxyl group was subsequently converted to the vinyl sulfone through coupling with divinyl sulfone in the presence of base (Fig. 2.39) [257]. This synthetic route enabled the conjugation of the streptavidin to the polymer. It was possible to bind biotin to streptavidin below the LCST and its binding activity dropped sharply above the LCST, when the polymer formed globules and hided streptavidin active sites.

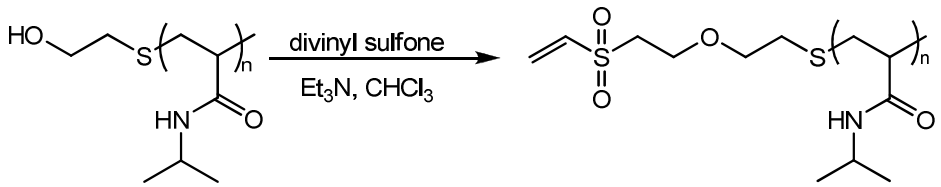

Figure 2.39: *Synthesis of vinyl sulfone end-functionalised PNIPAAm*

Velonia *et al.* [260] reported that synthesis of maleimide end-functionalised polystyrene (PS) can be performed in two steps: reaction of the polymer terminal carboxyl group with $SOCl_2$, and then maleimide addition in the presence of base (Fig. 2.40). Lipase B (CAL B) was coupled to PS via this modification. The conjugate molecule possessed amphiphilic nature and in the solvent mixture of tetrahydrofuran and water assembled into fibres of 25 – 30 nm in diameter.

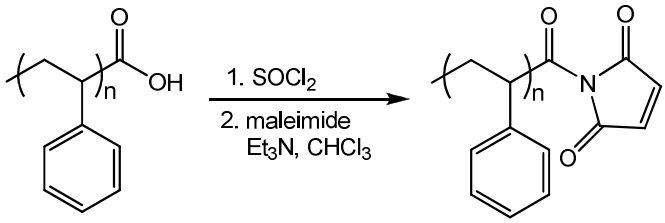

Figure 2.40: *Synthesis of maleimide end-functionalised polystyrene*

Chilkoti *et al.* [261] reported the synthesis of PNIPAAm by FRP with 2-aminoethanethiol as the chain-transfer agent. This was then coupled with a NHS-activated maleimide derivative to form α-maleimide PNIPAAm that was used for the modification of the protein cytochrome b5.

Polymers with pyridyl, alkoxycarbonyl and *o*-nitrophenyl disulfide end-groups form peptide-polymer conjugates *via* disulfide bridge formation. The advantage of this strategy was the reversibility of the protein conjugation because it could be released under reducing conditions. Li *et al.* reported the synthesis of an α,ω-pyridyl disulfide functionalised Pluronic® (PEG-*b*-poly(propylene oxide)-*b*-PEG) for protein immobilisation on a surface (Fig. 2.41). The functionalised Pluronic® was adsorbed onto a polystyrene resin, thus allowing the immobilisation of β-galactosidase [262].

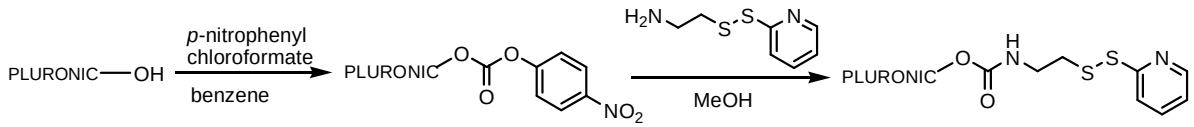

Figure 2.41: *Synthesis of a,ω-pyridyl disulfide activated Pluronic*

Smeenk *et al.* [263] synthesised a triblock copolymer with PEG end-blocks and the central block of the β-sheet forming polypeptide $[(AG)_3EG]_n$ (AG – alanylglycine, EG – glutamylglycine; n = 10, 20). The central block contained cysteine residues at both ends which reacted with maleimides from PEG, thus linking PEGs to the peptide. Both conjugates PEG-$[(AG)_3EG]_{20}$-PEG and PEG-$[(AG)_3EG]_{10}$-PEG formed fibrillar structures with 12 nm wide fibres in the first case and smaller width in the later case due to the shorter peptide block.

2.4.2.1.3. Oxime formation

Oxime formation between a hydroxylamine and a ketone/aldehyde-functionalised polymer or peptide is another method to form site-specific conjugates (Fig. 2.42). Aminooxy or ketone functionalities can also be introduced into a peptide.

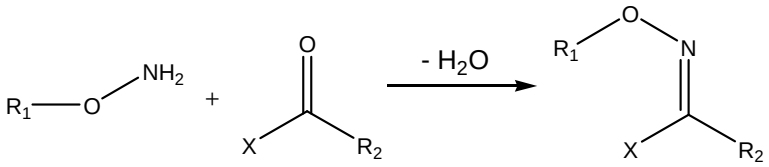

Figure 2.42: *Oxime formation*

Using this method Kochendoerfer *et al.* prepared the conjugate of the protein chemokine ((C-C motif) ligand 5 (CCL-5), responsible for the sending the leukocytes to inflammatory sites, with an aldehyde end-functionalised linear PEG (Fig. 2.43) [264]. This conjugate was reported as anti-HIV protein derivative. HIV uses CCR-5 receptors to enter cells and PEG-CCL-5 showed the ability to bind to CCR-5 receptor and block the virus. The conjugate also showed prolonged *in vivo* circulation in rats [265].

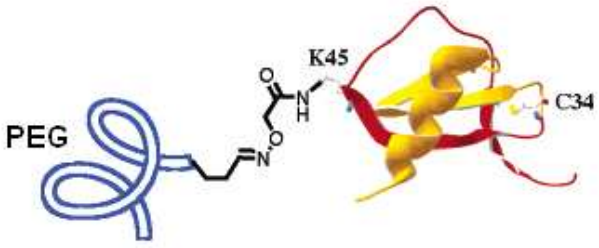

Figure 2.43: *Synthesis of the PEG modified CCL-5 via oxime formation (adapted from [264])*

2.4.2.1.4. Conjugate formation via cycloaddition

Azide-alkyne 1,3-dipolar cycloaddition offers another fast and efficient way to obtain bioconjugates (Fig. 2.44). This reaction is within the concept known as "click" chemistry introduced by Sharpless *et al.* [266] and relies on the quick and selective reaction between relatively small units. The reaction conditions are mild and the product is obtained in high

yields. The peptide to be conjugated should be modified with an azide or alkyne moiety before the conjugation reaction. The conjugate of an azide-terminated PS and alkyne-functionalised bovine serum albumin (BSA) was obtained successfully using the [3 + 2] cycloaddition as outlined in Fig. 2.44 [267].

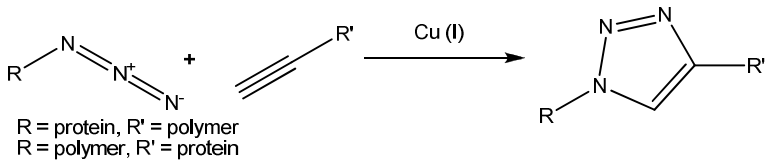

Figure 2.44: *Bioconjugate formation via [3+2] cycloaddition*

2.4.2.1.5. Ligand-modified polymers

One other approach is to use polymers containing ligand end-groups such as biotin (vitamin H) that can bind to avidin or streptavidin. Therefore biotinylated stimuli-responsive polymers have been synthesised with the perspective to be conjugated with avidin or streptavidin. Kulkarni *et al.* [268] reported the conjugates of PNIPAAm with streptavidin and biotin. As outlined in Fig. 2.45, below the LCST PNIPAAm was hydrophilic and the conjugate was also soluble. Above the LCST the aggregation of the conjugate into particles occurred due to the hydrophobic nature of PNIPAAm.

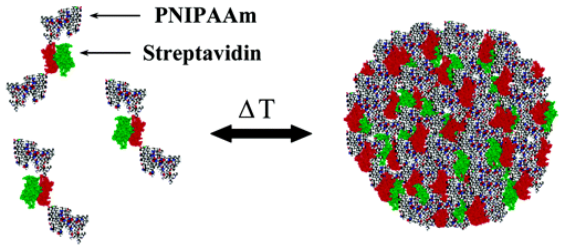

Figure 2.45: *Formation of PNIPAAm-streptavidin thermo-responsive nanoparticles (adapted from [268])*

Particles were stabilised by charged and hydrophilic streptavidin, thus preventing further aggregation. The results showed that particles with the size of 250 – 900 nm were obtained, depending on conjugate concentration, polymer molecular weight and also rate of temperature change. On the contrary, conjugates with biotin showed continuous aggregation over the same time period (16 h). Streptavidin-functionalised particles can selectively attach to biotinylated antibodies, thus enabling their isolation.

2.4.2.2. Divergent conjugation

In divergent conjugation the conjugates are obtained via polymerisation using peptide macroinitiators, peptide macromonomers or conventional SPPS.

2.4.2.2.1. Polymerisation from a peptide

Polymerisation from a peptide is one of the most straightforward conjugate synthesis strategies. It involves modification of a peptide with chemical groups that can initiate polymerisation, hence the peptide becomes a polymerisation initiator [29, 234]. Direct polymerisation from the peptide offers an advantage of simplified purification of the bioconjugate from the unreacted monomer or catalyst. At the same time polymerisation can be affected by other functional groups of the peptide.

Maynard *et al.* [269] used the high reactivity of streptavidin towards biotin to create a macroninitiator, which was later employed in ATRP of 2-hydroxyethyl methacrylate (Fig. 2.46). This approach can also be applied to other monomers. For example, conjugates of poly(ethylene glycol) methyl ether methacrylate were also reported. The results showed that the polymerisation reaction did not affect streptavidin activity.

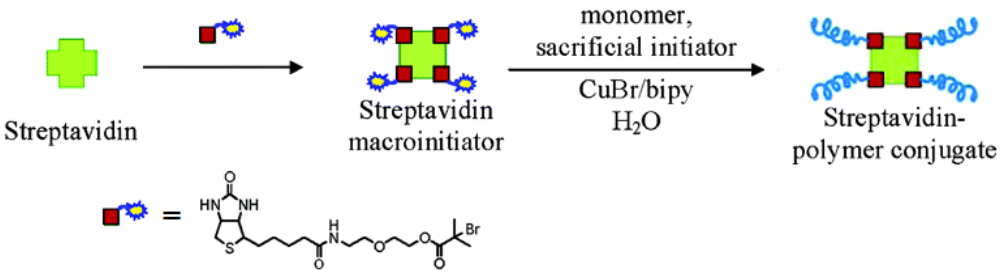

Figure 2.46: *PNIPAAm polymerisation from streptavidin macroinitiator (adapted from [269])*

Heredia *et al.* [270] reported the synthesis of bovine serum albumin (BSA) and T4 lysozyme-PNIPAAm conjugates *in situ*. Free cysteines, Cys-34 of BSA and Cys-131 of T4 lysozyme V131C, were modified with initiators for ATRP (Fig. 2.47). Polymerisation of NIPAAm from the protein macroinitiators resulted in thermo-responsive conjugates BSA-PNIPAAm and lysozyme-PNIPAAm with yields greater than 65%. Maynard *et al.* [271] also reported thermo-responsive conjugates of PNIPAAm with streptavidin and of PNIPAAm with BSA using ATRP.

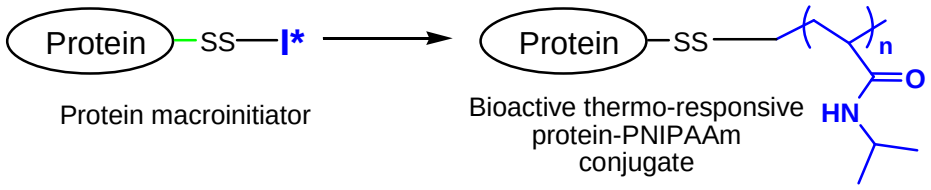

Figure 2.47: *ATRP polymerisation of NIPAAm from the protein macroinitiator [270]*

The functional groups of ovalbumin [272], casein [273] and gelatine [274] have been used for preparing the graft-copolymers. The polymerisation was initiated with ceric ions, benzoyl peroxide and potassium persulfate accordingly. The conjugated materials were not well-defined because of the grafting of the polymers at random and multiple sites of the protein, for example, polydispersity of acrylonitrile-grafted-casein copolymers varied between 2.6 and 4.5 [273].

During the conjugation process the protein activity could decrease due to some properties of the conjugated polymer, such as molecular weight, length, volume, and its closeness to the active site of the protein [1, 237].

One other example of the divergent conjugation strategy is conjugate formation in the solid state. In this case the peptide is formed via SPPS and then functionalised with a group that can initiate ATRP of a monomer. Following this procedure Washburn *et al.* [275] prepared the conjugate of GRGDS peptide with 2-hydroxyethyl methacrylate (HEMA). They also showed that incorporation of the RGD sequence promoted fibroblasts adhesion and proliferation in cell culture experiments, whereas PHEMA polymer on its own did not show such an effect. RGD sequence was recognised by cell receptors, thus promoting cell proliferation [229].

Lynn *et al.* reported a conjugation method in which a PEG segment was coupled to the solid support and the peptide was grown from the PEG using SPPS [276]. They studied the properties of a dilute solution of a diblock copolymer of amyloid peptide and PEG. TEM studies revealed that these aggregates formed long fibrils separated from each other, as the PEG hid the peptide hydrophobic domains and reduced the association of the fibrils. This was an important finding, contributing to the development of the strategies to prevent fibrilogenesis, which was typical to the symptoms of Alzheimer's disease.

In summary, a great variety of chemical reactions are available for the conjugation of the polymer with the peptide. These reactions can be convergent and divergent. The choice of the conjugation strategy depends on the polymer and peptide functional groups and also polymer and peptide individual characteristics.

2.4.3. Self-assembly of polymer-peptide conjugates

As mentioned previously, polymer-peptide conjugates combine the characteristics of synthetic polymers, such as solubility, ability to include various functionalities, with those of peptides, such as secondary structure, ability to change reversibly the structure in response to stimuli (pH, temperature, ionic strength), biocompatibility and biofunctionality. In aqueous

solutions polymer-peptide conjugates typically self-assemble into different stimuli-responsive structures, for example, micelles, vesicles or hydrogels composed of β-sheet fibres, owing to their amphiphilic nature. Lecommandoux and Carlsen [128] published a comprehensive review on self-assembly of polypeptide-based block copolymer amphiphiles.

If the peptide segment shows greater hydrophilicity to the solvent than the polymer, the micelles with polymer inner core and peptide outer shell are formed. An example of this system was reported by Lecommandoux *et al.* [277]. They studied the self-assembly of polyisoprene-*b*-poly(L-lysine) block copolymer (PI-*b*-PLLys) in aqueous media as a function of pH. The block-copolymer assembled into spherical micelles with a hydrophobic PI core and hydrophilic corona of PLLys. In acidic conditions PLLys was charged and adopted a coiled conformation, resulting in larger micelles. In basic conditions, the transition from a coil conformation to α-helical conformation occurred and the micelles shrank. Klok *et al.* [278] studied a similar system: polystyrene-*b*-poly(L-lysine) (PS-*b*-PLLys) block copolymer. SANS and static light scattering (SLS) results confirmed the formation of cylindrical micelles with a hydrophobic core of PS and hydrophilic shell.

When the polymer segment shows greater affinity to the solvent than the peptide segment, micelles with a polypeptide core and polymer shell are formed. To illustrate this, Zhang *et al.* [279] reported the effect of pH on the self-assembly of copolymer poly(*N*-isopropylacrylamide)-*b*-poly(L-glutamic acid-*co*-L-lysine) (PNIPAAm(PLG-*co*-PLLys)). They observed that at pH < 6 and pH > 10 the copolymer was soluble in aqueous solution, due to the protonated lysine residues and negatively charged glutamic acid residues respectively (Fig. 2.48). In the pH range from 6 to 10, glutamic acid and lysine residues were partially protonated and deprotonated respectively and charged peptide-peptide interactions were facilitated. Clear solution turned to opaque due to the formation of compact aggregates. Copolymer chains self-assembled into particles of 300 – 800 nm in diameter with aggregated polypeptide chains into the core.

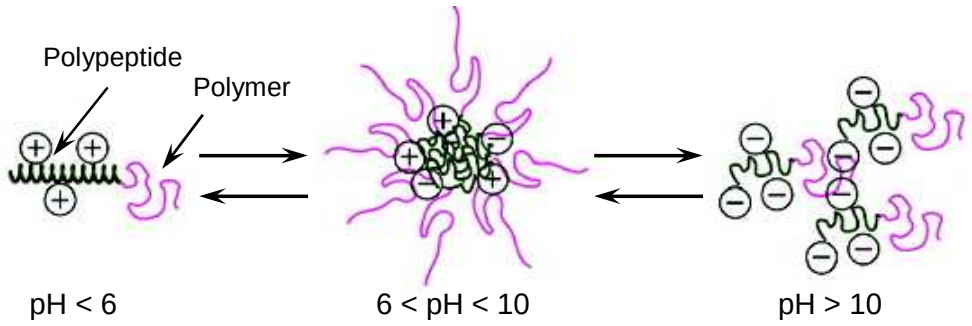

Figure 2.48: *Schematic representation of different structures of copolymer PNIPAAm(PLG-co-PLLys) at different pH (adapted from [279])*

Amphiphilic block copolymers also form vesicles or fluid-filled sacs [280]. An example of this behaviour was reported by Lin *et al.* [281]. They studied the self-assembly of poly(L-glutamic acid)-*b*-poly(propylene oxide)-*b*-poly(L-glutamic acid) (PLGA-*b*-PPO-*b*-PLGA) triblock copolymer in aqueous solution. Lin *et al.* observed that vesicles were formed in acidic conditions when PLGA was in helical conformation and also when the length of PLGA block decreased. The walls of the vesicles were formed by PPO and the inner layer by PLGA chains. In contrast, basic conditions or longer PLGA chains facilitated the formation of spherical micelles with PPO in the core and PLGA in its corona. These vesicles showed great potential to be used as drug vehicles in controlled drug delivery.

Cornelissen *et al.* [282] reported the self-assembly behaviour of conjugate composed of a short peptide GGR and hetero-telechelic polystyrene (PS) which was obtained *via* copper-catalysed azide-alkyne 1,3-dipolar cycloaddition, or simply "click" chemistry. Self-assembly was triggered in two ways: by injecting THF solution into water or by dialysing THF solution against water. Spherical aggregates were obtained by both methods. After a closer examination of the aggregates, the researchers concluded that conjugates assembled into vesicles, which could accommodate bioactive molecules into their core and used in diagnostics.

Kopeček *et al.* [283] observed gel formation by mixing synthetic His-tagged coiled coils with the copolymer of *N*-(2-hydroxypropyl)methacrylamide (HPMAAm) and *N*-(*N*′,*N*′-dicarboxymethylaminopropyl)methacrylamide (DAMAAm) and nickel(II) sulphate. The metal complex formed between terminal histidines and pendant acetate groups of the copolymer, thus linking them together. The coiled coil proteins self-assembled into superhelical quaternary structures, which lead to the formation of a non-covalent network. Upon heating from 25 to 70ºC the system collapsed due to unfolding of the coiled coil proteins. The transition was not reversible during 48 h. Authors proposed that several peptides, having coiled coil conformation and different protein unfolding temperatures, could be used to create a system with step-like transitions.

In one other study Kopeček *et al.* [284] described the synthesis of the conjugate of poly(*N*-(2-hydroxypropyl)methacrylamide) (PHMAAm) and β-sheet forming peptide NH2-QQEFQWQFRQQ (P11) using a thiol-maleimide coupling strategy. They hypothesised that the peptide would impose the β-sheet formation onto the conjugate (Fig. 2.49). Indeed, the results showed that the conjugates formed long fibrils of 10 – 15 nm in width at pH 11 due to the electrostatic interactions between negatively charged glutamic acid and positively charged arginine residues. CAC of P11 necessary for fibril formation was in the range from 0.005 to 0.01 mg ml^{-1}.

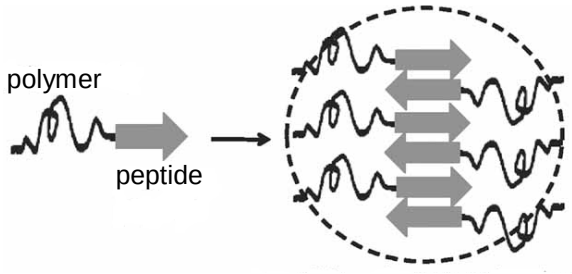

Figure 2.49: *Schematic representation of the self-assembly of polymer-peptide conjugates into β-sheet fibres (adapted from [284])*

Tzokova *et al.* [285] prepared PEG-*b*-poly(L-phenylalanine) (mPEG-F_4-OEt) diblock copolymer and studied its self-assembly. The conjugate was prepared via copper-catalysed 1,3-dipolar cycloaddition of azide-terminated PEO and alkyne-terminated tetrapeptide. They observed that the conjugate formed nanotubes with an inner radius of 2 nm and outer shell of 8 nm in a THF/water mixture in the concentration range from 2 to 10 mg ml^{-1}. Upon removal of THF during dialysis, the nanotubes entangled and formed gels. Self-assembly of this system was driven by the formation of antiparallel β-sheet packing between the peptides, which later assembled into nanotubes via lateral π-π stacking. In further studies [286] they examined the effect of the peptide sequence and PEG block length on self-assembly. They compared the conjugates with tetrapehylalanine and tetralanine and three lengths of PEG blocks (350, 1,200 or 1,800 g mol^{-1}). Results showed that as the length of PEG block increased, tetraphenylalanine-containing conjugates assembled into β-sheet-containing nanotubes, fibres and wormlike micelles. Whereas the conjugates of tetravaline showed the propensity to form the mixture of β-sheets and random coils, resulting in plank-like structures and tapes.

Hamley *et al.* [287] studied a similar system; the conjugate of tetraphenylalanine and PEG (5,000 g mol^{-1}). They observed that at low concentrations in aqueous solution the conjugate self-assembled into short rigid fibrils due to π-π stacking and hydrophobic interactions of the phenylalanine residues. At higher concentrations, well-defined β-sheets were detected. They postulated that PEG segments were considerably big and did not facilitate the formation of the fibrillar network.

In summary, polymer-peptide conjugates self-assemble in aqueous solution forming structures of various hierarchical level. The self-assembly process and the properties of the self-assembled systems depend on the polymer and peptide characteristics.

2.4.4. Applications of smart polymer-peptide/protein conjugates

Polymer-peptide conjugates have great potential in medicine, for example in therapeutic and protective medicine as drug and vaccines carriers, in biotechnology, and nanotechnology [1, 72, 257, 288, 289].

2.4.4.1. Drug delivery and tissue engineering

Polymeric micelles that can accommodate bioactive molecules in their core and then selectively release the drug, have attracted a lot of interest in cancer therapy applications. Peptide-polymer conjugates can be designed for drug delivery applications using the conjugation techniques already discussed in section 2.4.2. The peptide in these conjugates can either link particular drugs or genes, or mediate controlled delivery. Conjugate systems based on the copolymers of hydrophilic PEG with hydrophobic polymers gained a lot of interest due to their ability to form micelles that could accommodate bioactive molecules in their core and then selectively release them. These conjugate systems are biocompatible, ensure extended drug circulation time and increased efficiency of drug [290]. The design of these copolymers and conjugates depends on the type of application and the therapeutic molecules to be used.

Fig. 2.50 shows a typical micelle for controlled drug delivery where the hydrophobic core can accommodate various hydrophobic drugs and different ligation segments can be seeded across the exterior hydrophilic shell.

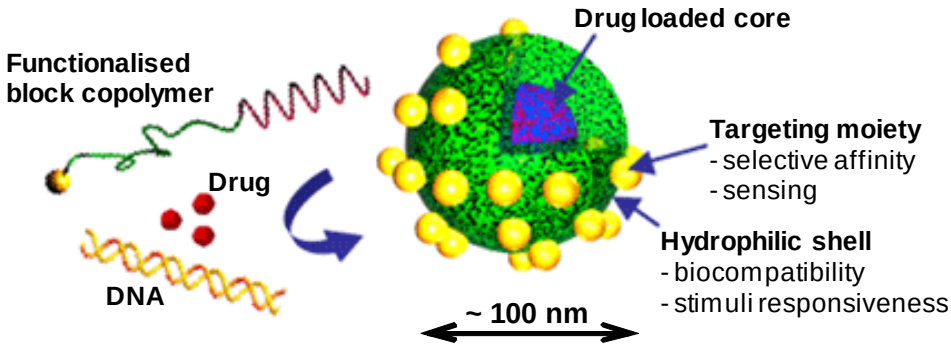

Figure 2.50: *Design of multi-functionalised polymeric micelles (adapted from [290])*

Kataoka *et al.* [291-294] were the first to study drug delivery using PEG as a polymer segment in polymer-peptide conjugate systems. They reported the self-assembly of the conjugate poly(ethyleneglycol)-*b*-poly(aspartic acid) (PEG-*b*-PD) and its ability to deliver the anticancer drug adriamycin (ADR) and doxorubicin (Dox) that were linked to the side chains of aspartic acid. The block copolymer formed amphiphilic micelles due to its amphiphilic character (Fig. 2.51). Hydrophilic PEG chains formed the outer shell. The inner core of the micelles was formed by drug molecules conjugated to the PD segment. If some free drug

molecules were present in solution during the micelles formation, the drug molecules would also be physically entrapped into the micelles due to hydrophobic and π-π interactions with the chemically conjugated drug molecules. Drug-loaded micelles ensured prolonged drug circulation times and showed anti-tumour activity mainly owing to the release of physically entrapped drug.

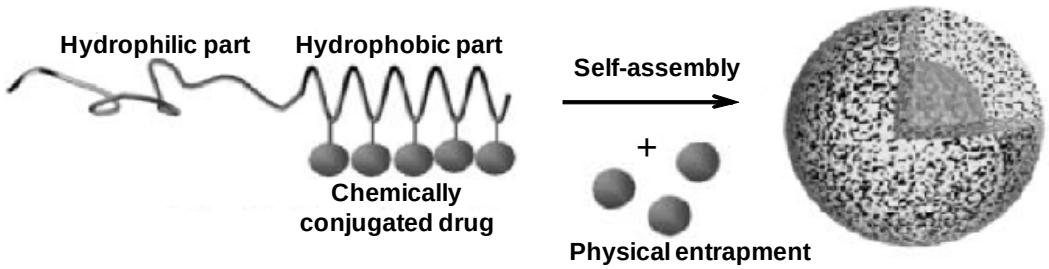

Figure 2.51: *Schematic representation of the formation of micelles of Dox-conjugated PEG-b-PD block copolymer (adapted from [290])*

Ghandehari *et al.* [295] designed a conjugate containing poly(*N*-(2-hydroxypropyl)-methacrylamide) (PHPMAAm) and the $\alpha_v\beta_3$ integrin-targeting peptide RGD4C. This conjugate was designed to deliver therapeutic radioisotopes to angiogenic sites in order to stop tumour growth.

Lowe *et al.* [296] prepared thermo-responsive and biodegradable linear dendritic conjugates with PNIPAAm and poly(L-lactic acid) (PLLA) as the central segment and poly(L-lysine) (PLL) dendrons at both its ends. Such conjugates formed nanoparticles in aqueous solution. The branched structure of PLL and its electrostatic interaction with the polyanionic phospholipids of cell membranes enhanced delivery of therapeutic agents into cells or across biological barriers. Results showed that the conjugate degraded in PBS at pH 7.4 and at 25ºC within 19 days due to the degradation of PLLA segment. Later these nanoparticles were used for delivery of therapeutic ceramide C_6 to solid tumour tissues upon heating [297]. Results showed that C_6 was released more rapidly in the lipophilic environment.

Cui *et al.* [298] developed a system for the controlled drug delivery to cancer cells. They prepared micelles from carboxyl group end-functionalised Pluronic triblock copolymers (PEG-*b*-PPO-*b*-PEG) (diameter < 50 nm) that accumulated the drug Paclitaxel in their core and conjugated them with anti-HIF-1α (human hypoxia-inducible factor 1 alpha subunit) antibody. Usually, HIF directed enzymes and growth factors stimulate the formation of blood vessels and HIF-1 activate genes that allowed the cancer cells to survive in the hypoxic tumour environment. Results of the study showed that when the micelles were incubated with the stomach cancer MGC-803 cells with the over-expression of HIF-1α, drug-loaded micelles were internalised into cytoplasm, released the drug and killed the cells. No cytotoxicity was

observed with human dermal fibroblast (HDF) cells which did not show the over-expression of HIF-1 α.

Shi and coworkers [299] prepared well-defined block copolymers of poly(*N*-isopropylacrylamide)-*b*-poly(L-glutamic acid) ($PNIPAAm_{55}$-*b*-$PLGA_{35}$) by combining RAFT and ring opening polymerisation (ROP). This block copolymer exhibited pH and temperature triggered micellisation behaviour in aqueous solution. At pH > 10 and below the LCST of PNIPAAm the copolymers were soluble in the form of unimers. At pH > 10 and above the LCST, elongated micelles with a PNIPAAm core were formed, while at pH < 4 and below the LCST, round-shaped micelles with a PLGA core were observed.

Peptides can not only induce conjugate self-assembly, but also exhibit the possibility to integrate short peptide sequences into synthetic hydrogels which makes them biologically active. Hubbell *et al.* reported hydrogels consisted of star-shape polymers with four PEG arms functionalised with vinylsulfone and two different peptide sequences: GPQGIWGQ [300] and RGDSP [301]. The peptide sequences served to mediate cell adhesion and acted as substrates for matrix metalloproteinase (MMP).

Klok *et al.* [302] prepared polymer brushes of poly(2-hydroxyethyl methacrylate) (PHEMA) and poly(poly(ethylene glycol)methacrylate) (PPEGMA) and functionalised them with RGD peptide sequence which promoted the endothelialisation of blood-contacting biomaterials. Results showed that human umbilical vascular endothelial cells (HUVEC) successfully adhered and proliferated on these surfaces. Some differences in cell size and morphology were noticed on PHEMA and PPEGMA brushes due to the increased PEG spacer length the hydrophilic nature of PPEGMA. This resulted in an increase of RGD peptide mobility and a decrease in its communication with cell receptors.

Polymer in the protein-polymer conjugate can also control the biological activity of the protein. Hoffman *et al.* [303] studied the separation and recovery of the enzyme β-D-glucosidase using thermo-responsive *N*-hydroxysuccinimide (NHS) end-functionalised PNIPAAm. The enzyme retained its activity after the conjugation and no significant loss of activity was observed during heating cycles. Also, end-functionalised PNIPAAm with vinylsulfone was used to control biotin binding to streptavidin [257].

Alexander *et al.* [304] showed that not only bioactive molecules could be encapsulated into thermo-responsive particles but also cells. They prepared the thermo-responsive copolymers of poly(ethylene glycol) methacrylate (PEGMA) and poly(propylene glycol) methacrylate (PPGMA) (PPGMA-*co*-PEGMA). During copolymer aggregation into microparticles in water, the solution of poly(lactic-*co*-glycol acid) (PLGA) in ethylacetate was introduced, resulting in the PLGA entrapment into the core of PPGMA-*co*-PEGMA particles.

Below 37°C the particles were dissolved, but above 37°C a gel formed. This property was later used to encapsulate C2C12 myoblasts (Fig. 2.52), and results showed that the porous gel structure formed was acceptable for successful cell growth allowing the formation of a cell-matrix that promoted cell communication.

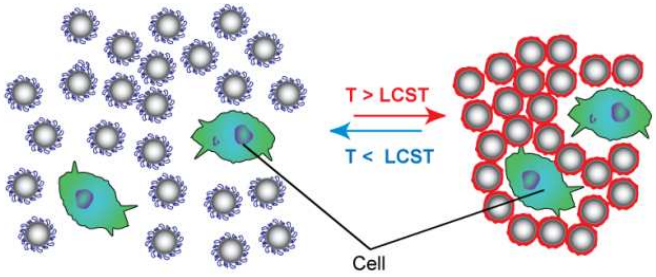

Figure 2.52: *Schematic representation of cell encapsulation above the LCST of the PPGMA-co-PEGMA particles (adapted from [304])*

2.4.4.2. Separation and purification technology

Conjugates of polymers and peptides can be also used in separation technology when one of the conjugate components exhibits high affinity towards a co-solute, e.g. protein that needs to be separated. Bioconjugates have also been used to selectively isolate an analyte from a complex mixture like a serum sample [84]. If the conjugate includes a thermo-responsive polymer in its structure, such as PNIPAAm, the protein-binded conjugate can easily be separated by precipitation upon heating. The most popular examples of such conjugates are the complexes of biotinylated molecules with avidin or streptavidin [305]. Using the same approach, the enzyme β-D-glucosidase was separated from its reaction solution [252, 306]. Another example of the affinity precipitation is the complex formation between protein A in the form of PNIPAAm-protein A conjugate and IgG. Similarly, the complex precipitated upon heating, thus enabling the separation of IgG from solution [254].

2.4.5. Summary

In summary, section 2.4 described some synthesis strategies to obtain the conjugates of a polymer and a peptide/protein. The choice of the appropriate reaction conditions should be based on the functional groups of the polymer and the peptide. Functional groups of both components can also be modified to ensure efficient coupling.

Self-assembly of the conjugates is driven by their amphiphilic nature. A variety of structures can be formed including micelles, vesicles and hydrogels composed of β-sheet fibres. Since both polymer and peptide can change their characteristic properties in response to different stimuli, such as pH, temperature or ionic strength, the final aggregates are

considered to be doubly stimuli-responsive. This feature makes them attractive for drug delivery and tissue engineering applications, for example drug-loaded particles showed good potentials to be used in cancer therapy and diagnostics.

2.5. Aims of the study

There are two main aims for this project.

The first aim is to create soluble PNIPAAm-rich gels by doping in different quantities of PNIPAAm-peptide conjugate. It is postulated that the peptide segments will retain their self-assembling behaviour after conjugation and will form β-sheet rich fibres decorated with PNIPAAm chains once dissolved in water. The effect of the peptide sequence on the self-assembly and gel properties will also be explored. The gelling, mechanical and thermo-responsive properties of the materials will be investigated and related to the chemistry and ratio of the self-assembling blocks.

The second aim is to create thermo-responsive peptide-rich composite gels by incorporating pure polymer-peptide conjugate into pure peptide matrix. In this case it is postulated that the peptide part of the conjugate will be incorporated into the peptide fibres and the attached polymer will confer thermo-responsiveness to the gel. The focus will be on understanding how the conjugate behaves in the gel network upon heating and cooling and how it influences the overall mechanical properties of the gel.

References

1. A. S. Hoffman and P. S. Stayton, *Macromol. Symp.*, 2004, **207**, 139-151.
2. B. Jeong and A. Gutowska, *Trends in Biotechnol.*, 2002, **20**, 305-311.
3. D. Dhara and P. R. Chatterji, *J.M.S.-Rev. Macromol. Chem. Phys.*, 2000, **C40**, 51-68.
4. N. Bhattarai, F. A. Matse and M. Zhang, *Macromol. Biosci.*, 2005, **5**, 107-111.
5. S. K. Li and A. D'Emanuele, *J. Control. Release*, 2001, **75**, 55-67.
6. E. Stabenfeldt, A. J. Garcia and M. C. Laplaca, 2006, **77**, 718-725.
7. S. Ibusuki, Y. Fujii, Y. Iwamoto and T. Matsuda, *Tissue Eng.*, 2003, **9**, 371-384.
8. L. D. Taylor and L. D. Cerankowski, *J. Polym. Sci., Part A: Polym. Chem.*, 1975, **13**, 2551-2570.
9. I. Y. Galaev and B. Mattiasson, *Enzyme Microb. Technol.* , 1993, **15**, 354-366.
10. R. Liu, M. Fraylich and B. R. Saunders, *Colloid. Polym. Sci.*, 2009, **287**, 627-643.
11. F. Meeussen, E. Nies, H. Berghmans, S. Verbrugghe, E. Goethals and F. D. Prez, *Polymer*, 2000, **41**, 8597-8602.
12. H. G. Schild, *Progress in Polymer Science*, 1992, **17**, 163-249.
13. I. Dimitrov, B. Trzebicka, A. H. E. Muller, A. Dworak and C. B. Tsvetanov, *Prog. Polym. Sci.* , 2007, **32**, 1275-1343.
14. I. C. Burker, J. M. G. Cowie, T. N. Huckerby, D. A. Shaw, I. Soutar and L. Swanson, *Macromolecules,*, 2003, **36**, 7765-7770.
15. E. Ayano, K. Nambu, C. Sakamoto, H. Kanazawa, A. Kikuchi and T. Okano, *J. Chromatogr. A*, 2006, **1119**, 58-65.
16. Y. G. Takei, T. Aoki, K. Sanui, N. Ogata, T. Okano and Y. Sakurai, *Bioconjugate Chem.*, 1993, **4**, 42-46.
17. Y. Xia, N. A. D. Burke and H. D. H. Stover, *Macromolecules*, 2006, **39**, 2275-2283.
18. G. Masci, L. Giacomelli and V. Crescenzi, *Macromol. Rapid. Commun.*, 2004, **25**, 559-564.
19. Y. Xia, X. Yin, N. A. D. Burke and H. D. H. Stöver, *Macromolecules*, 2005, **38**, 5937-5943.
20. D. J. Kim, J.-Y. Heo, K. S. Kim and I. S. Choi, *Macromol. Rapid Commun.*, 2003, **24**, 517-521.
21. D. J. Kim, S. M. Kang, B. Kong, W.-J. Kim, H.-J. Paik, H. Choi and I. S. Choi, *Macromol. Chem. Phys.*, 2005, **206**, 1941-1946.
22. F. Ganachaud, M. J. Monteiro, R. G. Gilbert, M. A. Dourges, S. H. Thang and E. Rizzardo, *Macromolecules*, 2000, **33**, 6738-6745.
23. C. Schili, M. G. Lanzendörfer and A. H. E. Müller, *Macromolecules*, 2002, **35**, 6819-6827.
24. B. Ray, Y. Isobe and M. Sawamoto, *Macromolecules,*, 2004, **37**, 1702-1710.
25. A. J. Convertine, N. Ayres, C. W. Scales, A. B. Lowe and C. L. McCormick, *Biomacromolecules*, 2004, **5**, 1177-1180.
26. M. D. C. Topp, P. J. Dijkstra, H. Talsma and J. Feijen, *Macromolecules*, 1997, **30**, 8518-8520.
27. R. Motokawa, K. Morishita, S. Koizumi, T. Nakahira and M. Annaka, *Macromolecules*, 2005, **38**, 5748-5760.
28. H.-H. Lin and Y.-L. Cheng, *Macromolecules*, 2001, **34**, 3710-3715.
29. K. Matyjaszewski and J. Xia, *Chem. Rev.*, 2001, **101**, 2921-2990.
30. O. Chiantore, M. Guaita and L. Trossarelli, *Makromol. Chem.*, 1979, **180**, 969-973.
31. J. M. Asua, *Polymer reaction engineering [electronic source]*, Blackwell Publishing, 2007.
32. G. Moad and D. H. Solomon, *The Chemistry of Free Radical Polymerization*, 1998.
33. Z. Ding, G. Chen and A. S. Hoffman, *Bioconjugate Chem.*, 1996, **7**, 121-125.
34. M. Yasui, T. Shiraya, K. Fujimoto and H. Kawaguchi, *Colloid. Surface B*, 1997, **8**, 311-319.
35. E. Ayano and H. Kanazawa, *J. Sep. Sci.*, 2006, **29**, 738-749.
36. J. S. Scarpa, D. D. Mueller and I. M. Klotz, *J. Am. Chem. Soc.*, 1967, **89**, 6024-6030.
37. M. Heskins and J. E. Guillet, *J. Macromol. Sci. Part A Pure Appl. Chem.*, 1968, **2**, 1441 - 1455.

38. S.-Y. Lin, K.-S. Chen and L. Run-Chu, *Polymer*, 1999, **40**, 2619-2624.
39. T. Okano, A. Kikuchi, Y. Sakurai, Y. Takei and N. Ogata, *J. Control. Release*, 1995, **36**, 125-133.
40. S. Furyk, Y. Zhang, D. Ortiz-Acosta, P. S. Cremer and D. E. Bergbreiter, in *J. Polym. Sci.: Part A: Polym. Chem.*, Editon edn., 2006, vol. 44, pp. 1492-1501.
41. T. Kawaguchi, Y. Kojima and T. Yoshinazi, *Polymer J.*, 2008, **40**, 455-459.
42. J. E. Chung, M. Yokoyama, T. Aoyagi, Y. Sakurai and T. Okano, *J. Control. Rel.*, 1998, **53**, 119-130.
43. E. I. Tiktopulo, V. N. Uversky, V. B. Lushchik, S. I. Klenin, V. E. Bychkova and O. B. Ptitsyn, *Macromolecules*, 1995, **28**, 7519-7524.
44. K. Otake, H. Inomata, M. Konno and S. Saito, *Macromolecules*, 1990, **23**, 283-289.
45. H. Feil, Y. H. Bae, J. Feijen and S. W. Kim, *Macromolecules*, 1993, **26**, 2496-2500.
46. H. G. Schild and D. A. Tirrell, *J. Phys. Chem.*, 1990, **94**, 4352-4356.
47. I. Yamamoto, K. Iwasaki and S. Hirotsu, *J. Phys. Soc. Jpn.*, 1989, **58**, 210-215.
48. T. Kawaguchi, Y. Kojima, M. Osa and T. Yoshizaki, *Polymer J.*, 2008, **40**, 528-533.
49. X. Wang, X. Qiu and C. Wu, *Macromolecules*, 1998, **31**, 2972-2976.
50. K. Kubota, S. Fujishige and I. Ando, *Polymer J.*, 1990, **22**, 15-20.
51. F. Zeng and F. Tong, *Polymer*, 1997, **38**, 5539-5544.
52. H. Ohta, I. Ando, S. Fujishige and K. Kubota, *J. Polym. Sci., Part B, Polym. Phys.*, 1991, **29**, 963-968.
53. C. Boutris, E. G. Chatzi and C. Kiparissides, *Polymer*, 1997, **38**, 2567-2570.
54. C. Wu and S. Zhou, *Macromolecules*, 1995, **28**, 8381-8387.
55. C. Williams, F. Brochard and H. L. Frisch, *Ann. Rev. Phys. Chem.*, 1981, **32**, 433-451.
56. S. Fujishige, K. Kubota and I. Ando, *J. Phys. Chem.*, 1989, **93**, 3311-3313.
57. S. Fujishige, *Polym. J.*, 1987, **19**, 297-300.
58. C. K. Chee, S. Rimmer, I. Soutar and L. Swanson, *Polymer*, 2001, **42**, 5079-5087.
59. F. M. Winnik, *Polymer*, 1990, **31**, 2125-2134.
60. H. Ringsdorf, J. Venzmer and F. M. Winnik, *Macromolecules*, 1991, **24**, 1678-1686.
61. F. M. Winnik, H. Ringsdorf and J. Venzmer, *Langmuir* 1991, **7**, 905-911.
62. F. Eeckman, A. J. Moes and K. Amighi, *Int. J. Pharm.*, 2004, **273**, 109-119.
63. H. G. Schild and D. A. Tirrell, *Langmuir*, 1991, **7**, 665-671.
64. M. B. Huglin, Y. Liu and J. L. Velada, *Polymer*, 1997, **38**, 5785-5791.
65. J. L. Velada, Y. Liu and M. B. Huglin, *Macromol. Chem. Phys.*, 1998, **199**, 1127-1134.
66. W. Xue, M. B. Huglin and T. G. Jones, *Macromol. Chem. Phys.*, 2003, **204**, 1956-1965.
67. Z. Tong, F. Zheng and X. Zheng, *Macromolecules*, 1999, **32**, 4488-4490.
68. X. Zheng, F. Tong, X. Xie and F. Zheng, *Polym. J.*, 1998, **30**, 284-288.
69. X. P. Qiu, F. Tanaka and F. M. Winnik, *Macromolecules*, 2007, **40**, 7069-7071.
70. M. Shibayama, S.-Y. Mizutani and S. Nomura, *Macromolecules*, 1996, **29**, 2019-2024.
71. H. G. Schild and D. A. Tirrell, *Langmuir*, 1991, **7**, 1319-1324.
72. A. S. Hoffman, P. S. Stayton, V. Bulmuş, G. Chen, J. Chen, A. Chilkoti, Z. Ding, L. Dong, R. Fong, C. A. Lackey and C. J. Long, *J. Biomed. Mater. Res.*, 2000, **52**, 577-586.
73. H. M. Zareie, E. V. Bulmuş, A. P. Gunning, A. S. Hoffman, E. Pişkin and V. J. Morris, *Polymer*, 2000, **41**, 6723-6727.
74. H. M. Zareie, S. Dinçer and E. Pişkin, *J. Colloid. Interf. Sci.*, 2002, **251**, 424-428.
75. F. M. Winnik, M. A. Winnik, H. Ringsdorf and J. Venzmer, *J. Phys. Chem.*, 1991, **95**, 2583-2587.
76. A. L. Nguyen and J. H. T. Luong, *Enzyme Microb. Technol.*, 1990, **12**, 663-668.
77. L. C. Dong and A. S. Hoffman, *J. Control. Release*, 1986, **4**, 223-228.
78. F. M. Winnik, H. Ringsdorf and J. Venzmer, *Macromolecules*, 1990, **23**, 2415-2416.
79. F. Eeckman, K. Amighi and A. J. Moës, *Int. J. Pharm.*, 2001, **222**, 259-270.
80. Y. Zhang, S. Furyk, L. B. Sagle, Y. Cho, D. E. Bergbreiter and P. S. Cremer, *J. Phys. Chem. C*, 2007, **111**, 8916-8924.
81. J. Eliassaf, *J. Appl. Polym. Sci.*, 1978, **22**, 873-874.

82. A. Kikuchi and T. Okano, *Prog. Polym. Sci.*, 2002, **27**, 1165-1193.
83. T. Yakushiji, K. Sakai, A. Kikuchi, T. Aoyagi, Y. Sakurai and T. Okano, *Anal. Chem.*, 1999, **71**, 1125-1130.
84. N. Monji and A. S. Hoffman, *Appl. Biochem. Biotechnol.*, 1987, **14**, 107-120.
85. T. Okano, *Biorelated Polymer and Gels: Controlled of Release and Applications in Biomedical Engineering*, Academic Press, Chestnut Hill, 1998.
86. M. Kurisawa, M. Yokoyama and T. Okano, *J. Control. Release*, 2000, **69**, 127-137.
87. N. Yamada, T. Okano, H. Sakai, F. Karikusa, Y. Sawasaki and S. Y., *Macromol. Chem. Rapid Commun.*, 1990, **11**, 571-576.
88. M. Yamato, C. Konno, A. Kushida, M. Hirose, M. Utsumi, A. Kikuchi and T. Okano, *Biomaterials*, 2000, **21**, 981-986.
89. A. Kushida, M. Yamato, C. Konno, A. Kikuchi, Y. Sakurai and T. Okano, *J. Biomed. Mater. Res.*, 2000, **51**, 216-223.
90. T. Okano, N. Yamada, M. Okuhara, H. Sakai and Y. Sakurai, *Biomaterials*, 1995, **16**, 297-303.
91. H. Kitano, C. Yan and K. Nakamura, *Makromol. Chem.*, 1991, **192**, 2915-2923.
92. T. Shiroya, M. Yasui, K. Fujimoto and H. Kawaguchi, *Colloids Surf., B*, 1995, **4**, 275-285.
93. J.-P. Chen and M.-S. Hsu, *J. Mol. Catal. B: Enzym.*, 1997, **2**, 233-241.
94. J.-P. Chen, J.-J. Lee and H.-S. Liu, *Biotechnol. Tech.* , 1997, **11**, 109-112.
95. K. D. Vorlop and K. Steinke, *Chem. Ing. Tech.*, 1988, **60**, 790-791.
96. A. Chilkoti, M. R. Dreher, D. E. Meyer and D. Raucher, *Adv. Drug Deliv. Rev.*, 2002, **54**, 613-630.
97. D. E. Meyer, B. C. Shin, G. A. Kong, M. W. Dewhirst and A. Chikoti, *J. Control. Release*, 2001, **74**, 213-224.
98. F. Kohori, K. Sakai, T. Aoyagi, M. Yokoyama, M. Yamato, Y. Sakurai and T. Okano, *Colloid. Surface B - Biointerfaces*, 1999, **16**, 195-205.
99. Y. Y. Li, X. Z. Zhang, J. L. Zhu, H. Cheng, S. X. Cheng and R. X. Zhuo, *Nanotechnology*, 2007, **18**, 1-7.
100. A. Gutowska, Y. H. Bae, H. Jacobs, F. Mohammad, D. Mix, J. Feijen and S. W. Kim, *J. Biomed. Mater. Res.*, 1995, **29**, 811-821.
101. J. E. Chung, M. Yokoyama, M. Yamato, T. Aoyagi, Y. Sakurai and T. Okano, *J. Control. Rel.*, 1999, **62**, 115-127.
102. G.-H. Hsiue, S.-H. Hsu, C.-C. Yang, S.-H. Lee and I. K. Yang, *Biomaterials*, 2002, **23**, 457-462.
103. M. Yamato, M. Utsumi, A. Kushida, C. Konno, A. Kikuchi and T. Okano, *Tissue Eng.*, 2001, **7**, 473-480.
104. B. D. Ratner, T. Horbett and A. S. Hoffman, *J. Biomed. Mater. Res.*, 1975, **9**, 407-422.
105. B. R. McAuslan and G. Johnson, 1987, **21**, 921-935.
106. Y. Rochev, D. O'Halloran, T. Gorelova, V. Gilcreest, I. Selezneva, B. Gavrilyuk and A. Gorelov, *J. Mater. Sci.- Mater. M.*, 2004, **15**, 513-517.
107. R. M. P. da Silva, J. F. Mano and R. L. Reis, *Trends Biotechnol.*, 2007, **25**, 577-583.
108. M. T. Moran, W. M. Carroll, I. Selezneva, A. Gorelov and Y. Rochev, *J. Biomed. Mater. Res. Part A, 2007*, 2007, **81A**, 870-876.
109. M. T. Moran, W. M. Carroll, A. Gorelov and Y. Rochev, *J. R. Soc. Interface*, 2007, **4**, 1151-1157.
110. Y. S. Kim, J. Y. Lim, H. J. Donahue and T. L. Lowe, *Tissue Eng.*, 2005, **11**, 30-40.
111. D. Schmaljohann, J. Oswald, B. Jorgensen, M. Nitschke, D. Beyerlein and C. Werner, *Biomacromolecules*, 2003, **4**, 1733-1739.
112. T. Okano, N. Yamada, M. Okuhara, H. Sakai and Y. Sakurai, *Biomaterials*, 1995, **16**, 297-303.
113. M. Ebara, M. Yamato, M. Hirose, T. Aoyagi, A. Kikuchi, K. Sakai and T. Okano, *Biomacromolecules*, 2003, **4**, 344-349.

114. M. Ebara, M. Yamato, T. Aoyagi, A. Kikuchi, K. Sakai and T. Okano, *Biomacromolecules*, 2004, **5**, 505-510.
115. H. Vihola, A. Laukkanen, L. Valtola, H. Tenhu and J. Hirvonen, *Biomaterials*, 2005, **26**, 3055-3064.
116. J. Koolman and K.-H. Röhn, *Color Atlas of Biochemistry*, Thieme, 1996.
117. R. V. Ulijn and A. M. Smith, *Chem. Soc. Rev.*, 2008, **37**, 664-675.
118. N. Sewald and H.-D. Jakubke, *Peptides: Chemistry and Biology*, Wiley-VCH, 2002.
119. *Protein structure*, http://www.food-info.net/uk/protein/structure.htm, Accessed October, 2009.
120. C. N. Pace and J. M. Scholtz, *Biophys. J.* , 1998, **75**, 422-427.
121. B. Alberts, D. Bray, J. Lewis, M. Raff, K. Roberts and J. D. Watson, *Molecular biology of the cell*, 4th edn., New York: Garland Science, 2002.
122. R. B. Merrifield, *J. Am. Chem. Soc.*, 1963, **85**, 2149-2154.
123. *Novabiochem 2008/2009 Catalogue: Peptide Synthesis*, Merck.
124. G. M. Whitesides, J. P. Mathias and C. T. Seto, *Science*, 1991, **254**, 1312-1319.
125. M. C. Branco and J. P. Schneider, *Acta Biomater.*, 2009, **5**, 817-831.
126. A. E. Rösler, G. W. M. Vandermeulen and H.-A. Klok, *Adv. Drug Deliv. Rev.*, 2001, **53**, 95-108.
127. S.-H. Hua, Y.-Y. Li, Y. Liu, W. Xao, C. Li, F.-W. Huang, X.-Z. Zhang and R.-X. Zhuo, *Macromol. Rapid Commun.*, **31**, 81-86.
128. A. Carlsen and S. Lecommandoux, *Curr. Opin. Colloid Interface Sci.* , 2009, **14**, 329-339.
129. J. Rodríguez-Hernández, F. Chécot, Y. Gnanou and S. Lecommandoux, *Prog. Polym. Sci.* , 2005, **30**, 691-724.
130. J. Du and R. K. O'Reilly, *Soft Matter*, 2009, **5**, 3544-3561.
131. A. Blanazs, S. P. Armes and A. J. Ryan, *Macromol. Rapid Commun.*, 2009, **30**, 267-277.
132. N. Lefèvre, C.-A. Fustin and J.-F. Gohy, *Macromol. Rapid Commun.*, 2009, **30**, 1871-1888.
133. F. Chiti and C. M. Dobson, *Annu Rev. Biochem.*, 2006, **75**, 333-366.
134. K. E. Kadler, D. F. Holmes, J. A. Trotter and J. A. Chapman, *Biochem. J.*, 1996, **316**, 1-11.
135. *Biomolecular Self-Assembly* http://www.nanoword.net/library/weekly/aa051400a.htm, Accessed January, 2010.
136. K. Y. Lee and S. H. Yuk, *Prog. Polym. Sci.*, 2007, **32**, 669–697.
137. D. W. P. M. Lowik and J. C. M. v. Hest, *Chem. Soc. Rev.*, 2004, **33**, 234-245.
138. C. Xu and J. Kopeček, *Polym. Bull.*, 2007, **58**, 53-63.
139. A. Klug, *Biosci. Rep.* , 1983, **3**, 395-430.
140. M. L. Brader and M. F. Dunn, *Trends Biochem. Sci* 1991, **16**, 341-345.
141. S. Treusch, D. M. Cyr and S. Lindquist, *Cell Cycle*, 2009, **8**, 1668-1674.
142. M. J. Webber, J. A. Kessler and S. I. Stupp, *J. Intern. Med.*, 2010, **267**, 71-88.
143. M. E. Davis, J. P. M. Motion, D. A. Narmoneva, T. Takahashi, D. Hakuno, R. D. Kamm, S. Zhang and R. T. Lee, *Circulation*, 2005, **111**, 442-450.
144. E. Genove, S. Shen, S. Zhang and C. E. Semino, *Biomaterials*, 2005, **26**, 3341-3351.
145. A. Horii, X. Wang, F. Gelain and S. Zhang, *PLoS One*, 2007, **2:e190**, 1-9.
146. S. Kyle, A. Aggeli, E. Ingham and M. J. McPherson, *Trends Biotechnol.*, 2009, **27**, 423-433.
147. J. J. Panda, A. Mishra, A. Basu and V. S. Chauhan, *Biomacromolecules*, 2008, **9**, 2244-2250.
148. Z. Ge and S. Liu, *Macromol. Rapid Commun.*, 2009, **30**, 1523-1532.
149. S. Ghosh, S. K. Singh and S. Verma, *Chem. Commun.*, 2007, 2296-2298.
150. S. Toledano, R. J. Williams, V. Jayawarna and R. V. Ulijn, *J. Am. Chem. Soc.*, 2006, **128**, 1070-1071.
151. J. H. Collier, B.-H. Hu, J. W. Ruberti, J. Zhang, P. Shum, D. H. Thompson and P. B. Messersmith, *J. Am. Chem. Soc.*, 2001, **123**, 9463-9464.
152. L. Adler-Abramovich, R. Perry, A. Sagi, E. Gazit and D. Shabat, *ChemBioChem*, 2007, **8**, 859-862.
153. H. J. Chung and T. G. Park, *Nano Today*, 2009, **4**, 429-437.
154. J. D. Hartgerink, *Curr. Opin. Chem. Biol.*, 2004, **8**, 604-609.

155. S. Zhang, *Biotechnol. Adv.*, 2002, **20**, 321-339.
156. S. Fernandez-Lopez, H.-S. Kim, E. C. Choi, M. Delgado, J. R. Granja, A. Khasanov, K. Kraehenbuehl, G. Long, D. A. Weinberger, K. M. Wilcoxen and M. R. Ghadiri, *Nature*, 2001, **412**, 452-455.
157. S. Cavalli, F. Albericio and A. Kros, *Chem. Soc. Rev.*, 2010, **39**, 241-263.
158. S. Zhang, T. Holmes, C. M. DiPersio, R. O. Hynes, X. Su and A. Rich, *Biomaterials*, 1995, **16**, 1385-1393.
159. S. Zhang, L. Yanc, M. Altman, M. Lässlea, H. Nugenta, F. Frankele, D. A. Lauffenburgera, G. M. Whitesides and A. Rich, *Biomaterials*, 1999, **20**, 1213-1220.
160. T. D. Holmes, S. de Lacalle, X. Su, G. Liu, A. Rich and S. Zhang, *P. Natl. Acad. Sci. USA*, 2000, **97**, 6728-6733.
161. J. D. Hartgerink, E. Beniash and S. I. Stupp, *Science*, 2001, **294**, 1684-1688.
162. F. Gelain, A. Horii and S. Zhang, *Macromol. Biosci.*, 2007, **7**, 544-551.
163. S. G. Zhang and M. Altman, *React. Funct. Polym.*, 1999, **41**, 91-102.
164. S. Zhang, T. Holmes, C. Lockshin and A. Rich, *P. Natl. Acad. Sci. USA*, 1993, **90**, 3334-3338.
165. E. J. Leon, N. Verma and S. e. a. Zhang, *J. Biomat. Sci.-Polym. E.*, 1998, **9**, 297-312.
166. S. Zhang, *Materials Today*, 2003, **5**, 20-27.
167. S. Zhang and A. Rich, *P. Natl. Acad. Sci. USA*, 1997, **94**, 23-28.
168. M. Altman, P. Lee, A. Rich and S. Zhang, *Protein Sci.*, 2000, **9**, 1095–1105.
169. C. S. Chen, M. Mrksich, S. Huang, G. M. Whitesides and D. E. Ingber, *Science*, 1997, **276**, 1425-1428.
170. D. N. Woolfson and M. G. Ryadnov, *Curr. Opin. Chem. Biol.*, 2006, **10**, 559-567.
171. R. J. Mart, R. D. Osborne, M. M. Stevens and R. V. Ulijn, *Soft Matter*, 2006, **2**, 822-835.
172. S. Scanlon and A. Aggeli, *Nano Today*, 2008, **3**, 22-30.
173. P. Chen, *Colloids Surf., A*, 2005, **261**, 3-24.
174. J. Kisiday, M. Jin, M. Kurz, H. Hung, C. Semino, S. Zhang and A. J. Grodzinsky, *P. Natl. Acad. Sci. USA*, 2002, **99**, 9996-10001.
175. R. G. Ellis-Behnke, Y.-X. Liang, S.-W. You, D. K. C. Tay, S. Zhang, K.-F. So and G. E. Schneider, *P. Natl. Acad. Sci. USA*, 2006, **103**, 5054-5059.
176. J. P. Schneider, D. J. Pochan, B. Ozbas, K. Rajagopal, L. Pakstis and J. Kretsinger, *J. Am. Chem. Soc.*, 2002, **124**, 15030-15037.
177. B. Ozbas, J. Kretsinger, K. Rajagopal, J. P. Schneider and D. J. Pochan, *Macromolecules*, 2004, **37**, 7331-7337.
178. M. C. Branco, F. Nettesheim, D. J. Pochan, J. P. Schneider and N. J. Wagner, *Biomacromolecules*, 2009, **10**, 1374-1380.
179. K. Rajagopal, M. S. Lamm, L. A. Haines-Butterick, D. J. Pochan and J. P. Schneider, *Biomacromolecules*, 2009, **10**, 2619-2625.
180. T. H. Larsen, M. C. Branco, K. Rajagopal, J. P. Schneider and E. M. Furst, *Macromolecules*, 2009, **42**, 8443-8450.
181. R. V. Rughani, D. A. Salick, M. S. Lamm, T. Yucel, D. J. Pochan and J. P. Schneider, *Biomacromolecules*, 2009, **10**, 1295-1304.
182. S. Santoso, W. Hwang, H. Hartman and S. Zhang, *Nano Letters*, 2002, **2**, 687-691.
183. S. Vauthey, S. Santoso, H. Gong, N. Watson and S. Zhang, *P. Natl. Acad. Sci. USA*, 2002, **99**, 5355-5360.
184. J. D. Hartgerink, E. Beniash and S. I. Stupp, *P. Natl. Acad. Sci. USA*, 2002, **99**, 5133-5138.
185. A. M. Smith, E. F. Banwell, W. R. Edwards, M. J. Pandya and D. N. Woolfson, *Adv. Funct. Mater.*, 2006, **16**, 1022-1030.
186. S. Kojima, Y. Kuriki, T. Yoshida, K. Yazaki and K. Miura, *Proc. Jpn. Acad., Ser. B Phys. Biol. Sci.*, 1997, **73**, 7-11.
187. M. J. Pandya, G. M. Spooner, M. Sunde, J. R. Thorpe, A. Rodge and D. N. Woolfson, *Biochemistry*, 2000, **39**, 8728-8734.

188. S. A. Potekhin, T. N. Melni, V. Popov, N. F. Lanina, A. A. Vazina, P. Rigler, A. S. Verdini, G. Corradin and A. V. Kajava, *Chemistry & Biology*, 2001, **8**, 1025-1032.
189. M. Reches and E. Gazit, *Science*, 2003, **300**, 625-627.
190. M. Reches and E. Gazit, *Nat. Nanotechnol.* , 2006, **1**, 195-200.
191. M. Reches and E. Gazit, *Nano Lett.*, 2004, **4**, 581-585.
192. A. M. Smith, R. J. Williams, C. Tang, P. Coppo, R. F. Collins, M. L. Turner, A. Saiani and R. V. Ulijn, *Adv. Mater.*, 2008, **20**, 37-41.
193. V. Jayawarna, A. M. Smith, J. E. Gough and R. V. Ulijn, *Biochem. Soc. Trans*, 2007, **35**, 535-537.
194. C. Tang, A. M. Smith, R. F. Collins, R. V. Ulijn and A. Saiani, *Langmuir*, 2009, **25**, 9447-9453.
195. S. Zhang, C. Lockshin, R. Cook and A. Rich, *Biopolymers*, 1994, **34**, 663–672.
196. A. Saiani, A. Mohammed, H. Frielinghaus, R. Collins, N. Hodson, C. M. Kielty, M. J. Sherratt and A. F. Miller, *Soft Matter*, 2009, **5**, 193-202.
197. A. Mohammed, A. F. Miller and A. Saiani, *Macromol. Symp.*, 2007, **251**, 88-95.
198. C. J. Bowerman, D. M. Ryan, D. A. Nissan and B. L. Nilsson, *Mol. BioSyst.*, 2009, **5**, 1058-1069.
199. A. Aggeli, I. A. Nyrkova, M. Bell, R. Harding, L. Carrick, T. C. B. McLeish, A. N. Semenov and N. Boden, *P. Natl. Acad. Sci. USA*, 2001, **98**, 11857-11862.
200. P. Y. Chou and G. D. Fasman, *Biochemistry*, 1974, **13**, 211-222.
201. Y. Hong, R. L. Legge, S. Zhang and P. Chen, *Biomacromolecules*, 2003, **4**, 1433-1442.
202. M. L. de la Paz, K. Goldie, J. Zurdo, E. Lacroix, C. M. Dobson, A. Hoenger and L. Serrano, *P. Natl. Acad. Sci. USA*, 2002, **99**, 16052-16057.
203. M. R. Caplan, E. M. Schwarzfarb, S. G. Zhang, R. D. Kamm and D. A. Lauffenburger, *Biomaterials*, 2002, **23**, 219-227.
204. S. Y. Fung, C. Keyes, J. Duhamel and P. Chen, *Biophys. J.*, 2003, **85**, 537-548.
205. A. Aggeli, M. Bell, L. M. Carrick, C. W. G. Fishwick, R. Harding, P. J. Mawer, S. E. Radford, A. E. Strong and N. Boden, *J. Am. Chem. Soc.*, 2003, **125**, 9619-9628.
206. W. J. Li, F. Nicol and F. C. Szoka, *Adv. Drug Deliv. Rev.*, 2004, **56**, 967-985.
207. T. B. Wyman, F. Nicol, O. Zelphati, P. V. Scaria, C. Plank and F. C. Szoka, *Biochemistry*, 1997, **36**, 3008-3017.
208. S. Aluri, S. M. Janib and J. A. Mackay, *Adv. Drug Deliv. Rev.*, 2009, **61**, 940-952.
209. L. E. Gerweck and K. Seetharaman, *Cancer Res.*, 1996, **56**, 1194-1198.
210. T. Arakawa, *Arch. Biochem. Biophys.*, 1986, **248**, 101-105.
211. P. K. Nandi and D. R. Robinson, *J. Am. Chem. Soc.*, 1972, **94**, 1299-1308.
212. Y. Hong, L. S. Lau, R. L. Legge and P. Chen, *J. Adhes.*, 2004, **80**, 913-931.
213. M. A. Bokhari, G. Akay, S. Zhang and M. A. Birch, *Biomaterials*, 2005, **26**, 5198-5208.
214. D. A. Narmoneva, O. Oni, A. L. Sieminski, S. Zhang, J. P. Gertler, R. D. Kamm and R. T. Lee, *Biomaterials*, 2005, **26**, 4837-4846.
215. P. A. George, K. Quinn and J. J. Cooper-White, *Biomaterials*, 2010, **31**, 641-647.
216. K. v. d. Mark, J. Park, S. Bauer and P. Schmuki, *Cell Tissue Res.*, 2010, **339**, 131-153.
217. J. M. Anderson, A. Andukuri, D. J. Lim and H.-W. Jun, *ACS Nano*, 2009, **11**, 3447-3454.
218. K. M. Galler, A. Cavender, V. Yuwono, H. Dong, S. Shi, G. Schmalz, J. D. Hartgerink and R. N. D'Souza, *Tissue Eng.*, 2008, **14**, 2051-2058.
219. R. Orbach, L. Adler-Abramovich, S. Zigerson, I. Mironi-Harpaz, D. Seliktar and E. Gazit, *Biomacromolecules*, 2009, **10**, 2646-2651.
220. Y. Yang, U. Khoe, X. Wang, A. Horii, H. Yokoi and S. Zhang, *Nano Today*, 2009, **4**, 193-210.
221. H. Yan, A. Nykanen, J. Ruokolainen, D. Farrar, J. E. Gough, A. Saiani and A. F. Miller, *Faraday Discuss.*, 2008, **139**, 71-84.
222. C. P. Barnes, S. A. Sell, E. D. Boland, D. G. Simpson and G. L. Bowlin, *Adv. Drug Deliv. Rev.*, 2007, **59**, 1413-1433.

223. G. A. Silva, C. Czeisler, K. L. Niece, E. Beniash, D. A. Harrington and J. A. Kessler, *Science*, 2004, **303**, 1352-1355.
224. E. S. Place, N. D. Evans and M. M. Stevens, *Nat. Mater.* , 2009, **8**, 457-470.
225. J. P. Jung, A. K. Nagaraj, E. K. Fox, J. S. Rudra, J. M. Devgun and J. H. Collier, *Biomaterials*, 2009, **30**, 2400-2410.
226. J. H. Collier, *Soft Matter*, 2008, **4**, 2310-2315.
227. B. Kao, K. Kadomatsu and Y. Hosaka, *Tissue Eng. Part A*, 2009, **15**, 2385-2396.
228. F. Zhang, G.-S. Shi, L.-F. Ren, F.-Q. Hu, S.-L. Li and Z.-J. Xie, *J. Mater. Sci.- Mater. M.*, 2009, **20**, 1475-1481.
229. M. J. Humphries, *J. Cell Sci.*, 1990, **97**, 585-592.
230. R. O. Hynes, *Cell*, 1992, **69**, 11-25.
231. S. Koutsopoulos, L. D. Unsworth, Y. Nagai and S. Zhang, *P. Natl. Acad. Sci. USA*, 2009, **106**, 4623-4628.
232. M. C. Branco, D. J. Pochan, N. J. Wagner and J. P. Schneider, *Biomaterials*, 2009, **30**, 1339-1347.
233. M. E. Davis, P. C. H. Hsieh, T. Takahashi, Q. Song, S. Zhang, R. D. Kamm, A. J. Grodzinsky, P. Anversa and R. T. Lee, *P. Natl. Acad. Sci. USA*, 2006, **103**, 8155-8160.
234. J.-F. Lutz and H. G. Börner, *Prog. Polym. Sci.*, 2008, **33**, 1-39.
235. H. G. Borner, *Prog. Polym. Sci.*, 2009, **34**, 811-851.
236. S. Liu, R. Maheshwari and K. L. Kiick, *Macromolecules*, 2009, **42**, 3-13.
237. K. L. Heredia and H. D. Maynard, *Org. Biomol. Chem.*, 2007, **5**, 45-53.
238. M. A. Gauthier and H. A. Klok, *Chem. Commun.*, 2008, 2591-2611.
239. H. A. Klok, *Macromolecules*, 2009, **42**, 7990-8000.
240. H. Jatzkewitz, *Hoppe-Seyler's Z. Physiol. Chem.*, 1954, **297**, 149-156.
241. A. Abuchowski, T. Vanes, N. C. Palczuk and F. F. Davis, *J. Biol. Chem.*, 1977, **252**, 3578–3581.
242. Z. Ding, C. J. Long, Y. Hayashi, E. V. Bulmus, A. S. Hoffman and P. S. Stayton, *Bioconj. Chem.*, 1999, **10**, 395-400.
243. G. T. Hermanson, *Bioconjugate techniques*, 1st edn., Academic Press, 1996.
244. http://www.piercenet.com, Accessed February, 2010.
245. G. Pasut and F. M. Veronese, *Prog. Polym. Sci.*, 2007, **32**, 933-961.
246. M. J. Roberts, M. D. Bentley and J. M. Harris, *Adv. Drug Deliv. Rev.*, 2002, **54**, 459-476.
247. A. Abuchowski, J. R. Mccoy, N. C. Palczuk, T. Vanes and F. F. Davis, *J. Biol. Chem.*, 1977, **252**, 3582–3586.
248. S. Arpicco, F. Dosio, A. Bolognesi, C. Lubelli, P. Brusa, B. Stella, M. Ceruti and L. Cattel, *Bioconjugate Chem.*, 2002, **13**, 757–765.
249. S. M. Chamow, T. P. Kogan, M. Venuti, T. Gadek, R. J. Harris, D. H. Peers, J. Mordenti, S. Shak and A. Ashkenazi, *Bioconj. Chem.*, 1994, **5**, 133-140.
250. O. Kinstler, G. Molineux, M. Treuheit, D. Ladd and C. Gegg, *Adv. Drug Deliv. Rev.*, 2002, **54**, 477-485.
251. M. J. Roberts, M. D. Bentley and J. M. Harris, *Adv. Drug Delivery Rev.*, 2002, **54**, 459–476.
252. Z. Ding, G. Chen and A. S. Hoffman, *J. Biomed. Mater. Res.*, 1998, **39**, 498-505.
253. A. L. Nguyen and J. H. T. Luong, *Biotechnol. Bioeng.* , 1989, **34**, 1186-1190.
254. J. P. Chen and A. S. Hoffman, *Biomaterials*, 1990, **11**, 631-634.
255. Y. Hao, M. Andersson, C. Virto, I. Y. Galaev, B. Mattiasson and R. Hatti-Kaul, *Biocatal. Biotransform.* , 2001, **19**, 341-359.
256. V. Bulmus, S. Patir, S. A. Tuncel and E. Piskin, *J. Appl. Polym. Sci.*, 2003, **88**, 2012-2019.
257. P. S. Stayton, T. Shimoboji, C. Long, A. Chilkoti, G. H. Chen, J. M. Harris and A. S. Hoffman, *Nature*, 1995, **378**, 472-474.
258. V. Bulmus, Z. L. Ding, C. J. Long, P. S. Stayton and A. S. Hoffman, *Bioconjugate Chem.*, 2000, **11**, 78–83.
259. T. Shimoboji, E. Larenas, T. Fowler, A. S. Hoffman and P. S. Stayton, *Bioconjugate Chem.*, 2003, **14**, 517–525.

260. K. Velonia, A. E. Rowan and R. J. M. Nolte, *J. Am. Chem. Soc.*, 2002, **124**, 4224–4225.
261. A. Chilkoti, G. H. Chen, P. S. Stayton and A. S. Hoffman, *Bioconjugate Chem.*, 1994, **5**, 504–507.
262. J. T. Li, J. Carlsson, J. N. Lin and K. D. Caldwell, *Bioconjugate Chem.*, 1996, **7**, 592–599.
263. J. M. Smeenk, M. B. J. Otten, J. Thies, D. A. Tirrell, H. G. Stunnenberg and J. C. M. van Hest, *Angew. Chem. Int. Ed.*, 2005, **44**, 1968-1971.
264. H. Shao, M. M. Crnogorac, T. Kong, S. Y. Chen, J. M. Williams, J. M. Tack, V. Gueriguian, E. N. Cagle, M. Carnevali, D. Tumelty, X. Paliard, L. P. Miranda, J. A. Bradburne and G. G. Kochendoerfer, *J. Am. Chem. Soc.*, 2005, **127**, 1350–1351.
265. L. P. Miranda, H. Shao, J. Williams, S.-Y. Chen, T. Kong, R. Garcia, Y. Chinn, N. Fraud, B. O'Dwyer, J. Ye, J. Wilken, D. E. Low, E. N. Cagle, M. Carnevali, A. Lee, D. Song, A. Kung, J. A. Bradburne, X. Paliard and G. G. Kochendoerfer, *J. Am. Chem. Soc.*, 2007, **129**, 13153-13159.
266. H. C. Kolb, M. G. Finn and K. B. Sharpless, *Angew. Chem. Int. Ed.*, 2001, **40**, 2004-2021.
267. A. J. Dirks, S. S. v. Berkel, N. S. Hatzakis, J. A. Opsteen, F. L. v. Delft, J. J. L. M. Cornelissen, A. E. Rowan, J. C. M. v. Hest, F. P. J. T. Rutjes and R. J. M. Nolte, *Chem. Commun.*, 2005, 4172-4174.
268. S. Kulkarni, C. Schilli, A. H. E. Muller, A. S. Hoffman and P. S. Stayton, *Bioconjugate Chem.*, 2004, **15**, 747–753.
269. D. Bontempo and H. D. Maynard, *J. Am. Chem. Soc.*, 2005, **127**, 6508–6509.
270. K. L. Heredia, D. Bontempo, T. Ly, J. T. Byers, S. Halstenberg and H. D. Maynard, *J. Am. Chem. Soc.*, 2005, 16955-16960.
271. H. D. Maynard, K. L. Heredia, R. C. Li, D. P. Parra and V. Vazquez-Dorbatt, *J. Mater. Chem.*, 2007, **17**, 4015-4017.
272. Y. Imai and Y. Iwakura, *J. Appl. Polym. Sci.*, 1967, **11**, 1529–1538.
273. Q. Z. Dong and Y. L. Hsieh, *J. Appl. Polym. Sci.*, 2000, **77**, 2543–2551.
274. H. Keles, M. Celik, M. Sacak and L. Aksu, *J. Appl. Polym. Sci.*, 1999, **74**, 1547–1556.
275. Y. Mei, K. L. B. Beers, M., D. L. VanderHart and N. R. Washburn, *J. Am. Chem. Soc.*, 2004, **126**, 3472-3476.
276. T. S. Burkoth, T. L. S. Benzinger, D. N. M. Jones, K. Hallenga, S. C. Meredith and D. G. Lynn, *J. Am. Chem. Soc.*, 1998, **120**, 7655-7656.
277. J. Babin, J. Rodríguez-Hernández, S. Lecommandoux, H. A. Klok and M.-F. Achard, *Faraday Discuss.*, 2005, **128**, 179-192.
278. A. Lubbert, V. Casteletto, I. W. Hamley, H. Nuhn, M. Scholl, L. Bourdillon, C. Wandrey and H. A. Klok, *Langmuir*, 2005, **21**, 6582-6589.
279. J. T. Li, T. Wang, D. Wu, X. Zhang, J. Yan, S. Du, Y. Guo, J. Wang and A. Zhang, *Biomacromolecules*, 2008, **9**, 2670-2676.
280. D. E. Discher and A. Eisenberg, *Science*, 2002, **297**, 967-973.
281. J. Cai, L. Zhang, J. Lin and L. Wang, *J. Phys. Chem. B*, 2008, **112**, 12666-12673.
282. A. J. Dirks, S. S. v. Berkel, H. I. V. Amatdjais-Groenen, F. P. J. T. Rutjes, J. J. L. M. Cornelissen and R. J. M. Nolte, *Soft Matter*, 2009, **5**, 1692-1704.
283. C. Wang, R. J. Stewart and J. Kopecek, *Nature*, 1999, **397**, 417-420.
284. L. C. Radu, J. Yang and J. Kopecek, *Macromol. Biosci.*, 2009, **9**, 36-44.
285. N. Tzokova, C. M. Fernyhough, P. D. Topham, N. Sandon, D. J. Adams, M. F. Butler, S. P. Armes and A. J. Ryan, *Langmuir*, 2009, **25**, 2479-2485.
286. N. Tzokova, C. M. Fernyhough, M. F. Butler, S. P. Armes, A. J. Ryan, P. D. Topham and D. J. Adams, *Langmuir*, 2009, **25**, 11082-11089.
287. V. Casteletto and I. W. Hamley, *Biophys. Chem.*, 2009, **14**, 169-174.
288. A. S. Hoffman, *Clin. Chem.*, 2000, **46**, 1478–1486.
289. M. L. Nucci, R. Shorr and A. Abuchowski, *Adv. Drug Deliv. Rev.*, 1991, **6**, 133–151.
290. K. Osada and K. Kataoka, *Adv. Polym. Sci.*, 2006, **202**, 113– 153.
291. M. Yokoyama, G. S. Kwon, T. Okano, Y. Sakurai, T. Seto and K. Kataoka, *Bioconjugate Chem.*, 1992, **3**, 295–301.

292. M. Yokoyama, S. Fukushima, R. Uehara, K. Okamoto, K. Kataoka, Y. Sakurai and T. Okano, *J. Control. Rel.*, 1998, **50**, 79– 92.
293. M. Yokoyama, *Expert Opin. Drug Deliv.*, 2010, **7**, 145-158.
294. K. Kataoka, A. Harada and Y. Nagasaki, *Adv. Drug Deliv. Rev.*, 2001, **47**, 113-131.
295. A. Mitra, A. Nan, J. C. Papadimitriou, H. Ghandehari and B. R. Line, *Nucl. Med. Biol.* , 2006, **33**, 43– 52.
296. Y. S. Kim, E. S. Gil and T. L. Lowe, *Macromolecules*, 2006, **39**, 7805-7811.
297. T. C. Stover, Y. S. Kim, T. L. Lowe and M. Kester, *Biomaterials*, 2008, **29**, 359-369.
298. H. Song, R. He, K. Wang, J. Ruan, C. Bao, N. Li, J. Ji and D. Cui, *Biomaterials*, 2010, **31**, 2302-2312.
299. L. Deng, K. Shi, Y. Zhang, H. Wang, J. Zeng, X. Guo, Z. Du and B. Zhang, *J. Colloid Interface Sci.*, 2008, **323**, 169-175.
300. M. P. Lutolf, G. P. Raeber, A. Zisch, N. Tirelli and J. A. Hubbell, *Adv. Mater.*, 2003, **15**, 888-892.
301. M. P. Lutolf, F. E. Weber, H. G. Schmoekel, J. C. Schense, T. Kohler, R. Muller and J. A. Hubbell, *Nat. Biotechnol.*, 2003, **21**, 513-518.
302. S. Tugulu, P. Silacci, N. Stergiopulos and H. A. Klok, *Biomaterials*, 2007, **28**, 2536-2546.
303. G. Chen and A. S. Hoffman, *Bioconjugate Chem.*, 1993, **4**, 509-514.
304. W. Wang, H. Liang, R. C. Al Ghanami, L. Hamilton, M. Fraylich, M. Shakesheff, B. Saunders and C. Alexander, *Adv. Mater.*, 2009, **21**, 1809-1813.
305. J. E. Morris, A. S. Hoffman and R. R. Fisher, *Biotech. Bioeng.*, 1993, **41**, 991-997.
306. G. Chen and A. S. Hoffman, *Bioconj. Chem.*, 2002, **4**, 509-514.

Chapter 3

Materials and Methods

3.1. Introduction

In this chapter the experimental procedures for the free radical polymerisation (FRP) of NIPAAm, solid phase peptide synthesis using Fmoc protocols and the conjugation of PNIPAAm with the peptides will be described. The basic principles of the instrumental techniques will be also described along with the general methods for sample preparation and analysis.

3.2. Materials

N-isopropylacrylamide (Aldrich, 97%) was recrystallised from hexane. NIPAAm-d7 (Polymer Source Inc., 98%) was used as received. Azobisisobutyronitrile (Fisher Scientific, laboratory grade) was recrystallised from methanol. 3-Mercaptopropionic acid (Acros Organics) was used as received. Propan-2-ol, hexane, absolute ethanol were purchased from Fisher Scientific and used as received. Dichloromethane (99.9%), tetrahydrofuran, (99+%), *N,N*-dimethylformamide (anhydrous, 99.8%), *N*-methyl-2-pyrrolidinone (99%), anisole (99%), ninhydrin (97%), potassium cyanide (97% ACS, reagent grade), phenol (99+%), DMSO-d_6 (99.9 atom% D with 0.03% v/v TMS) were purchased from Aldrich and used as received. Trifluoroacetic acid (99%), acetonitrile (Chromasolv for HPLC), water (Chromasolv Plus for HPLC), piperidin (99%), *N,N*-diisopropylethylamine (99%) were purchased from Sigma-Aldrich and used as received. Fmoc-Glu(OtBu)-OH, Fmoc-Lys(Boc)-OH, Fmoc-Phe-OH, Fmoc-Lys(Boc)-Wang resin were purchased from Novabiochem and used as received.

3.3. Synthetic procedures

3.3.1. Solid phase peptide synthesis (SPPS)

Peptide synthesis was performed on a ChemTech ACT 90 peptide synthesiser using *N*-methyl-2-pyrrolidone (NMP) as a solvent and standard 9-fluorenylmethoxycarbonyl (Fmoc) protocols [1]. The peptide synthesis usually includes several steps which are described below.

1) Swelling of the resin

For FEFEFKFK synthesis a preloaded Fmoc-Lys(Boc)-Wang resin was used (bead size 100–200 mesh, substitution – 0.70 mmol g^{-1}). The N-terminus of the amino acid was protected by a base-labile Fmoc protecting group and the side groups were protected by acid-labile tertiary-butyl (tBu) groups. In a typical procedure ~ 2.5 g of resin were placed into the reaction vessel. First 30 ml of dichloromethane (DCM) were added and the vessel was agitated for 2 h to swell the solid support. Then 20 ml of NMP were added to continue swelling for an additional hour.

2) Deprotection

The Fmoc group was cleaved by solvent mixture of piperidine:NMP = 2:1 to allow coupling of another amino acid. 30 ml of piperidine:NMP mixture were added, the reaction vessel was agitated for 20 min. Then the deprotected amino acid on the solid support was washed 5 times with 20 ml of NMP, each time mixing for 1 minute. To check if all Fmoc groups were removed and the N-terminus was ready for reaction with the next amino acid, the Kaiser test was performed [2, 3]. The Kaiser test is a qualitative test for free primary amines based on their reaction with ninhydrin. The blue colour of the beads indicates that free amino groups are present and the amino acid is deprotected and ready for the coupling. No colour indicates that no free amine groups are present and the deprotection should be repeated.

For the Kaiser test two solutions were prepared: solution A and solution B. To prepare solution A, 8 g of phenol were initially dissolved in 2 ml of absolute ethanol and 13 mg of potassium cyanide (KCN) were dissolved in 20 ml of water. Then 20 μl of the aqueous KCN solution was diluted with 980 μl of pyridine and added to 100 μl of the phenol/ethanol solution. Solution B contained 1 g of ninhydrin in 20 ml of absolute ethanol. Both solutions are light sensitive and were kept in covered containers. The Kaiser test was performed by adding 3 drops of solution A and three drops of solution B to an aliquot of resin beads from the reaction vessel and incubating at 100ºC for 2 minutes.

3) Coupling

The quantities of amino acids and activating agent were calculated taking into consideration the amount of resin loaded in the vessel:

$$n = m_{resin} \times n_{resin\ substitution} \qquad (Eq.\ 3.1)$$

where n – number of moles per gram of resin (mmol g^{-1}), m – mass of resin in g, $n_{resin\ substitution}$ – number of moles (mmol) of first pre-loaded amino acid per gram of resin

All amino acids and activating agent were added to the reaction vessel in an 8 fold excess to ensure a quantitative reaction. Amino acid coupling was facilitated using 2-(6-chloro-1H-benzotriazole-1-yl)-1,1,3,3-tetramethylaminium hexafluorophosphate (HCTU) which activated the carboxyl group by forming an activated ester and making nucleophilic attack by an amino group more efficient.

The amino acid required for coupling and HCTU were dissolved in 40 ml of DMF prior to loading into the reaction vessel. HCTU is light sensitive, so the lights were turned off and the vessel was covered with foil. 20 ml of deprotonating agent *N*,*N*-diisopropylethylamine (DIPEA) were added to the reactor to facilitate the formation of the peptide bond. The reaction mixture was agitated for 1 hour. Then the peptidyl resin was cleaned.

4) Cleaning

The cleaning step included the addition of 20 ml of NMP to the vessel to wash the peptidyl resin and then the beads were filtered. This washing was repeated once. Then, 30 ml of NMP were added and the vessel was agitated for 1 min. The reactor was emptied and washing with NMP was repeated 4 times.

The Kaiser test was performed subsequently to see if all the amino acids were coupled and that there were no free amines left. The beads and the solution should be yellow indicating that all the amino groups are protected.

5) n times deprotection and coupling

According to the desired length of the peptide, the deprotection of Fmoc N-terminus and coupling of the next amino acid were repeated until the peptide was fully synthesised (steps 2 - 4).

6) Final cleaning

The final cleaning of the peptidyl resin involved three steps:

- 3 × 20 ml of DMF were added manually to the reactor and agitated for 15 min, then the solvent was drained leaving the beads in the vessel;

- 2 × 20 ml of ethanol were added and agitated for 10 min, then the solvent was drained;

- 2 × 20 ml of DCM were added and agitated for 10 min, then the solvent was drained.

The peptidyl resin was left in the reactor to dry overnight.

7) Cleavage

Liberation of the final peptide from the support was accomplished by treating the system with 20 ml of a cleavage mixture (95 vol.% of trifluoroacetic acid (TFA) and 5 vol.% of anisole) and agitating the vessel for 3 hours. Anisole was added to prevent highly reactive TFA participating in side reactions. Subsequently, the peptide solution in TFA was poured into a round-bottom flask and TFA was evaporated using a rotary evaporator, leaving a concentrated peptide solution. The peptide was isolated by precipitation into diethyl ether and centrifugation. The washing with diethyl ether and centrifugation were repeated 4 times. Finally, the peptide was lyophilised from water, resulting in a white powder material with the yield of ~ 80%. The peptide structure was confirmed by ^{1}H NMR (Appendix 1 Fig. A1.1 and A1.2), its molar mass was confirmed by mass spectroscopy (MS) (1121 g mol^{-1}) (Appendix 1 Fig. A1.3) and its purity was found to be ~ 85% using reverse phase high performance liquid chromatography (RP-HPLC) (Appendix 1 Fig. A1.4 and A1.5)

3.3.2. Modification of FEFEFKFK with 3-mercaptopropionic acid (MPA)

The synthesis of SH-modified peptide was performed in a similar way as for a normal peptide using the method developed by Stoica *et al.* [4]. Once all standard amino acid coupling

steps were complete and the N-terminus of the last amino acid was deprotected, 8 fold excess of 3-mercaptopropionic acid (MPA) and HCTU were added. The reaction mixture was agitated for 24 h to ensure the coupling of MPA to the free amino group of the peptide. The functionalised peptide was then cleaned, cleaved and purified, following the same procedures described above. The peptide modification was confirmed by proton nuclear magnetic resonance (^{1}H NMR) (Appendix 1 Fig. A1.1 and A1.2), the peptide molar mass was confirmed by MS (1209 g mol^{-1}) (Appendix 1 Fig. A1.3) and its purity was found to be ~ 85% using HPLC (Appendix 1 Fig. A1.4 and A1.5).

3.3.3. Polymerisation of *N*-isopropylacrylamide (NIPAAm)

NIPAAm was polymerised via FRP with AIBN as initiator. NIPAAm and AIBN were both recrystallised prior to use from hexane and methanol respectively. Typically 3 g (26.5 mmole) of NIPAAm and 40 mg (0.244 mmole) of AIBN were placed in a reaction vessel with a magnetic stirrer. 40 ml of deaerated iso-propanol were added to dissolve the reagents. The reaction mixture was stirred for 24 h at 65°C under N_2. After that the reaction mixture was cooled to room temperature. It was concentrated by evaporating the majority of organic solvent using a rotary evaporator. The product was dissolved in THF and precipitated into hexane. This dissolution/precipitation and evaporation was repeated several times until a white powder was obtained. The polymer was characterised by gel permeation chromatography (GPC), by micro differential scanning calorimetry (micro DSC) and ^{1}H NMR.

3.3.4. PNIPAAm functionalisation with peptide

A series of polymer-conjugate mixtures were obtained using the conditions given in Table 3.1.

Table 3.1: *PNIPAAm functionalisation with FEFEFKFK and FEFKFEFK*

Sample*	n_{NIPAAm} (moles)	$n_{AIBN} \times 10^{-4}$ (moles)	SH-FEFEFKFK (S) or SH-FEFKFEFK (A)	
			m (mg)	n × 10^{-5} (moles)
PS1 and PA1	0.0265	2.44	100	8.27
PS2 and PA2	0.0265	2.44	200	16.5
PS3 and PA3	0.0265	2.44	400	33.1

* S and A stand for sequential and alternating peptides FEFEFKFK and FEFKFEFK respectively.

The reagents were dissolved in 30 ml of deoxygenated DMSO and the reaction mixture was stirred at 65ºC for 24 h under N_2. The reaction mixture was subsequently cooled to room temperature and the majority of solvent was evaporated using a rotary evaporator. The viscous liquid left was diluted with deionised water to 500 ml. This solution was placed in dialysis

membranes with 3,500 g mol^{-1} molecular weight cut-off (MWCO) (Medicell Ltd., UK) and dialysed against water for 4 days to remove short polymer chains and unreacted reagents. After purification, the solution was lyophililysed to give a white powder product with yield > 85%. The products were characterised by ^{1}H NMR (see Appendix 2 Fig. A2.1 – A2.3), SLS, viscometry, GPC and micro DSC.

It should be noted that Michael addition of NIPAAm monomers to the primary amine on the side chains of lysine may occur. Previous experiments in the beginning of this project using the coupling of carboxyl group functionalised PNIPAAm to the peptide with unprotected side chain groups via *N*-hydroxysuccinimidyl (NHS) and carbodiimide strategy showed that polymer attachment to the side chains of lysine resulted in products insoluble in water. The products obtained in this study using the polymerisation of NIPAAm and peptidic chain-transfer agent were fully soluble suggesting that only linear conjugates were obtained.

3.3.5. Determination of the polymer/conjugate ratio

50 mg ml^{-1} of polymer/conjugate mixture was dissolved in 1 ml of H_2O. Centrifugation was used to separate unconjugated polymer from the conjugate. It was anticipated that after centrifugation the conjugate would start to self-assemble into fibres and would precipitate at the bottom due to their increased density. As to the less dense polymer, it would be extracted and present in upper liquid phase. Polymer was extracted a further 3 times and the resulting polymer and conjugate fractions were separately collated, freeze-dried, analysed by ^{1}H NMR in DMSO-d_6 and weighed to calculate the ratios.

3.3.6. Gelation and phase behaviour of polymer-rich and peptide-rich gels

In Chapter 4 polymer/conjugate mixture solutions were prepared in the sample concentration range from 5 to 200 mg ml^{-1}. The samples were mixed thoroughly for 30 sec using the Vortex mixer and left at room temperature to dissolve completely. Gel behaviour was studied after ~ 12 h. The concentration at which self-supported gels were formed was registered as a critical gelation concentration of a sample using a tilt-test.

The phase behaviour of the gels was studied as a function of temperature. The test tubes were placed in a thermo-regulated water bath and the phase behaviour of each sample was recorded visually at 10°C intervals during heating/cooling cycle from 25 to 80°C. When each temperature was reached, the samples were equilibrated for 15 minutes, and the observations were recorded.

In Chapter 5 and 6 the samples were prepared in a similar fashion as described previously in section 3.3.6. Gelation was studied after ~ 12 h. To study the phase behaviour gels were placed in the thermo-regulated oven at 40 and 80°C for 15 min and their state was recorded by removing the samples from the oven and taking the pictures of the phase separated samples.

3.4. Instrumental techniques

3.4.1. Nuclear magnetic resonance (NMR) spectroscopy

3.4.1.1. Theory behind NMR spectroscopy

NMR is a technique to analyse the structure and stereochemistry of chemical molecules, mainly organic compounds which consist of carbon, hydrogen and oxygen. Every NMR experiment involves three steps: sample placement in a static magnetic field, excitation of the nuclei of the sample with a radio frequency pulse and measurement of the frequency of the signals emitted. Typically the NMR active nuclei in the sample resonate at different frequencies which are called **resonance frequencies**. These are the frequencies emitted by the nuclei when the sample is excited by the radio frequency pulse. The type of nucleus and local atomic environment influence the value of the resonance frequency.

Electrons, protons and neutrons are spinning on their axes. In many atoms like ^{12}C these spins are paired against each other, so that the nucleus of the atom has no overall spin. These atoms are inactive towards radio frequency. The atoms in which the nucleus possess an overall spin (*I*) are active, for example, ^{1}H and ^{13}C. ^{1}H is also the most abundant isotope in nature (99.98%). A natural abundance of ^{12}C is 98.89%, but it is inactive. Hence ^{13}C is used even if its natural abundance is only 1.11%.

In the magnetic field atomic nuclei align depending on their spin, and electrons interact with the magnetic field and begin to circulate around the nucleus. Electrons generate a magnetic field which is opposite to the main magnetic field and therefore decrease it. In other words the electrons shield the nucleus from the applied magnetic field. The difference between the applied field and the field at the nucleus is termed the nuclear shielding. This decrease in the main magnetic field is small and can be measured in parts per million (ppm). The **chemical shift** represents the ratio of the change in magnetic field with the respect to the magnetic field required to bring nuclei with no shielding effects into resonance. The size of chemical shift is dependent on the neighbouring atoms. NMR signal frequencies are measured in Hertz (Hz – cycles per second) or Megahertz (MHz). All the frequencies are measured with respect to a reference. For ^{1}H NMR the recommended reference is tetramethylsilane $Si(CH_3)_4$ (TMS) and its peak is taken as a reference of zero. The advantage of the ppm unit is that

frequency measurements are independent of magnet strength which simplifies the comparison of spectra obtained on different instruments. To covert the frequency from ppm to Hertz, the frequency of the emitted signal in Hz should be multiplied by the carrier frequency in MHz. To convert Hertz to ppm, Hertz should be divided by the carrier frequency in MHz. Most protons display chemical shifts within 14 ppm of TMS.

Splitting of NMR signals may occur due to magnetic interaction between neighboring protons. For example, two protons can combine and exist in three possible magnetic states as a result of spin orientation. The effect of spin-spin coupling can be removed by a technique called "decoupling" when the presence of a particular proton group can be masked.

During the acquisition of the signals emitted by the excited atoms in the sample the raw data is acquired and the received signal is called an Free Induction Decay (FID). The FID is then transformed into the frequency spectrum using mathematical operation (Fourier transformation). In the FID the signal intensity varies with time. An NMR spectrum is a plot of signal frequency versus signal intensity. The frequency provides qualitative information about the local atomic environment. The intensity gives quantitative information as the integral of the peak is directly related to the number of nuclei contributing to a signal at a particular frequency [5, 6].

^{13}C NMR follows the same principles as ^{1}H NMR and identifies carbons in organic molecules. TMS is also used as the reference (0 ppm), however the chemical shift range is approximately 20 times larger than that of ^{1}H NMR [7].

3.4.1.2. General procedure for NMR spectroscopy

^{1}H NMR spectra were measured on a Bruker DPX 400 Spectrometer operating at 400 MHz. Deuterated dimethyl sulfoxide (δ (DMSO-d_6) = 2.50 ppm) with 0.03% tetramethylsilane (TMS) was used as a solvent reference. All the spectra used for the comparison were collected under identical conditions with 256 scans. The spectra were analysed using MestreNova software (CambridgeSoft).

3.4.2. Static Light Scattering (SLS)

3.4.2.1. Principle of SLS

In light scattering the light beam (electromagnetic wave) is scattered by the atoms or molecules of the medium. The intensity of the scattered light depends on the polarisability of the molecules (molecules posses a dipole moment) which in turn depends on the molecular weight. Therefore light scattering is one of the techniques for determining $\overline{M}_w$ of polymers [8-10].

For gases, Rayleigh showed that the reduced intensity of the scattered light R_θ at any angle θ to the incident beam of wavelength λ could be related to the molar mass of the gas *M*, its concentration *c*, and the refractive index increment (*dn*/*dc*) using the following equation:

$$R_\theta = \frac{4\pi^2 n^2}{N_A \lambda^4}\left(\frac{dn}{dc}\right)^2 (1+\cos^2\theta) M_c \qquad (Eq.\ 3.2)$$

where $R_\theta = i_\theta r^2 / I_0$ is Rayleigh ratio, where I_0 is the intensity of the incident beam, i_θ is the quantity of light scattered per unit volume by one centre at an angle θ to the incident beam, *r* is the distance of the centre from the observer, and N_A is the Avogadro's number. This equation is valid only for gases where all the particles are considered as independent scattering centres.

For polymer solutions, both scattering from the solvent and polymer contribute to scattering, therefore

$$R_\theta = R_\theta(\text{solution}) - R_\theta(\text{solvent}) \qquad (Eq.\ 3.3)$$

and the change of polymer concentration is related to the change in Gibbs energy (ΔG) which in turn is related to the osmotic pressure π, then:

$$R_\theta = \frac{4\pi^2 {n_0}^2}{\lambda^4}\left(\frac{dn}{dc}\right)^2 (1+\cos^2\theta)\frac{NM}{N_A}\frac{RT}{(d\pi/dc)_T} \qquad (Eq.\ 3.4)$$

where n_0 and *n* are the refractive indices of the solvent and solution respectively measured by differential refractometer, *c* is polymer concentration, and *N* is the number of polymer molecules. The refractive index increment $\frac{dn}{dc}$ is defined as $\frac{n-n_0}{c}$. Differentiation of the virial expansion for π with respect to *c*, followed by substitution in Eq. 3.4 and rearrangement gives:

$$\frac{K'(1+\cos^2\theta)c}{R_\theta} = \frac{1}{M_w} + 2A_2 c \qquad (Eq.\ 3.5)$$

$$\text{where } K' = \frac{4\pi^2 n_0^2 (dn/dc)^2}{\lambda^4 N_A} \qquad (Eq.\ 3.6).$$

These equations are valid for molecules smaller than λ'/20 when the angular scattering is symmetrical, λ' being the wavelength of light in solution, i.e. $\lambda' = \lambda/n_0$. Molecular weigth for small particles can be calculated using the Eq. 3.5. When polymer molecules are larger than λ'/20, intramolecular interactions become predominant and cause the light scattering from two or more centres. In this case the scattering depends on the shape of the molecule.

Guinier found that using the scattering originated from large particles a characteristic shape-dependent geometric function called the radius of gyration $\left\langle R_g^{\,2}\right\rangle^{1/2}$ can be obtained.

One of the methods for determining $\langle R_g^2 \rangle^{1/2}$ employs the double extrapolation method proposed by Zimm. This method uses the assumption that the scattering at zero angle is independent of size and the form factor $P(\theta)$ is unity when $\theta = 0$. In practice, it is difficult to measure scattering at zero angle, therefore an exptrapolation method has been developed that is based on the following equation:

$$\frac{Kc}{R_\theta} = \frac{1}{M_w}(1 + \frac{q^2 \langle R_g^2 \rangle^{1/2}}{3}) + 2A_2 c + \ldots \qquad (Eq.\ 3.7)$$

where q is the scattering vector: $q = \frac{4\pi}{\lambda'}\sin(\frac{\theta}{2})$.

Experimentally, the scattering intensity for each polymer concentration in a dilution series is measured at different angles and the data is plotted as (Kc/R_θ) versus $(\sin^2(\theta/2) + k'c)$, where k' is an arbitrary constant. A double extrapolation is performed by joining all points of equal concentration and extrapolating to zero angle, and then all points of equal angles and extrapolating them to zero concentration. The lines of $\theta = 0$ and c = 0 should have a common interseption. This gives a grid-like graph presented in Fig. 3.1. The intercept with y axis gives the value of $1/\overline{M}_w$, the slope of the $\theta = 0$ gives the value of A_2 and R_g is calculated from the slope of the $c = 0$ divided by the intercept.

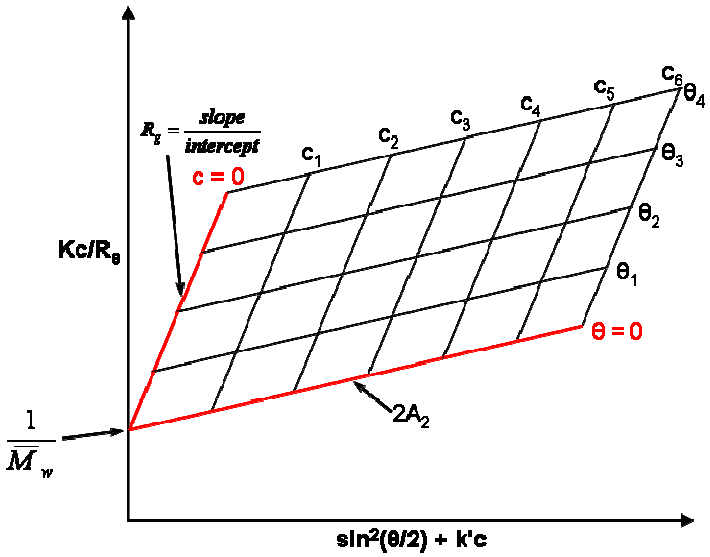

Figure 3.1: *A Zimm plot using the double extrapolation method*

3.4.2.2. General procedure for SLS

SLS measurements were carried out to determine the weight-average molar mass ($\overline{M}_w$), the radius of gyration (R_g) and the second virial coefficient (A_2). SLS measurements were carried out on a Brookhaven Instruments Corporation thermally regulated (± 0.1°C) motor

driven goniometer (BI-200SM) equipped with the digital autocorellator (BI-9000AT), multidiode detector (BT-APD) and with a He-Ne laser at 632.8 nm (Melles Griot). A series of polymer and polymer-conjugate solutions with concentration ranging from 0.5 to 2% were prepared in 1 mM phosphate buffer (pH 7) and filtered prior to the measurements using 0.45 μm filter (Millipore) at 5ºC. The specific refractive index increment (*dn/dc*) necessary for the SLS analysis was determined for each sample dilution series using Abbe refractometer (Model 60/ED) connected to water bath HAAKE F3 digital at 20ºC and Na lamp. BI-ZPW Static Light Scattering Software was used to calculate $\overline{M}_w$, R_g and A_2 values.

3.4.3. Viscometry

3.4.3.1. Introduction to viscometry

When polymer is dissolved in a solvent, its chains interact with solvent molecules changing their conformation and thus affecting the viscosity of a solution. Viscosity of the polymer solution depends also on polymer concentration and on polymer molecular weight [8].

Viscometry of a dilute solution provides a rapid method for the average-viscosity molecular weight ($\overline{M}_v$) determination. For a given polymer/solvent system at a given temperature the intrinsic viscosity, [η] represents the volume occupied by a polymer per mass unit and is related to $\overline{M}_v$ through the Mark-Houwink-Sakurada equation:

$$[\eta] = K\overline{M}_v^a \qquad (Eq.\ 3.8)$$

where *K* and *a* are empirical constants determined experimentally for the polymer/solvent system at a specified temperature using fractions of known molar mass. When *a* is equal to 0.5, the polymer is in theta solvent (ideal solvent). If $0.5 < a < 0.8$, polymer chains are in a "good" solvent and they are in expanded conformation. When $a > 0.8$, the quality of the solvent decreases and polymers are in "poor" solvent where intra-molecular interactions become dominant [240].

The viscosity of a dilute solution is measured in a capillary viscometer. The estimation of polymer molar mass from viscosity measurements does not require absolute viscosities. Hence the absolute calibration of viscometers is not necessary. The relative viscosity, $\eta_{rel,}$ is defined as the ratio of the viscosity of the solution to the viscosity of the solvent. If the flow time of solvent is t_0 is equal to that of the solution t_s, then

$$\eta_{rel} = \frac{\rho_S t_S}{\rho_0 t_0} \qquad (Eq.\ 3.9)$$

For the dilute solutions employed in the viscosity measurements, the densities of the solvent, ρ_0, and the solution, ρ_s, are assumed to be equal. Therefore,

$$\eta_{rel} = t_s / t_0 \qquad (Eq.\ 3.10)$$

The specific viscosity, η_{sp}, expresses the increase in viscosity due to the solute and is defined by $\eta_{sp} = \eta_{rel} - 1.$ (*Eq. 3.11*).

Even in dilute solution molecular interactions occur, therefore η_{sp} is expressed either as a reduced viscosity η_{sp}/c according to the Huggins relation at infinite dilution:

$$\eta_{red} = \lim_{c\to 0} \frac{\eta_{sp}}{c} = [\eta]_H + k_H [\eta]_H^{\,2} c \qquad (Eq.\ 3.12)$$

or as an inherent viscosity $\ln\eta_{rel}/c$ according to the Kraemer relation at infinite dilution:

$$\eta_{inh} = \lim_{c\to 0} \frac{\ln \eta_{rel}}{c} = [\eta]_K - k_K [\eta]_K^{\,2} c \qquad (Eq.\ 3.13).$$

A double extrapolation to $c = 0$ gives the common intercept with y axis which gives the value of $[\eta]$ which is a characteristic parameter for the polymer in a particular solvent. k_H and k_K are shape-dependent factors and are called the Huggins and Kraemer constants accordingly.

Experimentally, both η_{sp}/c and $\ln\eta_{rel}/c$ are calculated by measuring the flow times (in modern viscometers the time of fall of the ball in a capillary) for pure solvent and for a series of polymer solutions over a certain polymer concentration range.

3.4.3.2. General procedure for viscometry measurements

Viscosity measurements were performed on automated micro viscometer AMVn (Anton Paar) using the glass capillary with diameter of 1.6 mm and the ball with diameter of 1.5 mm. The most concentrated solution of each sample in 1 mM PB (pH 7) was prepared first and the solutions of lower concentrations were obtained by successive dilution. A series of solutions for each conjugation product and polymer with concentration ranging from 0.5 to 2% was prepared. The measurements of dynamic viscosity as well as the time of fall of the ball in the capillary for pure solvent, conjugation products and pure polymer solutions were taken at 10°C.

3.4.4. Reversed phase high performance liquid chromatography (RP-HPLC)

3.4.4.1. Principle of RP-HPLC

Typically, every HPLC system consists of a pump with solvents and a degassing unit, a column and a detector. When the sample is injected into the system, the mobile phase carries

it through the column where the separation occurs. In this case, the separation is based on the chemical or physical affinity of the analyte to the column and mobile phase. The stationary phase consist of silica beads covered with hydrophobic saturated carbon chains. The degree of interaction between the mobile phase and the stationary phase affects the retention time of the analytes. If the sample does not exhibit any affinity towards the columns, it is readily eluted from the column at short retention times and vice versa. If the stationary phase is nonpolar, then a polar mobile phase is used (most commonly methanol or acetonitrile with water) and the technique is called reversed phase chromatography (RPC). In RP-HPLC the retention time can be increased by adding more water to the solvent, thus increasing the interaction time of hydrophobic analyte with hydrophobic stationary phase. These interactions can be reduced, by adding organic solvent, thus reducing the retention time [11].

3.4.4.2. General procedure for RP-HPLC analysis

HPLC measurements were performed on a Dionex Ultimate 3000 HPLC system, fitted with an Acclaim 300 column (particle size 3 μm, pore size 100 Å, surface chemistry C18) using a gradient of two solvents (Table 3.2): solvent A is HPLC grade water + 0.1% TFA and solvent B is acetonitrile (ACN) + 0.1% TFA.

Table 3.2: *Gradient of solvents used for the RP-HPLC method*
Solvent A: water + 0.1% TFA, solvent B: ACN + 0.1% TFA

Time (min)	Solvent B (%)
0	20
4	20
35	80
40	80
42	20

Samples were prepared by dissolving 0.5 mg of peptide in 1 ml of deionised water and 0.5 ml acetonitrile. The sample injection volume was 100 μl and the flow rate in the column was maintained at 1 ml min^{-1}. The software Chromeleon CHM-1 6.80 was used to acquire and process the data.

3.4.5. Size exclusion chromatography (SEC)

3.4.5.1. Introduction to SEC

Chromatography is a physico-chemical process that enables the separation of the components of a mixture. SEC, also called *gel filtration chromatography* when the mobile phase is aqueous, and *gel permeation chromatography* (GPC) when the mobile phase is organic, is a high

performance liquid chromatography (HPLC) technique where macromolecules are separated according to differences in their hydrodynamic volume. SEC is widely used for the determination of polymer molecular weight and molecular weight distribution (MWD) or polydispersity index (PDI). The separation is possible by using columns packed with porous spherical particles of crosslinked polystyrene or macroporous silica (3 to 20 μm). During separation the mobile phase with the macromolecular solute molecules is exchanged with the stagnant liquid phase that occupies the interior of the pores. Large molecules are excluded from the smaller pore sizes of the packing material and consequently pass quickly through the column and are eluted first (Fig. 3.2). Smaller molecules diffuse into the many smaller pores, thus retarding their elution. Refractive index (RI), ultraviolet (UV) or infrared (IR) detectors are used to obtain the mass distribution as a function of retention or elution volume. The resulting chromatogram in an SEC experiment represents a molecular size distribution [12].

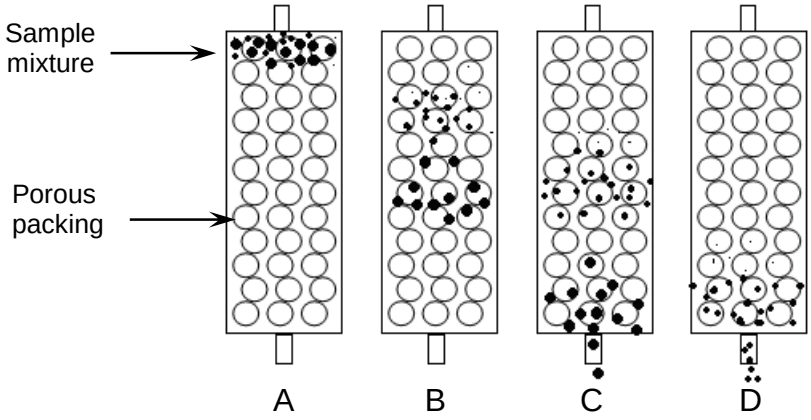

Figure 3.2: *Schematic representation of the separation process in SEC: A) sample injection, B) size separation, C) elution of large molecules, D) elution of small molecules*

During synthetic polymerisation a distribution of macromolecular chains with different length is produced. SEC is widely used for the determination of the number-average ($\overline{M}_n$) and weight-average ($\overline{M}_w$) polymer molecular weights and polydispersity index (PDI):

$$\overline{M}_n = \frac{\sum_i N_i M_i}{\sum_i N_i} = \frac{\sum_i W_i}{\sum_i W_i / M_i} \quad (Eq.\ 3.14); \qquad \overline{M}_w = \frac{\sum_i N_i M_i^2}{\sum_i N_i M_i} = \frac{\sum_i W_i M_i}{\sum_i M_i} \quad (Eq.\ 3.15)$$

where N_i and W_i are the number and weight, respectively, of molecules having molecular weight M_i. The subscript i is an index representing all molecular weights present in the ensemble of chains. M_i is obtained via calibration with appropriate standards where a series of narrow-dispersed molecular weight standards of known peak molecular weight (M_p) are injected into the SEC system and the retention volumes determined. Then log M_p is plotted

versus retention volume and this gives the calibration curve, from which $\overline{M}_n$ and $\overline{M}_w$ are calculated.

Molecular size (radius of gyration, R_g) and molecular weight are related to each other the following relationship: $R_g \sim M^{\alpha}$, where α is a constant which depends on the solute composition, the temperature and the solvent. This relationship depends also on different macromolecular chain conformations. The majority of synthetic polymers form random coils in solution. Once $\overline{M}_n$ and $\overline{M}_w$ of a polymer are obtained, the PDI is calculated using Eq. 3.16. For FRP the PDI values are about 2.0, but larger and slightly smaller values are possible [11, 12].

$$PDI = \frac{\overline{M}_w}{\overline{M}_n} \qquad (Eq.\ 3.16)$$

3.4.5.2. General procedure for GPC

GPC studies were undertaken to determine $\overline{M}_w, \overline{M}_n$ and PDI of the polymeric products obtained in the study. Samples were prepared by dissolving 20 mg of product in 10 ml of DMAc. GPC measurements were performed using *N*,*N*-dimethylacetamide (DMAc) with 0.05% $LiNO_3$ as an eluent and PLgel 500 Å + 2 Mixed B column (column temperature was 75°C, flow rate was 1 ml min^{-1}, injection volume was 100 µl, pump Waters 501). The detection was performed with a refractive index (RI) detector (ERC-7515A, detector temperature was 50°C). PEG/PEO standards were used for calibration.

3.4.6. Oscillatory rheology

3.4.6.1. Principle of rheology

Viscous materials resist shear flow and strain linearly with time when stress is applied. Elastic materials strain instantaneously when stretched and return to their initial state once the stress is removed. Soft (visco-elastic) materials exhibit mechanical properties that lie between those of a pure solid and those of a viscous liquid. In oscillatory rheology a sinusoidal shear deformation is applied to the sample and the resultant stress response is measured. Typically the sample is placed between two parallel plates, as shown in Fig. 3.3.

The top plate rotates imposing a time dependent strain on the sample,

$$\gamma(t) = \gamma \cdot \sin(\omega t) \qquad (Eq.\ 3.17)$$

where γ – strain, ω – oscillation frequency, t - time, while the bottom plate stays stationary and measures stress response. Simultaneously, measurements of the torque that the sample

imposes on the bottom plate give the time dependent stress, $\sigma(t)$. A Peltier element provides temperature control.

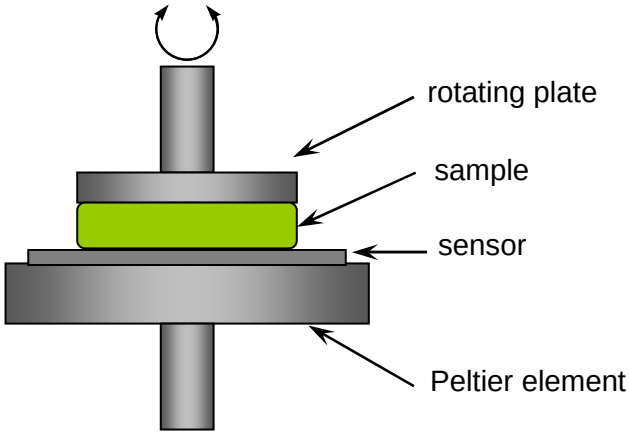

Figure 3.3: *Schematic representation of a typical oscillatory rheometer with the sample placed between two parallel plates*

The visco-elastic behaviour of the system at ω is characterised by the storage, or elastic modulus, $G'(\omega)$, and by the loss, or viscous, modulus, $G''(\omega)$, which characterise the solid-like and liquid-like contributions to the measured stress response respectively. For a sinusoidal strain deformation (Eq. 3.18), the stress response of a visco-elastic material is given by

$$\sigma(t) = G'(\omega)\gamma_0 \sin(\omega t) + G''(\omega)\gamma_0 \cos(\omega t) \qquad (Eq.\ 3.18)$$

Initially, amplitude sweeps are performed to determine the linear visco-elastic region (LVR) of the material (to determine the strain) where material is independent of the extent of deformation. Then frequency sweeps are performed in the LVR. Frequency-dependent G' and G'' are recorded when the material is an undisturbed state, where the applied strain deformations are sufficiently small to affect the material properties [13, 14].

3.4.6.2. General procedure for oscillatory rheology

Mechanical studies were performed on a stress-controlled Bohlin C-CVO rheometer, equipped with a Peltier device to control the temperature. A parallel plate geometry (Ø = 20 mm, 0.25 mm gap) was used with a solvent trap to minimise evaporation.

Rheological experiments of all samples consisted of three stages for each sample. Firstly, a strain amplitude sweep (γ = 0.001 - 10) was performed at constant frequency (ω = 1 rad s^{-1}) to identify the LVR. Secondly, the frequency sweep (ω = 6.28 – 62.8 rad s^{-1}) at constant strain amplitude (γ = 0.01) was performed to determine the elastic (G') and viscous (G'') moluli within LVR. Both measurements were performed at 20°C. Finally, temperature sweeps were performed at a constant strain amplitude (γ = 0.01, ω = 1 rad s^{-1}) and in the temperature range

from 20 to 80°C at a heating/cooling rate of 1 °C/min. Silicon oil was placed around the sample to minimise evaporation. Heating/cooling cycles were performed three times.

3.4.7. Micro differential scanning calorimetry (micro DSC)

3.4.7.1. Principle of micro DSC

The phase transitions of different materials, even having them in small quantities, can be studied by micro DSC with an ultra-high analytical sensitivity. This technique measures the difference in heat flow necessary to increase or decrease the temperature of a sample and reference. The calorimetric block of the micro DSC instrument consists of a metal cylinder with high thermal conductivity (Fig. 3.4A).

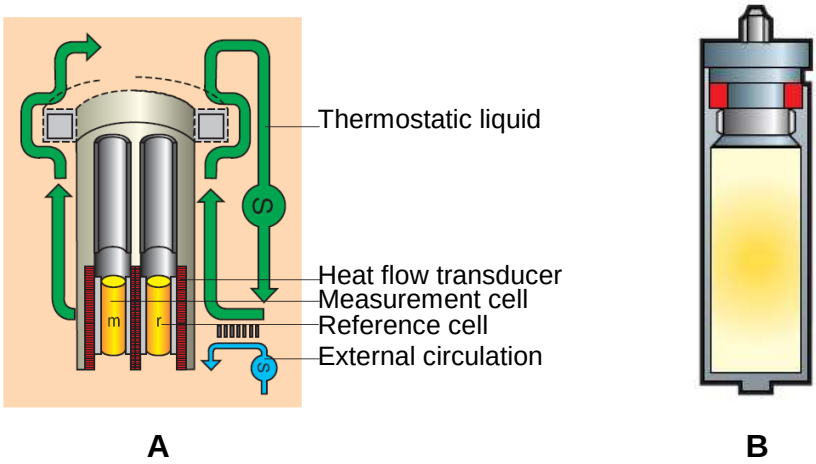

Figure 3.4: *Schematic representation of: A) the calorimetric block and (B) experimental vessel of the micro DSC instrument [15]*

Solid or liquid samples are placed in the "measurement" cell, while the "reference" cell contains an inert material to compensate the heating. There are different types of experimental cells depending on the application. For the experiments closed "batch" cells were used (Fig. 3.4B) which are typically used to determine the phase transitions of liquid samples, e.g. aqueous solutions of polymers or biopolymers.

During the experiment the heating block delivers different heat flow to maintain the temperature of the sample equal to that of the reference. The difference in the heat flows between two cells is related to the thermal characteristic of the sample and gives information about the thermal properties of the material such as melting, crystallisation, polymerisation and decomposition.

The difference in heat flows is related to the specific heat capacities of the sample. The heat flow U_S necessary to increase the temperature of the sample of mass M_S by a degree is expressed as:

$$U_S = M_S \times C_S \qquad (Eq.\ 3.19)$$

Similarly, the heat flow U_R necessary to increase the temperature of the reference of mass M_R by a degree is expressed as:

$$U_R = M_R \times C_R \qquad (Eq.\ 3.20)$$

C_S and C_R are the specific heat capacities of the sample and reference respectively. The difference of the heat capacities can be written as:

$$\Delta C = C_R - C_S = \frac{U_R}{M_R} - \frac{U_S}{M_S} \qquad (Eq.\ 3.21).$$

For each sample a thermogram is obtained by plotting ΔC as a function of temperature. In the case when no thermal transitions occur, only the baseline showing the variation of ΔC with temperature is observed.

During the first order transitions the specific heat capacity becomes infinite and the latent heat (amount of energy released or absorbed by a sample during the change of state) becomes predominant and the thermogram shows a peak The maximum or minimum of the peak describes the temperature of a transition and the area of the peak is related to the enthalpy of the transition. Total enthalpy changes between the sample and reference is defined by the following equation:

$$\Delta H_{tot} = \int_{T_0}^{T} \Delta C \cdot dT \qquad (Eq.\ 3.22)$$

where T_0 and T are initial and final temperatures.

The equation can also be written as:

$$\Delta H_{tot} = \int_{T_0}^{T} (\Delta C_b + \Delta C_t) \cdot dT \qquad (Eq.\ 3.23)$$

where ΔC_b is the difference of the heat capacities when no thermal transition is observed (baseline), ΔC_t is the difference of the heat capacities due to the thermal transition.

Finally, the total enthalpy of the thermal transition corresponds to the peak area is written as:

$$\Delta H_{tot} = \int_{T_0}^{T} \Delta C_t \cdot dT \qquad (Eq.\ 3.24)$$

Phase transitions of polymer solutions, biological materials and gels can be studied by micro DSC. Very slow temperature scanning rates (even lower that 0.001°C min^{-1}) allow a very accurate analysis of these transitions and very low detection limits that are much lower by a factor of ten in comparison to conventional DSC techniques. Calorimetric signal variations of less than one microwatt can be detected. The micro DSC operating temperature range is from -20 to 120ºC [15].

The results from micro DSC experiments are displayed as a thermal analysis curve in which the instrument signal ("heat flow") is plotted against sample temperature or time. From micro DSC plots the temperature values of the transition occurred and the enthalpy values associated with it can be extracted [5].

3.4.7.2. General procedure for micro DSC

Thermal analysis was performed on a micro differential scanning calorimeter III (SETARAM, France). A certain amount of polymeric material was dissolved in 1 ml of deionised water and then the samples were weighed directly in the experimental cell prior to analysis and the cells were sealed hermetically. Heating scans were recorded in the range of 20 – 80°C at a heating rate of 1 °C min^{-1}. Deionised water was used as a blank reference. The heating and cooling cycles were performed four times to study the reversibility of the phase transitions observed. For each sample onset temperature, peak temperature and enthalpy of the phase transition were determined from the DSC curves using Setsoft 2000 software.

3.4.8. Transmission electron microscopy (TEM)

3.4.8.1. Principle of TEM

TEM uses a high energy electron beam transmitted through a very thin sample to image and analyse the microstructure of materials with atomic scale resolution. The microscope operates on the same basic principles as the light microscope, but uses electrons instead of light. The schematic representation of a TEM is given in Fig. 3.5. A radiation source at the top of the microscope emits the electrons that travel through vacuum in the column of the microscope. The electrons are accelerated at several hundred kV, giving wavelengths much smaller than that of light thus offering a thousand times better resolution.

Electromagnetic lenses are used to focus the electrons into a very thin beam which travels through the specimen. Polymers are typically composed of elements that are low scatterers of electrons and have little spatial variation in the electron density, thus resulting in poor contrast. To overcome this, the sample is stained with a heavy metal solution (*e.g.* uranyl acetate). The metal ions attach to certain regions of the sample, enhancing the contrast. Depending on the density of the material, some of the electrons are scattered and disappear from the beam. The unscattered electrons hit a fluorescent screen at the bottom of the microscope, giving a "shadow image" of the specimen with its different parts displayed in varied darkness according to their density. The image can be studied directly by the researcher or recorded with a camera [15, 16].

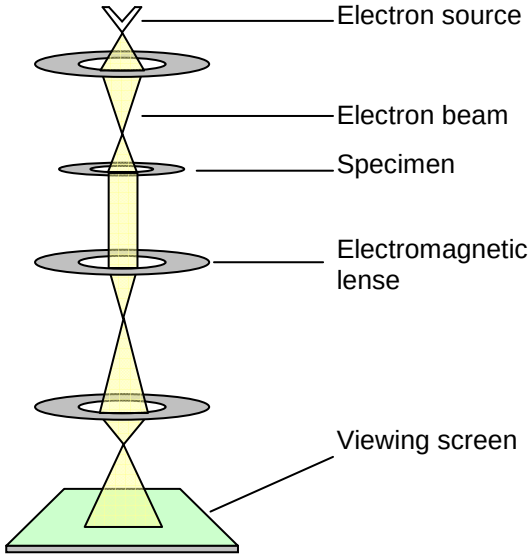

Figure 3.5: *Schematic representation of a transmission electron microscope*

3.4.8.2. General procedure for TEM

Sample morphology was studied using a JEM-1220 electron microscope (JEOL) equipped with Gatan digital camera. Carbon-coated copper grids (400 mesh, Agar scientific) were placed with the carbon-coated face on top of a 10 µl drop of aqueous sample solution for 10 s. After blotting on Whatman 50 filter paper, the grid was washed by placing the grid with the sample side on top of a 10 µl drop of deionised water for 10 s and blotted again. The sample was then negatively stained by placing the grids with the sample side on top of a 10 µl drop of 4 wt.% solution of uranyl acetate for 60 s and then blotted. After drying, the sample was examined by TEM at 100 kV accelerating voltage, at 70% saturation of the filament and at 5 µA of beam current. Images were obtained by a Gatan digital camera.

3.4.9. Atomic force microscopy (AFM)

3.4.9.1. Principle of AFM

AFM is a scanning probe technique, in which a sharp tip positioned on a cantilever is scanned along a surface to provide a three-dimensional image of a sample [17-19]. Fig. 3.6 shows the basic concept of AFM. Attractive or repulsive forces resulting from interactions between the tip and the surface cause a positive or negative bending of the cantilever. The bending is detected by means of a laser beam, which is reflected from the back side of the cantilever and collected in a photodiode. Cantilevers are usually made from silicon (Si) or silicon nitride (Si_3N_4).

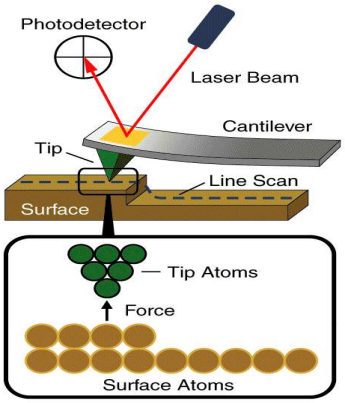

Figure 3.6: *Principle of AFM (adapted from [20])*

The relevant forces between the tip and the surface are van der Waals and the Coulomb forces. Fig. 3.7 represents the curve of force *versus* distance obtained during surface scanning. The distance between the surface and the tip, as well as horizontal movement, is controlled by an arrangement of piezoelectric elements controlling the *x,y* (horizontal) and *z* (vertical) coordinates of the sample surface. When the tip is far from the surface, no interaction between it and the surface is observed. As soon as the tip approaches the surface, atoms are brought together and the tip enters the attractive regime where it is pulled towards the surface. Then it enters the repulsive regime where it is pushed away from the surface due to the increased compactness of atoms and hence electrostatic repulsions of their electron clouds. Atoms come in contact and van der Waals force becomes positive (repulsive). Repulsive forces stop the tip getting closer to the surface.

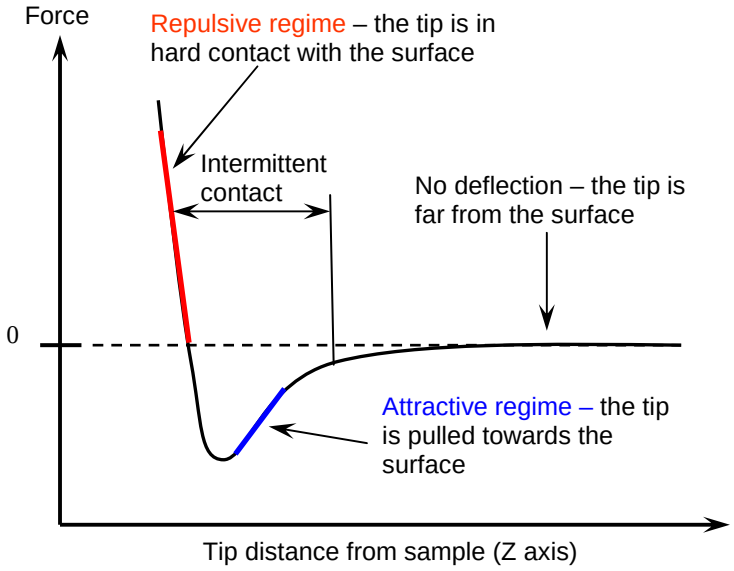

Figure 3.7: *Curve of interatomic force versus tip-to-sample distance (adapted from [20])*

There are several modes of operation in AFM, depending on the application:

- **Contact mode** – the tip operates in the repulsive regime and it makes soft contacts with the surface of the sample. The deflection of the cantilever Δz is proportional to the force, F acting on the tip, via Hook's law, $F = -k \cdot \Delta z$, where k is the spring constant of the cantilever. Topographic data can be acquired in two ways: the tip either scans at a constant height above the surface or at a constant force. Mainly hard materials are analysed in this mode using silicone nitride tips. Soft materials, such as soft gels, can be damaged by the tip.

- **Non-contact mode** – the tip is in the attractive force region where the tip-sample interaction is minimised. This mode is used for the analysis of attractive forces between the chemical surface (*e.g.*, polyelectrolytes) and the tip which is typically made of silicon.

- **Tapping mode (intermittent contact mode)** – the cantilever end oscillates with such amplitude that the tip touches the sample. Forces between the sample and the tip will affect the oscillation amplitude, the resonant frequency and phase of the cantilever. The piezoscanners are adjusted vertically in response to amplitude change, thus producing the height image (surface topography). At the same time, the phase changes are presented in the phase image, showing physical differences on the surface due to different chemistries of the materials and forces. This mode is mainly used for the analysis of soft and biological materials, such as hydrogels, tissues and cells [20].

3.4.9.2. General procedure for AFM

The morphology of the samples was studied using a Veeco Multimode atomic force microscope with a Nanoscope IIIa controller. Muscovite mica and metal specimen discs (Agar Scientific, UK) were used and films were cast by depositing a 80 μl aliquot of the sample ($\leq$ 5 mg ml^{-1} aqueous solution) onto a freshly cleaved mica surface for 60 s. Excess liquid was removed by capillary action and then the surface was washed twice with 1 ml of distilled H_2O; the first was performed straight after sample deposition and the second after the sample was air-dried overnight. The sample was subsequently air-dried again. Olympus high aspect ratio etched silicon probes with a nominal spring constant of 42 N m^{-1} (Veeco Instruments, France) were used for imaging. Samples were imaged via tapping mode at a relative humidity of < 45%. Cantilever oscillation varied in the range from 300 to 350 kHz, whilst the drive amplitude was determined by the Nanoscope software. Height and phase images were captured at a scan rate of 1.97 Hz with scan sizes of 5 and 2 μm^2. The instrument was periodically calibrated using a grating with 180 nm deep, 10 μm^2 depressions and tip deconvolution was performed using 10 mm gold particles deposited on mica. Height data was first-order flattened, and mean fibre diameters were determined using the software package WSxM (Nanotec Electronica S.L.) [21]. Correction for the overestimation of lateral dimensions due to tip geometry was performed as

reported by Sherratt *et al.* [22]. The true width (W_t) of a cylindrical polymer imaged by an AFM tip with a radius of curvature R can be calculated from the measured width at half maximum height (W_m) (Eq. 3.25):

$$W_m = 2\sqrt{R \times W_t + \frac{W_t}{4}} \qquad (Eq.\ 3.25)$$

3.4.10. Small-angle neutron scattering (SANS)

3.4.10.1. Principles of SANS

Scattering means the deflection of an incident beam from its original direction due to interaction with the scattering centres of a sample [16, 23-27]. The basic principle of any scattering technique is depicted in Fig. 3.8. The incident radiation is characterised by the wavelength λ, wave vector k_0 with magnitude $2\pi/\lambda$, and energy E:

$$E = \frac{hc}{\lambda} \qquad (Eq.\ 3.26)$$

where h is the Plank's constant equal to 6.626×10^{-34} J×s and c is the speed of light equal to 3×10^{8} m s^{-1}.

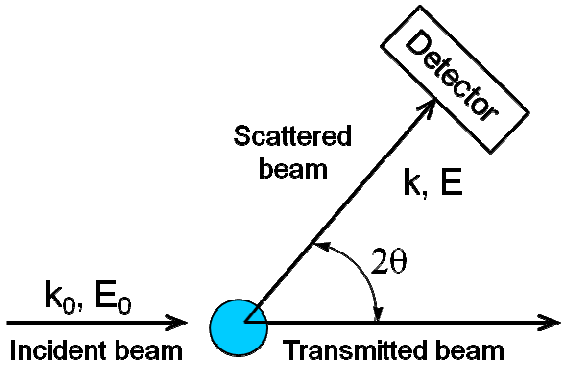

Figure 3.8: *Schematic representation of the scattering principle (adapted from [8])*

During elastic scattering incident and scattered radiation have the same energy, therefore the magnitude of the initial wave vector k_0 is equal to the final wave vector k. The direction of the scattered beam changes by the scattering angle, 2θ. The difference in wave vectors, $\vec{q} = \vec{k} - \vec{k}_0$ defines the change in the direction of traveling of the wave, and it is referred to as the scattering vector or momentum transfer, q:

$$q = \frac{4\pi}{\lambda}\sin\theta \qquad (Eq.\ 3.27)$$

Many forms of radiation can be used for scattering purposes: X-rays, neutrons, electrons, laser light and gamma rays. The characteristics for X-rays, neutrons and laser light are given in Table 3.3.

Table 3.3: *Types of radiation used in scattering*

	X-Rays	**Neutrons**	**Laser light**
Wavelength range	0.1 – 5 Å	1 -15 Å	1 μm
Scattering by	Electrons	Nuclei	Electrons
Sample thickness	< 1 mm	1 – 2 mm	1 – 5 mm
Problems with	Absorption	Low fluxes	Dust scattering

Neutron, X-ray and light scattering are complementary scattering techniques to study size, shape, and interactions of complex systems. In SAXS and LS electromagnetic radiation interacts with electrons in the sample and is scattered from the electron cloud. In SANS, neutrons interact with nuclei and the scattering depends on the contrast between a particle and environment. SANS is a very useful technique for the study of the concentrated solutions or condensed state systems which are inaccessible to SAXS and LS due to difficulties of distinguishing between the inter- and intra- chain contribution to the structure.

Conventional SANS instruments cover the q range from 10^{-3} to 10^{-1} Å^{-1} and the scattering angle range from 0.1° to 10°. This corresponds to length scales of 1 to 2000 Å. The interaction of neutrons with nuclei is characterised by the neutron-scattering length, b, which is usually of the order of 10^{-12} cm for all nuclei and by the scattering cross-section, $\sigma = 4\pi b^2$ which corresponds to the atom surface accessible for the radiation. The nuclei of proton (^{1}H) and deuterium (^{2}D) have very different scattering lengths: $b_H = -0.374\times10^{-12}$ cm^{-2} and $b_D = 0.667\times10^{-12}$ cm^{-2} respectively. This feature is in the basis of many SANS experiments when the contrast in scattering power between the particle and its environment can be easily manipulated by exchanging protons with deuteriums without affecting the physico-chemical properties of the sample. The technique is called contrast matching [24].

The scattering length density of a molecule of n atoms, ρ is the sum of the scattering lengths of the nuclei in the molecule, a divided by the molecular volume, V_m:

$$\rho = \frac{\sum_{i=1}^{n} b_i}{V_m} = \frac{a}{V_m} \qquad (Eq.\ 3.28)$$

where b_i is the scattering length of n atoms in a molecule. Table 3.4 shows the scattering length densities for the components used for the study of the composite gels: D_2O, H_2O, the mixture of H_2O and D_2O, hydrogenated peptide and deuterated NIPAAm.

Table 3.4: *Scattering length densities for the hydrogenated peptide, deuterated monomer and solvents*

Compound	Scattering length density (10^{-10} cm^{-2})
D_2O	6.37
H_2O	-0.56
58 vol.% H_2O /42 vol.% D_2O	2.35
FEFEFKFK	3.02 (in D_2O) / 1.87 (in H_2O)
NIPAAm-d7	6.52 (in D_2O) / 0.99 (in H_2O)

Table 3.5 shows the molar volumes for the amino acids. The molar volumes of the peptide were calculated by adding the molar volumes for each amino acid in the sequence [28].

Table 3.5: *Molar volumes of the amino acids*

Amino acid	Molar volume (Å^3)
Glutamic acid (E)	140.6
Lysine (K)	176.2
Phenylalanine (F)	203.4

The intensity scattered by any system in dilute regime (no cross-interaction between the components) depends on the physical properties of the system defined by the structure factor S(q), instrument, and sample geometry. If experimental parameters are included in constant B, the intensity scattered can be expressed as:

$$I(q) = BT_e\delta_e S(q) \qquad (Eq.\ 3.29)$$

with

$$B = F_i\,\Phi_o\,\delta\Omega_i\,tA \qquad (Eq.\ 3.30)$$

where:

	F_i	efficiency of the counter cell
	Φ_o	flux of the incident beam
	$\delta\Omega_i$	solid angle under which the cell *i* is visible looking from the sample
	t	counting time
	A	sample surface
	T_e	transmission of the sample
	δ_e	sample thickness

Structure factor depends on the number of the scattering centres and comprises of two terms: coherent, S^{coh} (reflects the spatial arrangement of the scattering centres and contains structural information of the system) and incoherent, S^{inc} (mainly coming from hydrogen molecules and independent of the scattering vector). Therefore the scattering intensity can be written as follows:

$$I(q) = BT_e\delta_e S^{coh}(q) + S^{inc} \qquad (Eq.\ 3.31)$$

During SANS experiments only S^{coh} provides information about the structure. S^{inc} results in a flat background which needs to be subtracted from raw data.

For a system of *N* components S(q) can written as:

$$S^{coh}(q) = \sum_{j,k=1}^{N} a_j a_k S_{jk}(q) \qquad (Eq.\ 3.32)$$

where $S_{jk}(q)$ is the correlation function between the species *j* and *k* and a_j, a_k are their scattering lengths.

In SANS, correlation lengths measured are considerably large in comparison to the inter-atomic distances. Therefore it is assumed that the fluctuations of the atomic densities are negligible and the system is incompressible. Following these conditions the scattering function for the system with *N+1* components is:

$$S^{coh}(q) = \sum_{j=1}^{N} (a_j - Y_j a_0)^2 S_{jj}(q) + \sum_{j \neq k=1}^{N} (a_j - Y_j a_0)(a_k - Y_k a_0) S_{jk}(q) \qquad (Eq.\ 3.33)$$

where a_j and a_0 — average scattering lengths for species j and 0

S_{jk} — correlation function that reflects intermolecular interactions

S_{jj} — correlation function that reflects intramolecular interactions

$Y_j = v_j/v_0$ — ratio of molar volumes for species j and 0

$Y_k = v_k/v_0$ — ratio of molar volumes for species k and 0

Eq. 3.33 does not contain the correlation function for species 0 (solvent molecules) because it is assumed that these species fill the space non-occupied by the species j and k.

In this study binary (hydrogenated peptide or deuterated polymer and solvent) and ternary (hydrogenated peptide, deuterated polymer and solvent) systems were used and they are presented below.

1) Binary system

In this case the coherent scattering the 2nd term from the Eq. 3.33 disappears and the equation can be rewritten as follows:

$$S^{coh}(q) = (a_P - Y_P a_S)^2 S_{PP}(q) \qquad (Eq.\ 3.34)$$

where a_P — average scattering length of a polymer (or a peptide)

a_S — average scattering length of a solvent

$S_{PP}(q)$ — correlation function comprising inter- and intramolecular interactions of a polymer (or a peptide)

$Y_P = v_P/v_S$ — ratio of molar volumes of a polymer (or a peptide) and a solvent

Usually the experiments are performed at low concentrations to exclude the intermolecular interactions of the components.

2) Ternary system

In this case the coherent scattering function reads as:

$$S^{coh}(q) = (a_{Pol} - Y_{Pol}a_S)^2 S_{PolPol}(q) + (a_{Pep} - Y_{Pep}a_S)^2 S_{PepPep}(q) + 2(a_{Pol} - Y_{Pol}a_S)(a_{Pep} - Y_{Pep}a_S)S_{PolPep}(q) \quad (Eq.\ 3.35)$$

where
- a_{Pep} — average scattering length of a hydrogenated peptide
- a_{Pol} — average scattering length of a deuterated polymer
- a_S — average scattering length of a solvent
- $S_{PepPep}(q)$ — correlation function comprising inter- and intramolecular interactions of a hydrogenated peptide
- $S_{PolPol}(q)$ — correlation function comprising inter- and intramolecular interactions of a deuterated polymer
- $S_{PepPol}(q)$ — correlation function comprising intermolecular interactions between a hydrogenated peptide and a deuterated polymer
- $Y_{Pep} = v_{Pep}/v_S$ — ratio of molar volumes of a hydrogenated peptide and a solvent
- $Y_{Pol} = v_{Pol}/v_S$ — ratio of molar volumes of a deuterated polymer and a solvent

The correlation functions $S_{Pep}(q)$ and $S_{Pol}(q)$ give structural information of the components. To study the polymer behaviour it is necessary to cancel the 3rd component in the Eq. 3.35, corresponding to the polymer and peptide interactions, by making the term $(a_{Pep} - Y_{Pep}a_S)$ of the peptide equal to 0. When the peptide contribution to the scattering is cancelled the coherent scattering function can be written as:

$$S^{coh}(q) = (a_{Pol} - Y_{Pol}a_S)^2 S_{PolPol}(q) \quad (Eq.\ 3.36)$$

The contrast matching can be done by using the mixture of hydrogenated and deuterated solvent. The fraction of a deuterated solvent is described by the following relations:

$$\frac{a_S}{v_S} = x_{SD}\frac{a_{SD}}{v_{SD}} + (1 - x_{SD})\frac{a_{SH}}{v_{SH}} = \frac{a_{Pep}}{v_{Pep}} \quad (Eq.\ 3.37)$$

$$x_{SD} = \frac{\frac{a_{Pep}}{v_{Pep}} - \frac{a_{SH}}{v_{SH}}}{\frac{a_{SD}}{v_{SD}} - \frac{a_{SH}}{v_{SH}}} \quad (Eq.\ 3.38)$$

where a_{SH}, v_{SH} and a_{SD}, v_{SD} are average scattering lengths and molar volumes for hydrogenated and deuterated solvents respectively.

Contrast matching is performed by preparing the sample in the mixtures of protonated and deuterated solvent and measuring the scattered intensity. At certain ratios of protonated and deuterated solvents, *i.e.* contrast match points, the scattering from the molecules to be

matched will be equal to that of the solvent and thus will be removed when the solvent background is subtracted from the raw data [24]. Fig. 3.9 shows the contrast matching of different parts of hydrogenated peptide fibres decorated with deuterated polymer by varying the proportions of deuterated and hydrogenated solvents. Fig. 3.9A shows the case when the hydrogenated and deuterated solvent mixture, hydrogenated peptide, deuterated polymer have different scattering densities. When the content of deuterated solvent increases, it is possible to reach the conditions when the deuterated polymer chains and hydrogenated peptide have the largest difference in contrast (Fig. 3.9B). The scattering originated from the hydrogenated peptide fibres. The study of the deuterated polymer chains is possible when the contrast of the hydrogenated peptide fibres matches that from the solvent. It is possible by increasing the amount of hydrogenated solvent in the solvent mixture (Fig. 3.9C) [9].

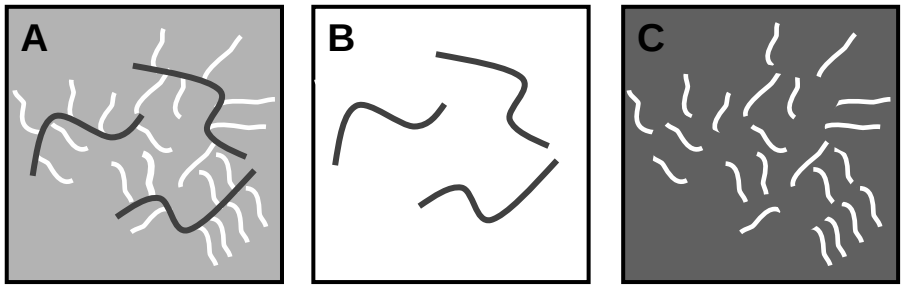

Figure 3.9: *Schematic illustration of the contrast matching concept in SANS(adapted from [9]). A) The hydrogenated peptide fibres, the conjugated polymer chains and the solvent have different contrasts. B) The deuterated polymer chains are contrast-matched with the solvent and the hydrogenated peptide fibres scatter neutrons. C) The hydrogenated peptide fibres are contrast-matched with the solvent and the deuterated polymer chains scatter neutrons.*

The study of the hydrogenated peptide fibres is possible in D_2O where peptide has better contrast due to small level of incoherent scattering. According to the Eq. 3.39, the contrast factor of the hydrogenated peptide in D_2O is 1.09×10^{-3}.

$$K = \frac{(a_p - Y_{ps} a_s)^2 N_A}{m_p^{\,2}} \qquad (Eq.\ 3.39)$$

where a_p and a_s are the scattering lengths of the peptide (or polymer) and the solvent accordingly, Y_{ps} is the molar volume ratio ($v_p/\ v_s$) between the peptide (or polymer) and the solvent, N_A is the Avogadro's number and m_p is the peptide (or polymer) molar mass.

Neither hydrogenated, nor deuterated polymers can be cancelled completely in D_2O. The contrast factors of the hydrogenated and deuterated polymers in D_2O are 2.03×10^{-3} and 9.95×10^{-5} respectively. For the experiments the composite gels were prepared in D_2O because the difference between the contrast factors of hydrogenated peptide and deuterated polymer is larger than that between the hydrogenated peptide and hydrogenated polymer.

The study of the deuterated polymer segments is possible when the hydrogenated peptide is contrast matched using the mixture of H_2O and D_2O. The contrast match points were first calculated using the following equations. For the **hydrogenated peptide** in the mixture of H_2O and D_2O the term $(a_{Pep} - Y_{Pep}a_S)$ can be written as:

$$(a_{Pep} - Y_{Pep}a_S) = (x_{D_2O}a_{D_2O}^{pep} + x_{H_2O}a_{H_2O}^{pep}) - (\frac{v_{D_2O}^{pep}}{x_{D_2O}v_{D_2O} + x_{H_2O}v_{H_2O}})(x_{D_2O}a_{D_2O} + x_{H_2O}a_{H_2O})$$

(Eq. 3.40)

where x_{D_2O}, x_{H_2O} and a_{D_2O}, a_{H_2O} are the volume fractions and scattering lengths for D_2O and H_2O accordingly; $a_{D_2O}^{pep}$ and $a_{H_2O}^{pep}$ are the scattering lengths for the hydrogenated peptide in D_2O and H_2O accordingly, $v_{D_2O}^{pep}$ is the molar volume of the peptide in D_2O.

Similar equation can be written for the **deuterated polymer** in the mixture of H_2O and D_2O:

$$(a_{Pol} - Y_{Pol}a_S) = (x_{D_2O}a_{D_2O}^{pol} + x_{H_2O}a_{H_2O}^{pol}) - (\frac{v_{D_2O}^{pol}}{x_{D_2O}v_{D_2O} + x_{H_2O}v_{H_2O}})(x_{D_2O}a_{D_2O} + x_{H_2O}a_{H_2O})$$

(Eq. 3.41)

where $a_{D_2O}^{pol}$ and $a_{H_2O}^{pol}$ are the scattering lengths for the deuterated polymer in D_2O and H_2O accordingly, $v_{D_2O}^{pol}$ is the molar volume of the deuterated polymer in D_2O.

The crossover term, showing the interaction of the peptide with polymer, can be written as: $2(a_{Pep} - Y_{Pep}a_S)\,(a_{Pol} - Y_{Pol}a_S)$

At certain x_{D_2O} the peptide will have the same scattering density as the solvent and the term $(a_{Pep} - Y_{Pep}a_S)$ will be equal to 0. x_{D_2O} can be determined by plotting the values of $(a_{Pep} - Y_{Pep}a_S)^2$ versus x_{H_2O} (Fig. 3.10). The contrast matching point corresponds to the cross-over point with the *x* axis when *y* = 0. The volume fraction of H_2O equals to $x_{H_2O} = 1 - x_{D_2O}$. It was found that the peptide was contrast matched at $x_{H_2O} = 0.58$ and $x_{D_2O} = 0.42$. This H_2O and D_2O ratio was used to prepare the composite gels and to study the polymer behaviour. By plotting $(a_{Pol} - Y_{Pol}a_S)^2$ of the deuterated polymer *versus* x_{H_2O} it is possible to find its scattering density at various ratios of H_2O and D_2O. The plot of the cross-over term $2(a_{Pep} - Y_{Pep}a_S)\,(a_{Pol} - Y_{Pol}a_S)$ versus x_{H_2O} shows its small values indicating that interactions between the peptide and the polymer are negligible. Then the calculated contrast match point is proven experimentally (see Chapter 6).

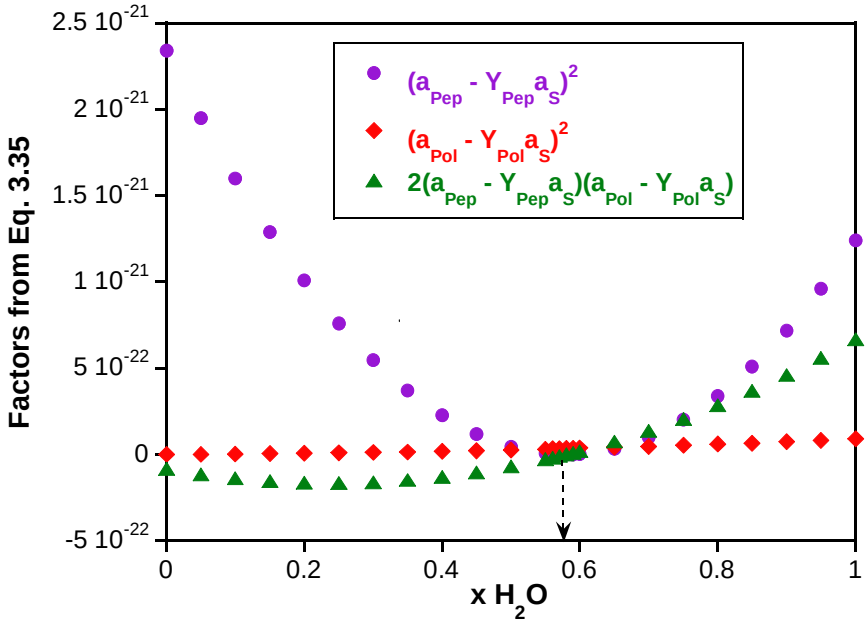

Figure 3.10: *The plots of* $(a_{Pep} - Y_{Pep}a_S)^2$, $(a_{Pol} - Y_{Pol}a_S)^2$ *and* $2(a_{Pep} - Y_{Pep}a_S)(a_{Pol} - Y_{Pol}a_S)$ *versus volume fraction of* H_2O

3.4.10.2. SANS spectrometer D22 and general procedure for SANS experiment

SANS experiments were performed at the D22 beam line at the Institut Laue-Langevin (ILL) in Grenoble, France [27, 29]. The schematic representation of the spectrometer D22 is given in Fig. 3.11. A neutron beam is produced by the horizontal cold source in the reactor. The wavelength then is selected using a mechanical velocity selector. The virtual source-to-sample distance is chosen by a collimation system consisting of eight sections. Each section consists of three tubes, any of each can be placed on the beam axis. At the end of the collimation the size of the beam in front of the sample is fixed by an aperture, made of Boron carbide (B4C) covered by Cadmium.

D22 possesses the largest area multidetector (^{3}He) of all small-angle scattering instruments, with an active area of 102 × 100 cm and pixel size of 8 × 8 mm. It is placed in a 2.5 m wide and 20 m long evacuated tube (to reduce scattering by air) and can move from 1.05 to 17.8 m from the sample position. The detector can also rotate around its vertical axis. D22 covers a total q range of up to 4×10^{-4} to 0.65 Å^{-1} depending on the sample and its environment.

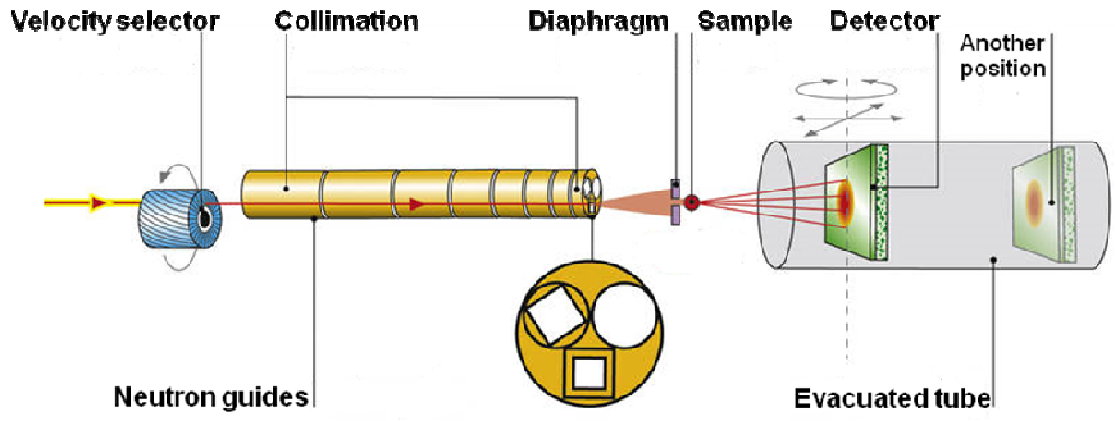

Figure 3.11: *D22 instrument layout (adapted from [30])*

For SANS experiments a neutron wavelength of 6 Å was used. The data were collected in the q range of $0.0043 < q\ (Å^{-1}) < 0.5$. The maximum accessible scattering vector modulus q range was covered by two detector distances of 5.6 and 11.2 m.

The composite gels samples were prepared in 2 or 5 mm path quartz cells in D_2O to study the fibres of hydrogenated peptide and in the solvent mixture of 58 vol.% H_2O and 42 vol.% D_2O to study the deuterated polymer segments. The scattering was measured below and above the LCST: at 25 and 45°C respectively. The temperature was controlled by an external thermostat. Data were corrected for background scattering (intensity scattered by the empty cell and the solvent). The incoherent (background) scattering, I_{inc}, was estimated using Porod's law which gave the scattered intensity of a two phase system at high q values:

$$I(q) = \frac{K_p}{q^4} + I_{Inc} \qquad (Eq.\ 3.42)$$

where K_p is the Porod constant. I_{inc} was estimated by fitting the last 10-20 data points of the scattering curves of Porod representation ($q^4I(q)$ versus q^4) and slope gave the value of I_{inc}.

The data were normalised by incoherent water scattering according to the standard procedures at the ILL. After ensuring the scattering was isotropic, the data were radially averaged to obtain a one-dimensional scattering plot. Under these conditions the normalised intensity scattered by the peptide is:

$$I_N(q) = \left[\frac{I_s(q)}{T_s \delta_s} - \frac{I_e(q)}{T_e \delta_e} \right] \qquad (Eq.\ 3.43)$$

where $I_N(q)$ is the normalised measured intensity, δ is the thickness of the sample and T is the transmission of the sample, s, and the empty cell, e.

To extract the absolute intensity scattered by the peptide, the coherent intensity scattered by the solvent and the incoherent intensity scattered by the peptide and the solvent have to be subtracted from total intensity scattered [31]:

$$I_A(q) = \frac{1}{K}\left[I_N(q) - (1 - c_p)I_D(q) - I_{inc}\right] \qquad (Eq.\ 3.44)$$

where c_p is the peptide concentration (g cm^{-3}), $I_D(q)$ is the normalised intensity scattered by the deuterated solvent, I_{inc} is the background scattering intensity due to the incoherent scattering of the hydrogenated peptide and K is the contrast factor described by Eq. 3.39 [31]:

References

1. W. C. Chan and P. D. White, *Fmoc Solid Phase Peptide Synthesis. A Practical Approach*, Oxford University Press, 2000.
2. E. Kaiser, R. L. Colescott, C. D. Bossinger and P. I. Cook, *Short Commun.*, 1970, **34**, 595-598.
3. V. S. Sarin, S. B. H. Kent, J. P. Tam and M. R.B., *Analytical Biochemistry*, 1981, **117**, 147-157.
4. F. Stoica, C. Alexander, N. Tirelli, A. F. Miller and A. Saiani, *Chem. Commun.*, 2008, 4433-4435.
5. *Avance. Beginners Guide. Version 003*, Bruker Biospin GmbH, 2003.
6. R. J. Anderson, D. J. Bendell and P. W. Groundwater, *Organic Spectroscopic Analysis*, Royal Society of Chemistry, 2004.
7. J. Keller, *Understanding NMR spectroscopy*, http://www-keeler.ch.cam.ac.uk/, Accessed March, 2010.
8. J. M. G. Cowie and V. Arrighi, *Polymers: Chemistry and Physics of Modern Materials*, 3rd edn., Taylor & Francis Group: CRC Press, 2008.
9. I. W. Hamley, *Introduction to Soft Matter: Synthetic and Biological Self-Assembling Materials. Revised edition*, Wiley, 2007.
10. B. I. Corporation, *Instruction Manual for BI-ZPW. Zimm Plot Software for Molecular Weight Determination in Dilute Polymer Solutions. Version 1.0.*, Brookhaven Instruments Corporation, 2000.
11. F. Rouessac and A. Rouessac, *Chemical Analysis: Modern Instrumentation Methods and Techniques*, John Wiley & Sons, 2000.
12. F. A. Settle, *Handbook of Instrumental Techniques for Analytical Chemistry*, Prentice Hall, 1997.
13. H. M. Wyss, R. J. Larsen. and D. A. Weitz, *G.I.T. Laboratory Journal*, 2007, **3-4**, 68-70.
14. J. W. Goodwin and R. W. Hughes, *Rheology for Chemists: an introduction*, RSC, 2000.
15. http://www.setaram.com, Accessed October, 2009.
16. J. M. G. Cowie and V. Arrighi, *Polymers: Chemistry and Physics of Modern Materials*, 3rd edn., Taylor & Francis Group: CRC Press, 2007.
17. F. J. Giessibl, *Rev. Mod. Phys.*, 2003, **75**, 949.
18. G. Binnig, C. F. Quate and C. Gerber, *Phys. Rev. Lett.*, 1986, **56**, 930-933.
19. V. M. G. Digital Instruments, *Scanning Probe Microscopy Training Notebook, version 3.0*, 2000.
20. A. Vilalta-Clement, K. Gloystein and N. Frangis, *Physics of Advanced Materials Winter School 2008*, 2008.
21. I. Horcas, R. Fernandez, J. M. Gomez-Rodriguez, J. Colchero, J. Gomez-Ferrero and A. M. Baro, *Rev. Sci. Instrum.*, 2007, **78**, 013705.
22. M. J. Sherratt, D. V. Bax, S. S. Chaudhry, N. Hodson, J. R. Lu, P. Saravanapavan and C. M. Kielty, *Biomaterials*, 2005, **26**, 7192-7206.
23. W. Brown and M. Kell, *Scattering in polymeric and colloidal systems* Amsterdam : Abingdon : Gordon & Breach ; Marston, c2000, 2000.
24. G. D. Wignall, in *Physical Properties of Polymers Hadbook*, ed. J. E. Mark, Springer New York, Editon edn., 2007, pp. 407 - 420.
25. J. Mark, K. Ngai, W. Graessley, L. Mandelkern, E. Samulski, J. Koenig and G. Wignall, *Physical Properties of Polymers*, 3rd edn., Cambridge University Press, 2004.
26. B. Hammouda, *A tutorial on small-angle neutron scattering from polymers*, National Institute of Standards and Technology, Materials Science and Engineering Laboratory, 1995.
27. I. Grillo, in *Soft Matter Characterization*, eds. R. Borsali and R. Pecora, Springer Netherlands, Editon edn., 2008, pp. 723-782.
28. B. Jacrot and G. Zaccai, *Biopolymers*, 1981, **20**, 2413-2426.
29. *Guide to Neutron Research Facilities at the ILL. The Yellow Book.*, Institut Max von Laue - Langevin, 1997.

30. http://www.ill.eu/instruments-support/instruments-groups/instruments/d22/, Accessed March, 2010.
31. J. S. Higgins and H. C. Benoit, *Polymers and Neutron Scattering*, Clarendon Press, Oxford, 1994.

Chapter 4

Results and Discussion

PNIPAAm-Peptide Conjugate Based Hydrogels: Synthesis and Characterisation

4.1. Introduction

The aim of this study is to modulate the gelling behaviour of PNIPAAm by targeting different degrees of functionalisation of PNIPAAm with the self-assembling peptides FEFEFKFK and FEFKFEFK. Polymer and peptide conjugation is possible by using a sulfhydryl end-functionalised peptide as the chain-transfer agent (CTA) in the free radical polymerisation (FRP) of NIPAAm. This procedure provides a mixture of pure polymer and polymer-peptide conjugate. The products prepared contain pure polymer and controllable quantities of PNIPAAm-FEFEFKFK or PNIPAAm-FEFKFEFK conjugate. In all samples in this chapter the free polymer concentration is much higher than conjugate concentration. It has been postulated that the peptide segments will retain their self-assembling behaviour after conjugation and will form β-sheet fibres decorated with PNIPAAm chains once dissolved in water. The effect of the peptide sequence on the self-assembly and gel properties has been studied.

The structural characteristics of the obtained conjugation products will be studied by ^{1}H NMR, SLS, viscometry and GPC. The thermal and mechanical properties of the resulting polymer/conjugate mixtures will be investigated by micro DSC and oscillatory rheology respectively. TEM and AFM will allow the gel morphology to be studied.

4.2. Synthesis and characterisation of polymer/conjugate mixtures

Two series of PNIPAAm samples containing various amounts of PNIPAAm-FEFEFKFK and PNIPAAm-FEFKFEFK conjugate were prepared by using an SH-modified FEFEFKFK and FEFKFEFK peptides as the CTA in the FRP of NIPAAm. The names of the peptides FEFEFKFK and FEFKFEFK in the conjugation products are abbreviated as "S" and "A" respectively which stand for the sequential and alternating peptides. The peptide modification with sulfhydryl group was achieved by coupling 3-mercaptopropionic acid (MPA) to the N-terminus of the peptide following the protocol of the solid phase peptide synthesis outlined elsewhere [1]. Both peptides were modified in the same way. It was anticipated that varying the quantity of CTA would influence the quantity of conjugate present in the final polymer-conjugate mixture, thus controlling material properties. The details of the preparative procedures of the polymer/conjugate mixtures are given in section 3.3.4 in Table 3.1. The chemical structures of the polymer-peptide conjugates present in the polymer/conjugate mixtures are given in Fig. 4.1. The effect of the peptide sequence on the self-assembly and gel properties has been studied.

Two series of the synthesised products were dialysed against water for 4 days using dialysis membrane with a pore size of 3,500 g mol^{-1} molecular weight cut-off to allow the unconjugated peptide (1,211 g mol^{-1}) to escape. ^{1}H NMR spectra were then used to confirm the presence of peptide residues in the samples, using pure PNIPAAm (P0) as a reference, which was obtained using the same polymerisation procedure as other products. The PNIPAAm spectrum given in Figure 4.2A shows a strong peak at 1.07 ppm corresponding to the methyl protons (H^f), broad peaks centred at 1.43 and 1.97 ppm corresponding to the backbone protons $H^{a,b}$ and H^c respectively, a peak at 3.95 ppm corresponding to the methylene group (H^e) and the very broad peak from 7.0-7.8 ppm corresponding to the amide group (H^d). The spectrum for polymerisation product PS3, given in Figure 4.2B, shows all peaks corresponding to the polymer, and additional multiplets at 4.0-4.8 ppm and 7.7-8.5 ppm, which become apparent in the magnified insets. These resonances arise from the protons in the peptide backbone and in the amide groups respectively. Furthermore the broad peak between ~7-7.5 ppm becomes more intense in comparison with the pure polymer due to the contribution of protons from the phenyl rings of the peptide. Similar spectra were also obtained for the PS1, PS2 and PA1, PA2, PA3 samples (Appendix 2: Fig. A.2.2 and A.2.3).

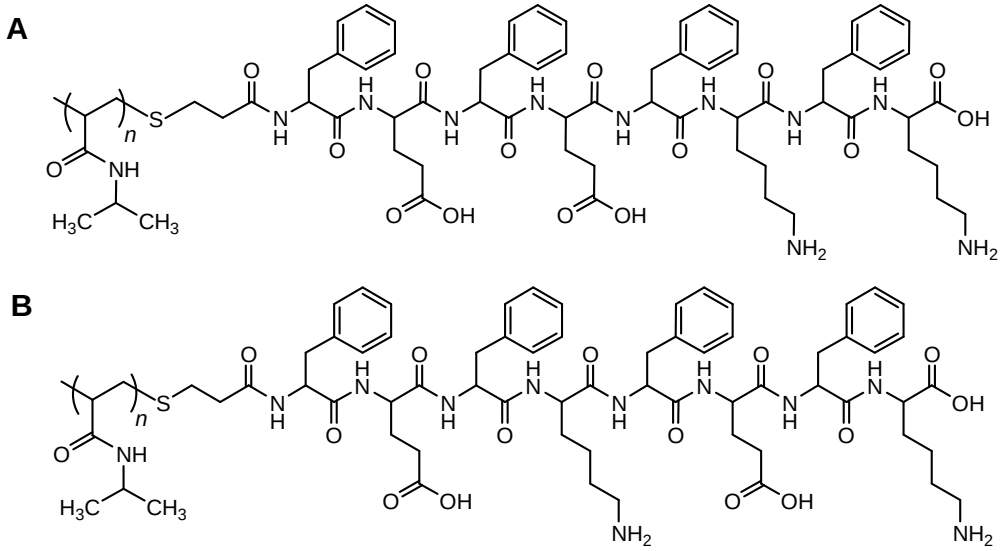

Figure 4.1: *Chemical structures of the polymer-peptide conjugates: A) PNIPAAm-FEFEFKFK and B) PNIPAAm-FEFKFEFK*

Figure 4.2C provides the ^{1}H NMR spectrum of the peptide FEFEFKFK with the typical regions of interest: resonance in the region of 3.7-4.4 ppm corresponding to the protons from the peptide backbone, a strong resonance from 7.0 to 7.3 ppm corresponding to the phenyl rings of the peptide and the resonance from 7.7 to 8.5 ppm corresponding to the amide bonds.

The presence of the peptide peaks in the ^{1}H NMR spectra could also be due to inefficient purification of possibly present free peptide. Physical mixtures of PNIPAAm and

the two peptides (20 mg of polymer and 10 mg of peptide) have been therefore prepared and dialysed against water under the same conditions used for polymer/conjugate mixture purification. The ^{1}H NMR after dialysis revealed the presence of PNIPAAm only, confirming the efficiency of the purification method and therefore ensuring that any peptide in the PS1, PS2, PS3 and PA1, PA2, PA3 samples was covalently linked to PNIPAAm.

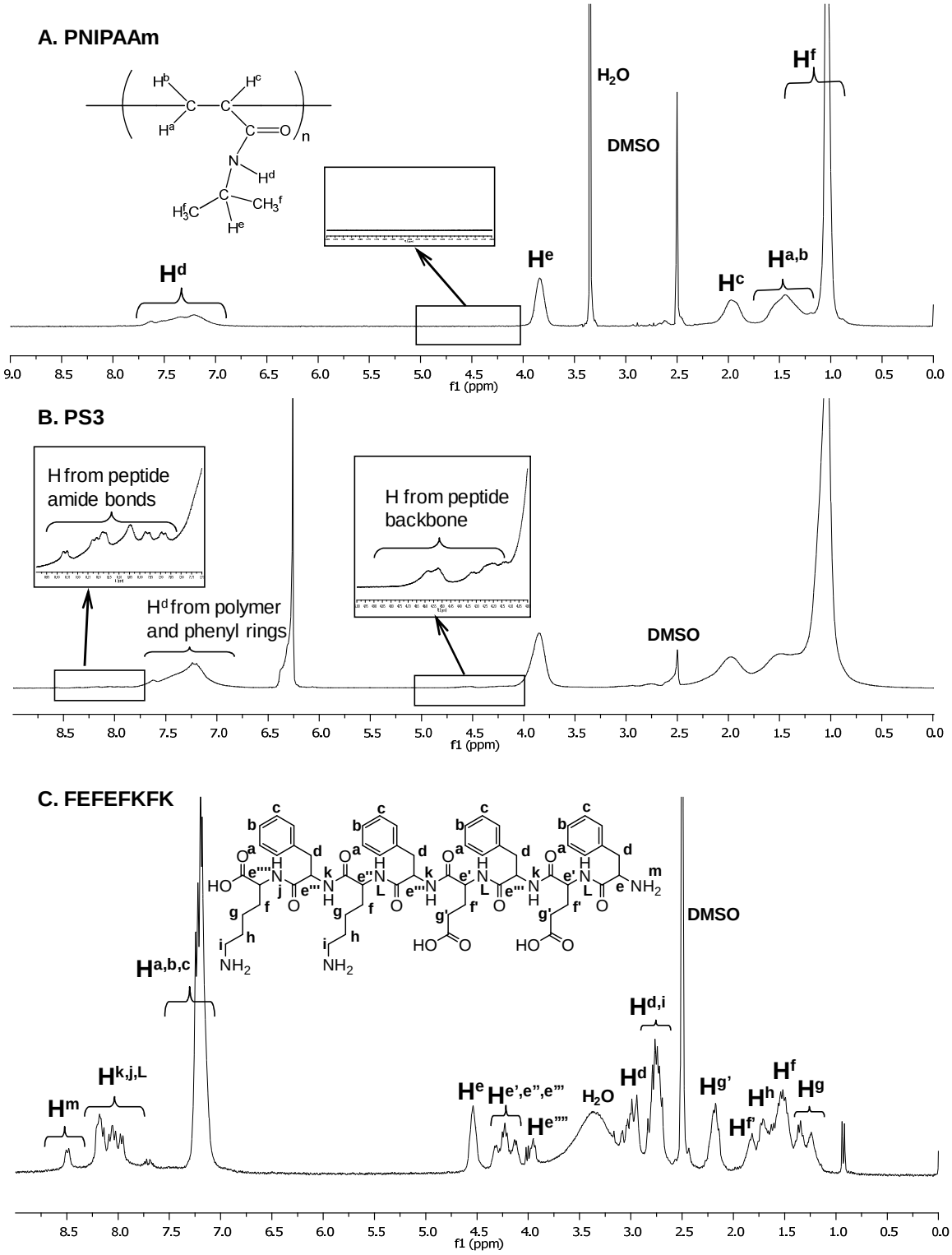

Figure 4.2: *^{1}H NMR spectra of: A) PNIPAAm (P0), B) PS3 and C) FEFEFKFK (DMSO-d_6, 400 MHz)*

Due to the likely different relaxation times of the protons in the polymer chain and in the peptidic groups, the average amount of peptide in the polymerised samples was evaluated by using the physical mixtures of peptide and PNIPAAm to generate a calibration curve relating the ratio of the signals at 3.95 ppm (H^e of PNIPAAm, Fig. 4.2A) and 4-5 ppm (peptide backbone, Fig. 4.2B) to the weight or molar fraction of peptide in the mixture (Fig. 4.3). The corresponding results are provided in Table 4.1 (4th column). These results showed that the peptide content increased with the increase of CTA used for polymerisation in each series.

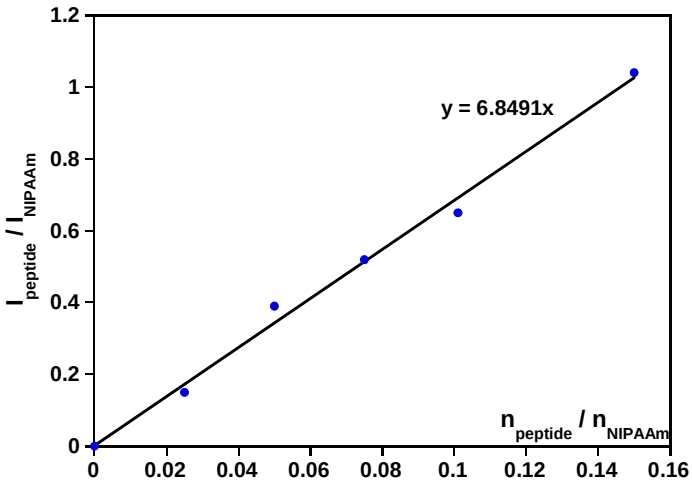

Figure 4.3: *Calibration curve for the determination of the peptide/monomer molar ratio in the polymer/conjugate mixtures*

Table 4.1: *Summary of the polymer/conjugate mixtures prepared in this study* [a]

Sample	Chain-transfer agent	Monomer / peptide weight ratio		$W_{peptide}$ in conj.	Polymer / conjugate weight ratio (centrifug.)	Conjugate	
		Feed	^{1}H-NMR			DP	$\overline{M}_n$ (g mol^{-1})
PS1	SH-FEFEFKFK	30 / 1	67 / 1	0.015	15 / 1	33	4850
PS2	SH-FEFEFKFK	15 / 1	17 / 1	0.060	5.8 / 1	16	3000
PS3	SH-FEFEFKFK	7.5 / 1	8 / 1	0.111	3.5 / 1	10	2250
PA1	SH-FEFKFEFK	30 / 1	69 / 1	0.014	20 / 1	23	3700
PA2	SH-FEFKFEFK	15 / 1	34 / 1	0.029	13 / 1	14	2740
PA3	SH-FEFKFEFK	7.5 / 1	17 / 1	0.056	4.8 / 1	21	3480
P0	-	-	-	-	-	-	-

[a] In each experiment 26.5 mmol of NIPAAm, 0.244 mmol of AIBN and 0, 82.7, 165 or 331 μmol of SH-modified peptide (corresponding to 0, 100, 200 or 400 mg) were used.

For analytical purposes the conjugated polymers were separated from unconjugated polymers by centrifuging 50 mg ml^{-1} of polymer/conjugate mixtures at 5,000 rpm for 5

minutes: this procedure produced a clear phase separation between an upper, less dense phase containing only pure polymer (confirmed by ^{1}H NMR) and a lower phase containing the polymer-peptide conjugate. Examples of ^{1}H NMR spectra for the products before and after centrifugation of PS3 are given in Fig. 4.4.

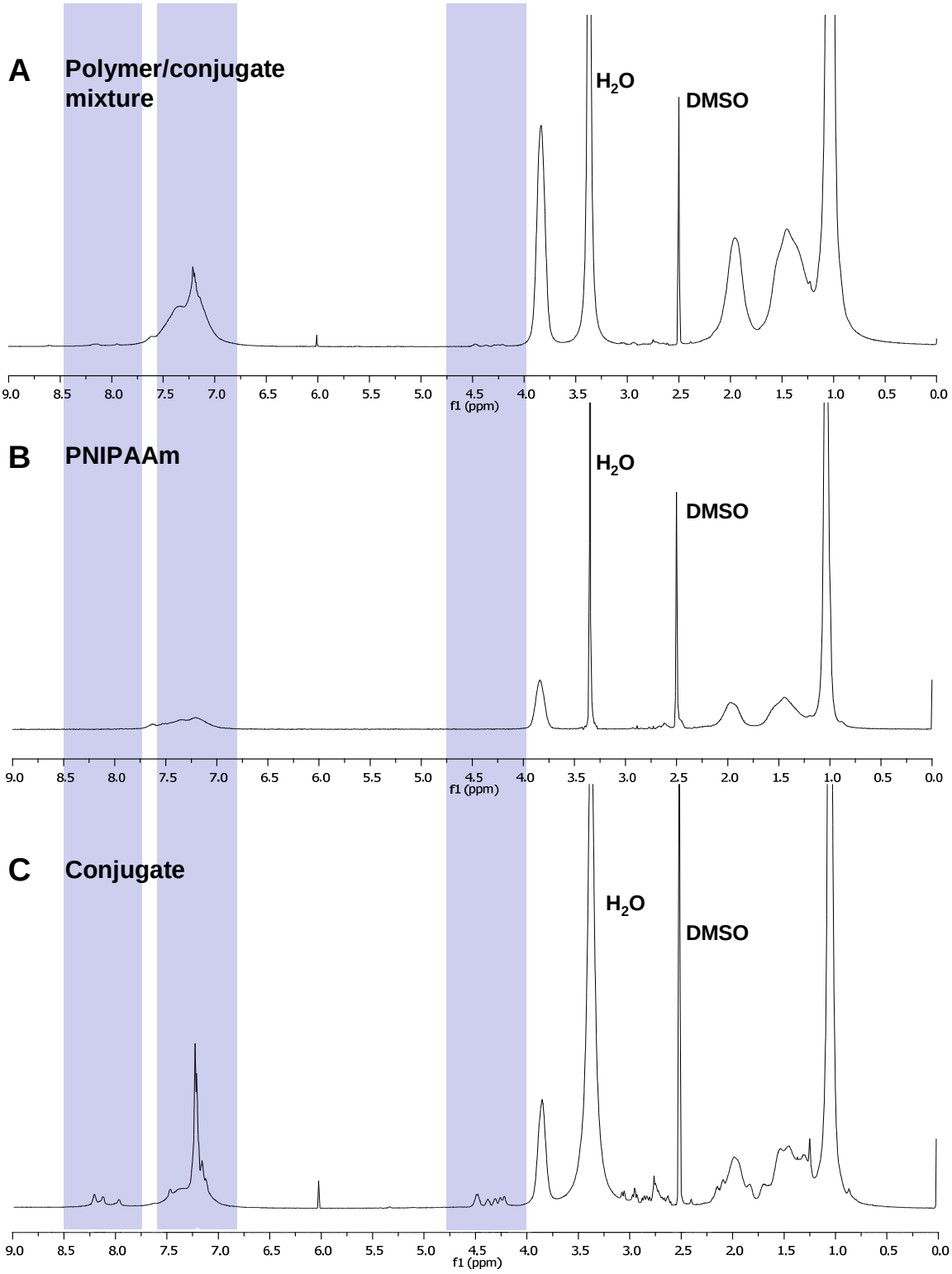

Figure 4.4: *^{1}H NMR spectra of: A) non-purified polymer/conjugate mixture PS3, B) PNIPAAm and C) conjugate after the purification via centrifugation (DMSO-d_6, 400 MHz)*

Fig. 4.4A shows the spectrum of the polymer/conjugate mixture PS3 with the characteristic polymer and peptide signals (see Fig. 4.2B). Fig. 4.4B shows the spectrum of the polymer obtained after the centrifugation with the characteristic polymer regions as in Fig. 4.2A. Fig. 4.4C shows the spectrum of the purified PNIPAAm-FEFEFKFK conjugate. The spectrum clearly shows the intensification of the signals after the purification: a resonance at 4 – 4.8 ppm corresponding to the protons from the peptide backbone, a resonance at 7 - 7.5 ppm corresponding to the aromatic rings of phenylalanine residues, and the peaks at 7.7 - 8.5 ppm corresponding to the peptide amide bonds.

After repeating three times the centrifugation and freeze-drying separately the sedimented phase and the combined supernatants, the weight fractions were obtained which are provided in Table 4.1 (5th column). The results also showed that conjugate content in the polymer/conjugate mixtures increased with increasing SH-modified peptide concentration in the synthesis. The mixtures PS1-PS3 showed slightly higher conjugate contents than the mixtures PA1-PA3. The ratios extracted from ^{1}H NMR were much higher than those obtained by centrifugation due to the use of the molar masses of the monomer units in the calculations.

The amount of unconjugated polymer in the mixture can be then subtracted from the monomer/peptide weight ratio, allowing the calculation of the peptide weight or molar fraction in the conjugated polymers, and thus also their degree of polymerisation or $\overline{M}_n$ (Table 4.1, 6th and 7th columns) assuming that only one peptide will be present per conjugated chain. For example, PS1 has a 1/16 weight fraction of conjugate and a 1/68 weight fraction of peptide; since the peptide is only present in the conjugate, the latter will have a 16/68 weight fraction of peptide. This corresponds to a 1/33 molar ratio, i.e. a degree of NIPAAm polymerisation of 33.

It was apparent that the amount of conjugate increased with increasing peptide content in the polymerisation; however, the conjugates were always a minor component of the samples, never exceeding 22% of the total weight. With the exception of PA3, also the $\overline{M}_n$ of the conjugates appeared to decrease with increasing amount of peptide.

The molecular weight distribution of the samples was investigated. The polymer/conjugate mixtures were analysed without separating the two components; however, due to the rather small amounts of conjugates present in the samples (ranging from 4.1 to 22% of the total weight), the results obtained were mostly related to the unconjugated polymer chains. The GPC results (Table 4.2, left part) showed that the $\overline{M}_w$ did not vary significantly as the concentration of SH-modified peptide increased; it remained roughly

constant at ~ 27,000 g mol^{-1} for PS1, PS2 and PS3 and at ~ 17,000 g mol^{-1} for PA1, PA2 and PA3. A certain influence of the presence of the chain-transfer agent was shown by a tendency towards decreasing $\overline{M}_n$ and increasing polydispersity, as the concentration of SH-modified peptide increased. This trend was somehow more apparent in the FEFEFKFK series (PS1-3), while the general decrease in $\overline{M}_n$ for the FEFKFEFK data (PA1-3) was more qualitative, since the very low molecular weights obtained likely fall outside the linear range of the GPC column. The $\overline{M}_n$ values, which were mostly attributed to the unconjugated polymers, were higher than those determined for the conjugates (centrifugation and ^{1}H NMR) for PS1-3, while they were rather similar for PA1-3. These differences, however, may also be related to a different form of aggregation of the polymers in the GPC solvent as a result of the different peptide structure. Indeed the determination of PNIPAAm molecular weight by GPC is a notoriously difficult task and is generally complicated by its unpredictable aggregation [2, 3].

Table 4.2: *Summary of the characterisation data for the polymer/conjugate mixtures prepared in this study*

Sample	GPC[a]			SLS			Viscometry			
	$\overline{M}_w$ [b]	$\overline{M}_n$ [b]	$\frac{\overline{M}_w}{\overline{M}_n}$	$\overline{M}_w$ [b]	R_g (nm)	A_2 (cm^3 mol g^{-2})	$[\eta]_H$ (dl g^{-1})	$[\eta]_K$ (dl g^{-1})	k_H	k_K
PS1	30	14	2.11	290	51±2	(4.4±0.5) 10^{-4}	0.877	0.828	0.43	0.17
PS2	24	7	3.39	390	61±4	(2.5±0.2) 10^{-4}	0.697	0.868	6.4	-0.06
PS3	28	7	4.21	300	51±6	(2.5±0.2) 10^{-5}	-0.163	0.369	133	-10.9
PA1	18	6	3.23	280	78±1	(4.9±1.0) 10^{-5}	0.480	0.492	0.52	0.95
PA2	17	5	3.32	230	41±2	(5.9±1.4) 10^{-5}	0.509	0.524	0.84	-0.08
PA3	17	9 [c]	1.98 [c]	260	50±3	(1.8±1.8)10^{-5}	0.428	0.459	3.6	-1.6
P0	27	13	2.08	80	21±6	(1.1±0.2) 10^{-3}	0.606	0.591	0.22	0.19

[a] in DMAc using PEG/PEO standards; [b] expressed in kg mol^{-1}; [c] molecular weight falls outside the linearity of the column

The effect of the presence, amount and type of the conjugate in PNIPAAm was then studied by static light scattering (SLS) and viscometry (Table 4.2, middle and right parts). SLS was performed in phosphate buffer (1 mM PB) and clearly showed a much higher tendency to aggregate for the polymer mixtures than for PNIPAAm. A first hint of aggregation is given by the very large values of $\overline{M}_w$ and radius of gyration (R_g) which were much higher for the polymer/conjugate mixtures than for the pure polymer. $\overline{M}_w$ and R_g for PS1 and for P0 were 290 kg mol^{-1} and 51 nm and 80 kg mol^{-1} and 21 nm respectively. The tendency for aggregation was further confirmed by the lower values of the second virial coefficient, A_2 for the polymer/conjugate mixtures than for pure polymer [4-6]. In particular, A_2 showed a clear

decrease with the increase in conjugate content while it was practically independent of $\overline{M}_n$ of conjugate (Fig. 4.5). An example from literature of the graft copolymer of PNIPAAm and polyoxythylene (PEO) with a terminal sulfobetaine group showed that the co-polymer aggregated intermolecularly. Its $\overline{M}_w$ was equal to 1.7×10^6 g mol^{-1} and showed A_2 of 5.7×10^{-4} cm^3 mol g^{-2} [4].

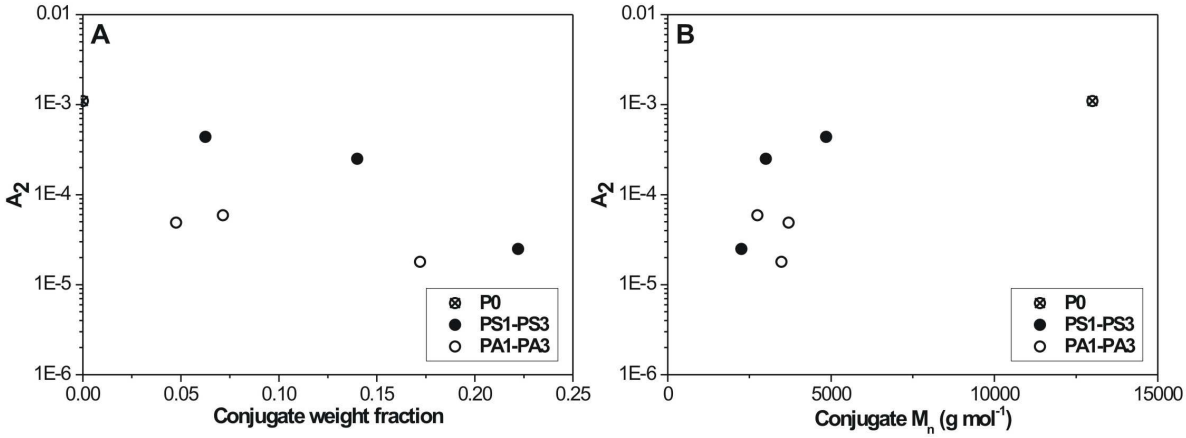

Figure 4.5: *A) Second virial coefficient as a function of the weight fraction of PNIPAAm-peptide conjugate in the polymer mixtures. For both peptides A_2 showed a clear decrease with increasing amount of conjugates. It can be noted that the FEFKFEFK-containing mixtures appeared to have lower values of A_2. B) Second virial coefficient as a function of the number-average molecular weight of the polymers. Although all the macromolecules had a rather similar size, A_2 showed variations of up two orders of magnitude without any clear pattern: the point on the right (PNIPAAm homopolymer) is reported only for comparison.*

Viscosity measurements were performed to confirm the tendency towards association of the conjugation products. A series of polymer/conjugate solutions with concentrations ranging from 0.5 to 2 wt.% were prepared in 1 mM PB and pure PNIPAAm (P0) was used as a reference. The dynamic viscosity of each solution was measured at 10°C. Plots of dynamic viscosity as a function of polymer/conjugate mixture and polymer concentration are given in Fig. 4.6.

Fig. 4.6A and 4.6B illustrate that for each sample the viscosity increased with solute concentration as expected. PS1 and PA1 had the viscosities very similar to those of P0 in the concentration range studied due to the lowest conjugate content in each series. At each sample concentration the viscosity increased with increasing conjugate content in the mixtures: for PS1 and PS3 at concentration of 0.015 g ml^{-1} the viscosity increased from 3.4 to 12 mPa×s accordingly and for PA1 and PA3 at the same concentration only slight increase in viscosity was observed: from 2.5 to 3.3 mPa×s accordingly. The viscosity increase rate was higher for polymer/conjugate mixtures PS1-PS3 than for PA1-PA3 presumably due to higher conjugate content. When a polymer is dissolved in a solvent, its chains interact with the solvent

molecules. Solvent influences the size and shape of the objects dissolved, which in turn influence the viscosity of the solution [7]. The conjugation products behaved differently than pure PNIPAAm most probably due to the presence of peptide segment that had tendency to self-assemble in larger aggregates thus increasing the viscosity. No substantial effect of the peptide sequence on the viscosity was observed.

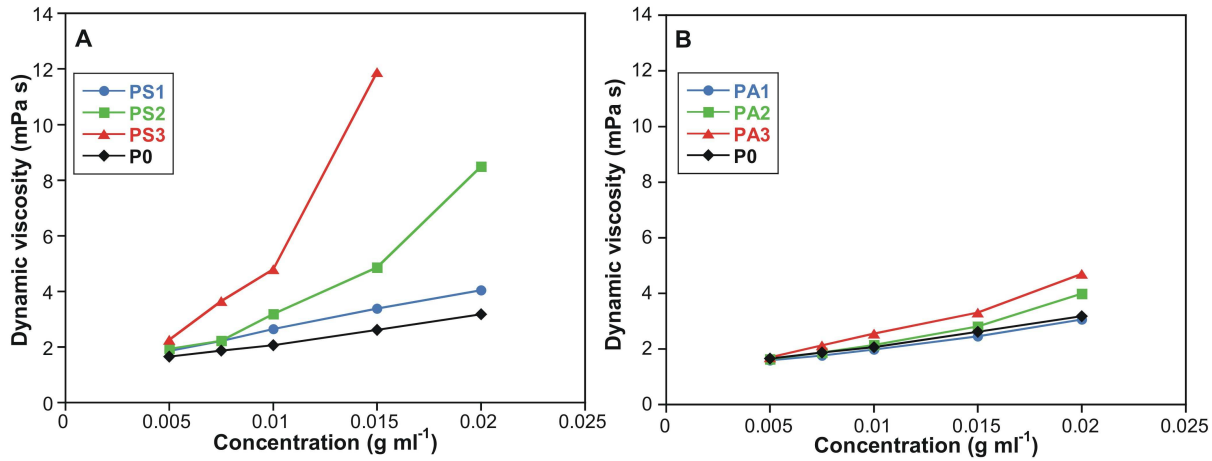

Figure 4.6: *Variation of dynamic viscosity with the concentration of the polymeric products in 1 mM PB at 10°C. In each series viscosity increased with increasing conjugate content in the mixtures. Polymer/conjugate mixtures with higher conjugate content PS1, P¨S2 and PS3 showed larger increase in viscosity than PA1, PA2 and PA3.*

Typically, viscometry measurements are performed to determine the intrinsic viscosity, [η] which depends not only on its molecular weight, but also on the balance of the interactions of the macromolecules with the solvent and between themselves [7]. It can be determined by plotting the reduced viscosity ($\eta_{red} = \eta_{spec}/c$) versus concentration, c (Huggins plot) or an inherent viscosity ($\eta_{inh} = (ln\eta_{rel})/c$) versus c (Kraemer plot). Plots of reduced and inherent viscosities of PNIPAAm (P0), PS1-3 and PA1-3 in 1 mM PB at 10°C are presented in Fig. 4.7. Double extrapolation of the lines connecting the reduced and inherent viscosities at different concentrations to $c = 0$ according to Eq. 3.12 and Eq. 3.13 respectively should provide a common intercept with the y axis which is the value of [η]. The slopes of the Huggins plots and the Kraemer plots give the values of Huggins (k_H) and Kraemer (k_K) coefficients accordingly. These coefficients are shape-dependent factors that provide additional information on the interactions between the polymer and the solvent and give an indication of the polymer compactness and/or tendency to aggregate. In particular, for aggregating polymers the $k_H = 0.3 - 0.5$ (from good to poor solvent) and $k_K > 0$, while for polymers exhibiting negligible aggregation at low concentration $k_K < 0$ and $k_H + k_K \sim 0.5$ [7-10].

The values of the intrinsic viscosities ($[\eta]_H$, $[\eta]_K$) and the coefficients (k_H, k_K), determined by the Huggins and Kraemer equations accordingly, are presented in Table 4.2 (right part). For PS3 and PA3 the calculations were performed disregarding the last points deviating from the straight line to give the approximate values of the intrinsic viscosities and the coefficients. Fig. 4.7 for P0 shows linear Huggins and Kraemer plots with similar intrinsic viscosities: $[\eta]_H$ = 0.606 dl g^{-1} and $[\eta]_K$ = 0.591 dl g^{-1} accordingly, indicating typical polymer behaviour with $k_H + k_K \sim 0.41$ (Table 4.2, right part). PS1, PA1 and PA2 also show behaviour similar to that of P0 with similar $[\eta]_H$ and $[\eta]_K$.

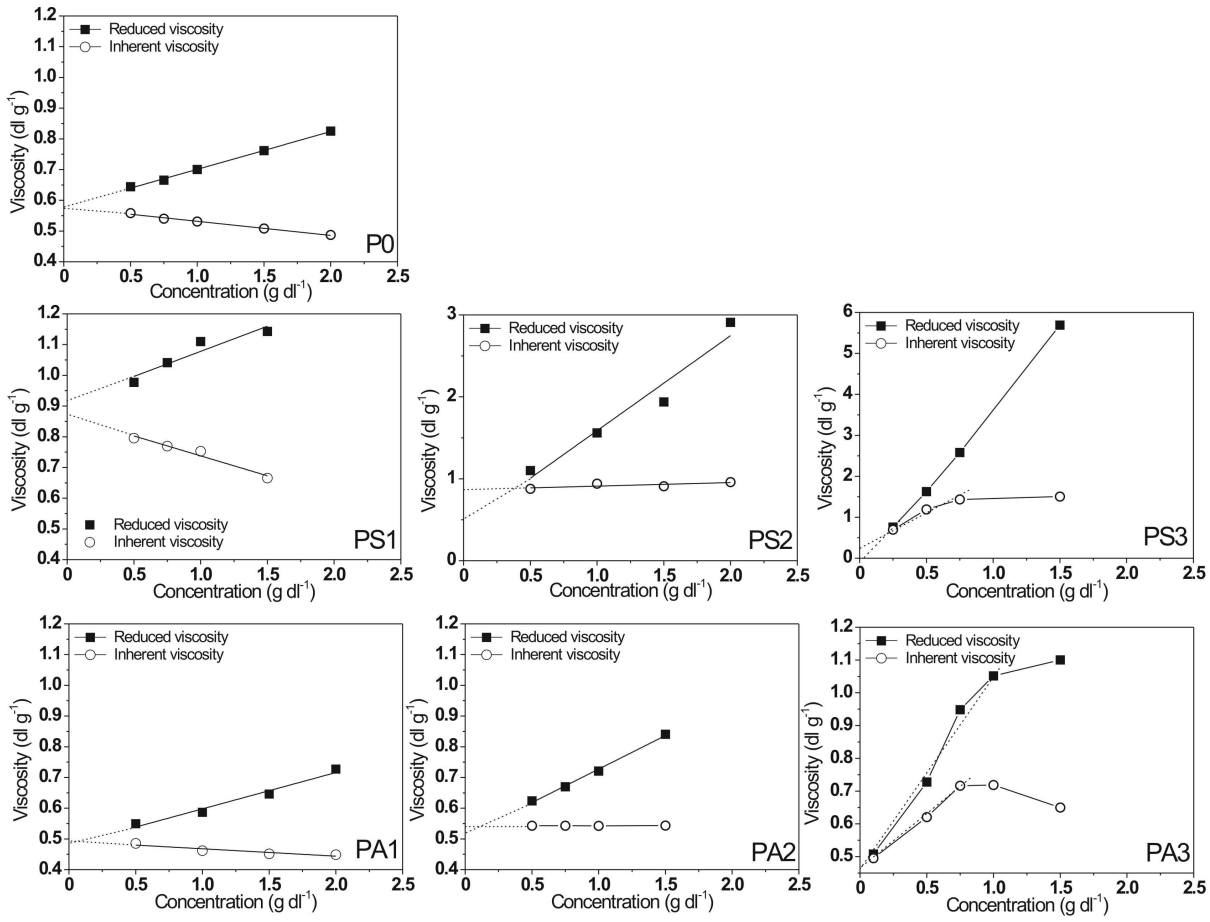

Figure 4.7: *Reduced and inherent viscosities for the different polymer/conjugate mixtures and for PNIPAAm (P0) as a function of their concentration in 1mM PB at 10°C*

The mixtures with low conjugate content, PA1 and PS1, maintained a certain similarity to the homopolymer, with the Kraemer and the Huggins plots still intersecting with slopes of opposite sign. However, k_H assumed values close to 0.5, indicating 1 mM PB as a poor solvent, and the sum $k_H + k_K$ increased above 0.5. The mixtures with higher conjugate content presented even stronger signs of deviation from the behaviour typical of a polymer solution, e.g. the inversion in the slope of the Kraemer plot, or $k_H \geq 1$. This demonstrated the

occurrence of aggregation phenomena in a fashion proportional to the weight fraction of the conjugate.

In particular, k_H. behaviour was studied As seen for the second virial coefficient, this parameter showed a clear dependence on the weight fraction of the conjugate in the mixture, and no pronounced dependence on the molecular weight (small variations in the molecular weight corresponding to large and random variations in k_H) (Fig. 4.8). It is noteworthy that the k_H dependence on the conjugate fraction did not highlight any significant difference between the two series of conjugates. In summary, SLS and viscometry measurements confirmed the tendency towards association of the conjugation products.

The results presented above demonstrated that the conjugation strategy provided an easy route to various polymer/conjugate mixtures where the higher the CTA concentration, the higher the fraction of conjugate present within the mixtures. The characteristic properties of the polymer/conjugate mixtures will be discussed in the following section. The behaviour of the pure polymer-peptide conjugate PNIPAAm-FEFEFKFK will be discussed in Chapter 6.

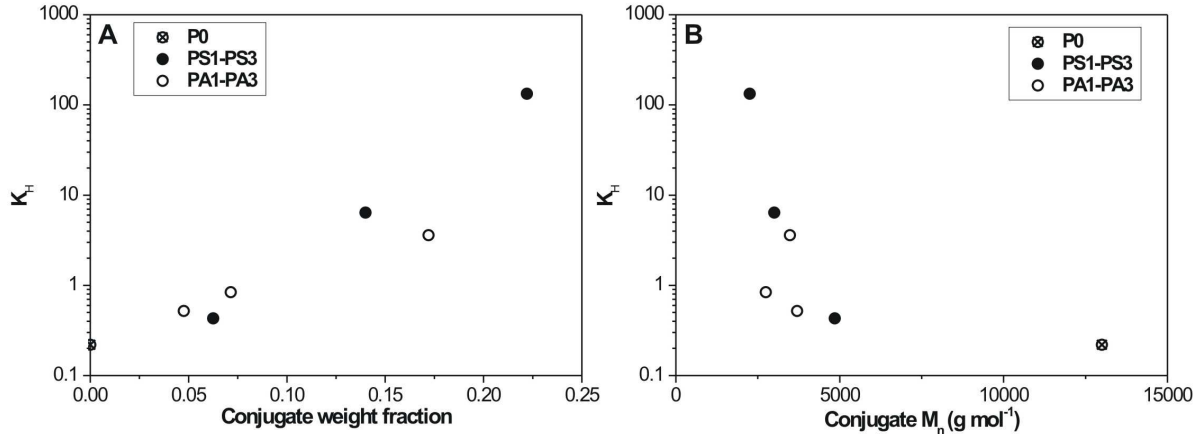

Figure 4.8: *A) Huggins coefficient as a function of the weight fraction of PNIPAAm-peptide conjugate in the polymer mixtures. k_H showed a clear (exponential) increase with increasing amount of conjugates. It can be noted that no significant difference was exhibited between FEFEFKFK- and FEFKFEFK -containing mixtures. B) Huggins coefficient as a function of the number average molecular weight of the polymers. Although all the macromolecules have rather similar size, k_H showed variations of up two orders of magnitude without any clear pattern: the point on the right (PNIPAAm homopolymer) is reported only for comparison.*

4.3. Characterisation of the mixtures of polymer and polymer-peptide conjugate

4.3.1. Gelation and thermal behaviour in water

To explore whether the six polymer/conjugate mixtures obtained had different macroscopic behaviour, a range of samples (5 - 200 mg ml^{-1}) were prepared by dissolving the

desired quantities of material in 1 ml of deionised water, vortexing for 60 s and leaving to equilibrate at room temperature overnight. For each sample a transition from a free flowing liquid to a self-supporting hydrogel occurred at a concentration that depended on the polymer/conjugate ratio. The critical gelation concentration, C^*, decreased with increasing amount of conjugate in the mixture, asymptotically approaching the values for the pure peptides: $140 < C^* < 150$, $40 < C^* < 50$ and $30 < C^* < 35$ mg ml^{-1} for PS1, PS2 and PS3 respectively and $180<C^*<190$, $140<C^*<150$ and $65<C^*<75$ mg ml^{-1} for PA1, PA2 and PA3 respectively. C^* for pure FEFEFKFK and FEFKFEFK peptides was found to be ~ 17 and 10 mg ml^{-1} respectively. Fig. 4.9 shows the variation of (C^*) with the conjugate weight fraction.

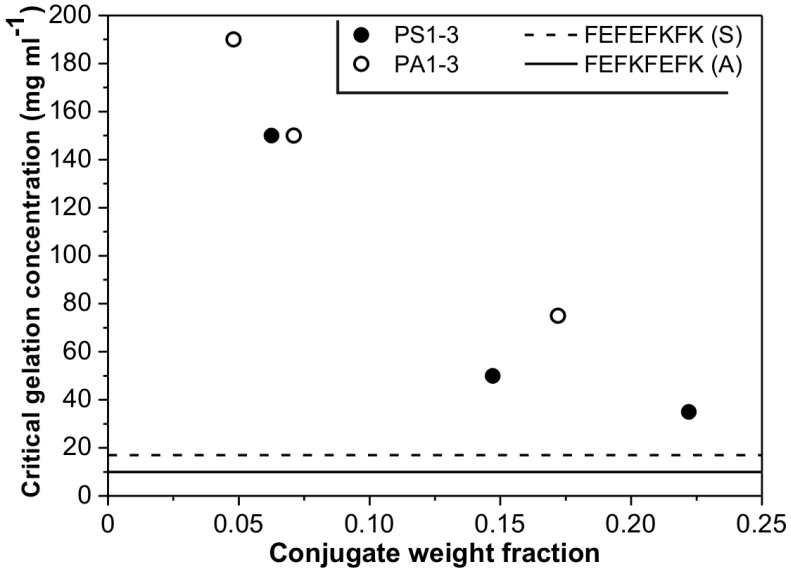

Figure 4.9: *Critical gelation concentration (measured with the tilt test on formulations in test tubes) as a function of the weight fraction of PNIPAAm-peptide conjugate in the polymer mixtures*

No significant difference could be recorded between the conjugates of the two peptides. The second virial coefficient data (Fig.4.5A) suggested slightly higher tendency of PAs to aggregation; however, these data were affected by relatively large errors, mostly due to their extrapolation from rather noisy Zimm plots. Additionally, both C^* and k_H appeared to demonstrate that, if differences in aggregation and gelling behaviour between the conjugates of the two peptides existed, they were rather minor and did not significantly affect the flow properties of the materials.

The amount of peptide in the mixtures at C^* was calculated using the calibration curve in Fig. 4.3 and the results showed that the peptide content in the polymer/conjugate mixtures at their C^* was very small (Table 4.3).

Table 4.3: *Peptide content in the polymer/conjugate mixtures at their C**

Sample	*C** (mg ml^{-1})	Peptide content (mg)
PS1	150	2.1
PS2	50	2.7
PS3	35	4.0
PA1	190	2.7
PA2	150	3.3
PA3	75	4.2

These results suggested that conjugated polymer modified the gelation behaviour of the peptides and it was postulated, therefore, that the peptide was able to self-assemble even if being attached to a large macromolecular chain. According to Table 4.3 the mixtures contained a small fraction of the conjugated peptide and a considerably high amount of pure polymer. Therefore it has been suggested that the free polymer might also influence the overall behaviour of the mixtures by creating the aggregates or additional entanglements with polymer segments in the conjugates and thus shifting the peptide gelation points to lower concentrations.

It is interesting to mention that the pH of the polymer/conjugate hydrogels was ~ 5.5. Usually the pH of the gels of pure peptides is ~ 2.3 due to the residual trifluoracetic acid (TFA) left after the peptide synthesis. TFA is a strong acid and forms salt-like complexes with lysine residues in the peptide. Since the polymer/conjugate mixtures were purified by dialysis, it was possible to eliminate some residual TFA and to increase the pH.

Concentrated solutions and gels of flexible polymers are characterised by entanglement points where polymer strands cross and loop around each other [11]. The elastic response of a network results from the tension in such chain segments as a function of the extension. Both the entanglement length and the mesh size (average spacing between chains or the size of voids between filaments) typically decrease with increasing concentration of polymeric or fibrillar chains [12]. FEFEFKFK and FEFKFEFK peptides were reported to form a network of anti-parallel β-sheet fibres at considerably low concentrations [13]. The stiffness of the fibres influences the visco-elastic behaviour of the gel. To confirm that the polymer/conjugate mixtures formed hydrogels, the mechanical properties of each of the samples over a range of concentrations slightly above the *C** were probed using oscillatory rheology where the sample was placed between parallel plates with the top plate of 20 mm in diameter.

The initial strain amplitude sweeps were performed when the hydrogels were exposed to an increasing stress at a constant frequency of 6.28 rad s^{-1}. Typical examples of the variation of elastic (*G′*) and viscous (*G″*) moduli as a function of shear strain are presented in Fig. 4.10 for 3 different concentrations of the polymer/conjugate mixtures PS3 (A) and PA3 (B).

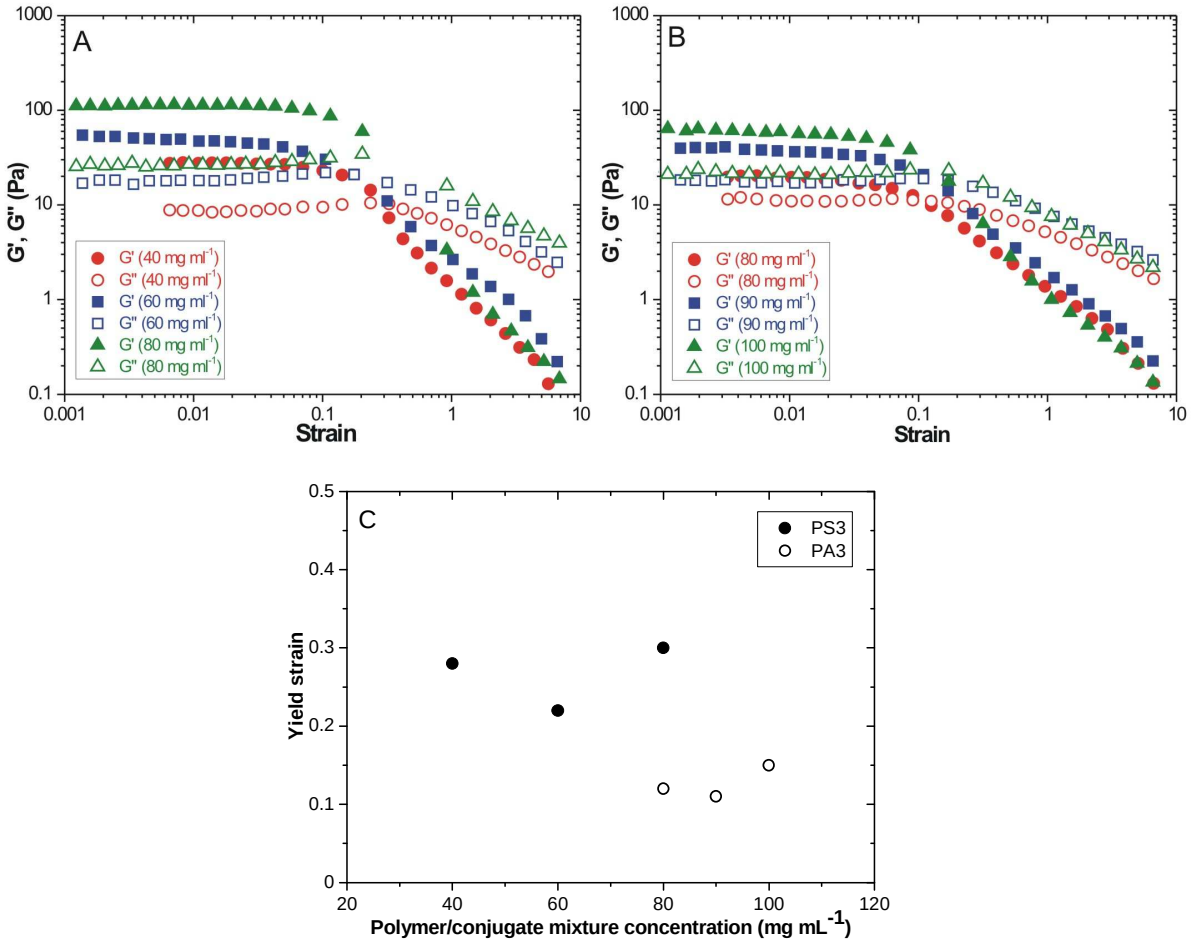

Figure 4.10: *Strain amplitude sweeps at angular frequency of 1 rad s^{-1} of: A) PS3 and B) PA3 at different concentrations at 20°C. G′ greater than G″ was observed for all samples indicating gel formation. Linear visco-elastic region was found to be at strain amplitudes lower than 0.1, above this value the breakdown of the gels was observed. Moduli increased with increasing sample concentration. C) Variation of yield strain with polymer/conjugate mixture concentration.*

Hydrogels are visco-elastic materials that combine properties of the elastic solid and the viscous fluid. Typically, when the sample is liquid-like, $G' < G''$. When the sample starts to behave more like the elastic solid, the behaviour changes and G' becomes higher than G'' [14, 15]. Fig. 4.10 shows that the elastic behaviour of the hydrogels dominated the viscous behaviour as elastic moduli (G') values were higher than viscous moduli (G'') values indicating the formation of a gel for all 3 concentrations for PS3 and PA3. The elastic response of the gels as measured by G' decreased rapidly above a concentration-dependent critical strain amplitude indicating a breakdown in the gels. Fig. 4.10C shows the variation of yield strain with polymer/conjugate mixture concentration. Yield strain (γ^*) shows the maximum strain which is necessary to break a sample in gel state and to make it flow. Below yield strain G' > G" (elastic behaviour dominates) and above the value of yield strain G" > G' (liquid behaviour dominates). In each series yield strain slightly increased with increasing

polymer/conjugate mixture concentration. PS3 series showed higher yield strain values (γ^*~0.25-0.3) than PA3 series (γ^*~0.15) presumably due to higher conjugate content. Fig. 4.10 also shows that moduli values increased with increasing polymer/conjugate mixture concentration. For example, *G′* of PS3 increased from 30 to 110 Pa when the sample concentration increased from 40 to 80 mg ml^{-1}. For PA3 the *G′* increase was smaller, from 20 to 50 Pa, when the sample concentration increased from 80 to 100 mg ml^{-1}. The same strain amplitude sweeps were performed for other mixtures in the series (PS1, PS2, PA1 and PA2). The results showed that for all samples *G′* > *G″* in the concentration range studied and that the gels were stable at strain amplitudes $\gamma < 0.1$.

The oscillation frequency sweeps were performed in the LVR at 1% strain by exposing all samples to a gradual increase in angular frequency from 6.28 to 62.8 rad s^{-1} and by varying the deformation in a sinusoidal fashion. The frequency sweep experiments were performed to reveal the strength of the gel networks. Evolution of *G′* and *G″* with frequency was studied over a range of concentrations for each polymer/conjugate mixture in both series. Fig. 4.11 compares the frequency sweeps of the gels of PS3 at 40, 60 and 80 mg ml^{-1} and of PA3 at 80, 90 and 100 mg ml^{-1}.

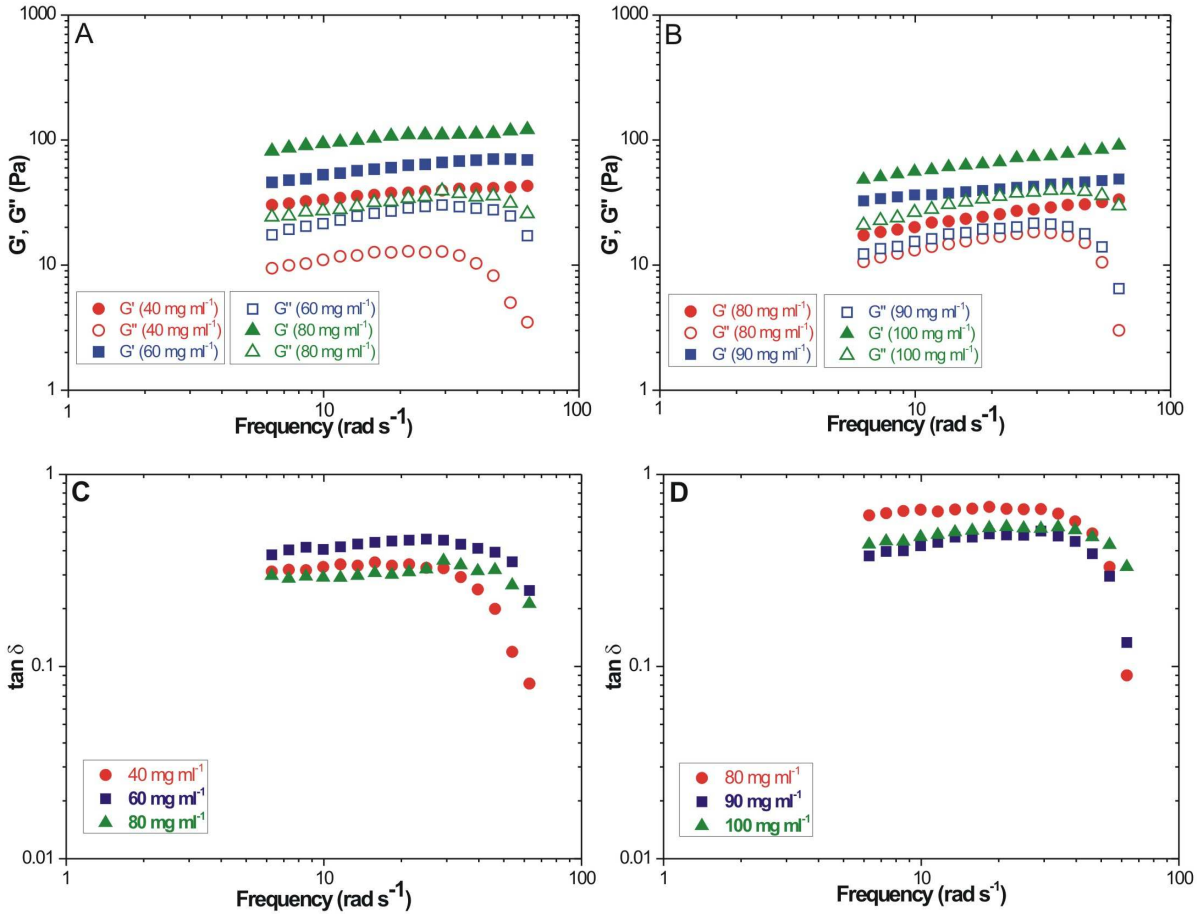

Figure 4.11: *Variation of G′ and G″ as a function of angular frequency of: A) PS3 and B) PA3 at different concentrations. G′ > G″was observed for all samples. Moduli were practically independent of the frequency over the range studied. Moduli increased with increasing sample concentration indicating the increase in gel strength. Variation of tan δ as a function of angular frequency of: C) PS3 and D) PA3 at different concentrations.*

For each concentration G' was found to be larger than G'', indicative of an elastic rather than viscous material. Both G' and G'' were practically independent of frequency over the range 6.28-62.8 rad s^{-1}, which indicated the dominant visco-elastic relaxations of the network were at lower frequencies. Such rheological behaviour matched the characteristic signature of a solid-like gels composed of long entangled fibres [16-18]. G' and G'' increased with increasing the concentration of PS3 and PA3. The long relaxation time of the polymer network was also consistent with the observation that polymer/conjugate mixture gels were resistant to flow, following sample inversion. Microstructure of the samples will be discussed later in section 4.3.3. Frequency sweeps of other samples (PS1, PS2, PA1 and PA2) showed similar mechanical behaviour. G' and G'' were practically independent of frequency over the range from 1 to 10 rad s^{-1} and G' was always higher than G'' for the samples above their C^*. However, G' values never exceeded the value of 100 Pa in the concentration range from 40 to 200 mg ml^{-1}.

Fig. 4.11C and D show the variation of tan δ with angular frequency. The results showed that the systems studied satisfy the Winter-Chambon criterion for the formation of a gel: tan $\delta = G''(\omega)/G'(\omega) \leq 1$. Tan δ is also independent of frequency in the linear visco-elastic region from 6.3 to 30 rad s^{-1} (Fig. 4.11C) confirming the gel state of the samples [19, 20]. As the samples approach higher frequencies they start to show strong dependency on the radial frequency presumably due to viscous behaviour becoming predominant and consequently tan δ decreases sharply.

Table 4.4 presents the G' values of gels composed of β-sheet fibres. The peptide structure as well as its concentration has a strong effect on the self-assembling behaviour and on the visco-elastic properties of the gel. The G' values obtained for PNIPAAm-rich gels (~100 Pa) were of the same order of magnitude as the modulus reported in the literature for other similar β-sheet fibres rich peptide hydrogels [17, 21].

Table 4.4: *Different β-sheet fibre forming peptides and G' values of their gels*

Entry	Peptide	G' (Pa)	Concentration (mg ml^{-1})	Ref.
1	EAK-II[a]	10	1	[17]
2	Poly-EAK-II[b]	100	1	[17]
3	Nap-FFGEY[c]	40	3	[22]
4	MAX1[d]	230	7	[23]
5	SSP2[e]	520	20	[24]
6	SSP3[f]	2800	20	[24]
7	Fmoc-FF[g]	21.2×10^3	11.8×10^3	[25]

[a] $(AEAEAKAK)_2$ (16 amino acid residues); [b] 168 amino acid residues; [c] Nap – naphthalene, F – phenylalanine, G – glycine, E – glutamic acid, Y – tyrosine; [d] $[(VK)_4\text{-}V^DPPT\text{-}(KV)_4\text{-}NH_2]$, V – valine, K – lysine, P – proline, T - threonine; [e] $[(VK)_3\text{-}V^DPPT\text{-}(KV)_5\text{-}NH_2]$; [f] $[(VK)_3\text{-}V^DPPT\text{-}(KV)_3\text{-}NH_2]$; [g] Fmoc – fluorenyl-9-methyloxycarbonyl, F - phenylalanine

MacKintosh *et al.* developed a theoretical framework for systems composed of semi-flexible fibrils based on chemically cross-linked F-actin fibrils [12]. The authors predicted that G' would vary with actin concentration as $C^{11/5}$ for entangled solution of linear semi-flexible biopolymer, when the persistence length was substantially larger than the mesh size. A slightly higher scaling factor of $G' \sim C^{5/2}$ was predicted for a densely cross-linked gel where the segment length approximated the mesh size [12]. Hinner *et al.* [26] predicted that $G' \sim C^{7/5}$ for a physically entangled network of linear semi-flexible fibres of actin.

One other theory relating the variation of the elastic modulus to polymer concentration has been developed for fibrillar gels by Jones and Marquès [27] and has been successfully applied by Guenet *et al.* to a number of thermo-reversible physical gels [28, 29]. According to Jones and Marquès, agarose gels that consisted of nearly straight fibrils (intrinsically rigid objects) exhibited $G' \sim C^{2}$ for systems at low-concentrations and $G' \sim C^{1.5}$ for higher concentrations [30]. In the case of poly(vinylchloride) gels that possessed a well-defined fibrillar morphology, G' varied as $C^{3.0}$ [28]. Fibrillar gels of isotactic polystyrene showed an exponent of 2.7 [31].

The theories presented above can be used for an approximate comparison of PNIPAAm-rich gels created in this study with other physically cross-linked networks. The scaling factors for the polymer/conjugate hydrogels were determined by plotting G' plateau values, measured at 1% strain as a function of peptide concentration in the mixtures in the logarithmic scale. The peptide content in the polymer/conjugate mixtures was recalculated using the calibration curve presented in Fig. 4.3. The values of scaling factors are presented in Fig. 4.12 and would possibly provide further structural information on the gel network. For comparison purposes the scaling factors of pure FEFEFKFK and FEFKFEFK gels are also included. The pH of FEFEFKFK and FEFKFEFK gels was adjusted to 5.5 by adding NaOH solution.

Fig. 4.12 shows that G' varied linearly with concentration for both polymer-conjugate systems and pure peptides. As Fig. 4.12A indicates FEFEFKFK showed a $C^{0.8}$ behaviour which is close to the physical network of actin fibres. As Table 4.2 showed the conjugate content in the polymer/conjugate mixture PS3 was the highest, hence it had the closest scaling factor of 2.6 to that of pure FEFEFKFK, however considerably larger. The scaling factors increased with decreasing conjugate content in the polymer/conjugate mixtures: PS2 and PS1 possessed higher scaling factors of 4.0 and 9.8 respectively.

Fig. 4.12B shows the variation of G' as a function of FEFKFEFK also extracted from the calibration curve in Fig. 4.3. Pure FEFKFEFK had the scaling factor of 1.1 which was close to that of FEFEFKFK at pH 5.5 and to the scaling factor predicted for physical actin

gels. PA1, PA2 and PA3 had rather similar and high scaling factors of 6.2, 6.7 and 5.3 presumably due to high polymer content in the polymer/conjugate mixtures.

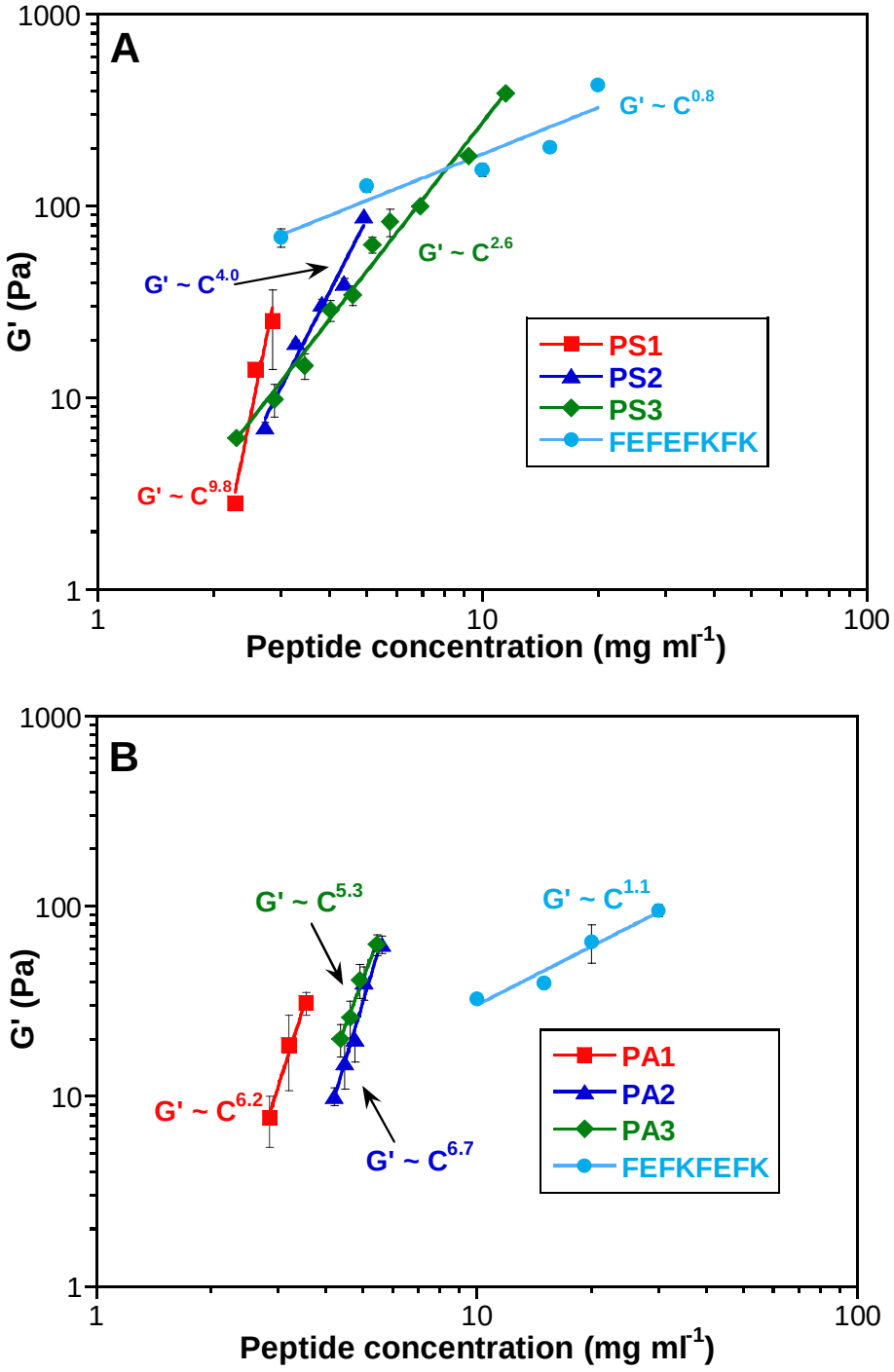

Figure 4.12: *Plateau values of G' as a function of concentration of: A) PS1, PS2, PS3 and FEFEFKFK; B) PA1, PA2, PA3 and FEFKFEFK at pH 5.5*

It has been observed by several researchers that *G'* values of physically cross-linked networks of gelatin and agarose showed typical to biopolymers C^2 dependence at high concentrations. At low concentrations much higher scaling factors were observed. In the case of agarose, it was suggested that at higher concentrations higher exponents were due to the

shorter and stiffer segments of single agarose chains [32]. These results showed higher scaling factor values for polymer/conjugate hydrogels presumably due to considerably high free polymer content in the samples.

It may be postulated that free polymer may interact with the peptide fibres and/or with the polymer segments present along peptide fibres thus contributing to the fibre stiffening, creating additional entanglements or physical cross-links and increasing gel stiffness.

In summary, rheological measurements confirmed the formation of self-supporting hydrogels above the C^*, since G' was higher than G''. The G' values for both polymer/conjugate mixture series were ≤ 100 Pa in the concentration range from 40 to 200 mg ml^{-1}. The results also suggested that not only peptide contributed to overall gel properties but also unconjugated polymer chains. The plots of scaling factors showed that the hydrogel visco-elastic properties increased not only with increasing conjugate content but also with increasing polymer content in the mixtures. The elastic, G' modulus scaling factors of the physically cross-linked hydrogels studied here do not correlate within the framework of the most widely accepted scaling factor theories for physically cross-linked gels. Further studies and theoretical concepts are suggested to describe complex PNIPAAm-rich networks.

4.3.2. Thermal behaviour

The thermal behaviour of the polymer/conjugate mixtures was studied to explore a reversible LCST, and possible melting and re-gelation in response to temperature. First, the macroscopic thermal behaviour of the polymer/conjugate mixtures was recorded visually at 10°C intervals during a heating/cooling cycle from 25-80ºC by placing the samples in a temperature controlled water bath and equilibrating for 15 min. Representative photographs of behaviour at 25, 40 and 80ºC are given in Fig. 4.13A for PS1, PS2 and PS3 at their C^* of: 150, 50 and 35 mg ml^{-1} respectively; and in Fig. 4.13B for PA1, PA2 and PA3 at their C^* of: 190, 150 and 75 mg ml^{-1} respectively. At 25ºC the formation of clear gel was observed. No change was noted until 40ºC when the gel turned opaque, presumably due to the collapse of PNIPAAm polymer chains, indicating the polymer had gone through its LCST. The samples remained self-supporting and the transition was thermally reversible if the samples were subsequently cooled at this stage, indicating both the conjugate and free polymer remained trapped within the hydrogel structure. When the gel samples were heated to 80°C, they appeared to shrink while expelling water. Such behaviour is typical of PNIPAAm solutions and has previously been related to the aggregation of the collapsed PNIPAAm chains [33, 34]. Upon cooling, the water was reabsorbed and the polymer redissolved to once again form clear

hydrogels. No significant difference in the macroscopic behaviour was observed between the two samples series.

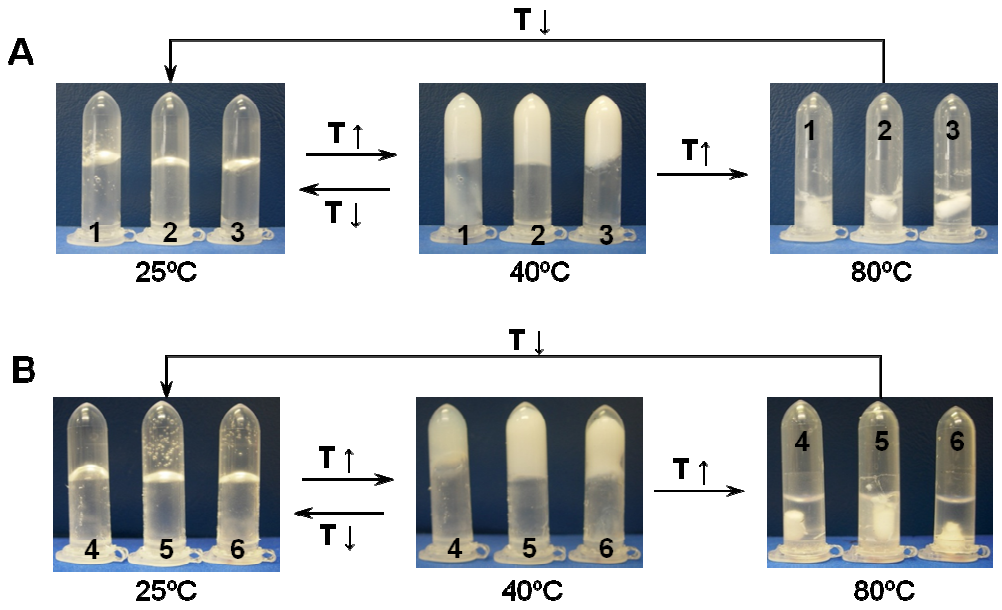

Figure 4.13: *Photographs showing phase behaviour of the polymer/conjugate mixtures at their critical gelation concentrations: A) 1-PS1: 150 mg ml^{-1}, 2-PS2: 50 mg ml^{-1}, 3-PS3: 35 mg ml^{-1} and B) 4-PA1: 190 mg ml^{-1}, 5-PA2: 150 mg ml^{-1}, 6-PA3: 75 mg ml^{-1} at 25°C, 40°C and 80°C. At 25°C self-supporting gels were formed. At 40°C gels became opaque due to the phase separation of PNIPAAm. At 80°C gel networks shrank releasing bound water. Upon cooling the transitions were reversible and collapsed polymer chains re-swelled absorbing water.*

To quantify the LCST and phase separation enthalpy values of these materials, the thermal behaviour of each sample was monitored using micro DSC between 20 and 80°C at a heating rate of 1 °C min^{-1} over a range of sample concentrations. Typical results for the initial heating scans for PS3 over a range of concentrations are given in Fig. 4.14A. Pure PNIPAAm was used as a reference. The onset points of the endothermic peaks, determined by the intersection of tangent lines from the baseline and slope of the endothermic peak, were used to determine the LCST.

A sharp endothermic transition at ~30°C for all samples was observed that was attributed to the LCST of PNIPAAm. This agreed well with visual observations. The enthalpy associated with this transition increased with increasing polymer concentration in the mixtures, as expected, while the temperature of transition remained constant (Fig. 4.14A). The latter indicated that the inclusion of the hydrophobic peptide and also sample gelation (C^* of PS3 is between 30 and 35 mg ml^{-1}) did not affect the LCST. Fig. 4.14B shows the reversibility of the phase separation upon cooling. All samples showed an exothermic peak of PNIPAAm. Fig. 4.15A and 4.15B compare the values of the LCST and enthalpies of the phase separation for both series of polymer/conjugate mixtures as a function of polymer concentration. The

polymer content in the mixtures was calculated using the calibration curve in Fig. 4.3. The results showed that the LCSTs remained practically constant ~30°C for all samples indicating that peptide conjugation to PNIPAAm did not affect the LCST and suggesting that the samples in each series contained polymer of similar $\overline{M}_w$. The figures also showed that the enthalpy of the LCST transition varied linearly with polymer content in the polymer/conjugate mixtures indicating that the more polymer was present, the more intensive the signal and the more sharp the transition would be.

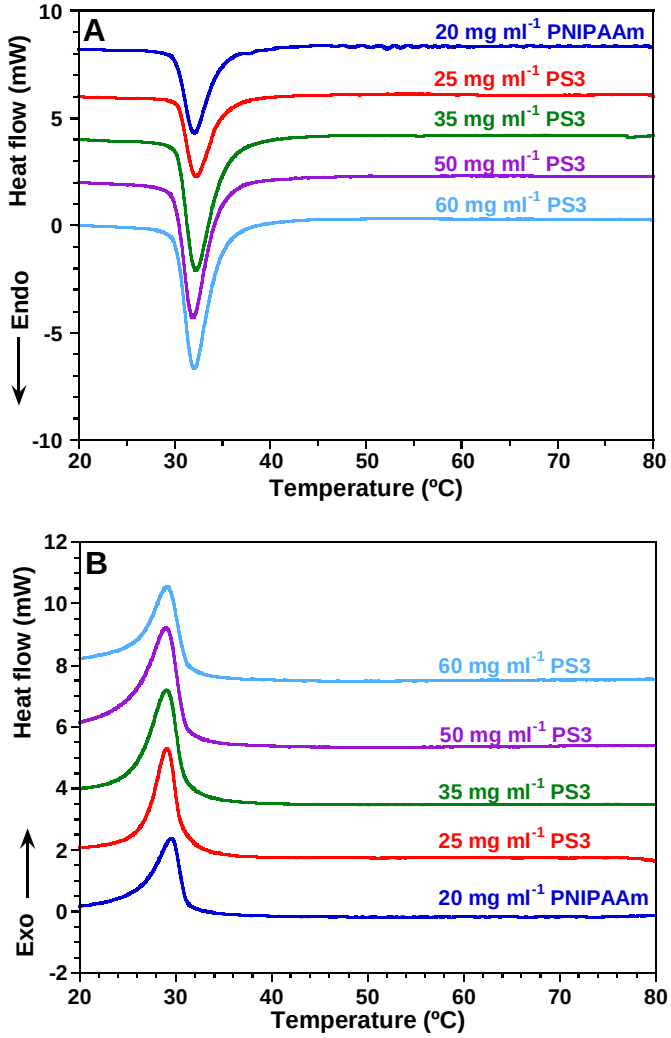

Figure 4.14: *Micro DSC thermographs of PS3 over a range of concentrations in comparison to pure PNIPAAm during: A) heating from 20 to 80°C and B) cooling from 80 to 20°C. During heating an endothermic peak at ~ 30°C characteristic to the LCST of PNIPAAm was observed. Upon cooling the LCST transition was reversible.*

The results showed that ΔH increased with increasing conjugate content in the mixtures. It is clear from Fig. 4.15 that the slope of the linear dependence of ΔH versus polymer concentration increased with the increase of conjugate content in the polymer/conjugate

mixtures. The slope for PNIPAAm and PS3 changed from 0.045 to 0.062 respectively (Fig. 4.15A). The slope corresponds to the ΔH (J per g of polymer solution) of the transition. Micro DSC detects the disruption of the hydrogen bonds among the amide groups of PNIPAAm and water molecules during the transition. Higher ΔH values for the polymer/conjugate mixtures indicated that the amount of hydrogen bonds to be disrupted was higher than that for pure PNIPAAm. Lysine (K) and glutamic acid (E) residues are capable of forming hydrogen bonds with water molecules. It can be assumed that the peptides can form intermolecular hydrogen bonds with polymer and/or among the peptide fibres below the LCST. At elevated temperatures the hydrogen bonds break resulting in slightly higher enthalpy values. This trend was also present but less pronounced in the PA1-PA3 mixture series (Fig. 4.15B). The slopes of PA1, PA2 and PA3 were not substantially different from that of PNIPAAm: 0.045 and 0.053 for PNIPAAm and PA3 respectively, possibly due to low conjugate content in the mixtures.

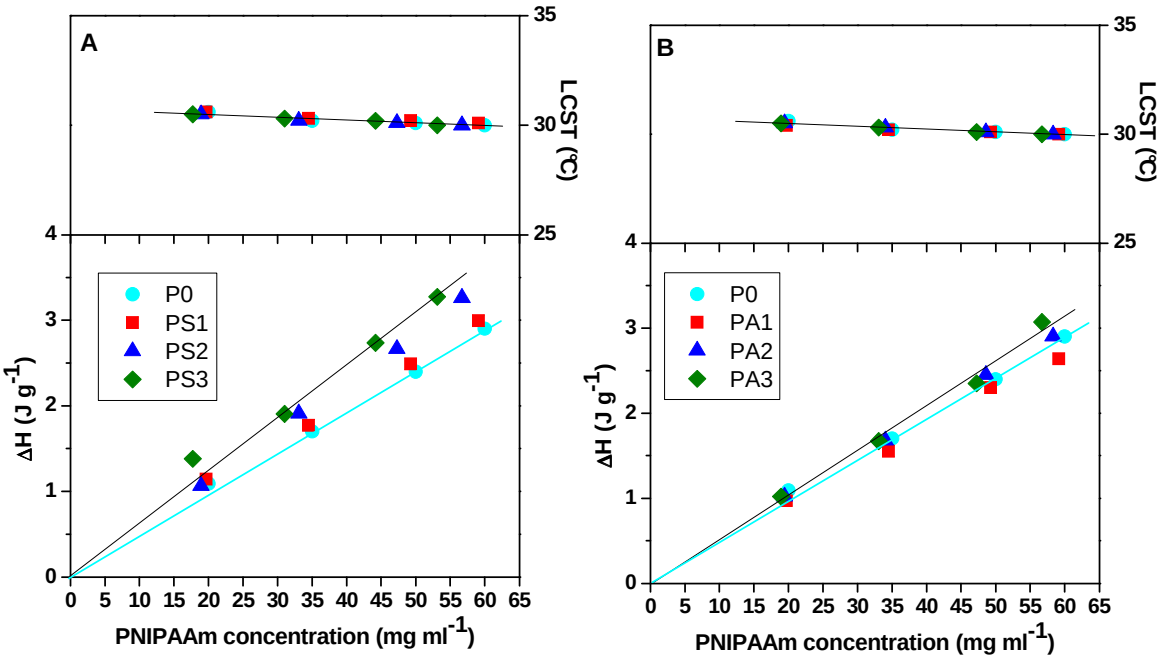

Figure 4.15: *Plots of the LCST transitions (upper) and enthalpies of phase separation (lower) as a function of PNIPAAm (P0) concentration and of polymer concentration in: A) PS1, PS2, PS3 and B) PA1, PA2, PA3*

Oscillatory rheology also allowed the mechanical behaviour of the polymer/conjugate gels to be studied as a function of temperature. Two polymer/conjugate mixtures were chosen for the study, i.e. PS3 and PA3, as they possessed the lowest *C** in their series. The variation of *G′* and *G″* at various concentrations was recorded in the temperature range from 20 to 45°C. Fig. 4.16A shows the variation of *G′* for PS3 during heating and cooling. The figure

shows that G' remained practically constant and G'' decreased slightly in the temperature range from 20 to 28°C. At ~ 30°C both moduli started sharply to increase presumably due to the phase separation of PNIPAAm when polymer chains collapsed and started to aggregate resulting in higher moduli. At ~ 35°C both moduli reached the maximum (G' ~ 680 Pa and G'' ~ 200 Pa) and started to decrease during further heating possibly due to further aggregation of collapsed polymers and water expulsion. This agreed with macroscopic phase separation when at high temperatures the polymer shrank while expelling water. Interestingly, upon cooling the thermal transition was reversible for both moduli, however a considerable hysteresis was observed in mechanical behaviour resulting in lower moduli values (G' ~ 30 Pa) than in the beginning of the experiment (G' ~ 100 Pa). Polymer aggregation above the LCST and re-solubilisation below the LCST may be a kinetically controlled process. This assumption indicated when the heating step was finished the system was still aggregating and expelling water and therefore the mechanical properties were weakening during cooling.

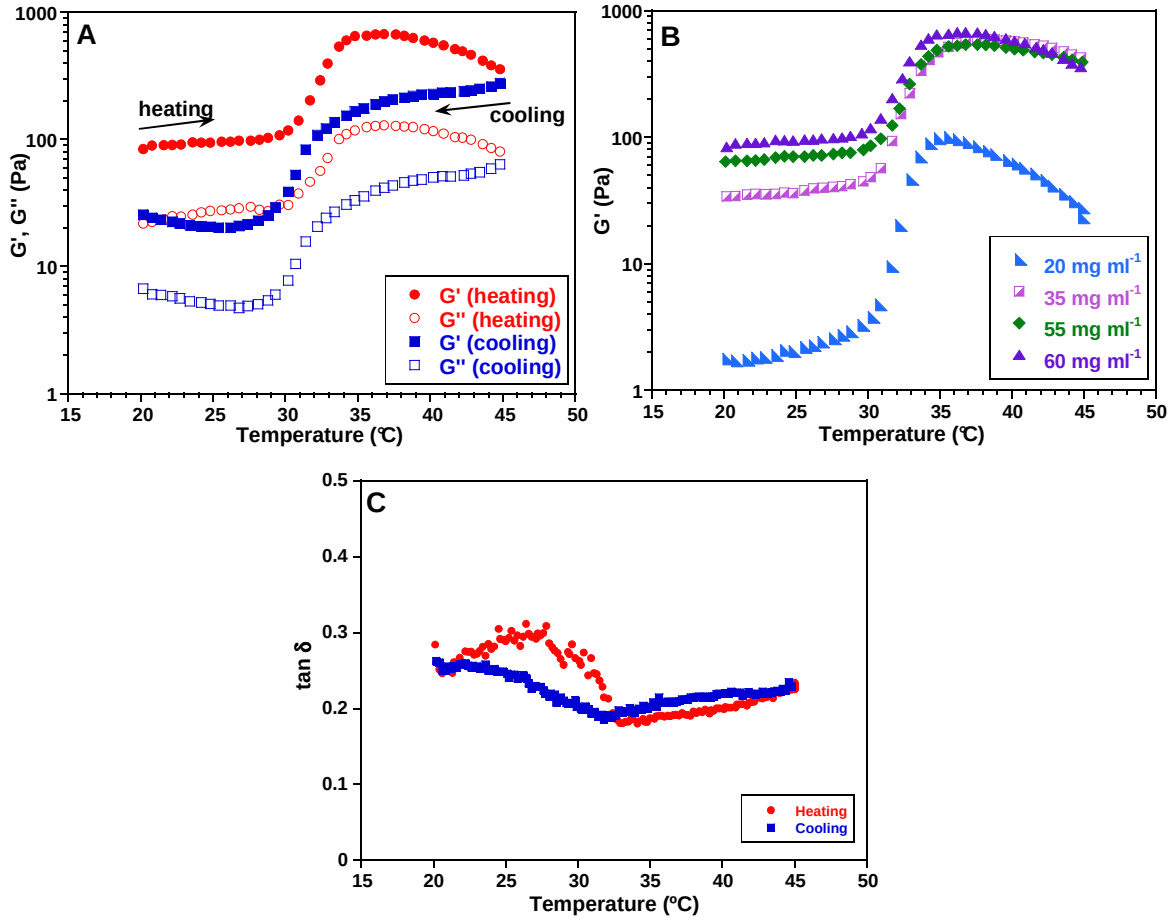

Figure 4.16: *A) Variation of G' and G'' of PS3 at 60 mg ml^{-1} during heating from 20 to 45°C and cooling from 45 to 20°C. B) Variation of G' of PS3 at different concentrations during heating from 20 to 45°C. C) Variation of tan δ of PS3 at 60 mg ml^{-1} with temperature.*

The observation that both moduli practically mirrored each other during heating and cooling may be explained by the presence of conjugated and free polymer chains (Fig. 4.16C). The conjugated polymer chains collapse along the peptide fibres resulting in a stiffening of the network and therefore an increase in G'. The free polymer chains will also collapse and in this state will behave as particulate fillers instead of long entangled polymer chains. Consequently the viscosity of the free polymer and water phase will decrease resulting in an increase in G'. The results also showed that the samples studied satisfy the Winter-Chambon criterion for the formation of a gel: $\tan \delta = G''(\omega)/G'(\omega) \leq 1$ indicating that the samples are in gel state [19, 20].

Fig. 4.16B shows the variation of G' for PS3 at 4 different concentrations as a function of temperature. In the temperature range from 20 to 28°C G' remained practically constant for all concentrations. At ~30°C G' started to increase considerably presumably due to the coil-to-globule transition of the polymer. The temperatures at which the phase separation occurred, at ~ 30°C, were in a good agreement with the LCST values from micro DSC studies. In the temperature range from 31 to 36°C G' continued to increase. Further heating resulted in slight decrease in G' due to the same reasons as explained above. The sample of 20 mg ml^{-1} showed a faster decrease in G' than the other 3 concentrations. This might be attributed to the fact that the sample of 20 mg ml^{-1} was a viscous liquid at room temperature and that the aggregation of the collapsed polymer chains was slightly faster than in the samples in gel state. It was assumed that dense peptide fibrillar network formed at higher PS3 concentrations ($30<C^*<35$) provided a stabilisation of the system and to some extent restricted or retarded the aggregation of the collapsed polymer chains. The hydrogels of PA3 (80 and 90 mg ml^{-1}) showed similar behaviour (data not shown) that G' increased from ~ 20 to 170 Pa during heating from 20 to 45°C presumably due to the collapse of the polymer. Such a substantial increase in G' values upon heating was found to be characteristic to other PNIPAAm-containing systems [19, 35-37].

4.3.3. Gel morphology and microstructure

TEM and AFM techniques were used to investigate the microstructure of the polymer/conjugate gels. Examples of typical TEM and AFM images for PS3, PA3 and pure FEFEFKFK are presented in Fig. 4.17 and 4.18 respectively. Both techniques showed that the structure observed consisted of a network of uniform, entangled fibres.

Fibre width for PS3 and PA3, estimated from TEM micrographs, was 5.5 ± 2 nm and 6 ± 1.5 nm respectively (Fig. 4.17A and B). PS2 and PA2 formed fibres of similar size. Polymer/conjugate mixtures with low conjugate content, PS1 and PA1, formed slightly larger

fibres of 7.5 ± 2 nm. Polymer content in the PS1 and PA1 samples was high and it might accumulate along the fibres allowing heavy metal ions, used for sample negative staining, to be deposited along the fibres. Therefore the fibres appear to look thicker and this may lead to the artefact and overestimation of fibre dimensions. Pure peptide formed 3.4 ± 2 nm wide fibres of similar appearance (Fig. 4.17C).

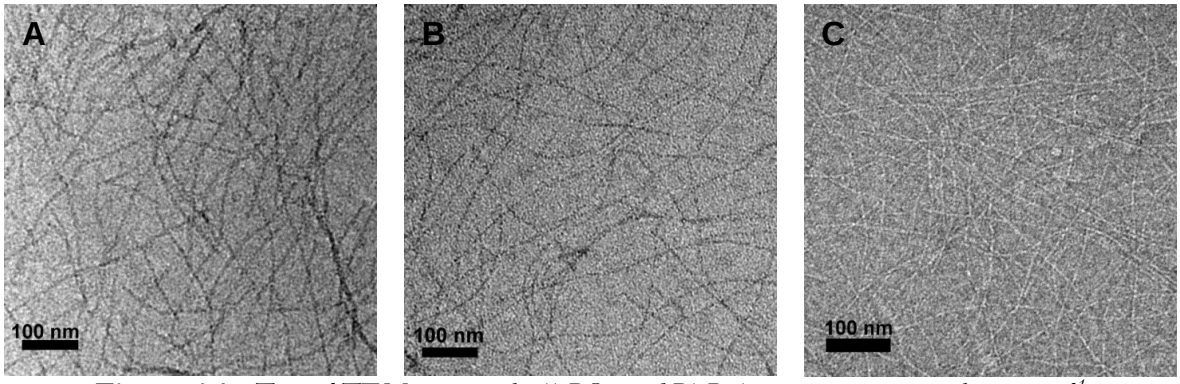

Figure 4.17: *Typical TEM images of: A) PS3 and B) PA3 at concentration of 10 mg ml^{-1}, C) FEFEFKFK at concentration of 1 mg ml^{-1}. TEM showed network of entangled fibres.*

AFM results showed that PS3 formed long 4 ± 1 nm wide and 0.7 ± 0.3 nm high fibres (Fig. 4.18A). Some shorter fibres of similar size were also present. The formation of short fibres as observed in Fig. 4.18A might occur due to low conjugate concentration (5 mg ml^{-1}) which was not enough for long fibre formation. Also shorter fibres might be more easily adsorbed on the mica surface than longer fibres. Longer fibres could also be easily removed during sample washing with water that was necessary for sample preparation. Fig. 4.18A shows light dots of 4.2 ± 1.5 nm in diameter and 0.8 ± 0.2 nm in height in the background of the AFM image and of 6.3 ± 1 nm in diameter and 2 ± 0.2 nm in height on the fibres. The height of the dots situated on the fibres was slightly overestimated due to the additional height of the fibre itself. These dots were attributed to the free polymer, or to small, fibrous subunits that did not incorporate into the fibre. The AFM image of the free polymer showed only the presence of similar light dots in the background (Fig. 4.18C). The AFM measurements on PA3 (Fig. 4.18B) showed slightly thicker fibres of 6.5 ± 2 nm in diameter and 1.3 ± 0.4 nm in height. Fig. 4.18B also shows 7.2 ± 1.5 nm wide and 2 ± 0.5 nm high light dots in the background of the image. It was worth mentioning that the fibre diameter was highly variable along the fibres. PS2 sample showed 4.9 ± 1 nm wide and 1.1 ± 0.4 nm high fibres and PA2 showed 4.9 ± 1 nm 0.9 ± 0.5 nm high fibres. The AFM measurements on PS1 and PA1 samples did not detect the fibres possibly due to low conjugate content that was not sufficient to form fibres for AFM measurements. Also the preformed fibres might be washed during sample preparation.

The AFM image of the free peptide showed only a fibrous network where fibres were 4.6 ± 1.7 nm wide and 0.9 ± 0.4 nm high (Fig. 4.18D). It is well documented that phenylalanine based peptides, i.e. FEFEFKFK and FEFKFEFK, were found to form gels composed of 4 nm wide β-sheet fibres [13]. The results obtained by both microscopic techniques as presented above correlated well with the fibre width obtained by Saiani *et al.* This supports the early assumption about the polymer-peptide conjugates able to self-assemble into β-sheet fibres.

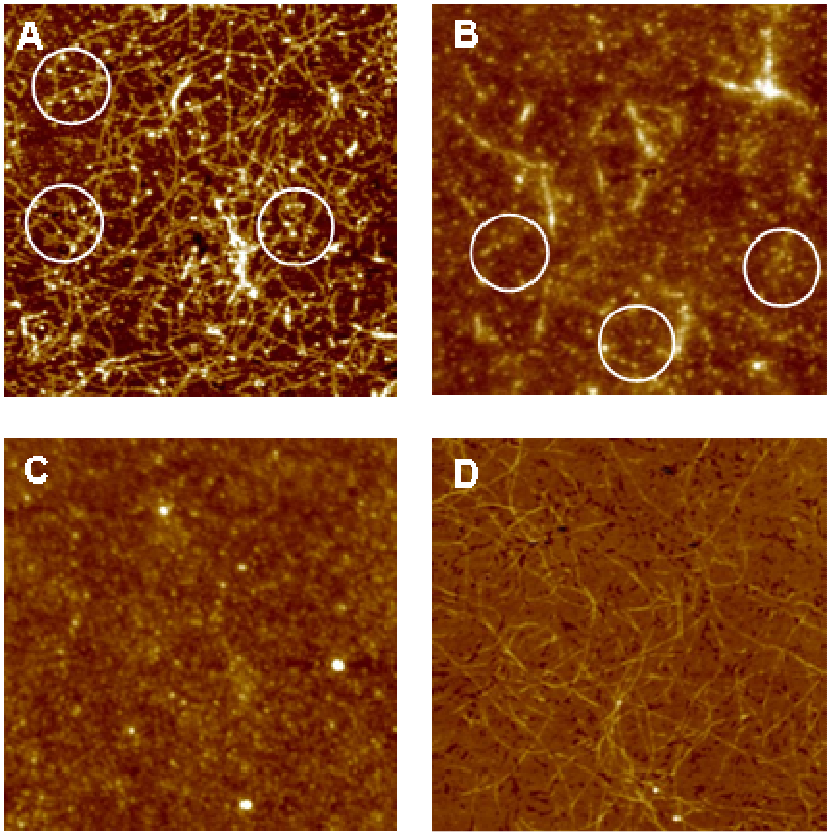

Figure 4.18: *Typical AFM images of: A) PS3 at concentration of 5 mg ml^{-1}, B) PA3 at concentration of 10 mg ml^{-1}, C) PNIPAAm at concentration of 5 mg ml^{-1} and D) FEFEFKFK at concentration of 2 mg ml^{-1}. Each image scan size is 2 μm^2. AFM also proved the formation of fibrillar network similar to that of pure peptide. Some light dots of polymer chains are highlighted in circles.*

4.4. Summary

Thermo-responsive, physical hydrogels of PNIPAAm were obtained by incorporating small quantities of polymer-peptide bioconjugate where the peptide self-assembled into elongated fibres that associated and entangled creating a gel network. Two series of such systems were prepared easily by using a thiol-modified FEFEFKFK and FEFKFEFK peptides as the chain-transfer agents in the free radical polymerisation of NIPAAm. The conjugation products were characterised by ^{1}H NMR. For analytical purposes the polymer was

separated from the conjugate to determine the polymer/conjugate weight ratio in each mixture. The results from both techniques showed that varying the quantity of SH-FEFEFKFK and SH-FEFKFEFK added offered control over the composition of the polymer/conjugate mixtures; the higher the peptide concentration, the higher the fraction of conjugate present in the mixtures. A series of mixture containing PNIPAAm-FEFEFKFK (PS1, PS2, PS3) showed higher conjugate content than the mixtures with PNIPAAm-FEFKFEFK (PA1, PA2, PA3). The combination of ^{1}H NMR and centrifugation allowed the $\overline{M}_n$ of the conjugates in the mixtures to be calculated and in each series the $\overline{M}_n$ values slightly decreased with increasing chain-transfer agent concentration. The $\overline{M}_n$ values from GPC, which were mostly attributed to the unconjugated polymer, were higher than those obtained from ^{1}H NMR and centrifugation for the conjugates. SLS and viscometry measurements showed the aggregation of the polymer/conjugate mixtures presumably due to the peptide presence and did not show substantial difference between the two series

The polymer/conjugate mixtures formed self-supporting hydrogels when above a critical gelation concentration which decreased with increasing conjugate concentration. Polymer/conjugate mixtures PS1, PS2, PS3 showed lower critical gelation concentrations (150, 50 and 35 mg ml^{-1} respectively) than PA1, PA2, PA3 (190, 150 and 75 mg ml^{-1} respectively). This difference in gelation behaviour was not ascribed to the differences in the peptide sequences but to the amount of the conjugate in the mixtures: conjugate content in the PS1-PS3 mixtures was higher than in the PA1-PA3. The elastic moduli of such hydrogels varied from ~ 10 Pa to 400 Pa depending on the sample and were found to be proportional to the quantity of the peptide present, as expected. The scalling exponents increased with decreasing peptide concentration and increasing free polymer concentration. The latter suggested that there were interactions between the free polymer and the peptide, and/or fibre, which were contributing to network formation. TEM and AFM studies proved the formation of the network composed of β-sheet fibres of ~ 4.5 ± 1.5 nm in diameter.

As the polymer/conjugate mixtures were heated, PNIPAAm exhibited an LCST transition ~ 30°C whose temperature was not influenced by the conjugate present, nor by the gelled state of the sample. All transitions were fully thermally reversible. In each series the mixtures with higher polymer-peptide conjugate content showed higher phase separation heats than pure PNIPAAm presumably due to additional intermolecular interactions between fibres and polymer chains. During the phase transition the mechanical properties of the hydrogel were enhanced, presumably due to the hydrophobic polymer chains collapsing and enhancing fibre-fibre interactions. Further heating led to the collapse of the gel network. Both

series showed very similar thermal, mechanical and morphological properties. By exploiting the self-assembly of the ionic-complementary peptides, it was possible to create PNIPAAm-rich, thermo-responsive hydrogels with controllable properties.

Fig. 4.19 gives a schematic representation of the behaviour of free polymer and polymer-peptide conjugate mixtures. In the scheme polymer chains are presented in red and peptide segments in the conjugates as arrows (Fig. 4.19A). In this case polymer concentration is much higher than peptide concentration. In water the peptide segments self-assemble into fibres (Fig. 4.19B, C), free polymer chains float around the fibres and PNIPAAm-rich gel is formed. Above the LCST phase separation occurs and conjugated polymer segments collapse onto the fibres whereas free polymer chains collapse and aggregate around the fibres (Fig. 4.19D). Upon cooling the phase separation is reversible and polymer chains re-swell.

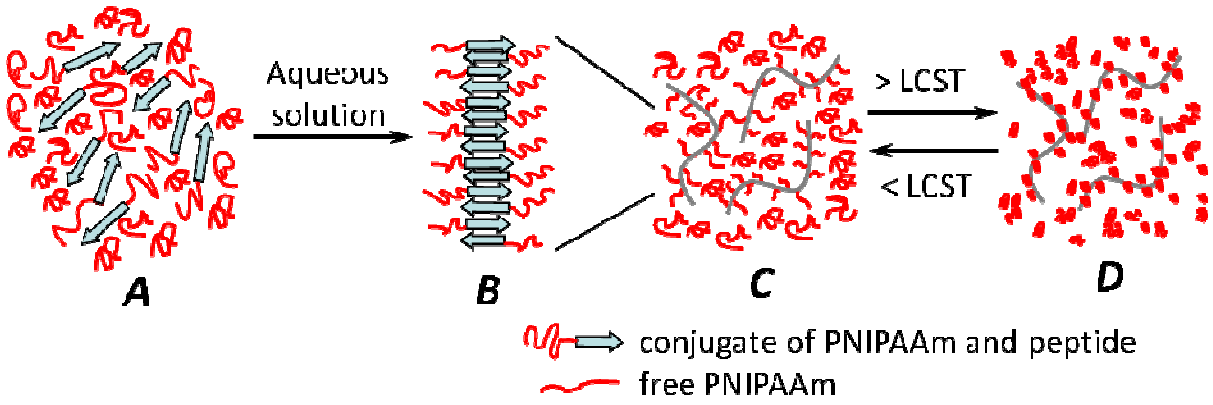

Figure 4.19: *Schematic representation of the polymer/conjugate gel. A) Polymer and polymer-peptide conjugate are dissolved in water. B, C) Self-assembly of the conjugates and fibre formation. Free polymers float around the fibrillar network. D) Phase separation due to the collapse of PNIPAAm above the LCST.*

References

1. F. Stoica, C. Alexander, N. Tirelli, A. F. Miller and A. Saiani, *Chem. Commun.*, 2008, 4433-4435.
2. F. Ganachaud, M. J. Monteiro, R. G. Gilbert, M. A. Dourges, S. H. Thang and E. Rizzardo, *Macromolecules*, 2000, **33**, 6738-6745.
3. C. Schili, M. G. Lanzendörfer and A. H. E. Müller, *Macromolecules*, 2002, **35**, 6819-6827.
4. I. V. Berlinova, I. V. Dimitrov, N. G. Vladimirov, V. Samichkov and Y. Ivanov, *Polymer*, 2001, **42**, 5963-5971.
5. M. Hahn, E. Gornitz and H. Dautzenberg, in *Macromolecules*, Editon edn., 1998, vol. 31, pp. 5616-5623.
6. T. Kawaguchi, Y. Kojima, M. Osa and T. Yoshizaki, *Polymer J.*, 2008, **40**, 528-533.
7. J. M. G. Cowie and V. Arrighi, *Polymers: Chemistry and Physics of Modern Materials*, 3rd edn., Taylor & Francis Group: CRC Press, 2008.
8. V. Wintgens, M. Charles, F. Allouache and C. Amiel, in *Macromol. Chem. Phys.*, Editon edn., 2005, vol. 206, pp. 1853-1861.
9. C. M. F. Oliveira, C. T. Andrade and D. M.C., *Polym. Bull.*, 1991, **26**, 657-664.
10. M. C. Delpech, F. M. B. Coutinho and M. E. S. Habibe, *Polymer Testing*, 2002, **21**, 155-161.
11. G. Pierre-Gilles de, *Scalling Concepts in Polymer Physics*, Ithaca, N.Y. ; London : Cornell University Press, 1979.
12. F. C. MacKintosh, J. Käs and P. A. Janmey, *Phys. Rev. Lett.*, 1995, **75**, 4425.
13. A. Saiani, A. Mohammed, H. Frielinghaus, R. Collins, N. Hodson, C. M. Kielty, M. J. Sherratt and A. F. Miller, *Soft Matter*, 2009, **5**, 193-202.
14. H. M. Wyss, R. J. Larsen. and D. A. Weitz, *G.I.T. Laboratory Journal*, 2007, **3-4**, 68-70.
15. J. W. Goodwin and R. W. Hughes, *Rheology for Chemists: an introduction*, RSC, 2000.
16. L. Haines-Butterick, K. Rajagopal, M. Branco, D. Salick, R. Rughani, M. Pilarz, M. S. Lamm, D. J. Pochan and J. P. Schneider, *P. Natl. Acad. Sci. USA*, 2007, **104**, 7791-7796.
17. N. L. Goeden-Wood, J. D. Keasling and S. J. Muller, *Macromolecules*, 2003, **36**, 2932-2938.
18. A. Aggeli, M. Bell, N. Boden, J. N. Keen, P. F. Knowles, T. C. B. McLeish, M. Pitkeathly and S. E. Radford, *Nature*, 1997, **386**, 259-262.
19. R. Liu, F. Cellesi, N. Tirelli and B. R. Saunders, *Polymer*, 2009, **50**, 1456-1462.
20. Y. Wang, A. Lue and L. Zhang, *Polymer*, 2009, **50**, 5474-5481.
21. M. C. Branco, F. Nettesheim, D. J. Pochan, J. P. Schneider and N. J. Wagner, *Biomacromolecules*, 2009, **10**, 1374-1380.
22. Z. Yang, G. Liang, L. Wang and B. Xu, *J. Am. Chem. Soc.*, 2006, **128**, 3038-3043.
23. B. Ozbas, K. Rajagopal, G. E. Schneider and D. J. Pochan, *Phys. Rev. Lett.*, 2004, **93**, 1-4.
24. R. A. Hule, R. P. Nagarkar, B. Hammouda, G. E. Schneider and D. J. Pochan, *Macromolecules*, 2009, **42**, 7137-7145.
25. V. Jayawarna, S. M. Richardson, A. R. Hirst, N. W. Hodson, A. Saiani, J. E. Gough and R. V. Ulijn, *Acta Biomater.*, 2009, **5**, 934-943.
26. B. Hinner, M. Tempel, E. Sackmann, K. Kroy and E. Frey, *Phys. Rev. Lett.*, 1998, **81**, 2614.
27. J. L. Jones and C. M. Marquès, *J. Phys.*, 1990, **51**, 1113-1127.
28. M. Dahmani, N. Fazel, J.-P. Munch and J.-M. Guenet, *Macromolecules*, 1997, **30**, 1463-1468.
29. J.-M. Guenet, *J. Rheol.*, 2000, **44**, 947-960.
30. M. Ramzi, C. Rochas and J.-M. Guenet, *Macromolecules*, 1998, **31**, 6106-6111.
31. G. B. McKenna and J.-M. Guenet, *J. Polym. Sci., Polym. Phys. Ed.*, 1988, **26**, 267-276.
32. K. Kamide, M. Saito, A. H. Clark and S. B. Ross-Murphy, *Biopolymers*, Springer-Verlag, 1987.
33. X. Wang, X. Qiu and C. Wu, *Macromolecules*, 1998, **31**, 2972-2976.

34. K. Kubota, S. Fujishige and I. Ando, *J. Phys. Chem.*, 1990, **94**, 5154-5158.
35. T. Aubry, B. F., G. Staikos and G. Bokias, *J. Rheol.*, 2003, **47**, 577-587.
36. F. Monti, S.-Y. Fu, I. Iliopoulos and M. Cloiter, *Langmuir*, 2008, **24**, 11474-11482.
37. F. Huang, R. Rotstein, S. Fraden, K. E. Kasza and N. T. Flynn, *Soft Matter*, 2009, **5**, 2766-2771.

Chapter 5

Results and Discussion

Thermo-Responsive Peptide-Rich Hydrogels from Physical Mixtures of Peptide and Polymer/Conjugate Mixture

5.1. Introduction

One strategy to obtain thermo-responsive gels is to create a chemically cross-linked network where the main polymer or co-monomer exhibits thermo-responsive behaviour. Another strategy consists of introducing thermo-responsive micelles, nanoparticles into non-responsive gel matrix or into already thermo-responsive gel to accentuate its thermo-responsiveness and to improve gel network swelling/shrinking and gel mechanical properties. Nguyen *et al.* [1] developed thermo-responsive composite gel by incorporating PNIPAAm nanoparticles into PEG matrix and the results showed that these gels were able to release bovine serum albumin (BSA) above the LCST. Later the same group prepared thermo-responsive hydrogel, in which poly(*N*-isopropylacrylamide-*co*-acrylamide) (PNIPAAm-AAm) nanoparticles, preloaded with drug, were incorporated into a photocrosslinkable poly(ethylene glycol) diacrylate (PEGDA) matrix [2]. Above the LCST the drug release occured due to the collapse of PNIPAAm. In one other study poly(*N*-isopropylacrylamide)/poly(ethylene glycol) diacrylate (PNIPAAm/PEG-DA) microgels were incorporated into PNIPAAm hydrogels. This additive improved gel swelling/shrinking ratios and thermal behaviour [3]. Zhang *et al.* [4] reported composite gels, containing poly(*N*-isopropylacrylamide)-*b*-poly(methyl methacrylate) (PNIPAAm-*b*-PMMA) micelles embedded in PNIPAAm hydrogel. Gels showed faster shrinking and slower swelling rates with increasing micelles content. When drug loaded micelles were used, drug release occurred in more controlled fashion in comparison to pure PNIPAAm gel.

Chapter 4 presented an easy way to prepare PNIPAAm polymers with various degrees of functionalisation with the self-assembling peptides FEFEFKFK and FEFKFEFK. These polymer/conjugate mixtures showed interesting phase behaviour and gelation properties, however the critical gelation concentrations were considerably high, which is not financially viable for any drug delivery or tissue engineering applications. **The aim** of Chapter 5 is to design peptide-rich thermo-responsive composite gels by incorporating the polymer/conjugate mixtures PS3 and PA3 described in Chapter 4 into a peptide gel: either FEFEFKFK or FEFKFEFK at different ratios. In these gels peptide concentration is greater than polymer (free and conjugated) concentration. It has been anticipated that the peptide segment will self-assemble into fibres, while the polymer, both conjugated and free, will confer the thermo-responsive behaviour to the gel. The effect of PS3 and PA3 on gelling, mechanical and thermal properties of the materials will be investigated.

5.2. Thermal behaviour of the peptide-rich gels

A range of physical mixtures were prepared by varying the quantities of peptide and polymer/conjugate mixtures in each sample (Table 5.1). Further in the text the sample names are reduced to the following abbreviations: 20-10, 15-10, 10-10, 10-15 and 10-20 where the 1st number represents peptide concentration in mg ml^{-1} and the 2nd one represents polymer/conjugate mixture concentration in mg ml^{-1}. The phase behaviour of these physical mixtures at 20, 40 and 80ºC was monitored visually using the standard tilt test tube method. Fig. 5.1A shows the mixtures of FEFEFKFK and PS3 at different weight ratios. Self-supporting transparent gels were formed for all samples at 20ºC suggesting the peptide component had self-assembled, as expected, into β-sheet rich fibrils that self-associated when above a critical gelation concentration, *C**. *C** for the pure FEFEFKFK and FEFKFEFK was typically ~17 and ~10 mg ml^{-1}.

Table 5.1: *Peptide weight fractions ($W_{pept.}$) in the conjugates PS3 and PA3 used for the preparation of the peptide-rich gels and conjugate weight fractions ($W_{conj.}$) in the peptide-rich gels studied*

Sample	FEFEFKFK/PS3		FEFKFEFK/PA3	
	$W_{pept.}$ in conjugate	$W_{conj.}$ in mixture	$W_{pept.}$ in conjugate	$W_{conj.}$ in mixture
20-10	0.115	0.074	0.055	0.057
15-10	0.115	0.089	0.055	0.069
10-10	0.115	0.111	0.055	0.086
10-15	0.115	0.133	0.055	0.104
10-20	0.115	0.148	0.055	0.115

As the samples were heated to 40°C, the gels became opaque presumably due to the PNIPAAm polymer chains collapsing as they went through their LCST. The samples remained self-supporting and the transition was thermally reversible if the samples were subsequently cooled at this stage, indicating the conjugate remained trapped within the hydrogel structure. As the samples were heated to 80°C, the gel samples with high polymer/conjugate mixture content appeared to shrink while expelling water (Fig. 5.1A samples Nr. 4 and 5). Such behaviour was typical of PNIPAAm solutions and have previously been related to the aggregation of the collapsed PNIPAAm chains [5, 6]. The samples did not shrink as dramatically as in Fig. 4.13 (Chapter 4) presumably due to the fibrillar network that appeared to hold the systems from shrinkage. The samples Nr. 1, 2 and 3 showed stable opaque gels with slight water expulsion probably due to high amount of pure peptide matrix in comparison to the polymer/conjugate mixtures. Upon cooling the water was reabsorbed and the polymer re-swelled to form clear hydrogels when cooled below 40°C. Such

temperature-responsive behaviour was reversible at least a further four thermal cycles. The gels of FEFKFEFK and PA3 showed similar thermal macroscopic behaviour (Fig. 5.1B): polymer underwent the LCST upon heating, showing slight gel shrinkage at 80°C with water expulsion (Fig. 5.1B samples Nr. 4 and 5) and reswelled upon cooling forming clear gels.

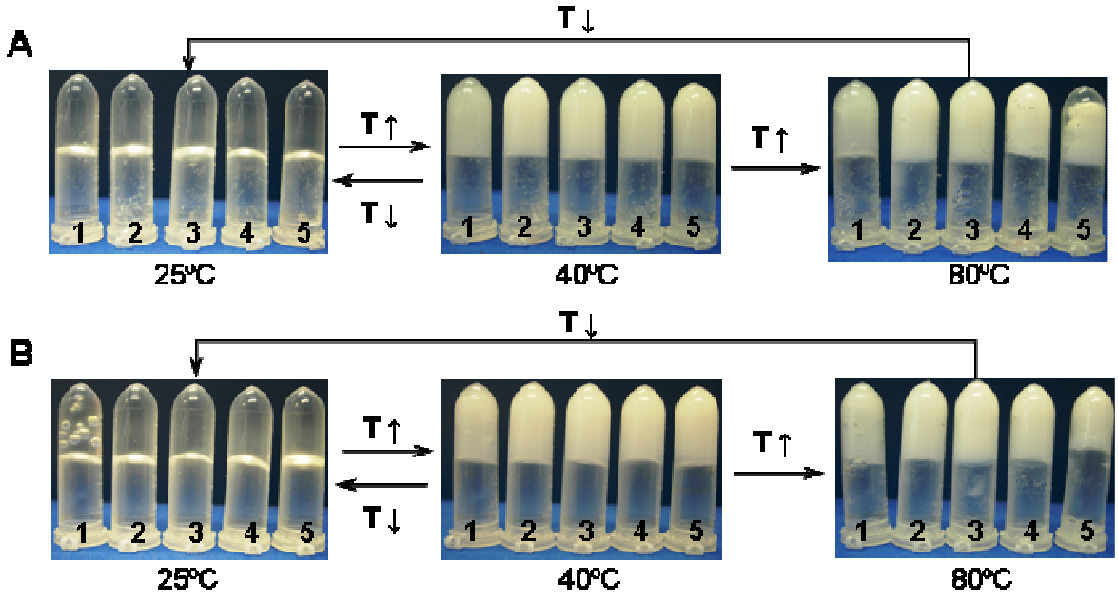

Figure 5.1: *Photographs of: A) FEFEFKFK/PS3 gels and B) FEFKFEFK/PA3 gels at the following peptide/(polymer/conjugate mixture) weight ratios: 1) 20-10, 2) 15-10, 3) 10-10, 4) 10-15, 5) 10-20 at 25°C , 40°C and 80°C. At 25°C self-supporting gels were formed. At 40°C gels became opaque due to the LCST transition of PNIPAAm. At 80°C gels remained opaque and stable; however slight water release was noticed in the samples with high polymer/conjugate mixture content (Nr. 4 and 5).*

The thermal behaviour of the gels of FEFEFKFK/PS3 and FEFKFEFK/PA3 at different ratios was monitored using micro DSC in the temperature range of 20-80ºC and the results for the initial heating scans for each sample are given in Fig. 5.2. Pure peptides FEFEFKFK and FEFKFEFK at 20 mg ml^{-1} are given for comparison.

Fig. 5.2A and 5.2C show that two endothermic transitions were observed for each mixture sample: a sharp transition at ~31°C and a second broader transition at ~ 63 - 68°C. The first transition corresponded to the LCST of the PNIPAAm and agreed well with the visual observations. The LCST values did not seem to vary with sample composition and the enthalpy of the phase separation increased with increasing polymer content (moving from the samples 20-10 to 10-20). The micro DSC plots for pure peptides showed no transition in the region of 30 - 40°C. Second transitions are more visible in the magnified images presented in Fig. 5.2B and 5.2D for FEFEFKFK/PS3 and FEFKFEFK/PA3 systems respectively. These endothermic peaks were much broader in nature and presumably corresponded to the macroscopic melting of the hydrogel mixture. The micro DSC measurements of pure

FEFEFKFK and FEFKFEFK gels at 20 mg ml^{-1} detected a very broad endothermic transition with the peak temperatures ~ 85-90°C (Fig. 5.2 B, D), therefore these peaks were not distinctive in Fig. 5.2B and D. Such a broad transition is typical of the melting of synthetic and biopolymer hydrogels with fibre-like morphology [7]. β-sheet rich fibres of FEFEFKFK and FEFKFEFK also entangled to form densely-packed networks at concentrations ≥ *C** and their gels showed slight metling upon heating.

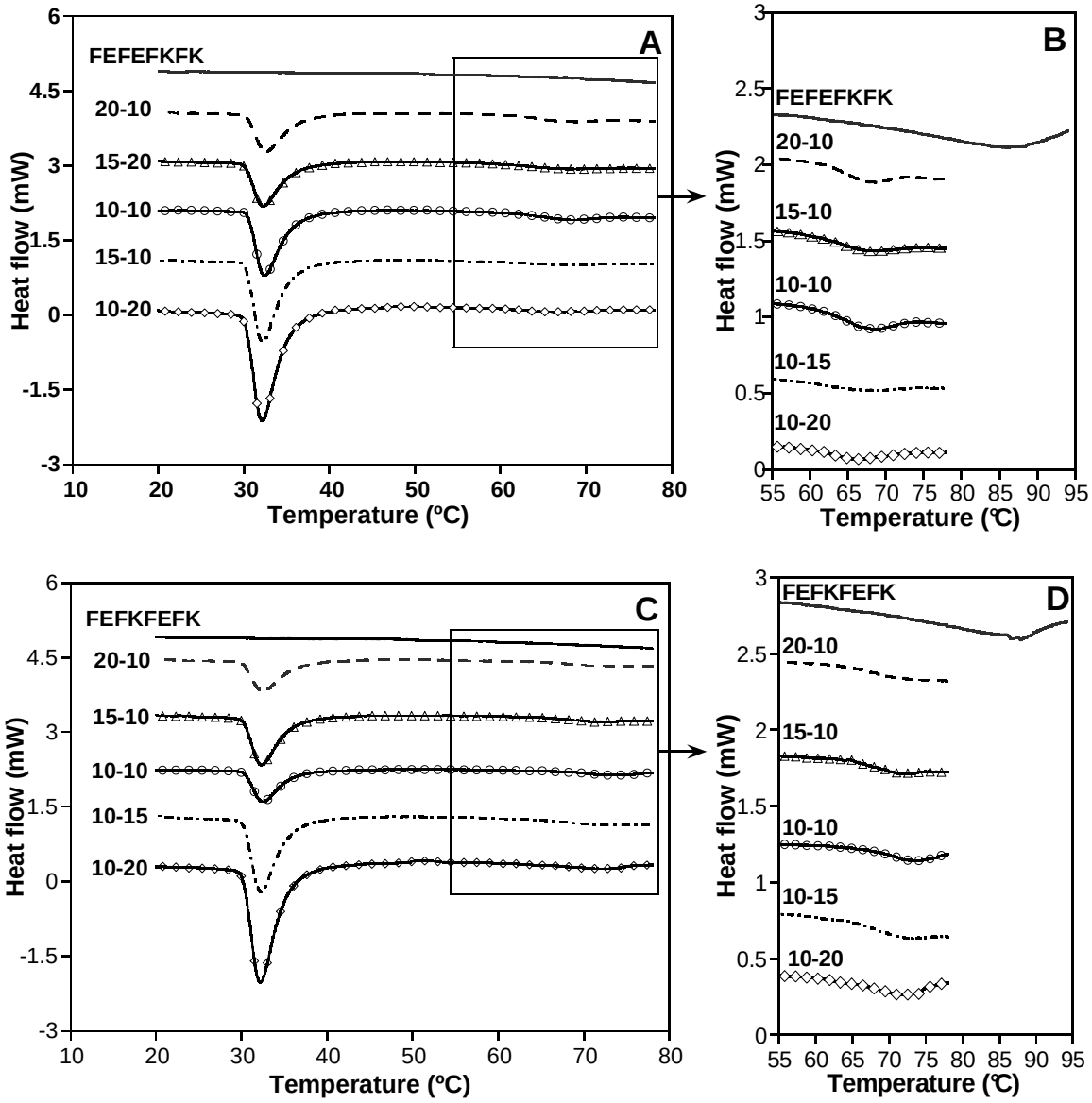

Figure 5.2: *Micro DSC thermographs of the gels of: A, B) FEFEFKFK/ PS3 and C, D) FEFKFEFK/PA3 at different weight ratios. B) and D) images correspond to the magnifications of the heating region from 55 to 80°C to show the 2nd endothermic transitions. Micro DSC plots for the peptides FEFEFKFK and FEFKFEFK at 20 mg ml^{-1} each are given for comparison.*

Fig. 5.3 A and B present the LCST values as a function of polymer and peptide weight fraction in the gels respectively and Fig. 5.3 C and D present ΔH changes with polymer and peptide weight fraction respectively. The enthalpy associated with the LCST transition (1st peak) increased with increasing polymer weight fraction in the gels, as expected, while the

temperature of transition remained constant (Figure 5.3A and C). However, the increase of enthalpy with polymer concentration was not purely linear. First three samples in each series (20/10, 15/10, 10/10) contained the same amount of polymer/conjugate mixture and only peptide concentration varied. Results showed that ΔH for these 3 samples in both series increased with decreasing peptide concentration. This might be due to the fact that gel fibrillar network partially suppressed the aggregation of the collapsed polymer chains. This correlated well with the macroscopic behaviour upon heating (Fig. 5.1A and B) and showed the effect of the gel strength on the aggregation of the collapsed polymers: the stronger the gel, the weaker the aggregation of collapsed polymer chains.

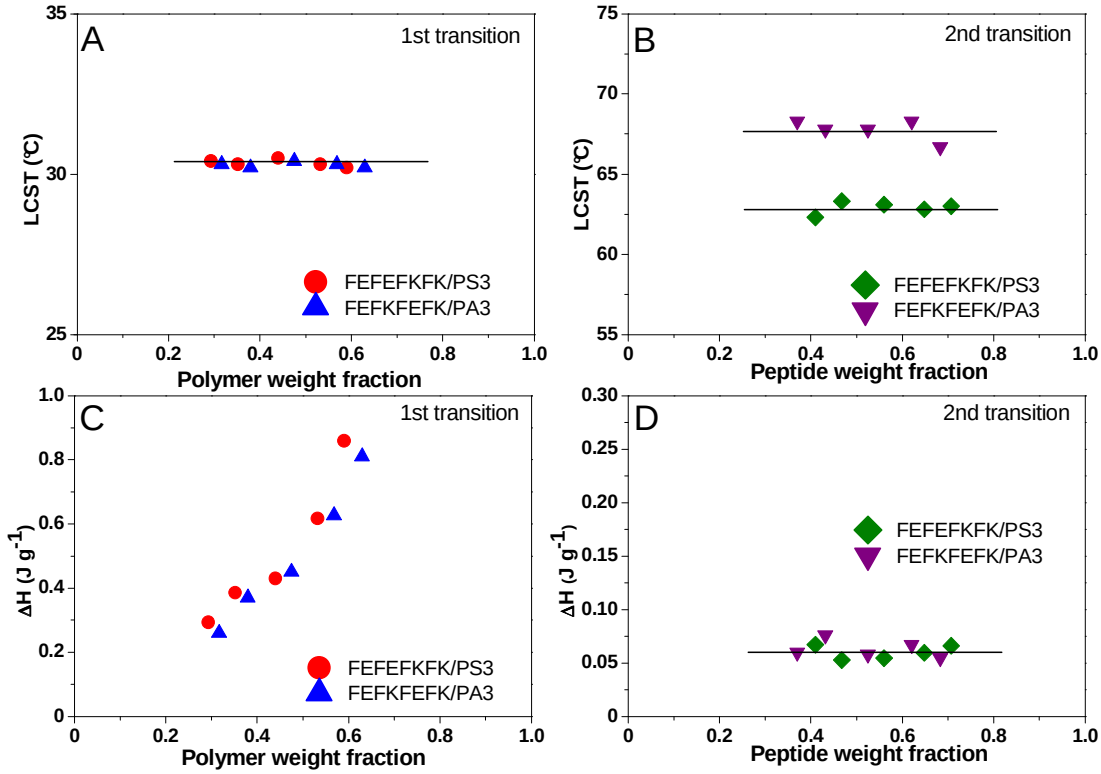

Figure 5.3: *Plots of the LCST (A, C) and enthalpy (B, D) values as a function of the weight fraction of polymer and weight fraction of peptide in the gels of FEFEFKFK/PS3 and FEFKFEFK/PA3*

The LCST values for the 2nd transition were slightly higher for the mixtures FEFKFEFK/PA3 than for FEFEFKFK/PS3, i.e. 68 and 63°C respectively (Fig. 5.3C). The enthalpies associated with the transitions practically did not vary with peptide weight fraction. ΔH were slightly higher for the mixtures FEFKFEFK/PA3 than for FEFEFKFK/PS3, i.e. 0.08 and 0.06 J g^{-1} (Fig. 5.3D). It may be assumed that the LCSTs of the 2nd transition, corresponding to the peptide gel melting, shifted to lower temperatures in comparison to pure peptide matrix possibly due additional interaction between the peptide matrix and polymer chains (free and conjugated) and possibly due to enhanced fibril-fibril and/or peptide-peptide interactions.

5.3. Rheological studies

Fig. 5.4 shows typical strain amplitude and angular frequency sweeps for 5 FEFEFKFK/PS3 and 5 FEFKFEFK/PA3 gels at 20ºC. Strain amplitude sweeps in Fig. 5.4A and 5.4B show that for each sample the elastic modulus (G') was greater that the viscous modulus (G'') indicative of an elastic rather than viscous material. The lowest moduli in the series were determined for the gels with equal amounts of peptide and polymer/conjugate mixture, 10-10. Visco-elastic properties of the gels increased with increasing free peptide content (20-10 and 15-10) and polymer/conjugate mixture content (10-15 and 10-20). The linear visco-elastic region of the gels was at strain values < 0.3 and the break down in the gel was observed at higher strain values. Fig. 5.4C and 5.4D show that for both gel series G' was essentially independent of frequency over the range 6.28 – 62.8 rad s^{-1}, which indicated that the hydrogels were relatively stable within this range. G'', however, showed some decrease at $\omega > 20$ rad s^{-1}. Such rheological behaviour matched the characteristic signature of a solid-like gel. The results showed that as the quantity of either peptide or conjugate from the polymer/conjugate mixtures increased, so did G'. Interestingly all G' values were higher than those obtained for an equivalent concentration of pure FEFEFKFK and FEFKFEFK peptides (G' was ~10 Pa for a sample of 20 mg ml^{-1}). This supported the earlier postulation that the peptide segment from the conjugate actively participated in fibre, and consequently, gel formation, resulting in stiffer fibres than in pure peptide gels. Fig. 5.4E shows the variation of yield strain (γ^*) with peptide concentration for the samples 10-10, 10-15 and 10-20. For both series a general trend was observed that γ^* increased slightly with overall peptide concentration presumably due to higher number of fibres formed which contributed to the increase of network elasticity.

The G' plateau values of the gels with high peptide content (20-10, 15-10 and 10-10) were plotted as a function of peptide concentration to determine the power law behaviour (Fig. 5.5). Pure peptides FEFEFKFK and FEFKFEFK are given for comparison. Since the polymer/conjugate mixtures were incorporated into the peptide matrix, the pH of the gels was ~ 2.3-2.5. Therefore the pH of the pure peptide gels was not either adjusted. Gels of FEFEFKFK/PS3 showed the scaling factor of 2.7 which was close to than the scaling factor of the corresponding peptide. Since the fibrillar matrix was formed mainly by the free peptide, the scaling factors were similar indicating the similar morphologies of pure peptide gel and peptide-rich gels with incorporated polymer/conjugate mixture. FEFKFEFK/PA3 and FEFKFEFK showed the exponent of 1.7 which was approximately half of that of pure FEFKFEFK.

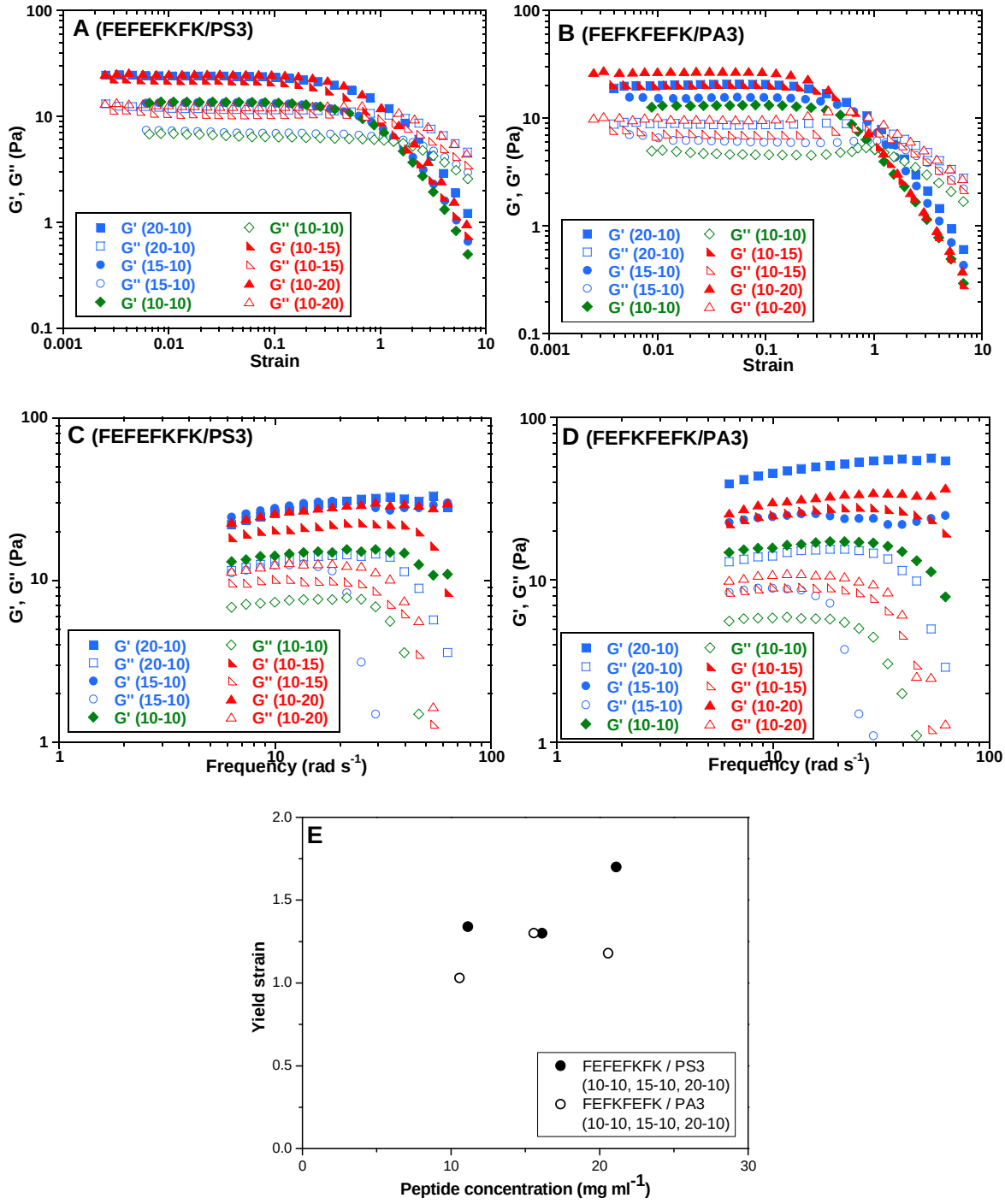

Figure 5.4: *Strain amplitude sweeps of the gels of: A) FEFEFKFK/PS3 and B) FEFKFEFK/PA3 at different peptide/(polymer/conjugate mixture) weight ratios at 20°C. Frequency sweeps of the gels of: C) FEFEFKFK/PS3 and D) FEFKFEFK/PA3 at different peptide/(polymer/conjugate mixture) weight ratios at 20°C. E) Variation of yield strain with peptide concentration.*

Figure 5.6A shows the variation of *G′* and *G″* moduli of FEFEFKFK/PS3 gel 20-10 as a function of temperature where a slight decrease in moduli values was observed from 20 to 30ºC, followed by a sharp increase to a much higher *G′* value of 300 Pa followed by a further decrease at ~ 60ºC. The thermal behaviour correlated well with both the transitions observed in micro DSC and those observed visually.

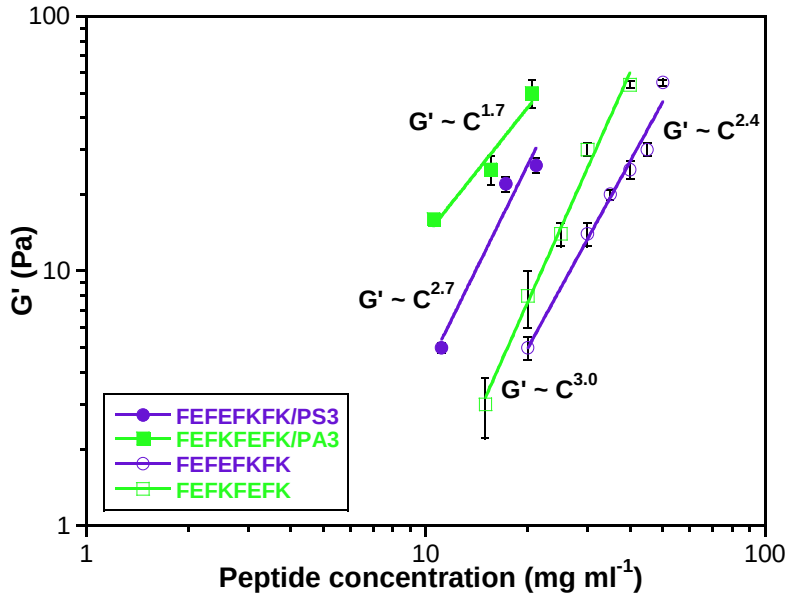

Figure 5.5: *Plateau values of G′ as a function of peptide concentration of the gels FEFEFKFK/PS3 and FEFKFEFK/PA3 at peptide/(polymer/conjugate mixture) ratios of 20-10, 15-10 and 10-10; and of pure FEFEFKFK and FEFKFEFK gels at pH 2.3-2.5*

The first transition led to an initial decrease in *G′* and *G″* presumably due to the collapse and shrinkage of the PNIPAAm polymer chains. The subsequent increase in moduli values could be due to a thickening in fibril diameter and possible enhancement of fibril-fibril interactions due to aggregation of the PNIPAAm chains, while the final decrease was due to further aggregation and sedimentation of collapsed polymer chains accompanied by slight macroscopic melting of gel. It has been reported that PNIPAAm-containing systems showed an increase in *G′* and *G″* moduli values upon heating due to the collapse and aggregation of PNIPAAm chains [8-11]. Upon cooling the transitions were thermally reversible, however *G′* and *G″* did not reach the initial values of ~ 30 and ~ 10 Pa accordingly but increased instead up to ~ 300 and ~ 100 Pa accordingly. Second heating/cooling cycle (Fig. 5.6B) showed that the systems underwent the same thermal transitions but less dramatic than during the 1st heating/cooling cycle: slight decrease of *G′* from 20 to 30ºC, an increase of *G′* from 30 to 45ºC, and a slight decrease ~60°C. During the 2nd heating/cooling cycles *G′* increased from ~ 270 to ~ 360 Pa, however *G″* remained roughly constant ~ 85 Pa.

The composite gel FEFKFEFK/PA3 20-10 showed slightly different mechanical spectra during heating and cooling (Fig. 5.6C, D). *G′* and *G″* were practically constant from 20 to 30°C and started to increase sharply at ~ 31°C presumably due to the collapse of PNIPAAm chains. Both moduli continued to increase during further heating to 72°C when they reached the maxima of 1,300 and 170 Pa for *G′* and *G″* respectively. Further heating from 72 to 80°C resulted in a sharp decrease in *G′* and *G″* values to 160 and 30 Pa respectively presumably due to the continuous process of aggregation of collapsed chains. At the end of

cooling cycle the moduli reached slightly lower values than in the beginning: G' = 110 Pa and G'' = 40 Pa. Again the values reached after cooling were higher than those before heating: G' =20 Pa and G'' = 10 Pa. Second heating from 31 to 68°C showed an increase in G' and then decrease at ~ 70°C to 50Pa. G'' mirrored the behaviour of G'. The increase of mechanical properties of the gels was less dramatic than during the first heating. Upon second cooling the moduli practically reached the initial values before the 2nd heating.

Interestingly, the elasticity of the hydrogels was significantly greater after each subsequent heating cycle. The values of G' before and after 4 heating/cooling cycles (samples taken after micro DSC measurements) are compared in Table 5.2 for both gel series. Before heating, G' increased with increasing pure peptide and polymer/conjugate mixture content in both series. The differences in moduli values between the series were not substantial indicating similar behaviour of both conjugated peptide sequences. After heating, the gels became rigid and G' reached ~150-200 Pa in comparison to initial G' ~ 25 Pa.

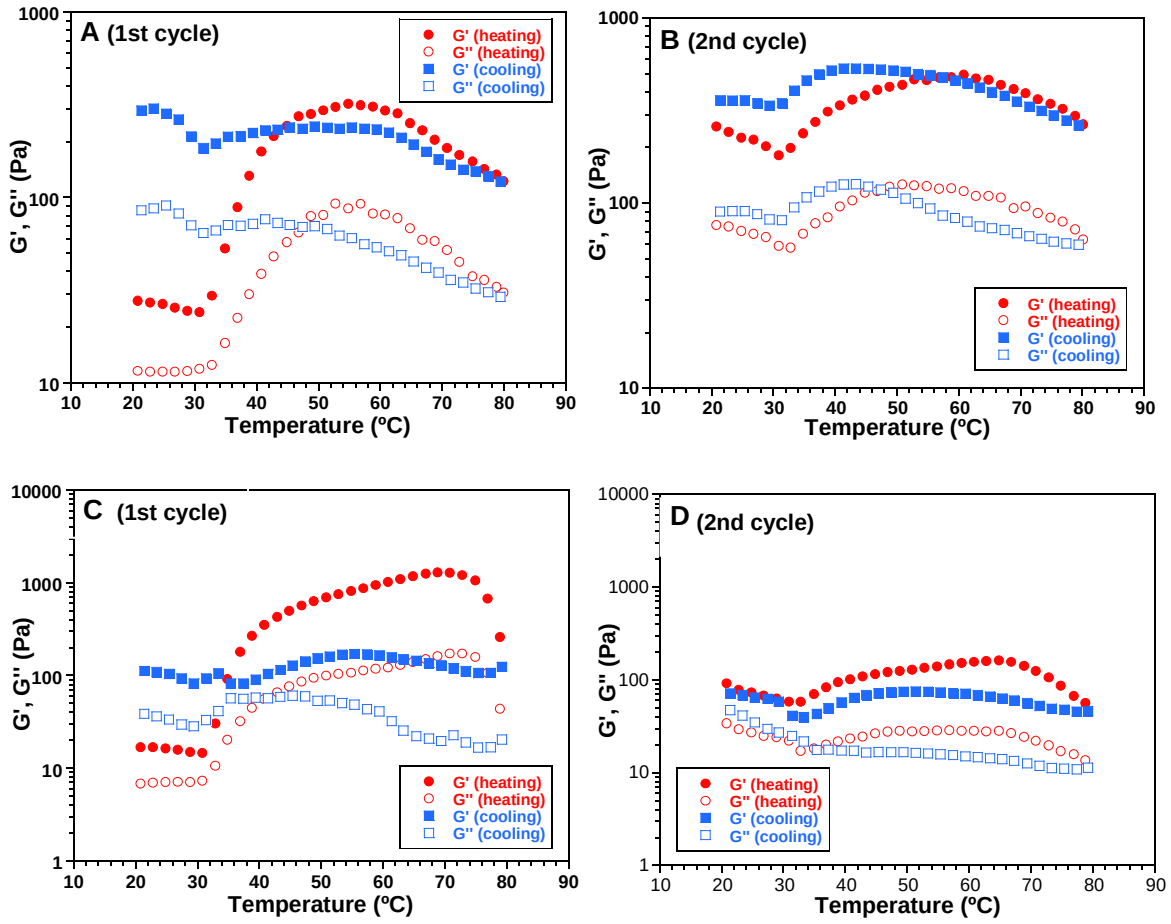

Figure 5.6: *Variation of G' and G'' of the gels: A, B) FEFEFKFK/PS3 (20/10) and C, D) FEFKFEFK/PA3 (20/10) during 1st heating/cooling cycle (A, C) and 2nd heating/cooling cycle (B, D) in the temperature range from 20 to 80°C*

The behaviour of the physical mixtures upon heating was similar to that observed earlier for the conjugation products PS3 and PA3 (see section 4.3.2): *G′* and *G″* increased upon heating. However, the decrease in mechanical strength was observed for PS3 and PA3 upon cooling, whereas the composite gels of FEFEFKFK/PS3 and FEFKFEFK/PA3 showed increase in moduli values upon cooling. This difference in behaviour might be attributed to considerably higher content of the polymer (free and conjugated) in PS3 and PA3 than in the peptide-rich gels and to considerably higher content of peptide in the peptide-rich gels than in PS3 and PA3.

During heating polymer chains collapse and aggregate and may form clusters of aggregated hydrophobic chains, which may cause some fibre rearrangements. Upon cooling the polymers start to re-swell which does not necessarily lead to the return of fibres and/or polymers in the initial position. The gel strengthening upon heating may also occur due to the formation of additional junctions between the peptide fibres. The mechanism behind such gel strengthening, as well as the rheology behaviour as a function of temperature, should be a subject to further investigation. Small angle neutron scattering in conjunction with rheology may help to understand such a phenomenon.

Table 5.2: *G′ values of the gels FEFEFKFK/PS3 and FEFKFEFK/PA3 before heating and after 4 consecutive heating/cooling cycles*

Gel sample	Peptide/(polymer-conjugate mixture) weight ratio	Peptide/conjugate/ polymer mol.% ratio	***G′*** **(Pa) (before heating)**	***G′*** **(Pa) (after heating)***
FEFEFKFK and PS3	20/10	89/5 /6	26	215
	15/10	86/6/7	22	200
	10/10	81/9/10	5	220
	10/15	74/12/14	15	210
	10/20	68/15/17	28	200
FEFKFEFK and PA3	20/10	93/3/5	50	200
	15/10	90/3/6	25	180
	10/10	86/5/9	16	160
	10/15	81/7/12	25	160
	10/20	76/8/16	30	130

* samples taken after 4 consecutive heating/cooling micro DSC cycles

Fig. 5.7 shows the state of the gel (FEFEFKFK/PS3 = 20/10) taken out of the vial after 4 consecutive heating and cooling cycles in the temperature range from 20 to 80°C. Fig. 5.7A shows the gel below the LCST of PNIPAAm and Fig. 5.7B shows the thermo-responsive nature of the same gel above the LCST. The gel held the shape upon heating and became opaque due to the collapse of the polymer. As shown in Fig. 5.7 the gels were stable,

visco-elastic and thermo-responsive. These properties are characteristic to the systems that could potentially be employed in controlled drug delivery and three-dimensional tissue engineering.

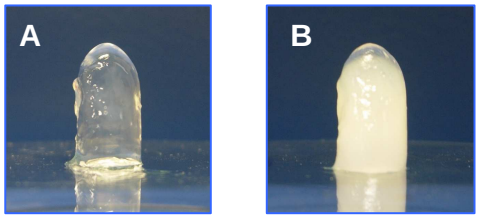

Figure 5.7: *Photographs of the stable gel of the physical mixture FEFEFKFK/PS3 after 4 consecutive heating/cooling cycles: A) below and B) above the LCST of PNIPAAm*

5.4. Summary

This chapter presented the research results on the peptide-rich hydrogels composed of pure peptides FEFEFKFK and FEFKFEFK and corresponding mixtures of polymer-peptide conjugates and polymer, PS3 and PA3. Two series of the gels by varying peptide and polymer/conjugate mixture concentration were studied. The gels showed thermo-responsive behaviour as expected and the LCST values were ~ 30°C for all the samples in both series. Micro DSC studies also detected the second endothermic transition upon heating ~63 - 68°C which was not observed previously. The second transition might be attributed to the macroscopic gel melting. Both thermal transitions were reversible upon cooling. Mechanical studies showed that gel strength increased with increasing polymer/conjugate mixture content, however G' values were < 50 Pa for the samples in both series. These peptide-rich gels again exhibited interesting mechanical behaviour upon heating, i.e. both elastic and viscous moduli values increased during heating from 20 to 80°C and did not reach the initial values upon cooling. G' values increased by approximately an order of magnitude after 4 consecutive heating/cooling cycles. These gels are complex systems with three components, i.e. peptide, polymer and polymer-peptide conjugate. During heating these components might form intermolecular aggregates which might not disaggregate upon cooling resulting in gel strengthening. Polymer re-swelling upon cooling was reported to be a thermodynamically slow process that might also contribute to enhancing gel visco-elastic properties during the study. Varying the peptide sequence in the peptide matrix and in the polymer/conjugate mixtures did not show a pronounced effect on the thermal behaviour and mechanical properties of the composite gels.

To understand the effect of pure polymer-peptide conjugate on the structural and mechanical properties of the peptide-rich gels, further studies are required. Hence, the

composite gels, where pure polymer-peptide conjugate was embedded into a peptide matrix, were designed, studied and the results are described in the following Chapter 6.

Fig. 5.8 gives a schematic representation of the behaviour of the pure peptide, free polymer and polymer-peptide mixtures. In the scheme free polymer chains are presented in red and all peptide segments as arrows (both free and components of the conjugates) (Fig. 5.8A). In this case peptide concentration is higher than polymer concentration. In water peptide segments self-assemble into fibres, free polymers float around the fibres and peptide-rich gels are formed (Fig. 5.8B, C). Above the LCST phase separation occurs and conjugated polymer segments collapse onto the fibres whereas free polymer chains collapse and aggregate around the fibres (Fig. 5.8D). Upon cooling the LCST transition is reversible and polymer chains re-swell.

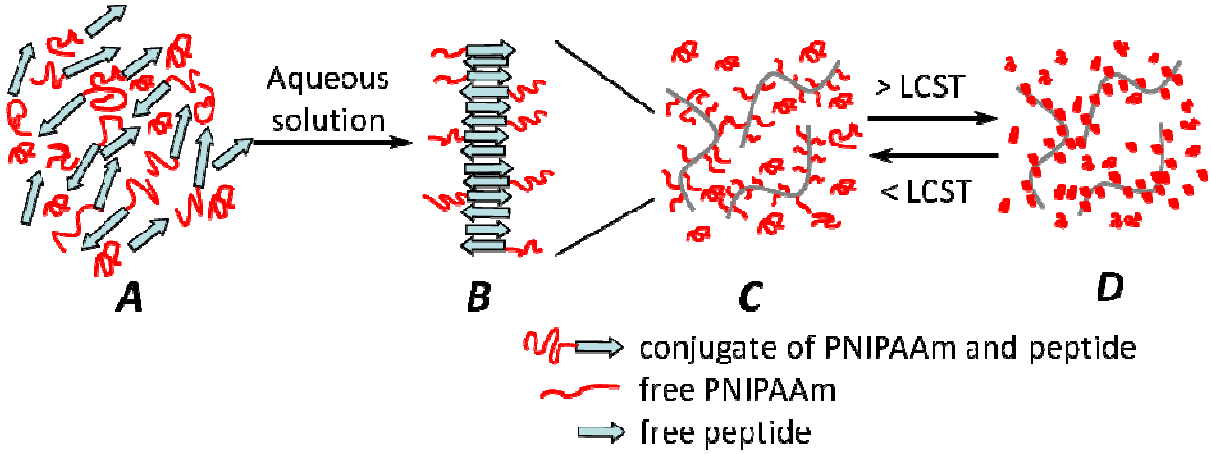

Figure 5.8: *Schematic representation of peptide-rich gel obtained by incorporating polymer/conjugate mixture into peptide matrix. A) Peptide and polymer/conjugate mixture are dissolved in water. B, C) Self-assembly and peptide fibre formation. Free polymers float around the fibrillar network. D) Phase separation due to the collapse of PNIPAAm above the LCST.*

References

1. R. M. K. Ramanan, P. Chellamuthu, L. Tang and K. T. Nguyen, *Biotechnol. Prog.*, 2006, **22**, 118-125.
2. A. Sabnis, A. S. Wadajkar, P. Aswath and K. T. Nguyen, *Nanomed. Nanotechnol. Biol. Med.* , 2009, **5**, 305-315.
3. X.-Z. Zhang and C.-C. Chu, *Polymer*, 2005, **46**, 9664-9673.
4. X.-D. Xu, H. Wei, X.-Z. Zhang, S.-X. Cheng and R.-X. Zhuo, *J. Biomed. Mater. Res. Part A* 2006, **81A**, 418-426.
5. H. G. Schild, *Progress in Polymer Science*, 1992, **17**, 163-249.
6. C. Wu and X. Wang, *Phys. Rev. Lett.*, 1998, **80**, 4092-4094.
7. J.-M. Guenet, *Themoreversible Gelation of Polymers and Biopolymers*, Academic Press, London, 1992.
8. T. Aubry, B. F., G. Staikos and G. Bokias, *J. Rheol.*, 2003, **47**, 577-587.
9. F. Monti, S.-Y. Fu, I. Iliopoulos and M. Cloiter, *Langmuir*, 2008, **24**, 11474-11482.
10. R. Liu, F. Cellesi, N. Tirelli and B. R. Saunders, *Polymer*, 2009, **50**, 1456-1462.
11. F. Huang, R. Rotstein, S. Fraden, K. E. Kasza and N. T. Flynn, *Soft Matter*, 2009, **5**, 2766-2771.

Chapter 6

Results and Discussion

Thermo-Responsive Peptide-Based Composite Gels

6.1. Introduction

The aim of this chapter is to study the effect of pure polymer-peptide conjugate on the structural and mechanical properties of the peptide-rich gels. The concept used here was to incorporate small quantities of purified polymer-peptide conjugate are added to pure peptide. In this case the peptide content is higher than conjugated polymer content. The peptide matrix undergoes slight melting upon heating but does not possess a transition similar to that of the LCST of PNIPAAm. The study focused only on FEFEFKFK and its conjugate with PNIPAAm. It has been hypothesised that the peptide part of the polymer-peptide conjugate will self-assemble with the peptide from the matrix which will allow the polymer segments to be distributed along the fibres. Polymer segments will exhibit LCST behaviour and confer their thermo-responsive behaviour to the composite gel. The study aims to reveal the thermo-responsive behaviour of the composite gels by micro DSC, to understand how the conjugate behaves in the gel network of β-sheets fibres upon heating and cooling using small angle neutron scattering (SANS) and to study fibre morphology by TEM and AFM. Also it is important to study the effect of conjugate incorporation on the mechanical properties of the composite gel.

6.2. Gels macroscopic phase separation

FEFEFKFK peptide and its corresponding conjugate with PNIPAAm were chosen for the study. It has been already discussed that this octapeptide FEFEFKFK self-assembles in aqueous solution into β-sheet fibres and forms a gel at considerably low concentration ($C^* \sim 17$ mg ml^{-1}) [1]. The polymer-peptide conjugate was synthesised using the same polymerisation method as for PS3, described in section 3.3.4. The product was dialysed similarly to PS3 and the separation of the unconjugated from conjugated polymers was performed by centrifugation. The sample purity was estimated was estimated by ^{1}H NMR to be ~ 90% .

The ^{1}H NMR spectrum of the purified conjugate is given in Fig. 6.1B where typical polymer (Fig. 6.1A) and peptide (Fig. 6.1C) signals can be distinguished.

GPC analysis of the conjugate showed $\overline{M}_w$ and $\overline{M}_n$ of 8,800 and 2,500 g mol^{-1} respectively. Two series of composite gels were prepared by mixing the peptide at 2 concentrations: below (10 mg ml^{-1}) and slightly above (20 mg ml^{-1}) the C^* of the peptide, with 3 polymer-peptide conjugate concentrations: 3, 5 and 10 mg ml^{-1} (Table 6.1). Further in the text the names of the composite gels are reduced to the following abbreviations: 10-3, 10-5, 10-10, 20-3, 20-5, and 20-10, where the first number stands for the peptide

concentration in mg ml^{-1} and the second number represents the conjugate concentration in mg ml^{-1}. These composite gels contain only pure peptide and polymer-peptide conjugate rather than the polymer/conjugate mixture as in Chapter 5 (Table 5.1). The gelling properties and macroscopic phase separation of the composite systems were studied below and above the LCST and typical images are given Fig. 6.2.

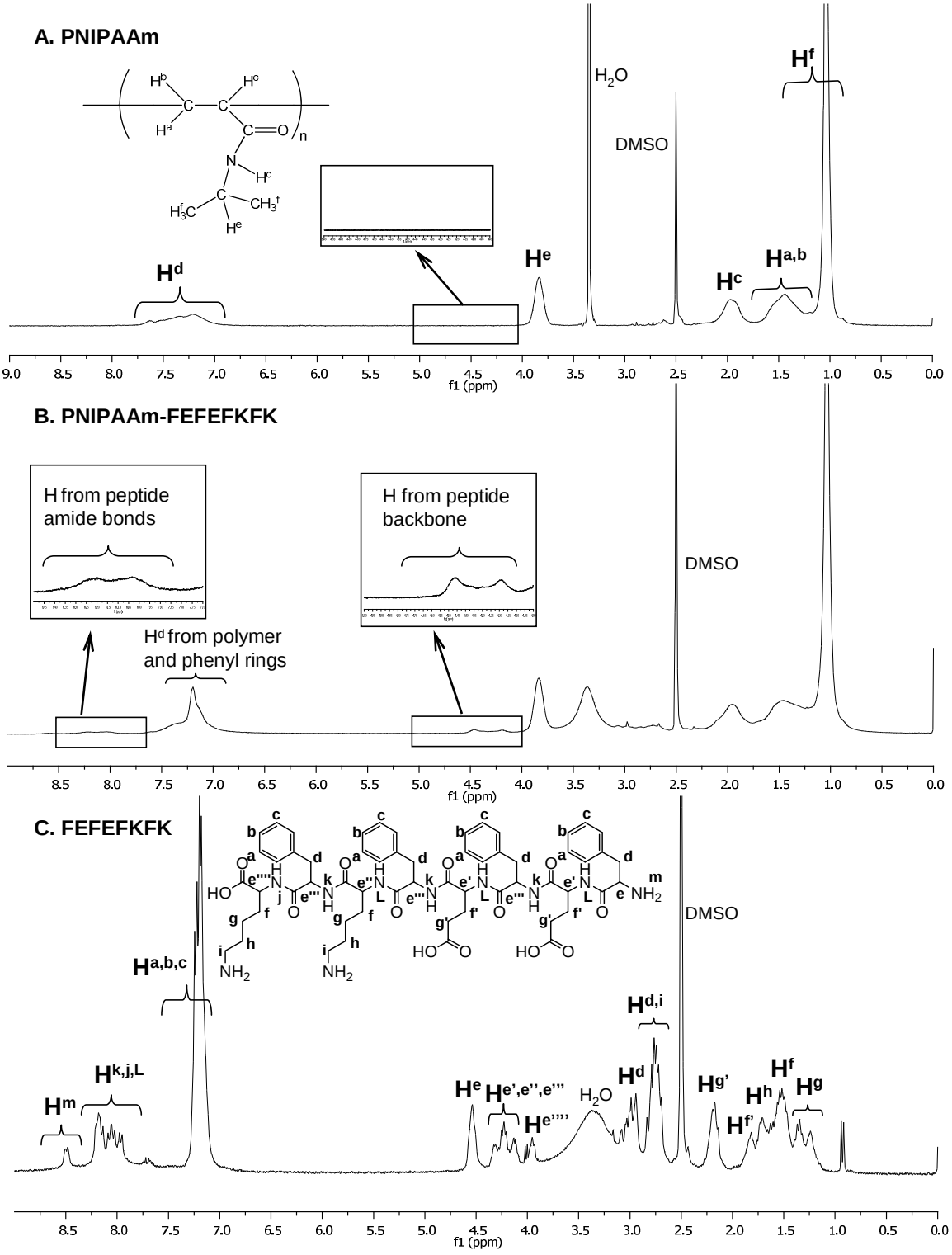

Figure 6.1: *^{1}H NMR spectra of : A) PNIPAAm, B) PNIPAAm-FEFEFKFK and C) FEFEFKFK (DMSO-d_6, 400 MHz)*

Table 6.1: *Peptide weight fraction ($W_{pept.}$) in the conjugate used for the preparation of the composite gels and conjugate weight fractions ($W_{conj.}$) in the peptide-rich gels studied*

Sample	$W_{pept.}$ in conjugate	$W_{conj.}$ in gel mixture
10-3	0.12	0.23
10-5	0.12	0.33
10-10	0.12	0.50
20-3	0.12	0.13
20-5	0.12	0.20
20-10	0.12	0.33

Fig. 6.2 (1A) shows that the composite gels 10-3 and 10-5 were liquid at ambient temperature as expected, whereas the sample 10-10 formed a self-supporting gel due to higher conjugate content and hence higher peptide content. 20-3, 20-5 and 20-10 samples formed self-supporting gels at ambient temperature (Fig. 6.2 (2A)). Typically at increased temperature a polymer solution becomes opaque due to the collapse and aggregation of the polymer [2] as it was observed for PNIPAAm-rich gels in Chapter 4 and for peptide-rich gels with the polymer/conjugate mixture in Chapter 5. In the case of the composite gels the opaqueness was not explicit (Fig. 6.2 (1B and 2B)).

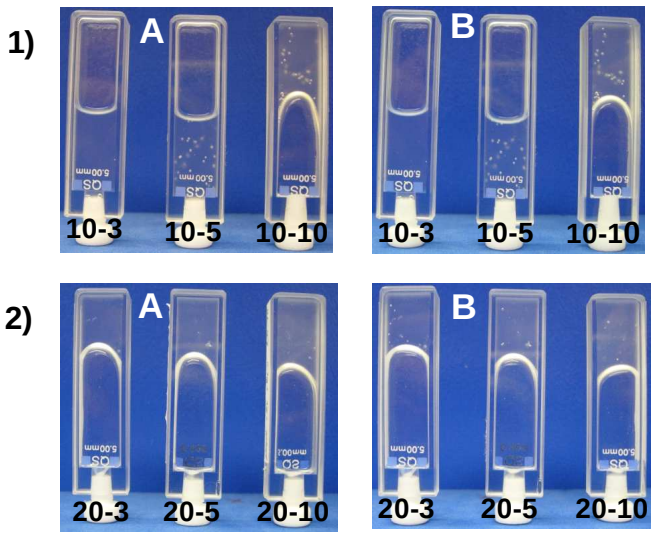

Figure 6.2: *Gelation and macroscopic phase behaviour of the composite gels: 1) series of 10 mg ml^{-1} of peptide and 2) series of 20 mg ml^{-1} of peptide and various conjugate content at: A) ambient temperature and B) 45°C*

UV-Vis spectroscopy is one of the techniques typically used to study the LCST behaviour of thermo-responsive polymers [3, 4] as it can easily detect a coil-to-globule transition of the macromolecular chains due to increased optical density above the LCST. A conjugate solution and a peptide/conjugate composite gel were studied by UV-Vis spectroscopy to prove that a coil-to-globule transition occurred (Fig. 6.3). Fig. 6.3A shows the S-shape increase of absorbance as a function of temperature for the conjugate solution which is typical of the LCST phenomenon. The composite gel showed similar behaviour, however, the increase in absorbance upon heating was not as large as in the conjugate solution (Fig. 6.3B). Usually, visible phase separation of polymer solution upon heating is due to the aggregation of the collapsed macromolecular chains [5]. Previously studied PNIPAAm-rich gels were predominantly formed by the polymer and peptide-rich gels contained a considerably large fraction of polymer/conjugate mixture (Chapter 4 and 5), hence they underwent the LCST transition which was visual macroscopically. The peptide-rich composite gels in this chapter contained ≤ 10 mol.% of pure polymer/peptide conjugate. UV-Vis spectroscopy showed that the LCST phenomenon was observed, however, the collapsed polymer chains did not form macroscopic aggregates presumably due to low density of polymer segments along the peptide fibres.

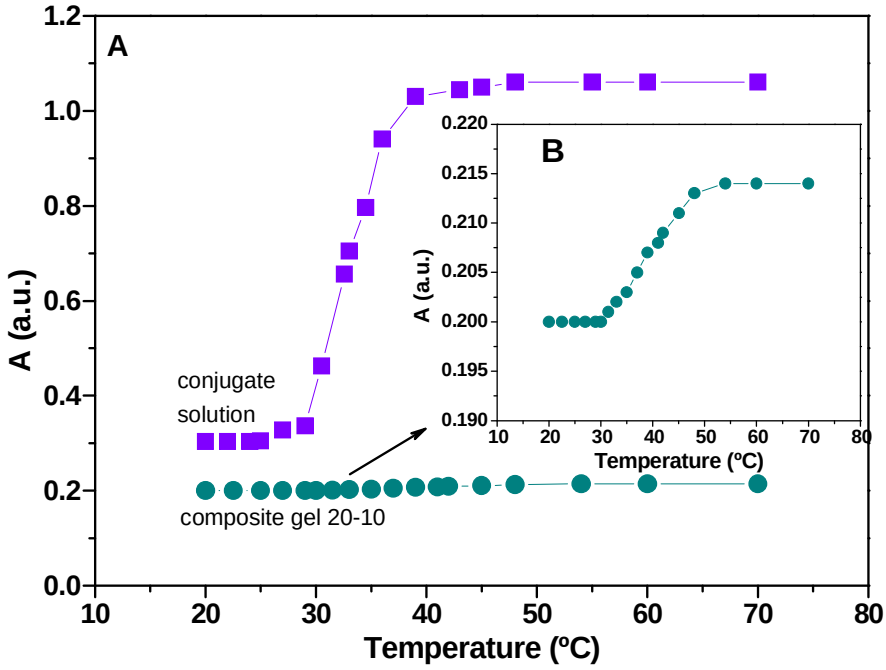

Figure 6.3: *A) Absorbance profile of an aqueous solution of the conjugate at 10 mg ml^{-1} and composite gel 20-10 at 500 nm and B) magnification of the composite gel profile*

6.3. Micro DSC studies of the composite gels

The thermo-responsive properties of the composite gels were analysed by micro DSC to reveal the effect of the incorporation of thermo-responsive polymer-peptide conjugate into peptide matrix. The onset points of the endothermic peaks, determined by the intersection of tangent lines from the baseline and slope of the endothermic peak, were used to determine the LCST. Fig. 6.4 shows typical micro DSC plots for 4 consecutive heating and cooling cycles for the composite gel 20-10. During each heating the endothermic peak characteristic to the LCST of PNIPAAm was detected (Fig. 6.4A) confirming the results from UV-Vis spectroscopy. The onset point of the transitions during the 1st heating was found to be at ~ 30°C which did not change during further heating cycles. Upon cooling the transition was completely reversible throughout all measurements (Fig. 6.4B). Other composite gels showed similar behaviour.

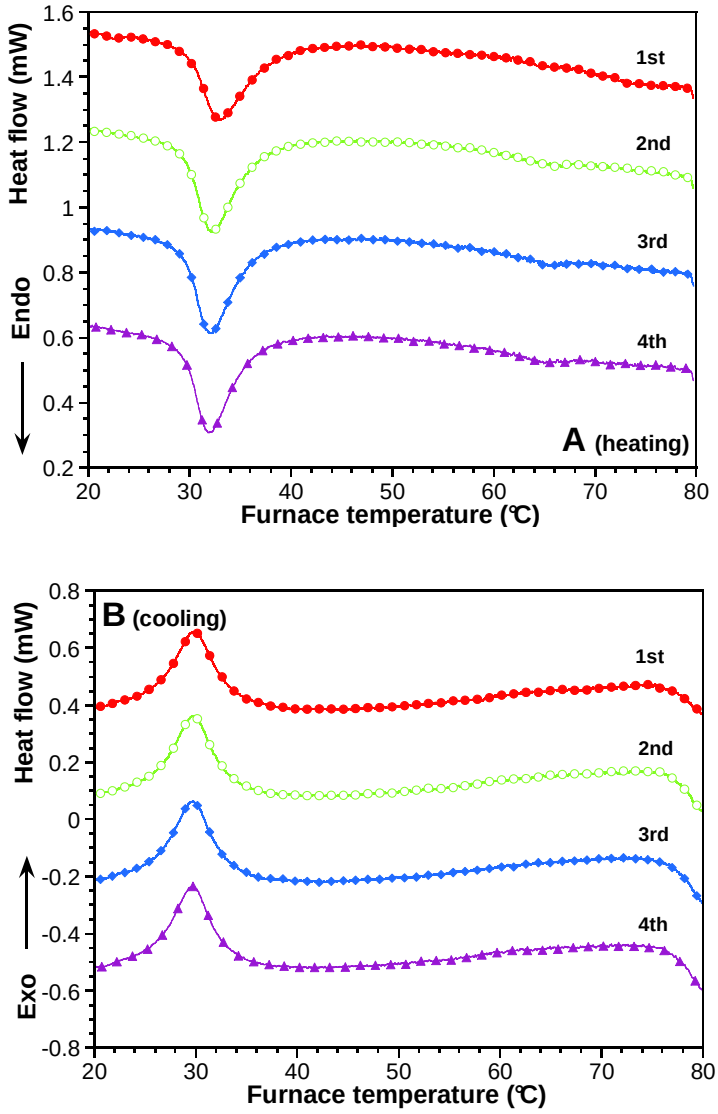

Figure 6.4: *Micro DSC plots of the composite gel 20-10 during 4 consecutive: A) heating and B) cooling cycles*

Fig. 6.5 compares the LCST and phase separation enthalpy values for polymer and polymer-peptide conjugate solutions and the two series of the composite gels as a function of polymer concentration which was calculated using the same calibration curve in Fig. 4.3.

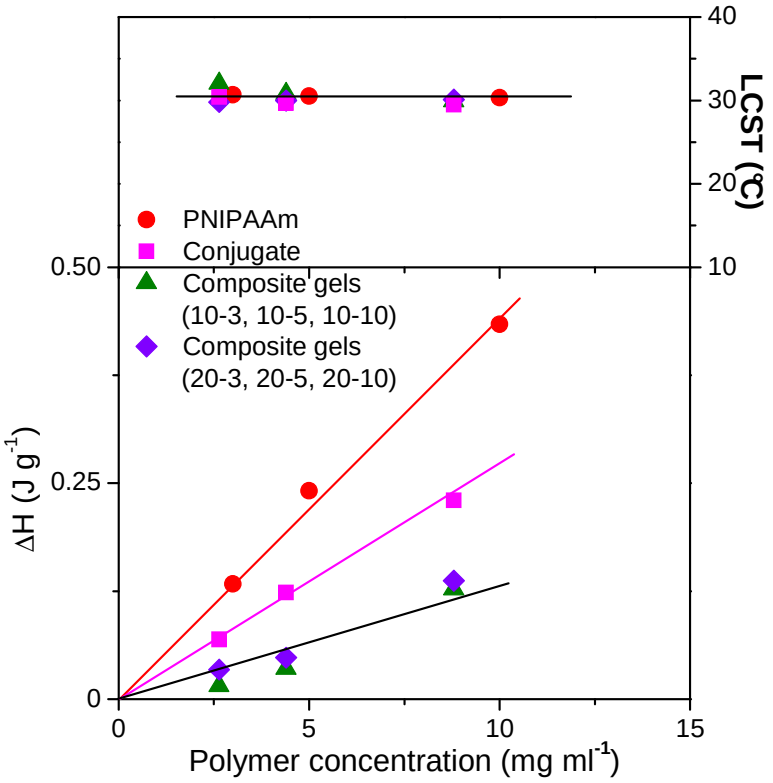

Figure 6.5: *LCST and phase separation enthalpy (ΔH) values for polymer and conjugate aqueous solutions and for the composite gels at peptide concentration of 10 mg ml^{-1} and 20 mg ml^{-1} with various conjugate content as a function of polymer concentration*

According to the micro DSC results both the polymer and conjugate samples exhibited LCST behaviour at ~30ºC indicating that the LCST of the polymer was not affected by its conjugation to the peptide FEFEFKFK. Fig. 6.5 also shows that polymer and conjugate enthalpy changed linearly with the concentration. The enthalpy of the phase separation of pure polymer was approximately twice that of the conjugate. This was due to lower $\overline{M}_w$ of the conjugate than that of PNIPAAm (8,800 and 15,000 g mol^{-1} respectively) and also due to the conjugate sample containing fewer polymer chains than pure polymer sample.

The micro DSC study of the composite gels showed the typical endothermic peaks, characteristic to PNIPAAm (Fig. 6.4.). The LCST values were also ~30°C, indicating that neither the peptide matrix nor the conjugate concentration had a considerable influence on the LCST values. Then it was noticed that the enthalpy values associated with the LCST transition of PNIPAAm in the composite gels were lower than those in pure conjugate solutions and varied slightly for different peptide concentrations. This might be due the

polymer chains being incorporated into the fibres that partially suppress their aggregation resulting in smaller phase separation enthalpies than in aqueous solution.

6.4. Mechanical properties of the gels

The mechanical properties of the composite gels were studied using oscillatory rheology. As previously, the samples were placed between the parallel plates with the top plate of 20 mm in diameter. Mechanical measurements were split in 3 types of tests: strain amplitude, angular frequency and temperature sweeps. The initial strain amplitude sweeps were performed for all samples when the material was exposed to an increasing strain at a constant frequency of 6.28 rad s^{-1}. The elastic (G') and viscous (G'') moduli as a function of strain amplitude were recorded for the two series of composite gels and compared to the pure peptide matrix. Fig. 6.6 shows the amplitude sweeps of both series of composite gels. The mechanical spectra for FEFEFKFK peptide at 10 and 20 mg ml^{-1} are included for comparison.

For both composite gel series elastic behaviour of the hydrogels dominated the viscous behaviour: $G' > G''$ as observed previously. Maximal G' value reached was ~ 100 Pa for both series. G' decreased rapidly above a concentration-dependent critical strain amplitude, indicating a breakdown in the gel. Fig. 6.7A shows that yield strain (γ^*) values shifted to lower values with increasing conjugate content as expected. Peptide fibres became stiffer and consequently more brittle with increasing conjugate content in each series. The results showed that lower concentration gels (peptide concentration 10 mg ml^{-1}) showed smaller γ^* values than the other series (peptide concentration 20 mg ml^{-1}) with no and 3 mg ml^{-1} of incorporated conjugate. At higher conjugate concentrations (5 and 10 mg ml^{-1}) γ^* became similar for both series indicating similar increase in gel stiffness.

Fig. 6.7B shows the increase of the moduli crosspoint values with increasing conjugate content for both series indicating the enhancement of mechanical characteristics.

G' and G'' increased with increasing quantity of polymer-peptide conjugate and hence quantity of peptide in the gels. The peptide segments from the conjugates contributed to the network formation and polymer segments, distributed along the fibres, influenced the stiffening of the fibres and overall network strength, hence the increase in moduli values. The results from strain amplitude sweeps for both composite gel series showed that both series exhibited similar behaviour.

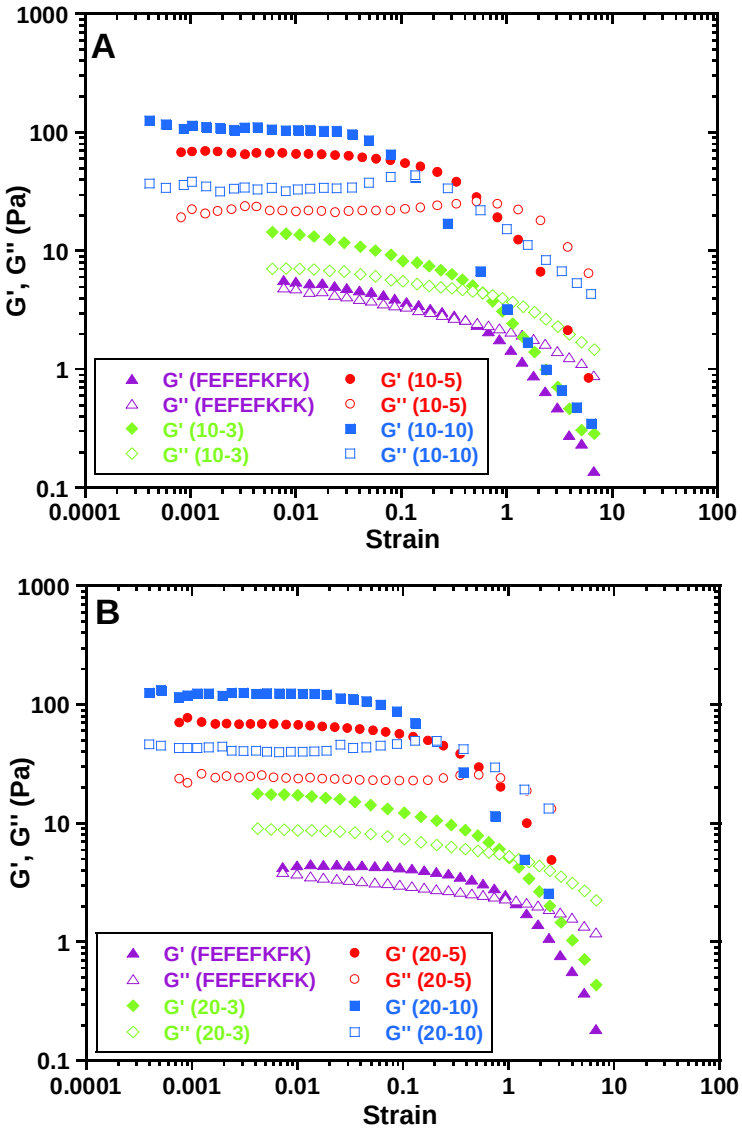

Figure 6.6: *Strain amplitude sweeps of: A) composite gels 10-3, 10-5, 10-10 and FEFEFKFK at 10 mg ml^{-1}, B) composite gels 20-3, 20-5, 20-10 and FEFEFKFK at 20 mg ml^{-1} at 20°C. G' was higher than G'' indicating gel formation. Moduli increased with increasing conjugate content.*

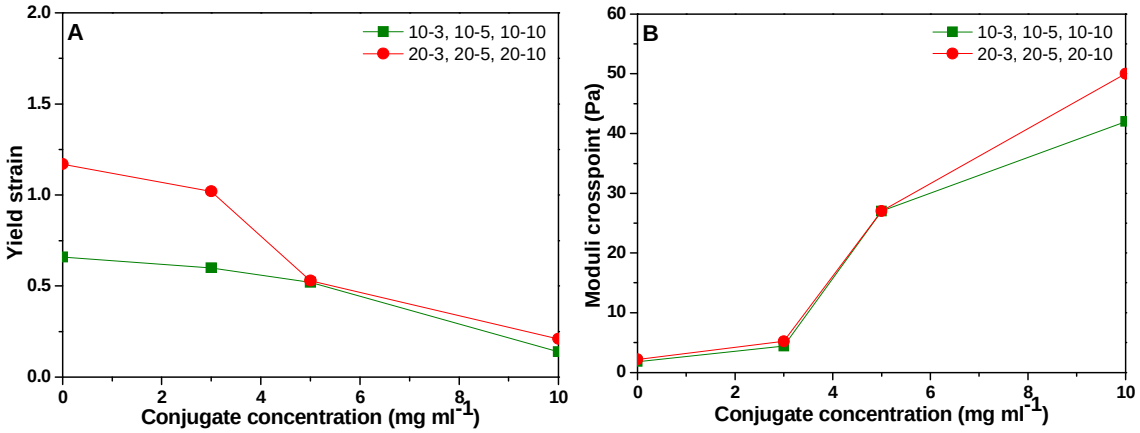

Figure 6.7: *Variation of: A) yield strain and B) modulus at the cross-over point of G' and G'' profiles with conjugate concentration incorporated into the peptide gels of 10 mg ml^{-1} and 20 mg ml^{-1}*

The oscillation frequency sweep measurements were performed in the LVR at 1% strain by exposing the samples to a gradual increase in angular frequency from 0.628 to 62.8 rad s^{-1} and varying the stress in a sinusoidal manner. Fig. 6.8A and Fig. 6.8B show the oscillation frequency sweeps for the gels 10-3, 10-5, 10-10 and 20-3, 20-5, 20-10 respectively. The results showed that all samples in both series exhibited a similar trend when $G' > G''$ and it was apparent that in each series the moduli increased with increasing conjugate content. In all cases, G' was nearly independent of frequency in the range from 0.1 to 10 rad s^{-1}, which was characteristic of solid-like behaviour of entangled network. G'', however, became more independent of frequency with increasing conjugate content.

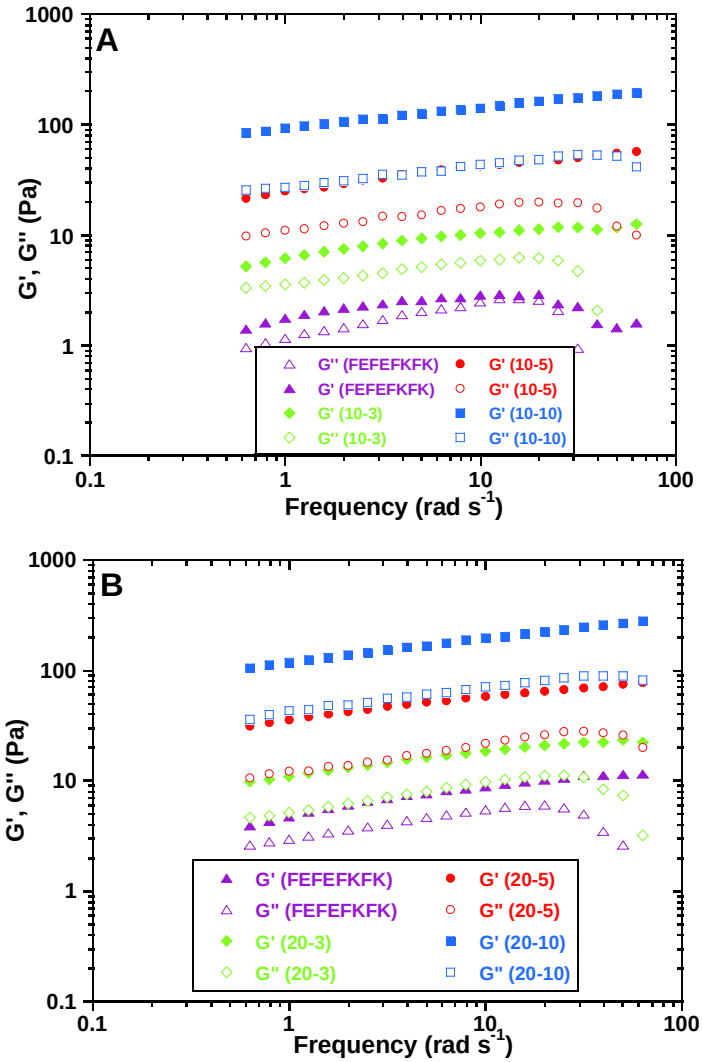

Figure 6.8: *Frequency sweeps for: A) composite gel series 10-3, 10-5, 10-10 and FEFEFKFK at 10 mg ml^{-1}, B) composite gel series 20-3, 20-5, 20-10 and FEFEFKFK at 20 mg ml^{-1} at 20°C*

Fig. 6.9A compares G' values extracted from the frequency sweep experiments for two series of composite gels. The results indicated that the gels became more rigid when the concentration of polymer-peptide conjugate increased. For example, G' increased from 5 and 9 Pa (peptide matrix at 10 and 20 mg ml^{-1} respectively) to the values of 150 and 180 Pa with

incorporation of 10 mg ml^{-1} of polymer-peptide conjugate. The increase in *G'* could be ascribed to the higher content of peptide included in the β-sheet fibres, to the increasing degree of entanglement of β-sheet fibres, and to the increased stiffness of the gel network due to pending PNIPAAm chains.

Fig. 6.9A also shows the opposing behaviour of the physical mixtures of FEFEFKFK (20 mg ml^{-1}) and different content of PNIPAAm. Network strength increased slightly from 9 to 32 Pa with 3 mg ml^{-1} of polymer and then decreased with further increase in polymer concentration: *G'* of 20-5 and 20-10 was 20 and 10 Pa respectively. This suggested that the network has been diluted with free polymer chains which freely floated in the fibrillar network rather than participated in its formation.

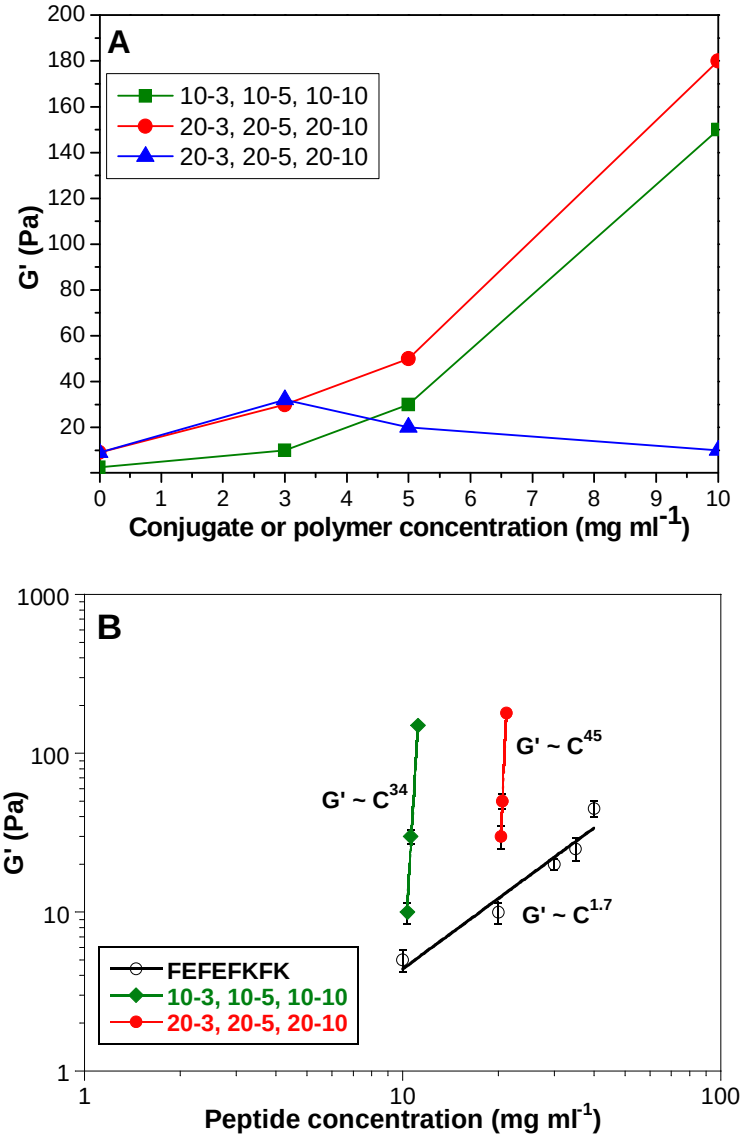

Figure 6.9: *A) Variation of G' of the composite gels of FEFEFKFK at 10 mg ml^{-1}, 20 mg ml^{-1} as a function of conjugate concentration and of the physical mixture of 20 mg ml^{-1} of FEFEFKFK as a function of polymer concentration at 20°C. B) Plateau values of G' as a function of peptide concentration in: pure FEFEFKFK, composite gels 10-3, 10-5, 10-10 and composite gels 20-3, 20-5, 20-10 at 20°C. pH 2.3 – 2.5*

Fig. 6.9B shows the power law behaviour of *G′* as a function of peptide concentration at pH 2.5. Variation of peptide concentration was minimal in each composite gel series and *G′* increased very quickly with increasing conjugate content. Both composite gels showed very high exponents (34 and 45 for the series 10-3, 10-5, 10-10 and 20-3, 20-5, 20-10 respectively) in comparison to pure peptide FEFEFKFK.

Mechanical properties of the gels were also studied as a function of temperature. Fig. 6.10 shows variations of *G′* and *G″* with temperature measured at angular frequency of 6.28 rad s^{-1} for two series of composite gels. The samples were heated from 20 to 80ºC and cooled down to 20°C and heating/cooling cycles were performed 3 times in total.

Dynamic temperature sweeps of both series showed that *G′* values increased during the first heating cycle and did not decrease to the initial *G′* values upon cooling. For both composite gel series the initial increase in moduli values was due to the phase-separation of the polymer (Fig. 6.10A, C). Upon cooling the behaviour of two series was slightly different. Gel series 10-3, 10-5 and 10-10 showed that *G′* continued to increase upon cooling (Fig. 6.10 B). For example, *G′* of 10-3 increased from 15 to 40 Pa upon heating and reached 120 Pa upon cooling. Gels samples 20-5 and 20-10 showed that upon cooling *G′* did not decrease but remained practically constant around the value reached upon heating (Fig. 6.10 D), except 20-3 that showed slight decrease of *G′*. For example, *G′* of 20-5 increased from 60 to 200 Pa upon heating and remained at the mark of 200 Pa upon cooling. The second and third heating/cooling cycles did not show further substantial increase or decrease in *G′* values which remained at the values reached after the 1st cooling. This behaviour had something in common with the peptide-rich gels studied in Chapter 5 when gel stiffness increased upon heating and upon cooling gels became more rigid than in the beginning of the experiment.

Another interesting observation was that for the composite gels 10-3, 10-5 and 10-10 (Fig 6.10A), *G′* values increased gradually until a certain temperature, which was 68, 60 and 50°C for 10-3, 10-5 and 10-10 accordingly, when *G′* values started to increase considerably. The temperature, at which *G′* started to increase rapidly, shifted to lower values with the increase in conjugate content. For the composite gels 20-3, 20-5 and 20-10 the increase of *G′* values was more continuous and gradual (Fig. 6.10C).

The results implied that polymer chains did not contribute significantly to the network elasticity because polymer concentration was much smaller than the peptide concentration. Therefore the variation of *G′* with temperature was slightly different from that observed in Chapter 4.

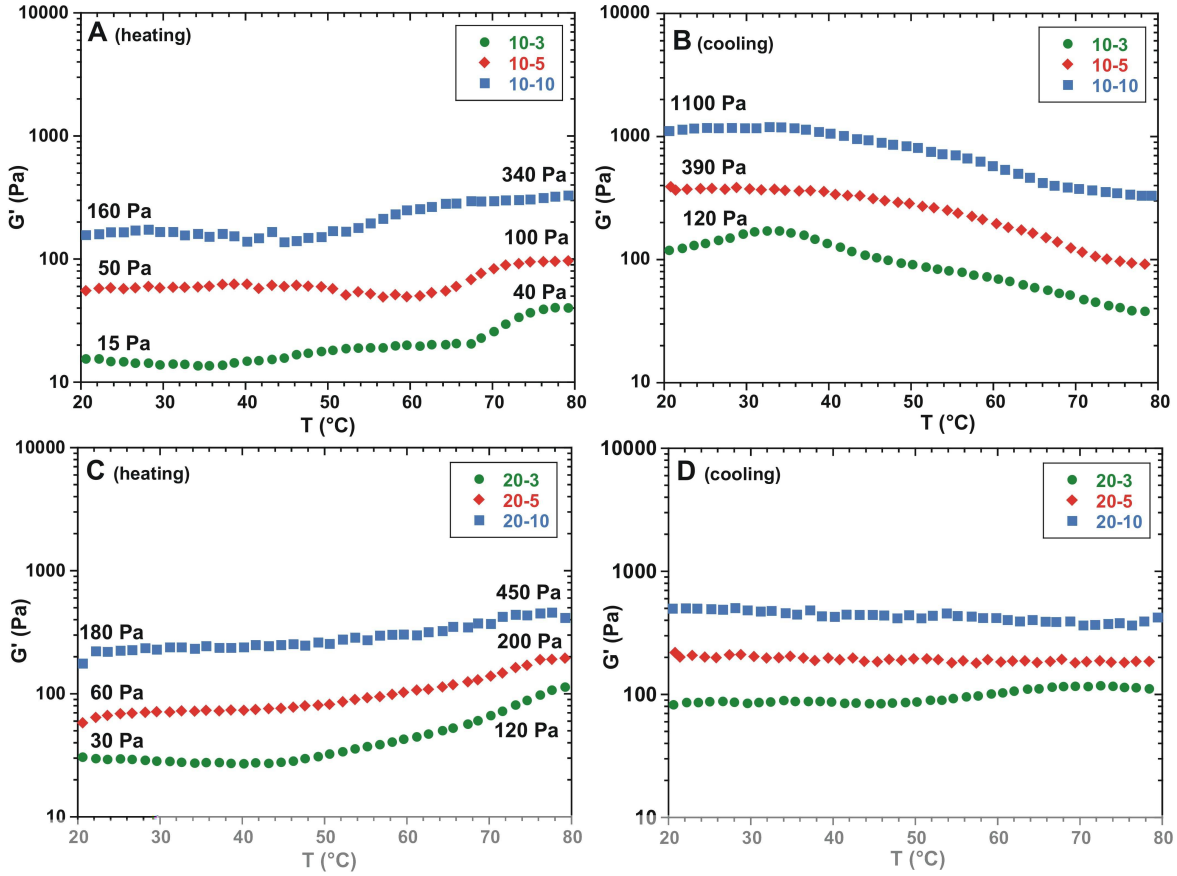

Figure 6.10: *Dynamic temperature sweeps of the composite gels: A) 10-3, 10-5, 10-10 and C) 20-3, 20-5, 20-10 during heating from 20 to 80°C. Dynamic temperature sweeps of the composite gels: B) 10-3, 10-5, 10-10 and D) 20-3, 20-5, 20-10 during cooling from 80 to 20°C. Heating rate 1 °C min*$^{-1}$.

Pure peptide matrix did not show a substantial increase in *G'* at elevated temperatures (Fig. 6.11). Both moduli varied slightly around 20 Pa during heating and cooling which indicated that the increase of the composite gel stiffness was not presumably due to the structural changes in peptide matrix.

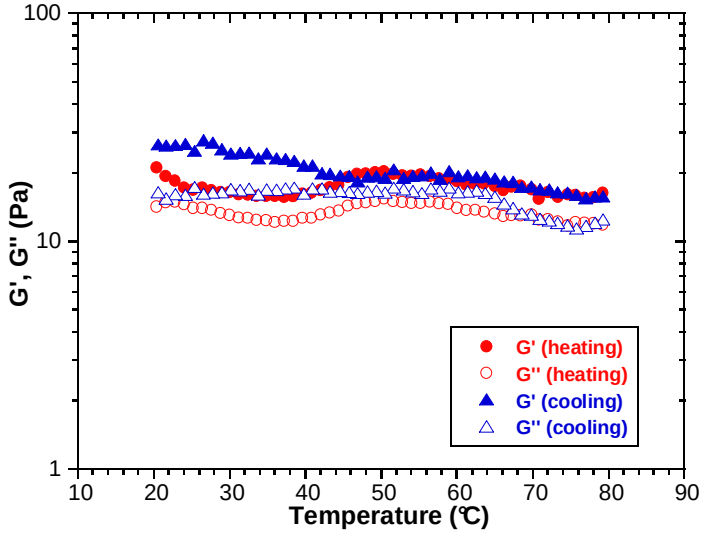

Figure 6.11: *Variation of G' and G'' of FEFEFKFK at 20 mg ml*^{1} *as a function of temperature*

High moduli values at elevated temperatures (70 - 80°C) indicated presumably strong interactions among the components of the gels. Wu *et al.* [6] studied PNIPAAm solution with light scattering and Fourier transform infrared spectroscopy (FT-IR) techniques and reported that at the temperatures, higher than the LCST, PNIPAAm chains were dehydrated and intermolecular hydrogen bonds were formed between the carbonyl and amide groups. These hydrogens bonds acted as cross-links making the collapsed polymer aggregates behave like a gel. When the temperature decreased, aggregates of the collapsed chains started to swell but did not disassociate due to the hydrogen bonds holding collapsed chains together. When the temperature was much lower than the LCST (~4°C), chain dissociation occurred. Therefore this also might be a reason for observed increase in gel strength in this study.

Similarly to other peptide-rich gels discussed in Chapter 5, these composite gels showed increase in gel strength at high temperatures and further investigations are required to elucidate this behaviour in more detail.

6.5. Gel network morphology

Gel network morphology was studied by SANS, TEM and AFM. First an overview of the peptide and conjugate concentration and temperature influence on SANS profiles is presented. Neutron scattering is sensitive to the difference in scattering density between phases [7]. Here, the scattering density difference between the peptide-rich phase, the network, and the peptide-poor phase, the solvent, and also between the polymer-rich phase and the solvent was employed. For SANS experiments the same two series of composite gels were prepared in different solvents allowing the behaviour of the peptide fibres and the polymer segments to be identified independently. To study the peptide behaviour, the gels were prepared in D_2O where the contrast between the hydrogenated peptide and the deuterated polymer was higher than between the hydrogenated peptide and the hydrogenated polymer (see section 3.4.10 for more detail). Fig. 6.12 shows a SANS plot for the deuterated PNIPAAm and the composite gel 10-3 in D_2O. The results showed that the scattering mainly originated from the peptide, however the deuterated polymer showed some scattering at low q (Fig. 6.12 inset).

As described in section 3.4.10 of Materials and Methods, the polymer could be studied when the peptide had the same contrast as the solvent, i.e. the peptide was contrast-matched. The calculations showed that it could be done in the solvent mixture of H_2O/D_2O = 58/42 vol.% when the scattering length density of the solvent mixture matched that of hydrogenated peptide and was equal to 2.35×10^{-10} cm^{-2}. As shown experimentally the experimental scattering length density obtained by looking at the peptide scattering extension

as function of solvent composition is in very good agreement with the calculated one (Fig. 6.13). Fig. 6.13 shows $I_N(q)$ versus q plots for the peptide samples of 10 mg ml^{-1} prepared in the mixtures of H_2O and D_2O at different ratios. The results obtained were in agreement with the theoretical calculations of the ratio that the peptide sample prepared in the mixture of 58 vol.% H_2O and 42 vol.% of D_2O would show no scattering. Consequently, this solvent mixture was used to study polymer behaviour in the composite gels.

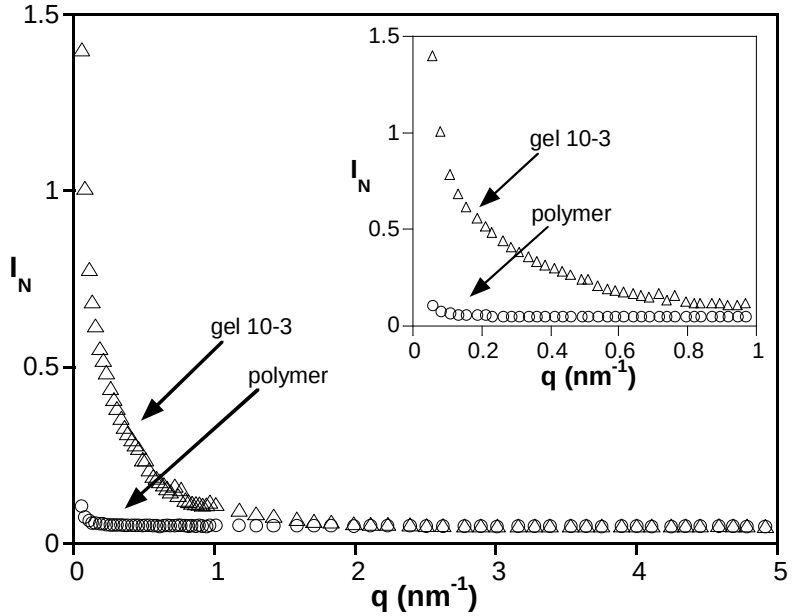

Figure 6.12: *$I_N(q)$ versus q plot of the deuterated PNIPAAm (3 mg ml^{-1}) and the composite gel of protonated peptide (10 mg ml^{-1}) and deuterated PNIPAAm (3 mg ml^{-1}) in D_2O. In the composite gel in D_2O main scattering originated from the peptide; polymer showed slight scattering at low q.*

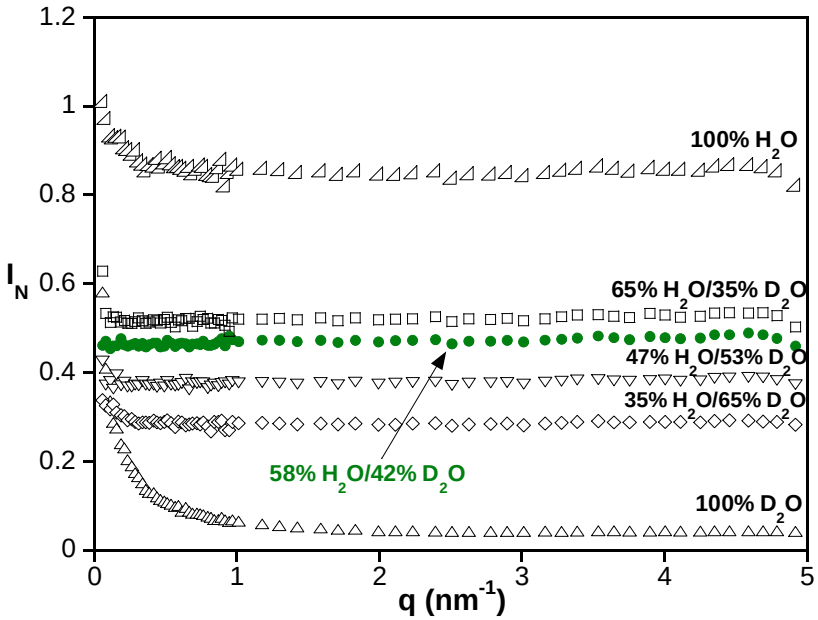

Figure 6.13: *$I_N(q)$ versus q plot for the peptide (10 mg ml^{-1}) in H_2O, D_2O and their mixtures. Peptide did not scatter in the solvent mixture of 58 vol.% H_2O / 42 vol.% D_2O.*

The scattering profiles for all samples for both sets of experiments (in D_2O and H_2O/D_2O = 58/42 vol.%) were collected at 25 °C to study the systems below the LCST, at 45°C to study the systems above the LCST, and again at 25°C to check the reversibility of the phase separation. Fig. 6.14 shows the variation of scattering intensity with *q* in the logarithmic scale for both series of the composite gels in D_2O at 25°C. The SANS profiles for the peptide FEFEFKFK at 10 and 20 mg ml^{-1} are given for comparison.

In D_2O the polymer part was "invisible" and the main contribution to the scattering originated from the peptide fibres (peptide matrix and peptide segments from the conjugate). Typically, the scattering intensity decreased for all samples with increasing *q*. At low *q* the pure peptide of 20 mg ml^{-1} showed asymptotic behaviour of the scattering intensity described by $I(q) \sim q^{-1}$ which is characteristic to the scattering of the rod-like objects (fibres) in solution [8-11]. The peptide at lower concentration showed slightly different dependence probably due to the concentration below its critical gelation concentration. The results showed that at both concentrations pure peptide formed concentrated microdomains due to the intermolecular interactions of the peptide fibres as expected. The scattering of these domains resulted in a correlation or structural peak in the SANS profiles. The maximum of this peak was found to be at ~ 0.32 nm^{-1} for both concentrations, however, the structural peak was more pronounced at higher peptide concentration than at 10 mg ml^{-1}. Using the Bragg's law, described by Eq. 6.1, it is possible to calculate the most probable distance between the aggregates or simply the mesh size, *d* of the network:

$$d = \frac{2\pi}{q} \qquad (Eq.\ 6.1).$$

The calculations showed that the network of FEFEFKFK fibres had the mesh size ~ 20 nm.

Composite gels 10-3, 10-5 and 10-10 showed no obvious structural peak probably due to the conjugated polymer slightly influencing the intermolecular interactions of the fibres. At low *q* values the intensity showed q^n dependence with *n* close to -1. When the conjugate concentration increased in the series, the curvature of the plots decreased indicating higher content of rod-like objects. The intensity of the structural peak was found to decrease as conjugate concentration increased. Similarly, the composite gels 20-3, 20-5 and 20-10 showed the exponent of -1 at low *q* characteristic to rod-like objects. The structural peak was also present in each sample at the same position as in that of pure FEFEFKFK at 20 mg ml^{-1}.

Fig. 6.15 shows the variation of scattering intensity with *q* in the logarithmic scale for both series of the composite gels in D_2O at 45°C when the polymer is in the collapsed state.

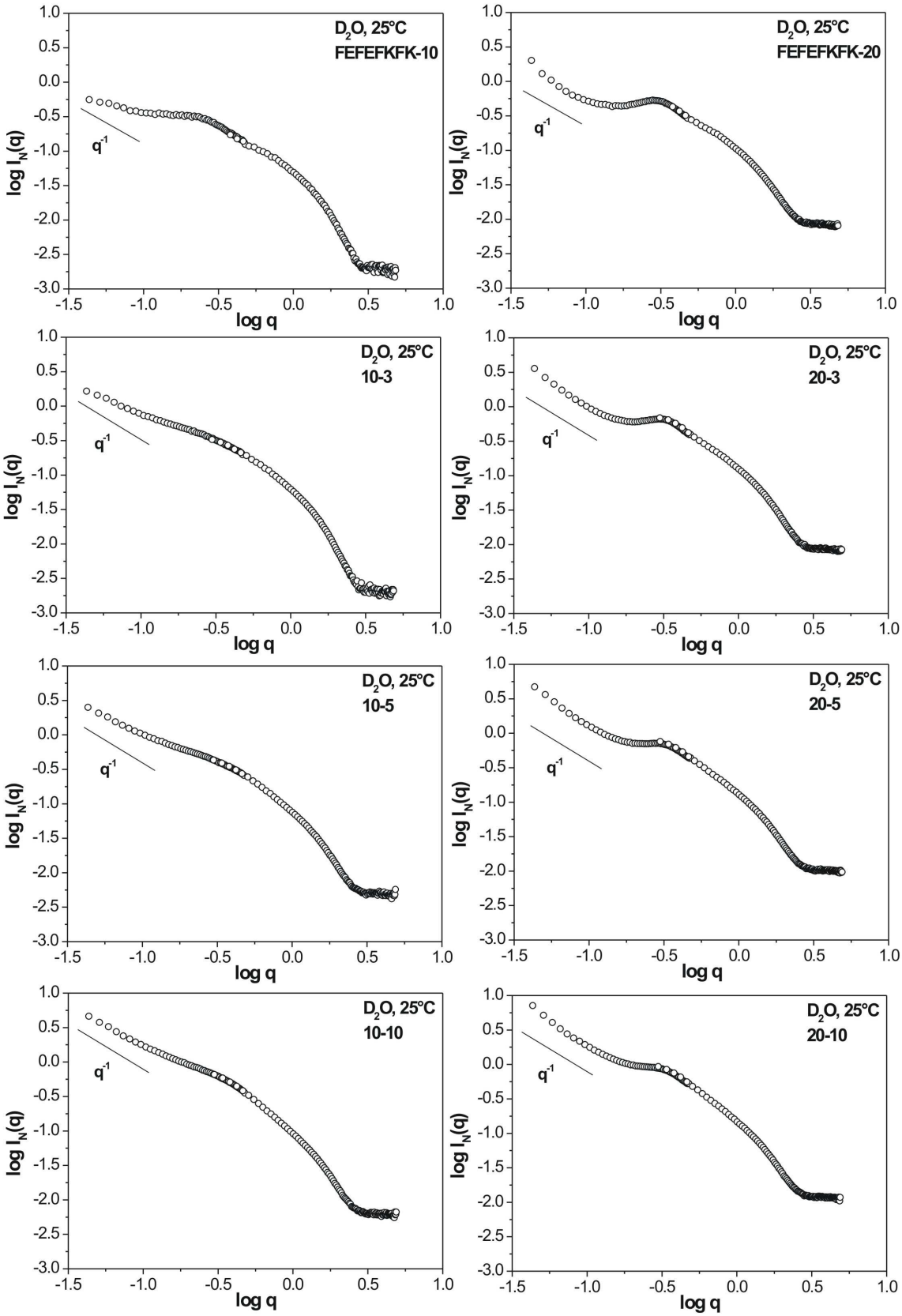

Figure 6.14: *SANS profiles of the two series of the composites gels in D_2O at 25°C. Pure petide FEFEFKFK at 10 and 20 mg ml^{-1} is given for comparison. In D_2O scattering originated mainly from the peptide. Scattering curves showed a q^{-1} behaviour at low q indicating the presence of rod-like objects. A correlation peak, centred at ~ 0.32 nm^{-1}, was present in the scattering profiles and became more intense with increasing peptide content, but its intensity decreased with increasing conjugate content.*

The scattering intensity decreased for all samples with increasing *q*. The composite gels 10-3, 10-5 and 10-10 showed the slopes close to -1 at low *q* indicating the presence of rod-like objects. The structural peak was not pronounced in the conditions studied. The composite gels 20-3, 20-5 and 20-10 showed the slopes of -1 at low *q* and the structural peak centred at ~ 0.32 nm^{-1} which decreased in intensity with increasing conjugate content and practically vanished for the sample 20-10. At 45°C the gels could melt slightly, showing the decrease in intermolecular fibre-fibre interactions. Sample of 20-10 contained the highest amount of conjugate in the series, which collapsed above the LCST and presumably influenced the fibre-fibre interactions.

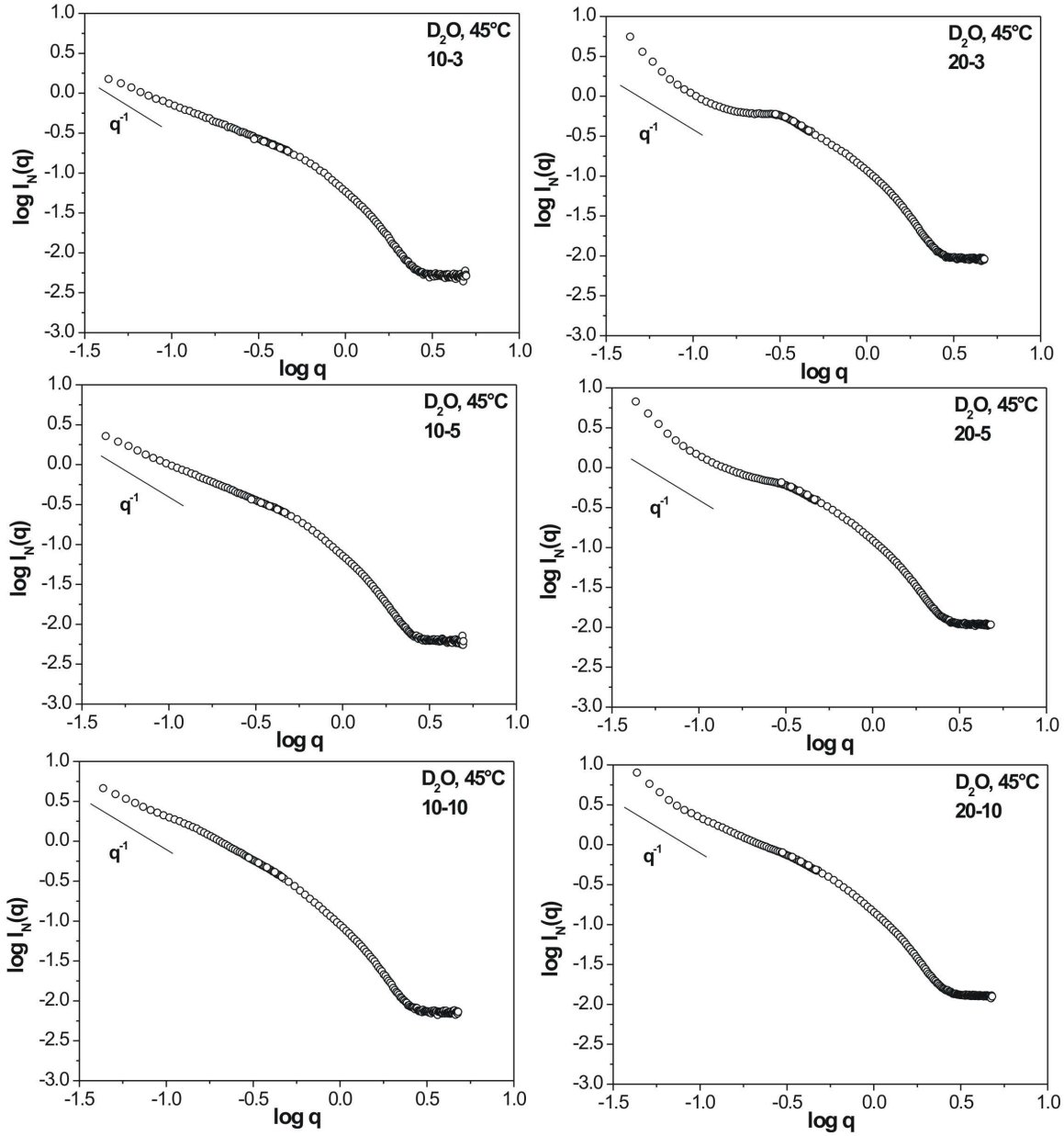

Figure 6.15: *SANS profiles of the two series of the composites gels in D_2O at 45°C. Scattering profiles showed q^{-1} behaviour at low q indicating the presence of the rod-like objects. The structural peak centred at ~ 0.32 nm^{-1} was more pronounced in the samples with higher peptide content.*

Kopeček *et al.* [12, 13] studied polymer-peptide conjugates and found that polymer presence in the conjugate influenced the conformational behaviour of the peptide. Therefore this might be also the reason for change of the network structure revealed as disappearance of the correlation peak as conjugate content in the composite gels increased.

Similar experiments using the solvent mixture were performed to study the behaviour of the polymer segments below and above the LCST. Fig. 6.16 shows the variation of scattering intensity with q in the logarithmic scale for both series of the composite gels in the solvent mixture of H_2O and D_2O at 25°C. In these conditions the peptide was "invisible" and did not scatter and only the polymer chains contributed to the scattering intensity. The scattering intensity decreased for all samples with increasing q and slightly increased with the increase of conjugate content in the series. It is worth mentioning that plots were slightly noisy for the samples with low conjugate content and became more linear with increasing conjugate content and hence polymer content that contributed to the scattering. Fig. 6.16 shows that all plots showed the slopes of -1 at low q confirming the presence of rod-like objects. It was postulated that the peptide segment of the conjugate would be incorporated into the fibrillar network following the self-assembly principle. Therefore the polymer chains would be placed outside the fibres and in the conditions, when the peptide fibres are "invisible", would repeat the contours of the fibres, creating a "hollow" fibre with inner core composed of peptide fibre and outer shell composed of polymer segments.

Fig. 6.17 shows the variation of scattering intensity with q in the logarithmic scale for both series of the composite gels in the solvent mixture of H_2O and D_2O at 45°C. Above the LCST, at 45°C, the scattering profiles changed drastically. Presumably at this stage the polymer chains collapsed along the fibres and according to rheology data at 45°C the gel structure was maintained. It was expected that the scattering profiles will also show the slopes of -1 at low q confirming the presence of fibres with collapsed polymer chains: rod-like objects. The scattering profiles were slightly similar to those in Fig. 6.14 obtained for the composite gels in D_2O at 25°C, however the structural peak in the solvent mixture at 45°C was very strong and overlapped the linear region with q^{-1} behaviour. This structural peak was presumably due to increased intermolecular interactions of the peptide fibres with collapsed PNIPAAm chains on them. It is suggested to study these systems with USANS (Ultra small-angle neutron scattering) technique which should allow the scattering profiles at small q^{-1} to be obtained and which would confirm the presence of rod-like objects.

The position of the structural peak shifted to lower q values and it was found to be at ~ 0.16 nm^{-1} that corresponded to the mesh size of ~ 40 nm according to the Bragg's law (Eq. 6.1). The mesh size of polymer network was twice that of the peptide network in D_2O. It

may postulated that at 45°C, when the polymer was in collapsed state, the fibres might tend to come together and form a bigger mesh.

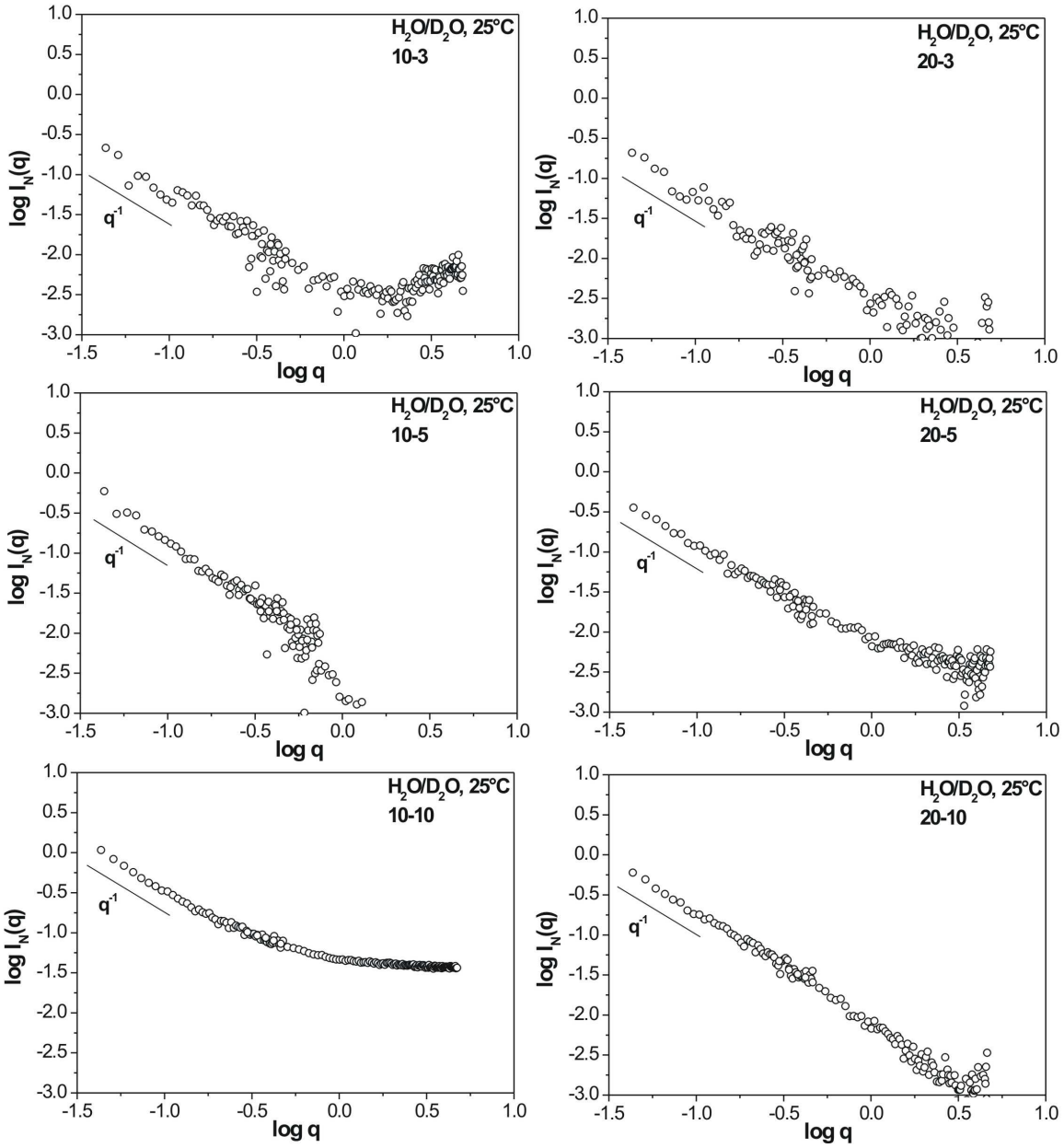

Figure 6.16: *SANS profiles of the two series of the composites gels in the solvent mixture of 58 vol.% H_2O / 42 vol.% D_2O at 25°C. Scattering profiles showed q^{-1} behaviour at low q due to the collapsed polymer chains along the peptide fibres.*

Fig. 6.18 shows the variation of scattering intensity with *q* in the logarithmic scale for the composite gel 20-10 in D_2O and in the solvent mixture of H_2O and D_2O at 25, 45 and 25°C. The log-log plot of intensity versus *q* of the composite gel in D_2O showed that the scattering intensity increased slightly at 45°C in comparison to that at 25°C (Fig. 6.18A). Also at 45°C the structural peak disappeared due to slight melting of the gel. Upon cooling the

log-log profile mirrored the profile before heating. At all 3 temperatures the slopes of the profiles at low *q* were equal to -1 indicating the presence of the rod-like objects (fibres). Similar results showing the reversible thermal behaviour were obtained in the solvent mixture of H_2O and D_2O and are presented in Fig. 6.18B. The log-log plot of intensity versus *q* of 20-10 showed that 45°C the scattering pattern changed dramatically presumably due to the collapse of PNIPAAm and returned to initial state upon cooling. The scattering plots at 25°C before and after heating were practically identical and had the slopes of -1 at low *q*. These results clearly showed the reversibility of the phase separation.

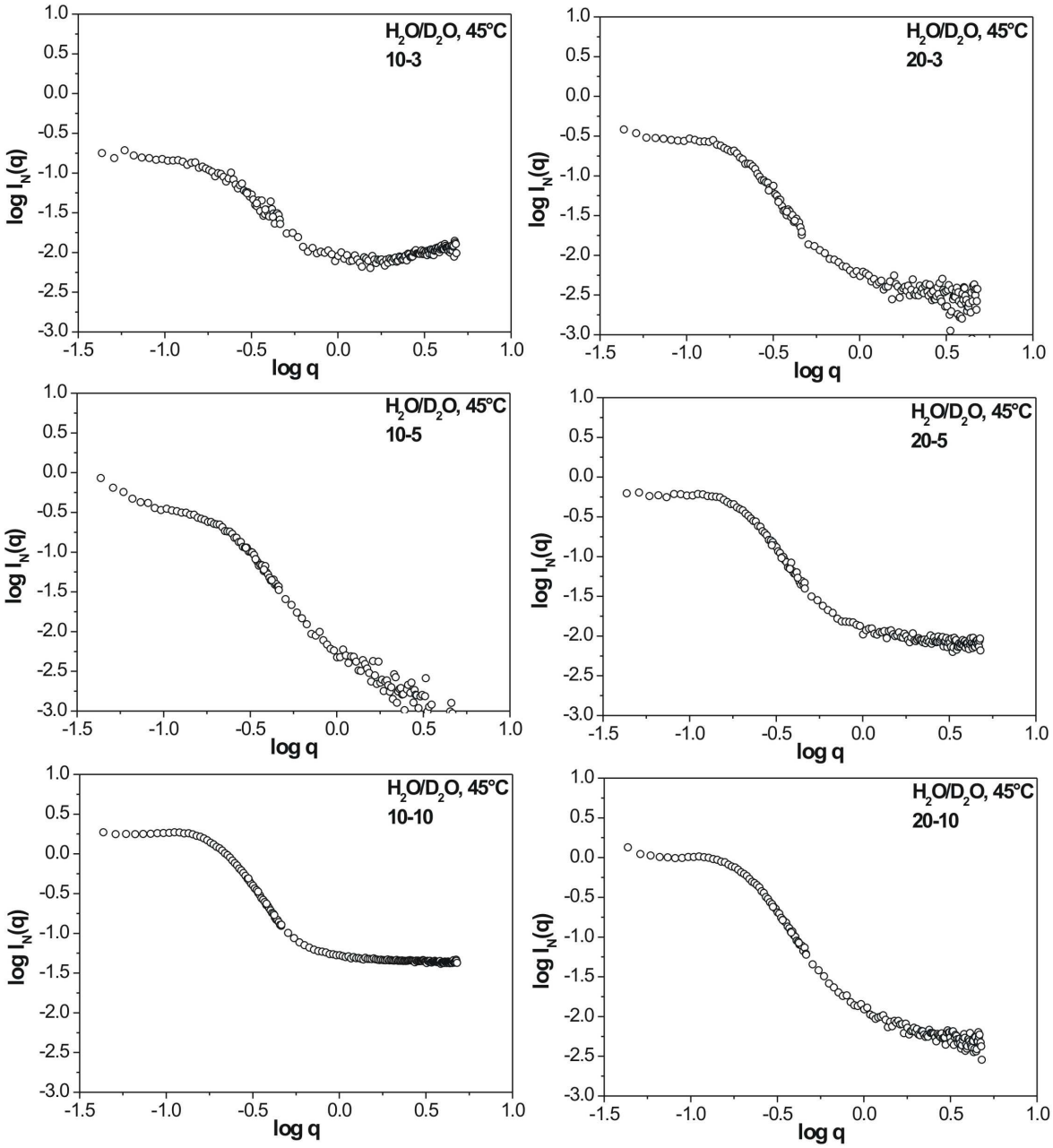

Figure 6.17: *SANS profiles of the two series of the composites gels in the solvent mixture of 58 vol.% H_2O / 42 vol.% D_2O at 45°C*

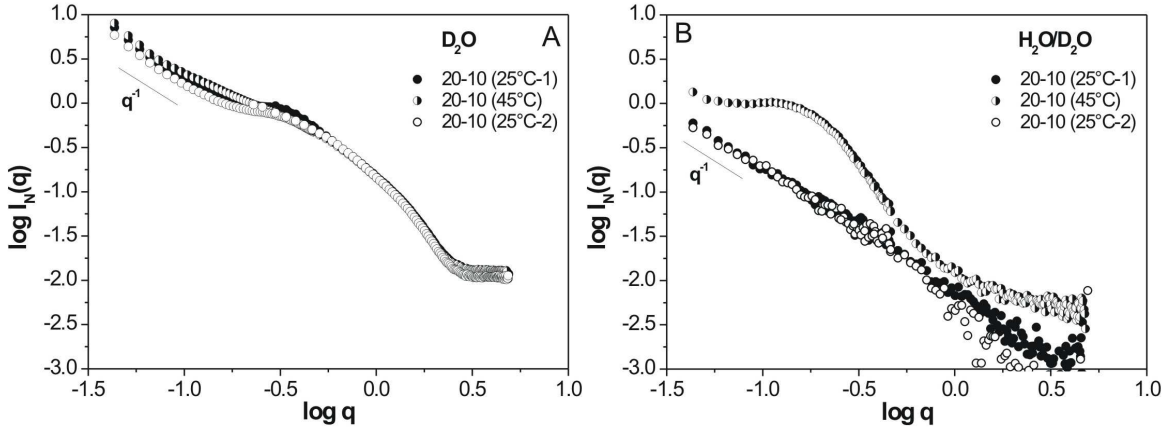

Figure 6.18: *SANS profiles of the composites gel 20-10 in: A) D_2O and B) in the solvent mixture of 58 vol.% H_2O / 42 vol.% D_2O at 25, 45 and 25°C. Scattering profiles showed the reversible thermal behaviour of the composite gels both in D_2O and in the solvent mixture.*

TEM and AFM studies were performed to provide a further insight into gel morphology and to confirm the presence of a fibrillar structure. Typical TEM micrographs of the composite gels with the highest conjugate content 10-10, 20-10 and of the peptide FEFEFKFK gel at a concentration of 10 mg ml^{-1} are presented in Fig. 6.19A, B and C respectively. The peptide concentration of 10 and 20 mg ml^{-1} is considerably high for TEM measurements when a dense fibrillar network is formed, therefore all samples for TEM measurements were diluted to final peptide concentration of 1 mg ml^{-1}. All TEM images showed a network of long and straight entangled fibres. It appeared that the entanglements were evenly distributed across the samples of the composite and pure peptide gels. Fibre diameter was found to vary in the range of 4.0 ± 0.8 nm. The fibrillar network of the composite gel did not seem to be different from that of pure peptide. The network mesh size varied from ~ 20 to 40 nm, however larger distances of ~ 100 nm were found.

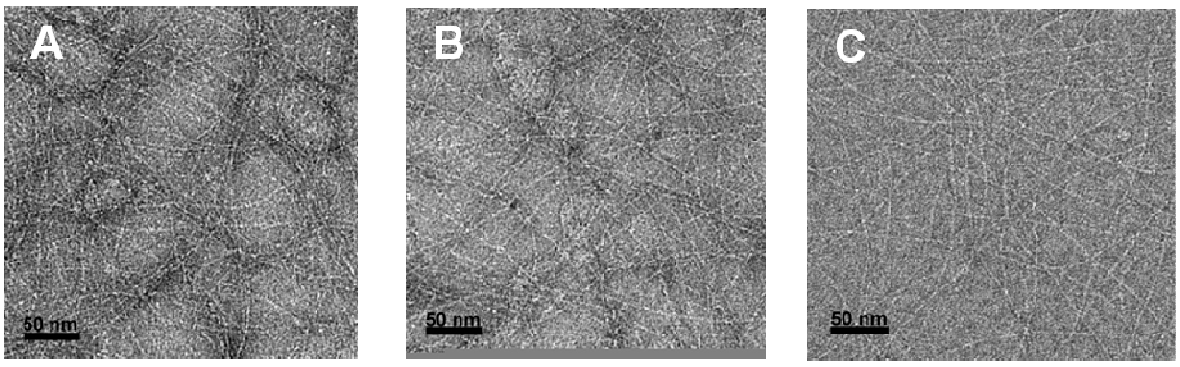

Figure 6.19: *Typical TEM images of: A) composite gel 10-3, B) composite gel 20-3 and B) FEFEFKFK at 10 mg ml^{-1}. Gels were diluted to the concentration of 1 mg ml^{-1} of peptide. TEM showed the formation of fibrillar network.*

Fig. 6.20 shows typical AFM images for the composite gels 10-10 and 20-10 which were diluted to the final peptide concentration of 0.5 mg ml^{-1} and of the pure peptide gel at 2 mg ml^{-1}. These are optimal concentrations found experimentally however they are slightly different from those used for TEM. Fig. 6.20A and 6.20B show the fibrillar network of the composite gel with some light dots distributed along the fibres. It was postulated that these light dots were polymer segments placed on the outside of the fibres. At higher magnification it was possible to distinguish that the fibres were not smooth and possibly polymer segments could be observed along the length of the fibre (Fig. 6.20 D, E). Fibre width was detected to be 4.5 ± 1 nm and fibre height ~1 nm. It was assumed that fibres were cylindrical, however the interactions between the substrate and the fibres might result in a deformation of the fibre shape pulling it towards the surface and flattening it. Also the fibres might be embedded in background matrix. This may result in the fibre width different from the height. Fig. 6.20C presents the AFM image of FEFEFKFK peptide at 2 mg ml^{-1} with a dense fibrillar network. Higher magnification showed that peptide fibres were rather smooth (Fig. 6.20F). The width of the fibres was similar to that observed in the composite gel and was in good agreement with the results obtained by Saiani *et al.* [1].

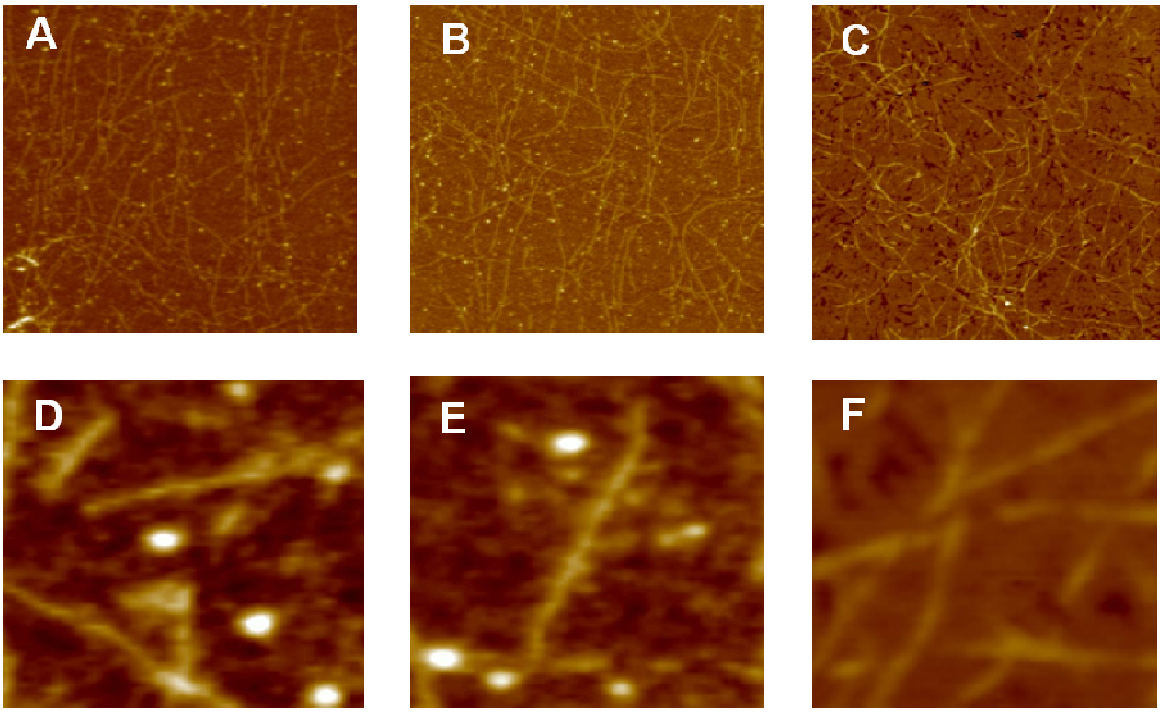

Figure 6.20: *AFM images of the composite gels 10-10 (A - scan size 2 μm^2, D - scan size 0.25 μm^2), 20-10 (B - scan size 2 μm^2, E - scan size 0.25 μm^2), and peptide solution at concentration of 2 mg ml^1 (C - scan size 2 μm^2, F - scan size 0.25 μm^2C) on mica at ambient temperature. AFM showed the formation of fibrillar network similar to that of pure peptide. In the case of composite gels fibres were not smooth as for pure FEFEFKFK and possibly polymer segments could be observed along the length of the fibre.*

The mesh size in the composite gels was measured and it varied from ~ 114 nm to 230 nm to 360 nm. Since the composite gels were diluted the mesh size measurements should be considered carefully as they may give misleading information about the real gel network. Also the substrate surface can direct the formation of mesh.

6.6. Self-assembly scheme

Following the results presented above, here is the proposed self-assembly scheme for the composite gels in water and their behaviour below and above the LCST (Fig. 6.21). In the figure the peptides are presented as arrows, the polymer segments in red, and the fibres in grey. Once peptides and polymer-peptide conjugates were dissolved in water (Fig. 6.21A), peptide segments self-assembled into β-sheet rich fibres (Fig. 6.21B and 6.21C). It was postulated that the peptide segment of the conjugate would participate in the formation of the fibres of ~ 3 nm in diameter and that the PNIPAAm segments from the conjugates would be placed outside the fibres. According to the initial peptide and conjugate weight ratios, the distance between the polymer segments on the peptide fibre was estimated to vary from 5 (for mixture 10-10) to 25 nm (for mixture 20-3). Below the LCST polymer chains were in good solvent and had an extended coil conformation. Radius of gyration for the polymer part was calculated to be ~ 3-5 nm according to the following equation: $<R_g^2>^{1/2} = 0.0188 \times \overline{M}_w^{0.54}$ where $<R_g^2>^{1/2}$ is radius of gyration and $\overline{M}_w$ is weight-average molecular weight [14]. When the temperature was increased above the LCST, PNIPAAm chains collapsed as tight globules along the length of the fibres, however the gel structure was maintained (Fig. 6.21D). The LCST transition was reversible upon cooling and polymer segments re-swelled.

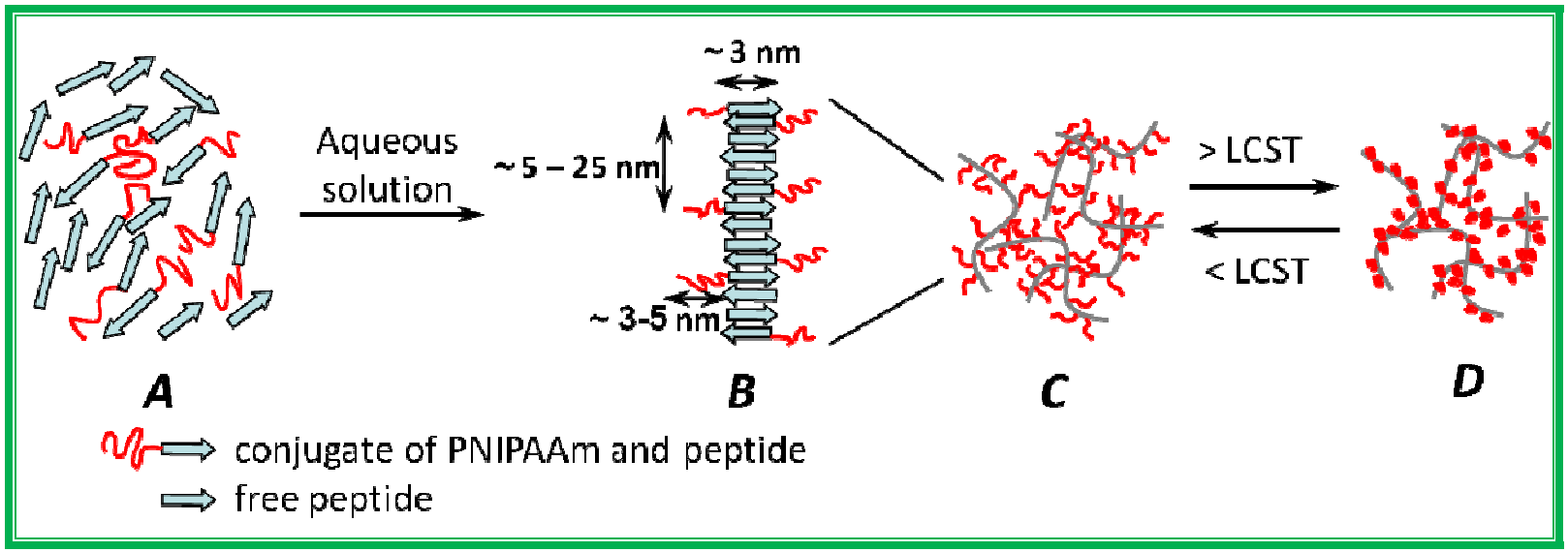

Figure 6.21: *Self-assembly scheme. A) Peptides and conjugates are dissolved in water. B, C) Self-assembly of peptides and conjugates into β-sheets and fibre formation. Polymer chains are placed outside the fibres. D) Phase separation due to the collapse of PNIPAAm. Polymer segments collapse along the length of the fibres. Phase separation reversible upon cooling.*

6.7. Summary

This chapter reported the results on the thermo-responsive composite gels prepared by embedding pure PNIPAAm-FEFEFKFK conjugate into the peptide FEFEFKFK matrix. Two series of the composite gels were prepared by varying peptide matrix concentration (10 and 20 mg ml^{-1}) and polymer-peptide conjugate concentration (3, 5 and 10 mg ml^{-1}). Micro DSC measurements revealed the thermo-responsiveness of the composite gels, showing the endothermic peak at ~ 30ºC which was characteristic of the LCST of PNIPAAm. No change in the LCSTs was noticed in comparison to pure polymer. The results showed that the composite gels had lower heats of the phase separation than corresponding conjugate solutions, suggesting that the aggregation of collapsed polymers was partially suppressed by the gel network. Oscillatory rheology studies showed that the composite gels became stronger with the increase in conjugate concentration (G' ~ 20 – 200 Pa). This behaviour was assigned to the increased number of fibres and entanglement points and to the fibre stiffening as the conjugate became incorporated into the fibrillar network. Network morphology was studied using SANS. Using contrast variation and contrast matching techniques it was possible to distinguish between the peptide fibres and the PNIPAAm segments. The scattering patterns showed the presence of rod-like objects (peptide fibres) showing the q^{-1} behaviour, as expected. Below the LCST, fibre morphology in the composite gels was similar to that of pure peptide hydrogel. Above the LCST, polymer segments presumably precipitated along the fibres. TEM and AFM also proved the formation of the fibrillar network. AFM studies showed that the fibres of the composite gel were decorated with polymer chains supporting the early hypothesis.

References

1. A. Saiani, A. Mohammed, H. Frielinghaus, R. Collins, N. Hodson, C. M. Kielty, M. J. Sherratt and A. F. Miller, *Soft Matter*, 2009, **5**, 193-202.
2. H. G. Schild, *Progress in Polymer Science*, 1992, **17**, 163-249.
3. S. Furyk, Y. Zhang, D. Ortiz-Acosta, P. S. Cremer and D. E. Bergbreiter, in *J. Polym. Sci.: Part A: Polym. Chem.*, Editon edn., 2006, vol. 44, pp. 1492-1501.
4. T. Kawaguchi, Y. Kojima and T. Yoshinazi, *Polymer J.*, 2008, **40**, 455-459.
5. S. Fujishige, *Polym. J.*, 1987, **19**, 297-300.
6. H. Cheng, L. Shen and C. Wu, *Macromolecules*, 2006, **39**, 2325-2329.
7. I. Grillo, in *Soft Matter Characterization*, eds. R. Borsali and R. Pecora, Springer Netherlands, Editon edn., 2008, pp. 723-782.
8. J. S. Higgins and H. C. Benoit, *Polymers and Neutron Scattering*, Clarendon Press, Oxford, 1994.
9. M.-H. Kim, C. J. Glinka, S. A. Grot and W. G. Grot, *Macromolecules*, 2006, **39**, 4775-4787.
10. A. Mohammed, A. F. Miller and A. Saiani, *Macromol. Symp.*, 2007, **251**, 88-95.
11. W. Zhou, M. F. Islam, H. Wang, D. L. Ho, A. G. Yodh, K. I. Winey and J. E. Fischer, *Chem. Phys. Lett.*, 2004, **384**, 185-189.
12. L. C. Radu, J. Yang and J. Kopecek, *Macromol. Biosci.*, 2009, **9**, 36-44.
13. L. C. Radu-Wu, J. Yang, K. Wu and J. Kopecek, *Biomacromolecules*, 2009, **10**, 2319-2327.
14. R. Nojima, T. Sato, X. Qiu and F. M. Winnik, *Macromolecules*, 2008, **41**, 292-294.

Chapter 7

General Conclusions and Future Work

7.1. General Conclusions

This research work focused on the design and characterisation of thermo-responsive hydrogels by functionalising PNIPAAm chains with self-assembling octapeptides FEFEFKFK and FEFKFEFK and thus modulating PNIPAAm gelation and by incorporating polymer-peptide conjugate into its respective peptide matrix.

Chapter 4 revealed that thermo-responsive, physical hydrogels of PNIPAAm can be obtained by incorporating small quantities of polymer-peptide bioconjugate where the peptide self-assembles into elongated fibres that associate and entangle creating a gel network. Two series of such systems were prepared easily by using a thiol-modified FEFEFKFK and FEFKFEFK peptides as the chain-transfer agents in the free radical polymerisation of NIPAAm. ^{1}H NMR was used to characterise the conjugation products and to determine the ratio of monomer/peptide in the mixtures. For analytical purposes the polymer was separated from the conjugate to determine the polymer/conjugate weight ratio in each mixture. ^{1}H NMR and centrifugation results showed that control over the composition of the polymer/conjugate mixtures was obtained by varying the quantity of SH-FEFEFKFK and SH-FEFKFEFK added; the higher the peptide concentration, the higher the fraction of conjugate present in the mixtures. A series of mixtures containing PNIPAAm-FEFEFKFK conjugates (PS1, PS2 and PS3) showed higher conjugate content than the mixtures with PNIPAAm-FEFKFEFK conjugates (PA1, PA2 and PA3). The combination of ^{1}H NMR and centrifugation allowed the $\overline{M}_n$ of the conjugates in the mixtures to be determined and in each series the $\overline{M}_n$ values decreased slightly with increasing chain-transfer agent concentration. The $\overline{M}_n$ values from GPC, which were mostly attributed to the unconjugated polymers, were higher than those obtained from ^{1}H NMR and centrifugation for the conjugates. SLS and viscometry measurements showed the aggregation of the polymer/conjugate mixtures presumably due to the presence of peptide and did not show substantial difference between the two series.

The polymer/conjugate mixtures formed self-supporting hydrogels when above a critical gelation concentration which decreased with increasing conjugate content in the mixtures. Polymer/conjugate mixtures PS1, PS2 and PS3 showed lower critical gelation concentrations (150, 50 and 35 mg ml^{-1} respectively) than PA1, PA2 and PA3 (190, 150 and 75 mg ml^{-1} respectively). This difference in gelation behaviour was not ascribed to the differences in the peptide sequences but to the amount of the conjugate in the mixtures: conjugate content in the PS1-PS3 mixtures was higher than in the PA1-PA3. The elastic moduli of such hydrogels

varied from ~ 10 Pa to 400 Pa depending on the sample and were found to be proportional to the quantity of the peptide present, as expected. The scalling exponents increased with decreasing peptide concentration and increasing free polymer concentration. The latter suggested that there were interactions between the free polymer and the peptide, and/or fibre, which were contributing to network formation. TEM and AFM studies proved the formation of the network composed of fibres of ~ 4.5 ± 1.5 nm in diameter.

As the polymer/conjugate mixtures were heated, PNIPAAm exhibited an LCST transition at ~ 30°C whose temperature was not influenced by the conjugate present, nor by the gelled state of the sample. All transitions were fully thermally reversible. In each series the mixtures with higher polymer-peptide conjugate content showed higher phase separation enthalpies than pure PNIPAAm presumably due to additional intermolecular interactions between fibres and polymer chains. During the phase transition the mechanical properties of the hydrogel were enhanced, presumably due to the hydrophobic polymer chains collapsing and enhancing fibre-fibre interactions. Further heating led to the collapse of the gel network. Both series of polymer/conjugate mixtures showed very similar thermal, mechanical and morphological properties. By exploiting the self-assembly of the ionic-complementary peptides, it was possible to create PNIPAAm-rich, thermo-responsive hydrogels with controllable properties.

Results for the peptide-rich hydrogels composed of pure peptides FEFEFKFK and FEFKFEFK and the corresponding mixtures of polymer-peptide conjugates and polymer were discussed in Chapter 5. Two series of the gels with various peptide and polymer/conjugate mixture contents were studied. The gels showed thermo-responsive behaviour as expected and the LCST values were at ~ 30°C for all samples. Micro DSC studies also detected the second endothermic transition upon heating at ~ 63 - 68°C which was not observed previously. At high temperatures the gels with high polymer/conjugate content started to shrink while releasing water. The second transition might be attributed to the formation of the complex between the peptide fibres and polymer, possibly accompanied by slight gel melting. Both thermal transitions were reversible upon cooling. Mechanical studies showed that gel strength increased with increasing polymer/conjugate mixture content, however G' values were < 50 Pa for the samples in both series. These peptide-rich gels again exhibited interesting mechanical behaviour upon heating, i.e. both elastic and viscous moduli values increased during heating from 20 to 80°C and did not decrease upon cooling. G' values increased by approximately an order of magnitude after 4 consecutive heating/cooling cycles. These gels were complex systems with three components, i.e. peptide, polymer and polymer-

peptide conjugate. During heating, these components might form irreversible intermolecular aggregates resulting in gel strengthening. Polymer re-swelling upon cooling was reported to be a thermodynamically slow process that might also contribute to enhancing gel visco-elastic properties during the study. Varying the peptide sequence did not influence thermal and mechanical properties of the hydrogels.

Chapter 6 reported the results on the thermo-responsive composite gels prepared by embedding pure PNIPAAm-FEFEFKFK conjugate into a peptide FEFEFKFK matrix. Two series of the composite gels were prepared by varying peptide matrix concentration (10 and 20 mg ml^{-1}) and conjugate concentration (3, 5 and 10 mg ml^{-1}). Micro DSC measurements revealed the thermo-responsiveness of the composite gels, showing an endothermic peak at ~ 30ºC which was attributed to the LCST of PNIPAAm. No difference in the LCSTs was noticed in comparison to pure polymer. The results showed that the composite gels had lower phase separation enthalpies than the corresponding pure conjugate solutions, suggesting that aggregation of collapsed polymers was partially suppressed by the gel network. Oscillatory rheology studies showed that the composite gels became stronger with the increase in conjugate concentration (G' ~ 20 – 200 Pa). This behaviour was assigned to the fibre stiffening as the conjugate became incorporated into the fibrillar network and also to the increased number of entanglement points. Network morphology was studied using small angle neutron scattering (SANS). Using contrast variation and contrast matching techniques it was possible to distinguish between the peptide fibres and the PNIPAAm chains. Below and above the LCST the scattering curves showed a q^{-1} behaviour which was typical of rod-like objects. TEM and AFM also proved the formation of fibres of ~4.0 ± 0.8 nm and ~4.5 ± 1 nm respectively. AFM studies showed that the fibres of the composite gels were decorated with polymer chains supporting the early hypothesis of the peptide fibres decorated with PNIPAAm chains.

Thermo-responsive hydrogels, containing polymer-peptide conjugates, form an interesting class of new biomaterials. The results of the study showed that PNIPAAm-based gels (Chapter 4) and thermo-responsive peptide-rich composite gels (Chaptes 5 and 6) possess interesting properties such as stability, visco-elasticity and thermo-responsiveness. These are essential properties of polymer-based biomaterials for applications in controlled drug delivery and tissue engineering. Gel mechanical stability is essential during the administration of the drugs- or cells-containing hydrogels indicating that they can easily be injected and retained by surrounding tissues. Thermo-responsive behaviour is important in controlled-drug delivery when the drug release can be targeted by the changes in temperature and also in tissue

engineering when the cells detachment is facilitated upon cooling due to the hydrophilic nature of PNIPAAm below the LCST.

Fig. 7.1 gives a comparison of *G'* (A) and yield stress (B) values as a function of conjugate weight fraction for all systems studied in Chapters 4, 5 and 6. Fig. 7.1A shows that *G'* increased with increasing conjugate content for all systems. PS3 and PA3 gels showed the closest slope values in the series to those of pure corresponding peptides ($c^{0.8}$ and $c^{1.1}$ for FEFEFKFK and FEFKFEFK respectively at pH 5.5), however substantially high (see section 4.3 for more detail). The mechanical strength of peptide-rich gels with the polymer/conjugate mixture was also close to that of pure peptides FEFEFKFK and FEFKFEFK at pH 2.5 ($c^{2.4}$ and $c^{3.0}$ respectively) (see section 5.3 for more detail). The highest slopes were observed for the gels containing pure peptide and the corresponding purified polymer-peptide conjugate (see section 6.4 for more detail). Fig. 7.1B shows that a general trend was observed when yield strain decreased with increasing conjugate fraction ($W_{conjugate}$) in the gels. This trend was more pronounced for peptide-rich systems when polymer/conjugate mixtures (Chapter 5) or purified polymer-peptide conjugate (Chapter 6) were incorporated into pure peptide gel. These results indicate that the gels become more brittle as more conjugate is incorporated into the fibres. PNIPAAm-rich systems showed slight variation with conjugate content presumably due to high free polymer content that did not contribute to formation of fibrillar network.

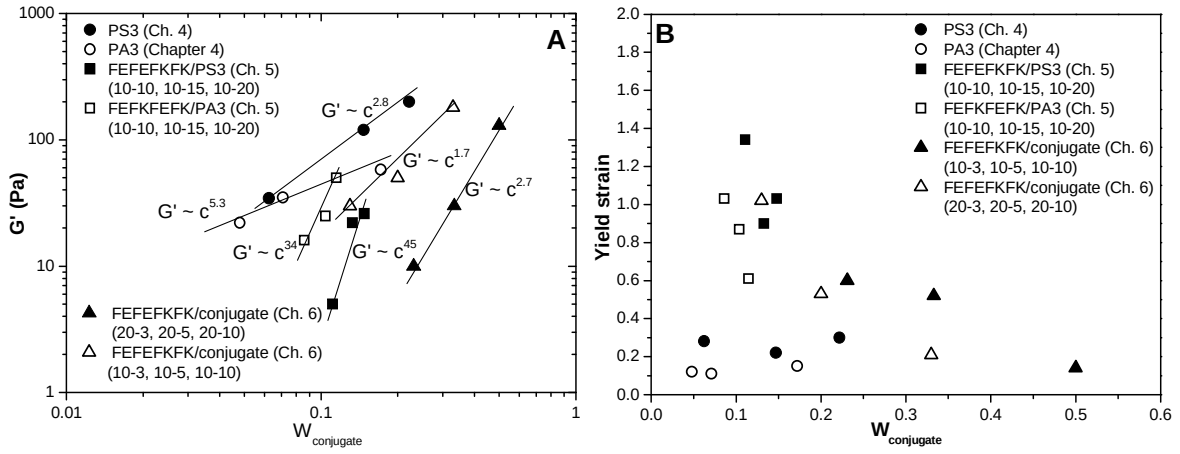

Figure 7.1: *Variation of: A) G' and B) yield strain with conjugate weight fraction ($W_{conjugate}$) in the gels studied*

7.2. Future work

Mechanical properties of the polymer-conjugate containing systems were studied as a function of temperature. The results showed a rather interesting behaviour: *G′* and *G″* values increased upon heating and remained practically unchanged upon cooling. It has been suggested that some additional intermolecular interactions between the fibres and polymer chains might contribute to this increase of the gels rigidity. Therefore it is proposed to use small angle neutron scattering in conjunction with rheology to study gel behaviour upon heating and cooling in more detail. This will provide a further insight into the network behaviour below and above the LCST.

Future work can be focused on other ionic-complementary peptide sequences, such as arginine-based peptides. It is anticipated that arginine would form larger diameter fibres and would influence the gelation properties by shifting the critical gelation concentration to lower values. This would result in stiffer gels than those made of FEFEFKFK and FEFKFEFK peptides.

PNIPAAm behaviour in the bioconjugates can be compared to other polymers, for example to PEG-based polymers. NIPAAm can also be co-polymerised with pH-responsive monomers to introduce additional stimulus to the system. Moreover, enzyme-cleavable linkers and fluorescent labels can be introduced into the conjugates. Such enzyme-responsive materials would provide a non-invasive assessment of enzyme activity and function, and can be used as a model for studying enzyme-triggered release of macromolecules. Fluorescent labels would also be useful for tracking the cellular internalisation pathways of drug molecules.

Appendices

Appendix 1

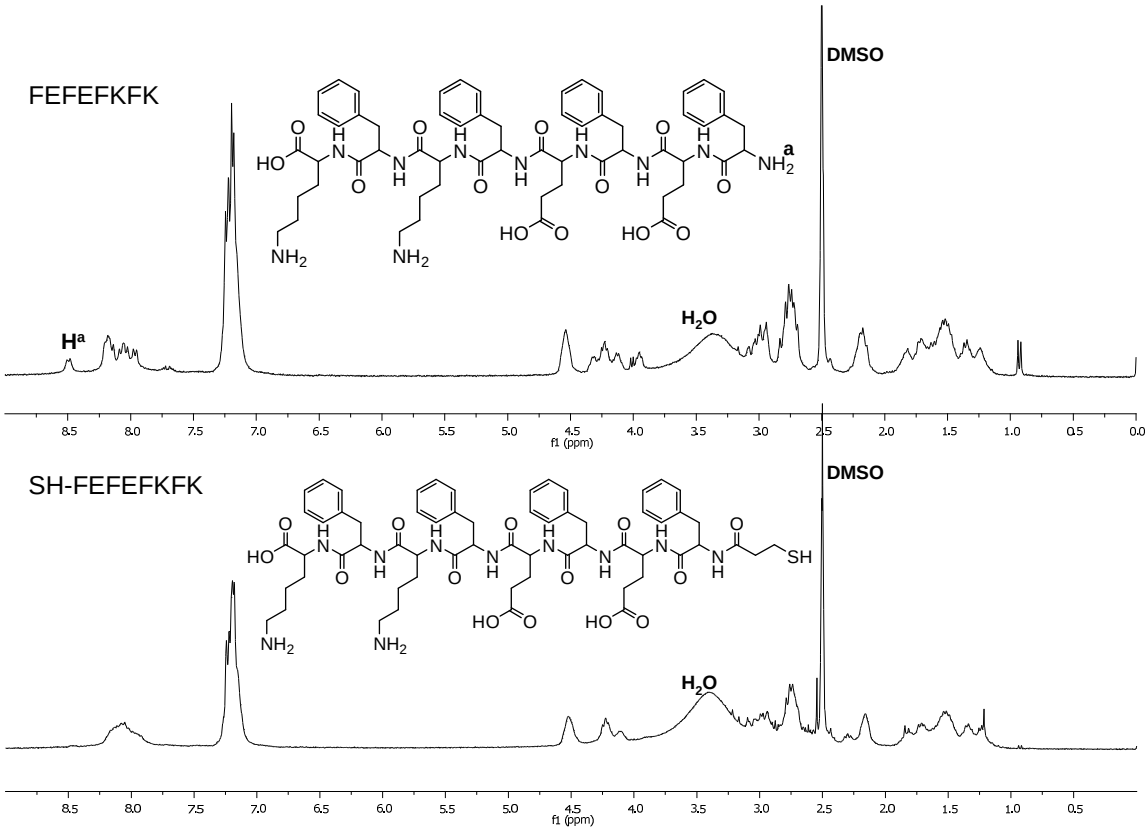

Figure A1.1: *^{1}H NMR spectra of FEFEFKFK and SH-FEFEFKFK (DMSO-d_6, 400 MHz)*

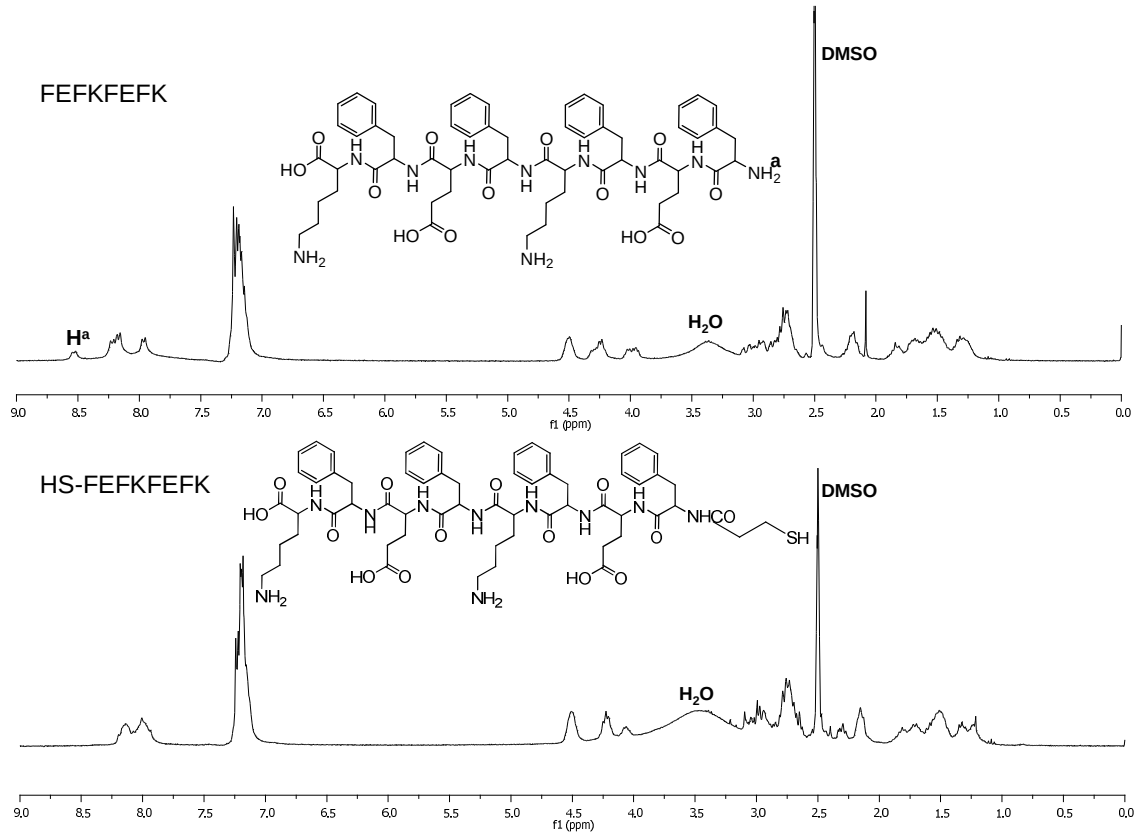

Figure A1.2: *^{1}H NMR spectra of FEFKFEFK and SH-FEFKFEFK (DMSO-d_6, 400 MHz)*

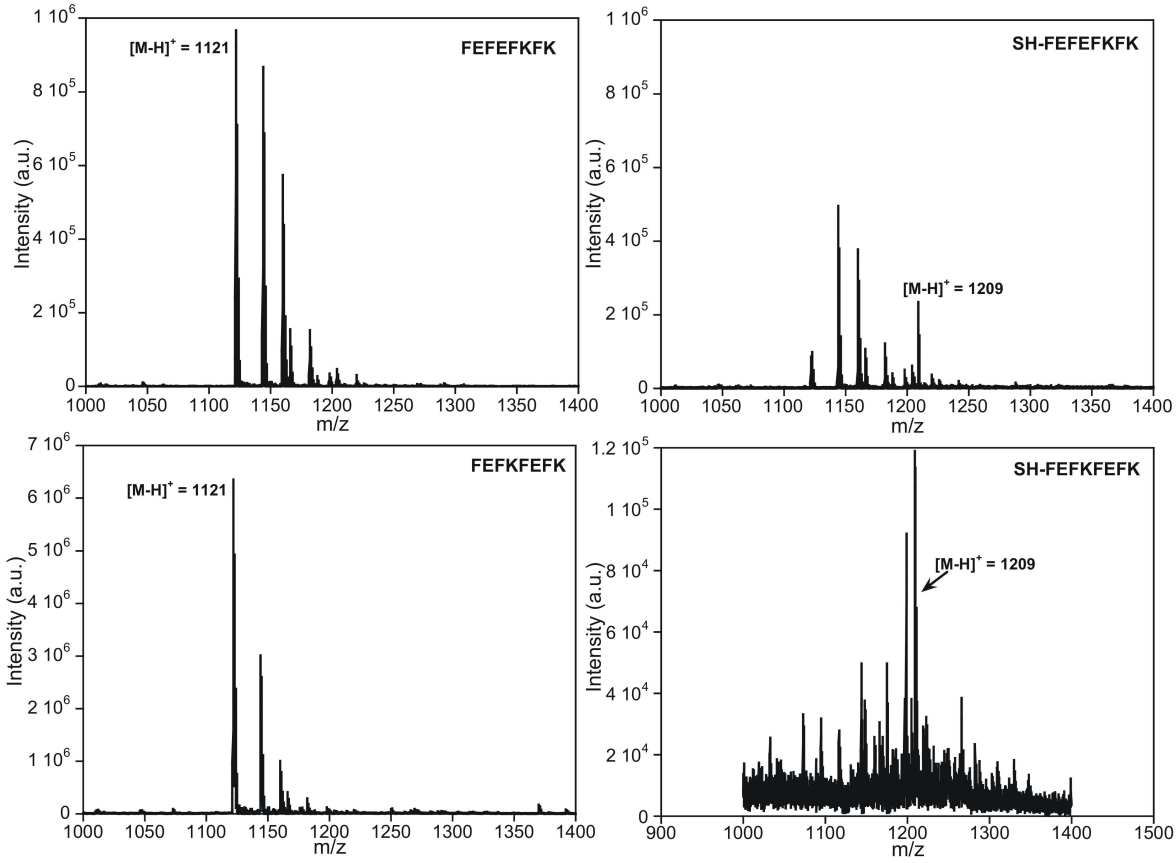

Figure A1.3: *MALDI-ToF spectra of the peptides FEFEFKFK, SH-FEFEFKFK, FEFKFEFK and SH-FEFKFEFK*

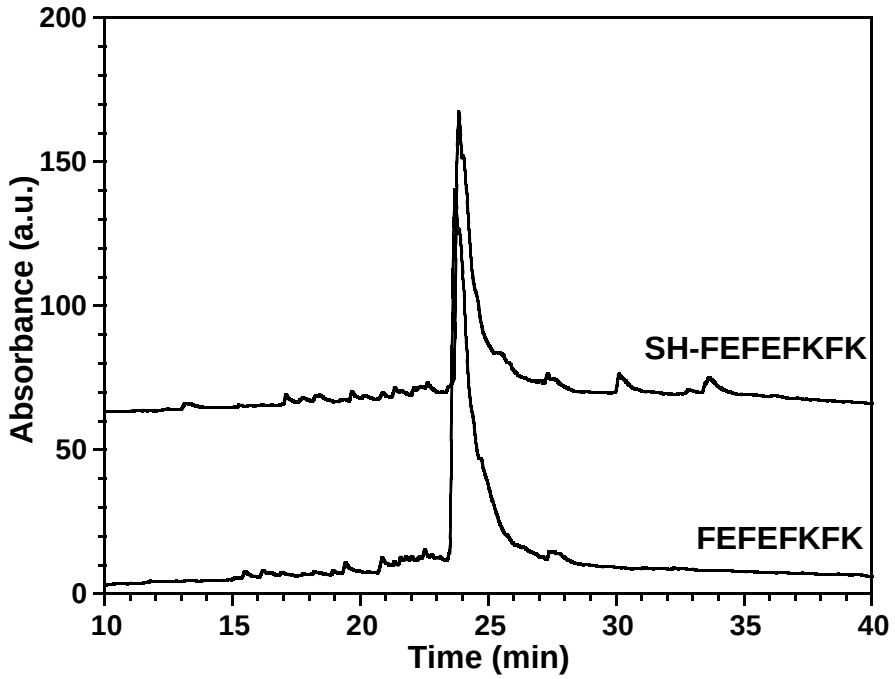

Figure A1.4: *HPLC chromatograms of FEFEFKFK and SH-FEFEFKFK with elution times of 23.7 and 23.9 minutes respectively*

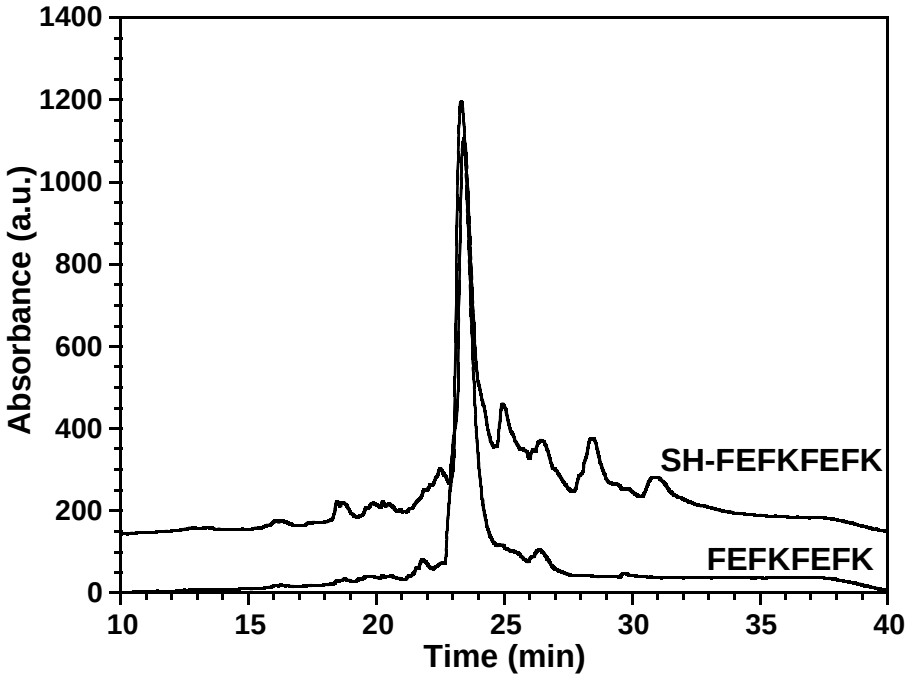

Figure A1.5: *HPLC chromatograms of FEFKFEFK and SH-FEFKFEFK with elution times of 23.3 and 23.5 minutes respectively*

Appendix 2

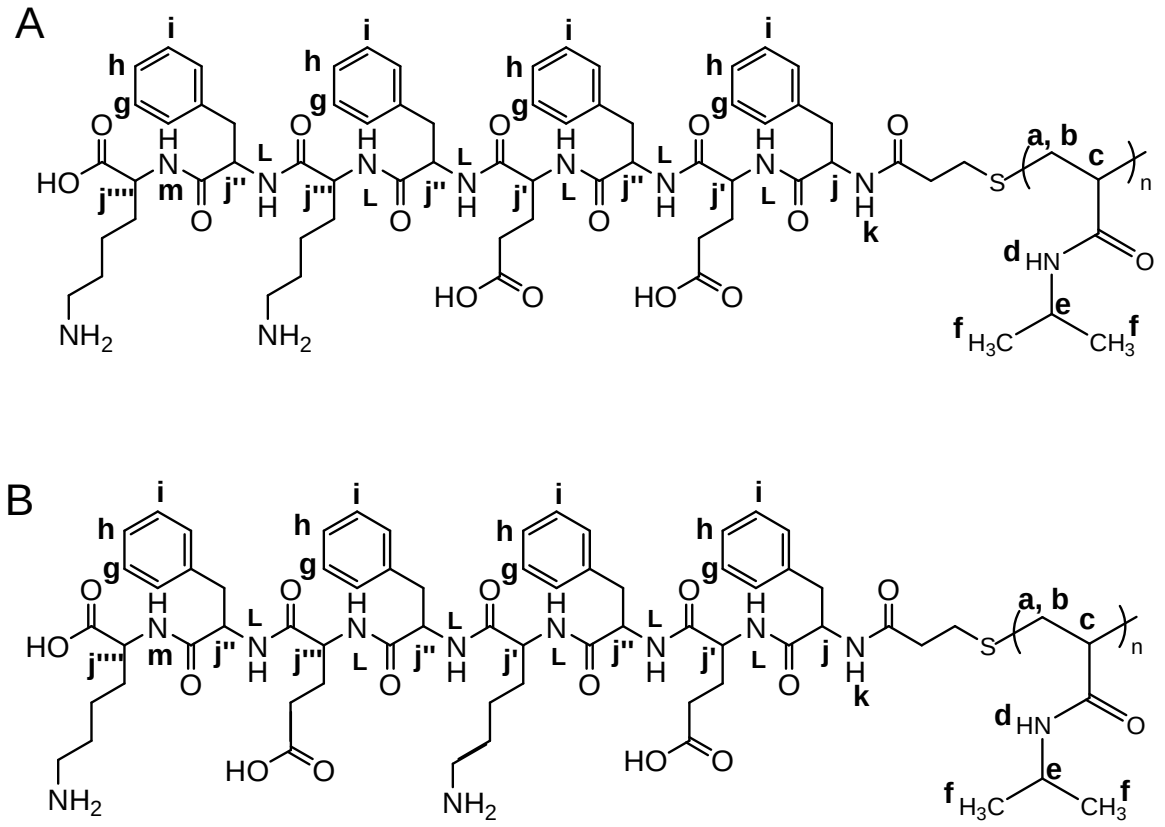

Figure A2.1: *Chemical structures of: A) FEFEFKFK-PNIPAAm and B) FEFKFEFK-PNIPAAm with the assignments of some characteristic protons for the ^{1}H NMR spectra in Fig. A2.2 and A2.3*

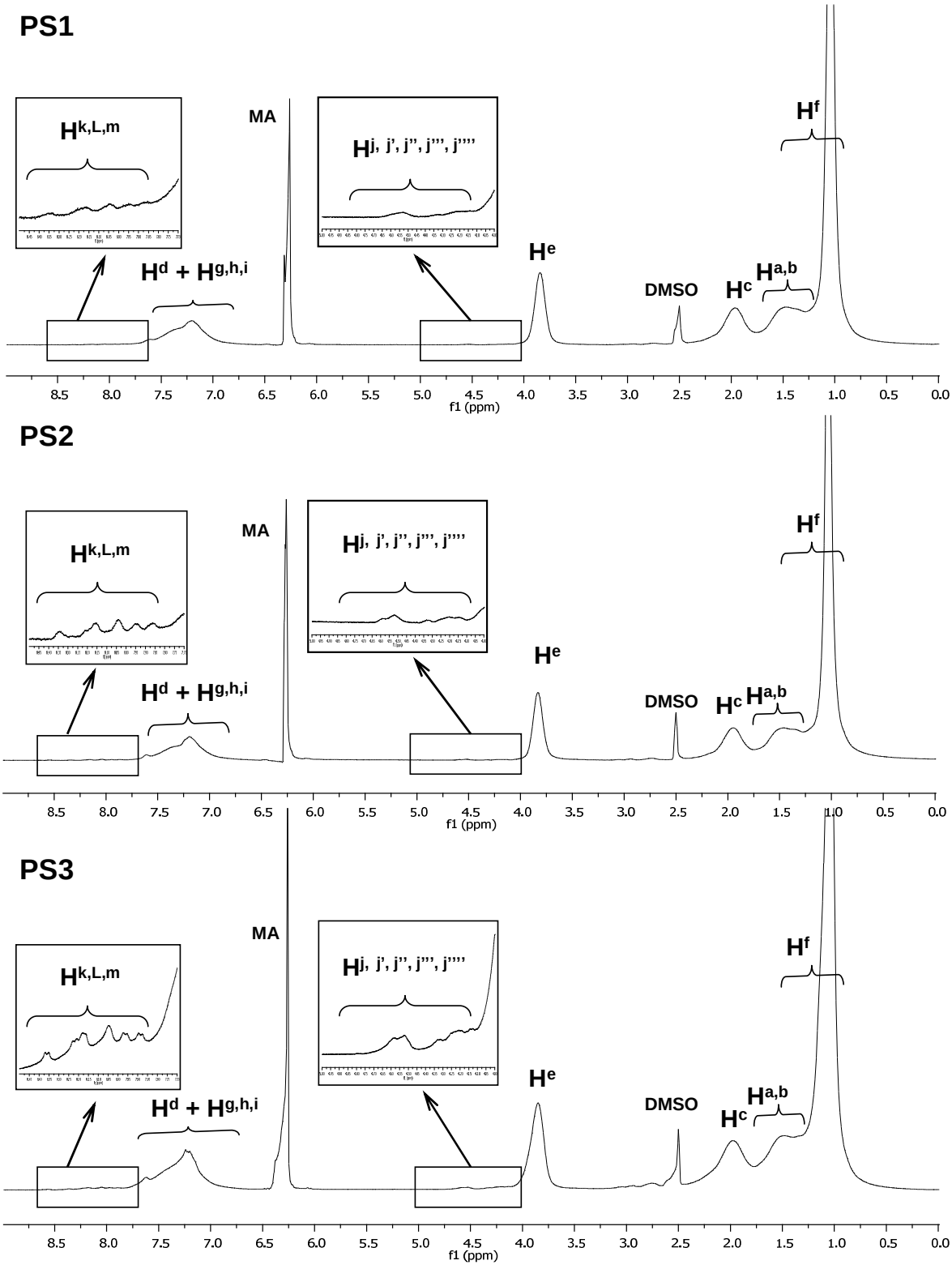

Figure A.2.2: *^{1}H NMR spectra of PS1, PS2 and PS3 with the characteristic peaks of the polymer and the peptide (DMSO-d_6, 400 MHz)*

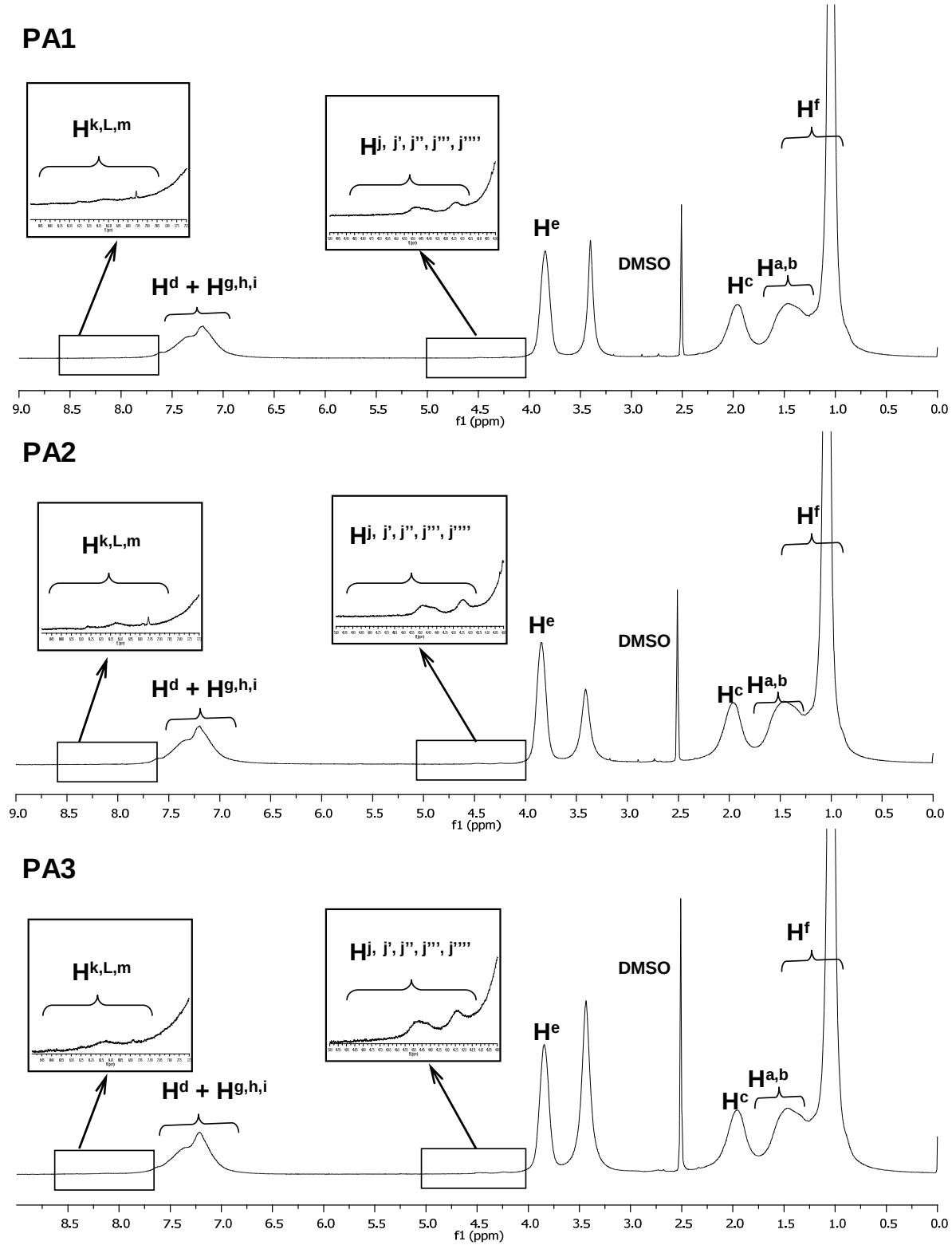

Figure A.2.3: *^{1}H NMR spectra of PA1, PA2 and PA3 with the characteristic peaks of the polymer and the peptide (DMSO-d_6, 400 MHz)*